INFLUENCE OF RADIATION THERAPIES ON LIVER CANCER

EDITED BY: John Varlotto, James M. Brindle and An Liu
PUBLISHED IN: Frontiers in Oncology

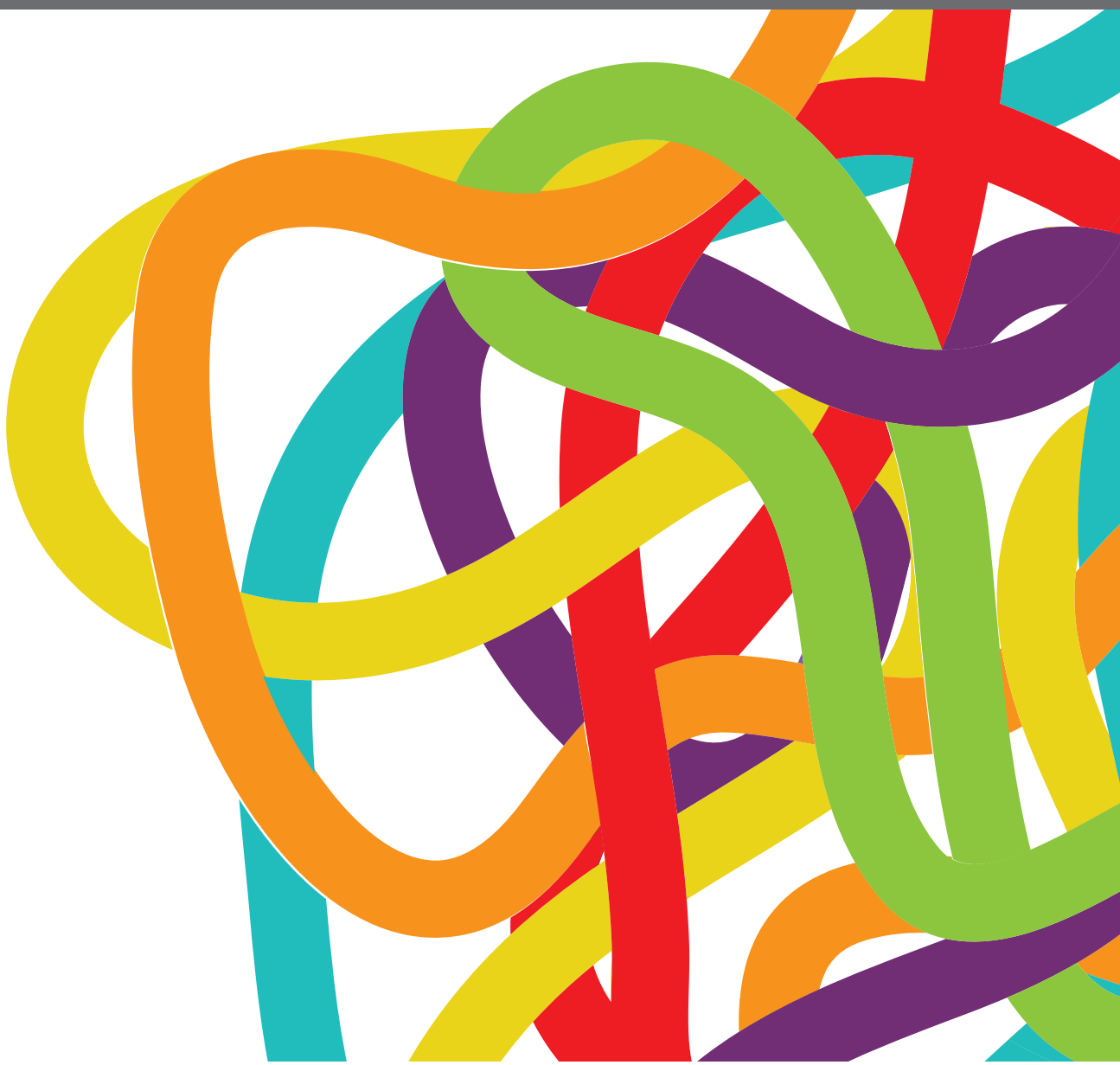

frontiers Research Topics

frontiers

ISSN 1664-8714
ISBN 978-2-83250-292-1
DOI 10.3389/978-2-83250-292-1

About Frontiers

Frontiers is more than just an open-access publisher of scholarly articles: it is a pioneering approach to the world of academia, radically improving the way scholarly research is managed. The grand vision of Frontiers is a world where all people have an equal opportunity to seek, share and generate knowledge. Frontiers provides immediate and permanent online open access to all its publications, but this alone is not enough to realize our grand goals.

Frontiers Journal Series

The Frontiers Journal Series is a multi-tier and interdisciplinary set of open-access, online journals, promising a paradigm shift from the current review, selection and dissemination processes in academic publishing. All Frontiers journals are driven by researchers for researchers; therefore, they constitute a service to the scholarly community. At the same time, the Frontiers Journal Series operates on a revolutionary invention, the tiered publishing system, initially addressing specific communities of scholars, and gradually climbing up to broader public understanding, thus serving the interests of the lay society, too.

Dedication to Quality

Each Frontiers article is a landmark of the highest quality, thanks to genuinely collaborative interactions between authors and review editors, who include some of the world's best academicians. Research must be certified by peers before entering a stream of knowledge that may eventually reach the public - and shape society; therefore, Frontiers only applies the most rigorous and unbiased reviews.
Frontiers revolutionizes research publishing by freely delivering the most outstanding research, evaluated with no bias from both the academic and social point of view. By applying the most advanced information technologies, Frontiers is catapulting scholarly publishing into a new generation.

What are Frontiers Research Topics?

Frontiers Research Topics are very popular trademarks of the Frontiers Journals Series: they are collections of at least ten articles, all centered on a particular subject. With their unique mix of varied contributions from Original Research to Review Articles, Frontiers Research Topics unify the most influential researchers, the latest key findings and historical advances in a hot research area! Find out more on how to host your own Frontiers Research Topic or contribute to one as an author by contacting the Frontiers Editorial Office: frontiersin.org/about/contact

INFLUENCE OF RADIATION THERAPIES ON LIVER CANCER

Topic Editors:
John Varlotto, Marshall University, United States
James M. Brindle, Rhode Island Hospital, United States
An Liu, City of Hope National Medical Center, United States

Citation: Varlotto, J., Brindle, J. M., Liu, A., eds. (2022). Influence of Radiation Therapies on Liver Cancer. Lausanne: Frontiers Media SA. doi: 10.3389/978-2-83250-292-1

Table of Contents

frontiers in Oncology

ORIGINAL RESEARCH
published: 24 March 2020
doi: 10.3389/fonc.2020.00347

Stereotactic Body Radiation Therapy vs. Transarterial Chemoembolization in Inoperable Barcelona Clinic Liver Cancer Stage a Hepatocellular Carcinoma: A Retrospective, Propensity-Matched Analysis

Ting-Shi Su[1], Ping Liang[2], Ying Zhou[2], Yong Huang[2], Tao Cheng[2], Song Qu[1], Long Chen[1], Bang-De Xiang[3], Chang Zhao[4], De-Jia Huang[4], Shi-Xiong Liang[1]* and Le-Qun Li[3]**

[1] Department of Radiation Oncology, Guangxi Medical University Cancer Hospital, Nanning, China, [2] Department of Radiation Oncology, Rui Kang Hospital, Guangxi Traditional Chinese Medical University, Nanning, China, [3] Department of Hepatobiliary Surgery, Guangxi Medical University Cancer Hospital, Nanning, China, [4] Department of Interventional Radiology, Guangxi Medical University Cancer Hospital, Nanning, China

Background and Objective: It is unclear if stereotactic body radiation therapy (SBRT) or transarterial chemoembolization (TACE) is better for the treatment of inoperable early-stage hepatocellular carcinoma (HCC). This study aimed to retrospectively compare the efficacy of SBRT to TACE in patients with inoperable Barcelona Clinic Liver Cancer (BCLC)-A stage HCC.

Materials and Methods: In this multi-institutional retrospective study, a total of 326 patients with inoperable BCLC-A stage HCC were enrolled. Totally, 167 patients initially received SBRT and 159 initially received TACE. Overall survival (OS), local control (LC), intrahepatic control (IC), and progression-free survival (PFS) were evaluated in univariable and propensity-score matched analyses.

Results: There was a smaller median tumor size in the SBRT group than in the TACE group (3.4 cm vs. 7.2 cm, $P < 0.001$). After propensity score matching in the selection of 95 patient pairs, SBRT had better LC, IC, and PFS than TACE but showed comparable OS. The accumulative 1-, 3-, and 5-year OS rates were 85.7, 65.1, and 62.8% in the SBRT group and 83.6, 61.0, and 50.4% in the TACE group, respectively ($P = 0.29$). The accumulative 1-, 3-, and 5-year PFS were 63.4, 35.9, and 27.5% in the SBRT group and 53.5, 27.4, and 14.2% in the TACE group, respectively ($P = 0.049$). The accumulative 1-, 3-, and 5-year LC were 86.8, 62.5, and 56.9% in the SBRT group and 69.3, 53.3, and 36.6% in the TACE group, respectively ($P = 0.0047$). The accumulative 1-, 3-, and 5-year IC were 77.3, 45.9, and 42.4% in the SBRT group and 57.3, 34.1, and 17.7% in the TACE group, respectively ($P = 0.003$). On multivariate analysis, treatment (SBRT vs. TACE) was a significant covariate associated with local and intrahepatic control (HR = 1.59; 95% CI: 1.03–2.47; $P = 0.04$; HR = 1.61; 95% CI: 1.13–2.29; $P = 0.009$).

OPEN ACCESS

Edited by:
Timothy James Kinsella, Warren Alpert Medical School of Brown University, United States

Reviewed by:
Shahed Nicolas Badiyan, Washington University in St. Louis, United States
Jaine Katharine Blayney, Queen's University Belfast, United Kingdom

****Correspondence:***
Ting-Shi Su
sutingshi@163.com
Shi-Xiong Liang
shixliang@vip.sina.com
Le-Qun Li
li_lequn@263.net

Specialty section:
This article was submitted to Radiation Oncology, a section of the journal Frontiers in Oncology

Received: *29 October 2019*
Accepted: *27 February 2020*
Published: *24 March 2020*

Citation:
Su T-S, Liang P, Zhou Y, Huang Y, Cheng T, Qu S, Chen L, Xiang B-D, Zhao C, Huang D-J, Liang S-X and Li L-Q (2020) Stereotactic Body Radiation Therapy vs. Transarterial Chemoembolization in Inoperable Barcelona Clinic Liver Cancer Stage a Hepatocellular Carcinoma: A Retrospective, Propensity-Matched Analysis. Front. Oncol. 10:347. doi: 10.3389/fonc.2020.00347

Conclusions: SBRT was an alternative to TACE for inoperable BCLC-A stage HCC with better local and intrahepatic control. Controlled clinical trials are recommended to evaluate the actual effects of this novel regimen adequately.

Keywords: hepatocellular carcinoma, SBRT, TACE, Barcelona Clinic Liver Cancer Stage A, overall survival

INTRODUCTION

Patients with early-stage hepatocellular carcinoma (HCC) are candidates for potentially curative treatment options, such as liver transplantation, liver resection, and radiofrequency ablation, and they have a 5-year survival rate of 40–70% (1). However, some patients with Barcelona Clinic Liver Cancer (BCLC) stage A disease refuse to undergo surgery, or the procedure may be deemed too high risk for them. There is an urgent clinical need for a more effective therapy for HCC. Transarterial chemoembolization (TACE) is an established local treatment for patients with unresectable and non-transplantable stages of HCC with compensated liver disease and without extrahepatic spread (2, 3). Although the aforementioned conditions define BCLC stage B disease, TACE can also be applied to those with earlier-stage (BCLC stage A) disease who are not considered for surgery or ablation (4, 5).

Stereotactic body radiation therapy (SBRT) is an advanced external beam radiation therapy technique that delivers large ablative doses of radiation and low fractionation (6). There is increasing evidence (primarily from non-randomized controlled trials) supporting the clinical application of SBRT as a non-invasive treatment in patients with unresectable or recurrent HCC (7–10). SBRT can provide encouraging outcomes comparable to those associated with curative treatment options, including liver resection and radiofrequency ablation (11–13). Several studies have reported good clinical outcomes using SBRT in HCC with or without TACE (14–17). However, few comparative studies have analyzed the use of SBRT vs. TACE in BCLC-A stage HCC. In this retrospective study, we aimed to compare the long-term survival rates after SBRT and TACE in patients with early-stage HCC who were ineligible for resection or ablation therapies.

MATERIALS AND METHODS

Patients

Datasets from January 2009 to January 2017 from two different institutions with a tertiary-A hospital in the Guangxi region of China, Cancer Hospital and Rui Kang Hospital, were used in this study. All cases of TACE were collected from Cancer Hospital, and cases of SBRT were collected from Rui Kang Hospital.

The eligibility criterion was the presence of BCLC stage A HCC in patients who were not considered for surgery, or refused to undergo surgery and/or local radiofrequency ablative therapies, and received SBRT or TACE as initial treatment. HCC diagnosis was established based on histopathology or according to the clinical criteria for HCC diagnosis (18). Exclusion criteria were as follows: (a) recurrence after other treatments, (b) intrahepatic cholangiocellular carcinoma, (c) gallbladder cancer, (d) liver metastases, and/or (e) prior history of conventional abdominal radiotherapy. All hospital charts and patients' documents were carefully reviewed.

Transarterial Chemoembolization (TACE)

A French catheter (4 F−5 F) was inserted into the abdominal aorta through the right femoral artery using the Seldinger technique. Selective arteriography of the hepatic artery was carried out for tumor location. Hepatic angiography was performed for the detection of any obvious tumor staining in the remaining liver. Subsequently, an emulsion of oxaliplatin or lobaplatin or cisplatinum (20–100 mg), pharmorubicin or pirarubicin (10–40 mg), and lipiodol (2–15 ml) was infused via the catheter (15, 19). The effect of TACE was evaluated by computed tomography (CT) at the 1-month follow-up. Treatment was repeated one to six times (median, 3) at 3–6-week intervals in the TACE group.

Stereotactic Body Radiation Therapy (SBRT)

SBRT was performed as described (7, 11, 20). Briefly, gross tumor volume was outlined under the fusion image of CT and magnetic resonance imaging (MRI) by comparing different imaging phases, and the gross tumor volume was expanded by 0–5 mm for the formation of the planning target volume (PTV). SBRT was implemented using a CyberKnife system (Accuray Inc., Sunnyvale, CA, USA). A 28–50 Gy dose of radiation was delivered in one to five fractions on consecutive days at the 55–80% isodose line that covered at least 97% of the planning target volume. Fractionation schedules and total doses were chosen according to the tumor size and dose–volume constraints of the organs at risk.

Response Evaluation and Follow-Up

The evaluations included laboratory tests and imaging with contrast-enhanced CT and/or MRI at 1 month after the procedure and every 3–6 months thereafter. The laboratory examinations assessed levels of alanine transaminase (ALT), aspartate transaminase (AST), prothrombin time, levels of total bilirubin, albumin, and alpha-fetoprotein. The modified Response Evaluation Criteria in Solid Tumors guideline was used to describe changes in the treated areas (21). Local recurrence/progress was defined as the reappearance of radiologic hallmarks of HCC for in-field-treated PTV lesions and/or progressive increase in tumor sizes during follow-up. Intrahepatic recurrence was defined as the reappearance of radiologic hallmarks of HCC (hypervascularity in the arterial phase with washout in the portal venous or delayed phases)

and out-field-treated (PTV) lesions in the whole parenchyma of the liver. For progressive increase in tumor sizes without typical CT/MRI characteristics, diagnosis was confirmed by histopathology.

Statistical Analysis

R version 3.6.1 software (2019 Microsoft Corporation) was used for the statistical analysis. $P < 0.05$ was considered statistically significant. Kaplan–Meier curves with the log-rank test were used to calculate patients' overall survival (OS), local control (LC) rate, intrahepatic control (IC) rate, and progression-free survival (PFS). In addition, accumulative overall survival (OS) was calculated starting from the date of the first treatment to death from any cause, with patients censored at the end of the study (April 11, 2019). Accumulative PFS was calculated starting from the date of the first treatment to the date of any tumor recurrence, progression, or death or the date of censoring. Accumulative LC was calculated starting from the date of the first treatment to the date of local tumor failure or the date of censoring. Accumulative IC was calculated starting from the date of the first treatment to the date of intrahepatic tumor failure or the date of censoring.

Variables without associations between each other by chi-squared/Mann–Whitney tests (**Figure S1**). We use univariate and least absolute shrinkage and selection operator (LASSO) to identify non-associated predictive variables that contribute toward the final multivariate. The report concordance index gives an indication of the predictive fit (**Figure S2**).

To reduce selection bias and potential confounding effect of treatment, a 1:1 nearest neighbor matching that pairs patients who have the closest propensity scores was performed to create a balanced cohort. The logit of the propensity score for matching was used with a caliper of 0.2 times its standard deviation as recommended by Austin (22), based on the potential confounding variables including age, gender, ALBI score, ALT, tumor size, and alpha-fetoprotein (AFP) levels. Only patients who were matched were included (**Figure S3**).

RESULTS

Patients

During the study period from January 2009 to January 2017, 326 patients with BCLC stage A HCC, who were not considered for surgery and/or radiofrequency ablative therapies were enrolled retrospectively. A total of 167 patients initially received SBRT, and 159 initially received TACE. Some variables differed between the groups, including age, ALT levels, tumor size, ALBI score, and AFP level. After propensity score matching, 95 paired patients were selected from the SBRT and TACE groups. There was no significant difference between the groups, and the balance of variables in the matched cohorts was markedly improved (**Table 1**).

SBRT vs. TACE

This study was concluded on April 11, 2019. The median follow-up time was 35.0 months in the SBRT group and 32.0 months in the TACE group. A total of 50 cases died, and 117 cases were right-censored, including 31 cases lost to follow-up, while 86 cases were still alive at the end of the study in the SBRT group. On the other hand, 66 cases died, and 96 cases were right-censored, including 41 cases lost to follow-up, while 55 cases were still alive at the end of the study in the TACE group. During the follow-up period, the total local and intrahepatic recurrence after SBRT was lower than that after TACE (69/167 vs. 98/159, $P = 0.037$).

Before propensity score matching, the accumulative OS (**Figure 1A**), PFS (**Figure 1B**), LC (**Figure 1C**), and IC (**Figure 1D**) at 12, 36, and 60 months were better in patients undergoing SBRT than in those undergoing TACE (**Table 2**). The accumulative 3-year OS was 64.7% in the SBRT group and 51.0% in the TACE group ($P = 0.005$, HR = 1.71, 95% CI: 1.17–2.51). The accumulative 3-year PFS was 38.1% in the SBRT group and 27.6% in the TACE group ($P = 0.0005$, HR = 1.62, 95% CI: 1.22–2.16). The accumulative 3-year LC was 63.1% in the SBRT group and 50.2% in the TACE group ($P = 0.0008$, HR = 1.93, 95% CI: 1.29–2.88). The accumulative 3-year IC 49.6% in the SBRT group and 33.5% in the TACE group ($P < 0.0001$, HR = 2.14, 95% CI: 1.54–2.96).

After propensity score matching in the selection of 95 well-pairs patients, we found no statistically significant difference in OS (**Figure 2A**); patients in the SBRT group had better long-term PFS (**Figure 2B**), LC (**Figure 2C**), and IC (**Figure 2D**) than those in the TACE group (**Table 2**). The accumulative 3-year OS was 65.1% in the SBRT group and 61.0% in the TACE group ($P = 0.55$, HR = 1.17, 95% CI: 0.7–1.96). The accumulative 3-year PFS was 35.9% in the SBRT group and 27.4%, in the TACE group ($P = 0.081$, HR = 1.37, 95% CI: 0.95–1.97). The accumulative 3-year LC was 62.5% in the SBRT group and 53.5% in the TACE group ($P = 0.0219$, HR = 1.81, 95% CI: 1.08–3.04). The accumulative 3-year IC was 45.9% in the SBRT group and 34.1% in the TACE group ($P = 0.01$, HR = 1.70, 95% CI: 1.12–2.58).

Multivariable Cox Analysis

Cox proportional hazards models accounting for clustering were used to compare the two treatment groups. The selection of influencing factors, which were considered for multivariate analysis, was based on LASSO analysis (**Table 3**). Multivariable cox regression analysis of OS (**Figure 3A**) showed that three independent predictors were size (HR = 1.12; 95% CI, 1.06–1.17; $P < 0.001$), ALBI score (HR = 2.01; 95% CI: 1.46–2.77; $P < 0.001$), and AFP level >400 (HR = 1.84; 95% CI: 1.12–3.02; $P = 0.02$). Multivariable cox regression analysis of PFS (**Figure 3B**) showed that three independent predictors were size (HR = 1.09; 95% CI: 1.05–1.14; $P < 0.001$), age (HR = 0.99; 95% CI: 0.98–1.00; $P = 0.05$), and AFP level >400 (HR = 1.52; 95% CI: 1.50–2.17; $P = 0.03$). Multivariable cox regression analysis of LC (**Figure 3C**) showed that three independent predictors were size (HR = 1.06; 95% CI: 1.01–1.12; $P = 0.02$), gender/male (HR = 2.69; 95% CI: 1.18–6.17; $P = 0.02$), and treatment (SBRT vs. TACE) (HR = 1.59; 95% CI: 1.03–2.47; $P = 0.04$). Multivariable cox regression analysis of IC (**Figure 3D**) showed that four independent predictors were size (HR = 1.10; 95% CI: 1.05–1.14; $P < 0.001$), gender/male (HR = 1.84; 95% CI: 1.06–3.21; $P = 0.031$), AFP level >400 (HR = 1.61; 95% CI: 1.06–2.46; P

TABLE 1 | Patient and treatment characteristics for different treatment groups.

		Before propensity matching			After propensity matching			
Factor	**Level**	**SBRT**	**TACE**	***p*-value**	**SBRT**	**TACE**	***p*-value**	**Test**
Number of patients		167	159		95	95		
Gender	Male	141 (84.4%)	139 (87.4%)	0.44	83 (87%)	84 (88%)	0.82	Pearson's chi-squared
Age, median (IQR)		56 (47, 65)	52 (44, 61)	0.007	55 (45, 63)	52 (44, 63)	0.31	Wilcoxon rank-sum
Age	>/=60	70 (41.9%)	49 (30.8%)	0.037	36 (38%)	29 (31%)	0.28	Pearson's chi-squared
HBV	Positive	145 (86.8%)	141 (88.7%)	0.61	83 (87%)	84 (88%)	0.82	Pearso's chi-squared
	Negative	22 (13.2%)	18 (11.3%)		12 (13%)	11 (12%)		
Tbil, median (IQR)		13.3 (9.3, 20.1)	14.4 (9.3, 21.5)	0.48	13.4 (9.7, 20.5)	14.9 (9.3, 22.4)	0.52	Wilcoxon rank-sum
Albumin, median (IQR)		37.9 (34.5, 41.7)	38.7 (34.2, 42)	0.63	37.6 (34.4, 41.8)	39.3 (33.9, 42.3)	0.26	Wilcoxon rank-sum
ALT, median (IQR)		31 (21, 44)	44 (35, 82)	<0.001	35 (23, 50)	39 (32, 60)	0.1	Wilcoxon rank-sum
AST, median (IQR)		31 (21, 50)	35 (24, 53)	0.13	36 (23, 52)	31 (22, 43)	0.24	Wilcoxon rank-sum
PT, median (IQR)		13.2 (12.5, 14)	13.1 (12.3, 14.4)	0.97	13.1 (12.5, 14.1)	13.3 (12.4, 14.8)	0.41	Wilcoxon rank-sum
Size, median (IQR)		3.4 (2.4, 5.2)	7.2 (4.2, 12.1)	<0.001	4.5 (3, 6.7)	5 (3, 7.1)	0.6	Wilcoxon rank-sum
Size status	1–5 cm	123 (73.7%)	53 (33.3%)	<0.001	53 (56%)	49 (52%)	0.47	Pearson's chi-squared
	5–10 cm	40 (24.0%)	54 (34.0%)		38 (40%)	38 (40%)		
	10–19.5 cm	4 (2.4%)	52 (32.7%)		4 (4%)	8 (8%)		
ALBI score, median (IQR)		−2.519 (−2.802, −2.179)	−2.511 (−2.878, −2.127)	0.88	−2.515 (−2.761, −2.127)	−2.530 (−2.967, −2.088)	0.5	Wilcoxon rank-sum
ALBI grade	1	73 (43.7%)	64 (40.3%)	0.48	41 (43%)	40 (42%)	0.29	Pearson's chi-squared
	2	88 (52.7%)	85 (53.5%)		51 (54%)	47 (49%)		
	3	6 (3.6%)	10 (6.3%)		3 (3%)	8 (8%)		
Child–Pugh score	5	105 (62.9%)	118 (74.2%)	0.2	59 (62%)	70 (74%)	0.24	Pearson's chi-squared
	6	32 (19.2%)	21 (13.2%)		17 (18%)	11 (12%)		
	7	18 (10.8%)	9 (5.7%)		12 (13%)	5 (5%)		
	8	5 (3.0%)	4 (2.5%)		3 (3%)	3 (3%)		
	9	7 (4.2%)	7 (4.4%)		4 (4%)	6 (6%)		
Child–Pugh class	A	137 (82.0%)	139 (87.4%)	0.18	76 (80%)	81 (85%)	0.34	Pearson's chi-squared
	B	30 (18.0%)	20 (12.6%)		19 (20%)	14 (15%)		
AFP	0–7	58 (34.7%)	35 (22.0%)	0.013	28 (29%)	22 (23%)	0.61	Pearson's chi-squared
	>7–100	50 (29.9%)	42 (26.4%)		23 (24%)	28 (29%)		
	>100–400	20 (12.0%)	22 (13.8%)		15 (16%)	12 (13%)		
	>400	39 (23.4%)	60 (37.7%)		29 (31%)	33 (35%)		

ALBI, albumin–bilirubin; AFP, alpha fetoprotein; TACE, transarterial embolization; SBRT, stereotactic body radiation therapy; PT, prothrombin time; AST, aspartate aminotransferase; ALT, alanine aminotransferase.

= 0.027), and treatment (SBRT vs. TACE) (HR = 1.61; 95% CI: 1.13–2.29; $P = 0.009$).

In our matched cohort, multivariable cox regression analysis showed that ALBI score was the only independent predictor of OS (HR = 1.84; 95% CI: 1.23–2.76; $P = 0.003$). Tumor size was the only independent predictor of PFS (HR = 1.12; 95% CI: 1.06–1.19; $P < 0.001$). Treatment (SBRT vs. TACE) was the only independent predictor of LC (HR = 2.19; 95% CI: 1.27–3.77; $P = 0.005$). Treatment (SBRT vs. TACE) and tumor size were two independent predictors of IC (HR = 1.99; 95% CI: 1.30–3.04; $P = 0.001$; and HR = 1.09; 95% CI: 1.02–1.16; $P = 0.014$).

In the SBRT cohort, multivariable cox regression analysis showed that AFP level and ALBI score were two independent predictors of OS (HR = 1.34; 95% CI: 1.04–1.73; $P = 0.02$; and HR = 2.84; 95% CI: 1.72–4.71; $P < 0.001$). The included influencing factors were not prognostic factors for PFS, LC, and IC.

In the TACE cohort, multivariable cox regression analysis showed that tumor size was an independent predictor of OS (HR = 1.09; 95% CI: 1.04–1.13; $P < 0.001$). Tumor size and age were two independent predictors of PFS (HR = 1.84; 95% CI: 1.23–2.76; $P = 0.003$; and HR = 0.97; 95% CI: 0.95–0.99; $P < 0.001$). Age was an independent predictor of LC (HR = 0.97; 95% CI: 0.95–0.99; $P = 0.02$). Tumor size and age were two independent predictors of IC (HR = 1.10; 95% CI: 1.05–1.15; $P < 0.001$; and HR = 0.98; 95% CI: 0.96–0.99; $P = 0.04$).

Complications and Mortality

Both treatment regimens have their own specific complications. In the TACE group, TACE-related deaths occurred in 2 (1.3%) of 159 patients after the initial TACE. The cause of death consisted of hepatic failure in one patient and liver abscess in the other. In the SBRT group, treatment-related deaths occurred in 2 (1.2%) of 167 patients after SBRT due to hepatic failure. Complications

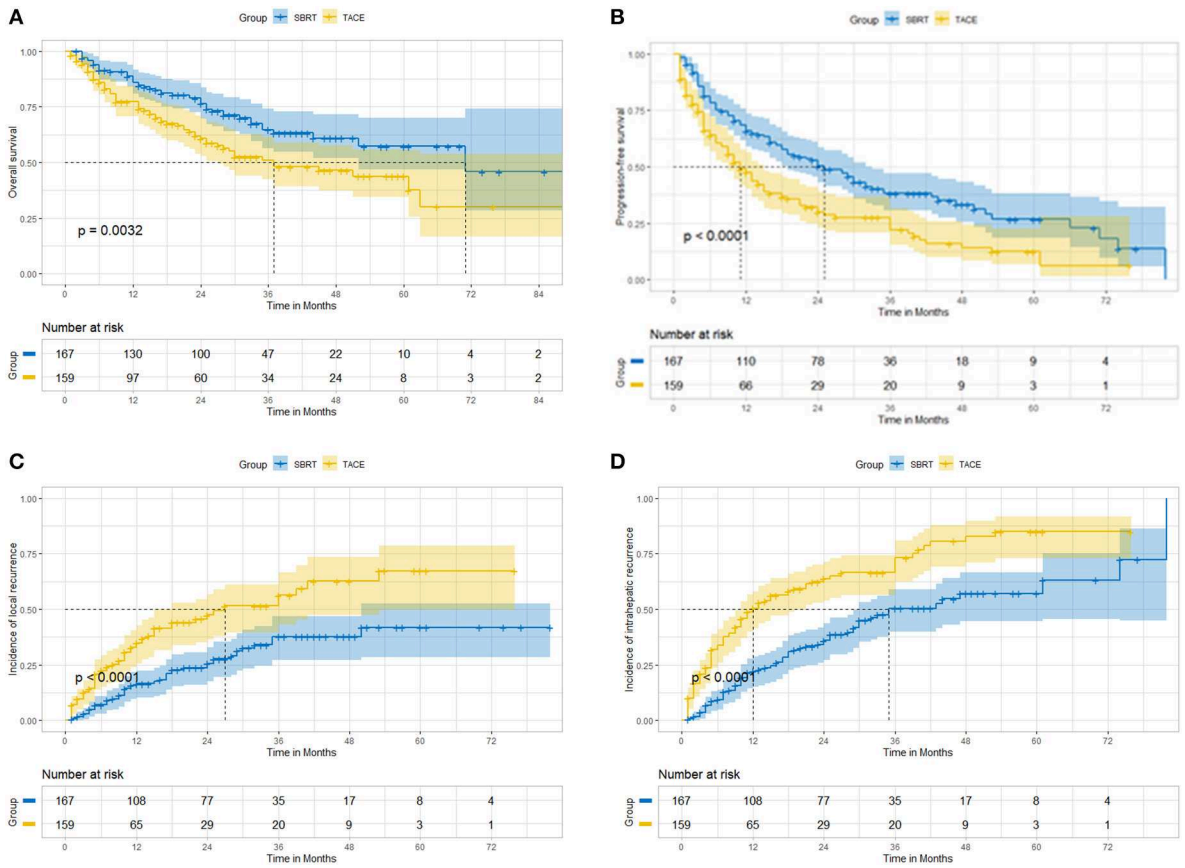

FIGURE 1 | Before propensity matching, SBRT vs. TACE. **(A)** overall survival; **(B)** progression-free survival; **(C)** local control; **(D)** intrahepatic control.

were graded according to the National Cancer Institute Common Terminology Criteria for Adverse Events version 4.03. The most common grades of acute complications in all groups were ≤3. Fever, hepatic pain, and increased levels of ALT or AST (≥3-fold) were the three most common TACE-related complications. Fatigue, nausea, and vomiting were the three most common SBRT-related complications. Elevated Child–Pugh score was common TACE or SBRT-related hepatotoxicity (+1 score: 28/159 vs. 20/167, $P = 0.22$; and +2 score: 8/169 vs. 17/167, $P = 0.11$). Most of the complications and hepatotoxicity were reversed by conservative and supportive treatment.

DISCUSSION

SBRT was shown to be an alternative option for patients with inoperable BCLC stage A disease. Our propensity match-based analysis after locoregional therapy for 326 inoperable patients with BCLC stage A disease in China, where hepatitis B virus (>86.8%) was predominant, suggests that patients undergoing SBRT have a similar OS to those undergoing TACE, with excellent local and intrahepatic control and PFS. On multivariate analysis, treatment (SBRT vs. TACE, HR = 1.59; 95% CI: 1.03–2.47; $P = 0.04$; HR = 1.61; 95% CI: 1.13–2.29; $P = 0.009$) and tumor size (HR = 1.06; 95% CI: 1.01–1.12; $P = 0.02$; HR = 1.10; 95% CI: 1.05–1.14; $P < 0.001$) were significant covariates associated with local and intrahepatic control. SBRT does not seem to compromise the measured survival outcomes after TACE. Sapir et al. (23) also reported that 209 patients with 287 HCC tumors, and 28 of these cases with portal vein branch thrombosis (BCLC-C), were treated with TACE ($n = 84$) or SBRT ($n = 125$) in western countries, where hepatitis C virus (70%) and alcohol abuse (20%) were the main cause of HCC. It was also found that SBRT can be an alternative to TACE for local HCC with one to two tumors and provided better LC, with no difference in OS. The 1- and 2-year OS were 74.1 and 34.9% after SBRT, and 75.3 and 54.9% after TACE, respectively. The 1- and 2-year LC were 47.1 and 22.9% after TACE compared to 96.5 and 91.3% after SBRT, respectively. The 1- and 2-year intrahepatic controls were better for patients after SBRT than after TACE (56.5, 26.9% vs. 35.9, 10.7%, respectively), favoring SBRT significantly (HR = 3.55, 95% CI 1.94–6.52, $P < 0.001$). In addition, higher AFP, previous treatment status, and branch thrombosis were significant covariates associated with intrahepatic control in multivariate analysis. Shen et al. compared the local control and overall survival between SBRT ($n = 46$) and TACE ($n = 142$) in medium-sized (3–8 cm) HCC in Taiwan. The 3-year local control rate was 73.3% for the SBRT group and 63.0% for the TACE group. Multivariable analyses also identified the

TABLE 2 | The accumulative OS, PFS, and local and intrahepatic control of different treatment groups.

		Before propensity matching					After propensity matching				
	Months	**SBRT**	**TACE**	**HR**	**95% CI**	***P***	**SBRT**	**TACE**	**HR**	**95% CI**	***P***
OS	12	86.0%	77.3%	1.79	1.05–3.03	0.031	85.7%	83.6%	1.19	0.57–2.49	0.65
	36	64.7%	51.0%	1.71	1.17–2.51	0.005	65.1%	61.0%	1.17	0.7–1.96	0.55
	60	57.3%	43.8%	1.69	1.17–2.46	0.0046	62.8%	50.4%	1.19	0.79–2.14	0.3
PFS	12	65.9%	47.5%	1.82	1.30–2.57	0.0003	63.4%	53.3%	1.46	0.93–2.28	0.092
	36	38.1%	27.6%	1.62	1.22–2.16	0.0005	35.9%	27.4%	1.37	0.95–1.97	0.081
	60	26.7%	12.4%	1.71	1.30–2.25	0.0001	27.5%	14.2%	1.44	1.01–2.04	0.037
LC	12	85.1%	67.2%	1.79	1.05–3.03	0.0031	86.8%	69.3%	1.93	1.18–3.18	0.0035
	36	63.1%	50.2%	1.93	1.29–2.88	0.0008	62.5%	53.5%	1.81	1.08–3.04	0.0219
	60	59.3%	35.6%	2.04	1.38–3.01	0.0002	56.9%	36.6%	1.93	1.18–3.18	0.0084
IC	12	77.8%	49.6%	2.94	1.99–4.32	0.0001	77.3%	57.3%	2.33	1.39–3.93	0.0016
	36	49.6%	33.5%	2.14	1.54–2.96	0.0001	45.9%	34.1%	1.7	1.12–2.58	0.01
	60	42.9%	15.1%	2.32	1.69–3.17	0.0001	42.4%	17.7%	1.85	1.23–2.77	0.0021

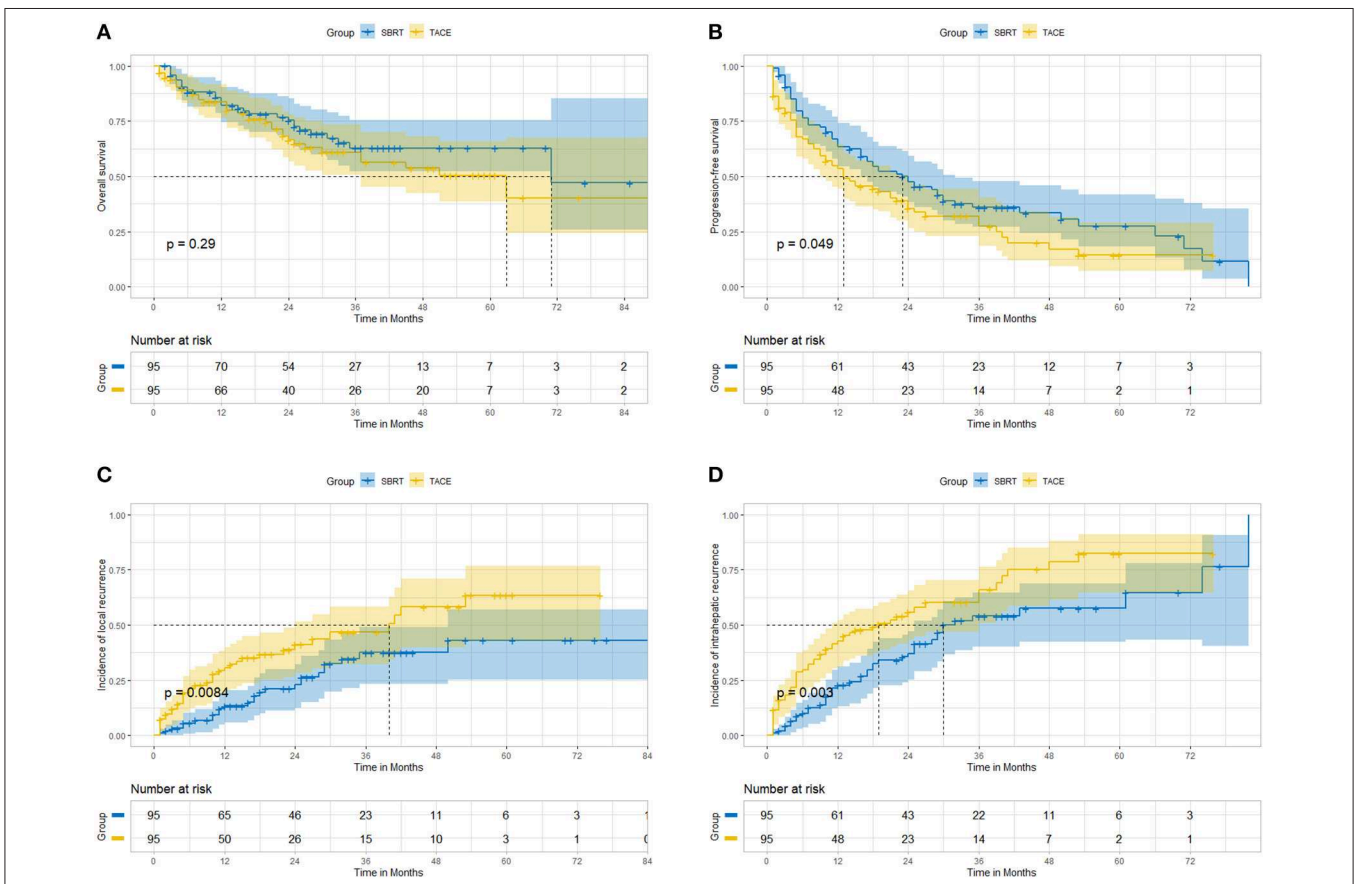

FIGURE 2 | After propensity matching, SBRT vs. TACE. **(A)** overall survival; **(B)** progression-free survival; **(C)** local control; **(D)** intrahepatic control.

independent predictors for local control as treatment modality (SBRT or TACE), gender (female vs. male), and recurrence HCC status (recurrence or primary diagnosis). After propensity score matching analysis, patients in the SBRT group also had better local control (3-year of 77.5 vs. 55.6%; $P = 0.007$) and OS (3-year OS of 55.0 vs. 13.0%; $P < 0.001$) than those in the TACE group. However, there was no difference in local control and OS between SBRT and TACE in newly diagnosed HCC cases. Sapisochin et al., in a retrospective study, reported that SBRT, RFA, and TACE were evaluated to have similar effectiveness in bridging therapy

TABLE 3 | Univariable and multivariable Cox analyses for OS, PFS, and local and intrahepatic control.

				OS									PFS							
				Univariable analysis				Multivariable analysis					Univariable analysis				Multivariable analysis			
Factor	**Level**	***N***	***n***	**HR**	***P***	**95% CI**		**HR**	***P***	**95% CI**		***n***	**HR**	**P**	**95% CI**		**HR**	***P***	**95% CI**	
Age		326	116	0.992	0.297	0.977	1.007					216	0.980	0.001	0.969	0.991	0.990	0.050	0.975	0.999
Gender	Female	46	17	1.000								27	1.000				1.000			
	Male	280	99	1.005	0.986	0.600	1.682					189	1.331	0.165	0.889	1.994	1.190	0.410	0.790	1.790
HBV	Positive	268	102	1.000								194	1.000				1.000			
	Negative	58	14	0.905	0.726	0.517	1.583					22	0.720	0.146	0.463	1.120	0.750	0.210	0.480	1.180
AFP	0–7	93	26	1.000				1.000				57	1.000				1.000			
	>7–100	92	33	1.446	0.160	0.864	2.421	1.550	0.100	0.920	2.620	59	1.146	0.467	0.794	1.653	1.260	0.230	1.260	0.230
	>100–400	42	15	1.477	0.229	0.782	2.791	1.660	0.120	0.870	3.150	27	1.338	0.216	0.844	2.121	1.390	0.170	0.870	2.210
	>400	99	42	2.041	0.004	1.249	3.333	1.840	0.020	1.120	3.020	73	1.796	0.001	1.264	2.552	1.502	0.030	1.040	2.170
PT		326	116	1.165	0.001	1.061	1.279					216	1.036	0.402	0.954	1.125				
Tbil		326	116	1.003	0.419	0.996	1.010					216	0.998	0.663	0.991	1.006				
Albumin		326	116	0.937	0.000	0.908	0.966					216	0.985	0.204	0.962	1.008				
AST		326	116	1.003	0.170	0.999	1.007					216	1.003	0.053	1.000	1.006				
ALT		326	116	1.003	0.034	1.000	1.007					216	1.003	0.030	1.000	1.005	1.000	0.929	0.997	1.003
Child-Pugh socre		326	116	1.294	0.001	1.116	1.499					216	1.098	0.142	0.969	1.243				
ALBI score		326	116	1.933	0.000	1.430	2.613	2.010	0.000	1.460	2.770	216	1.159	0.229	0.911	1.476				
Tumor size		326	116	1.120	0.000	1.073	1.168	1.120	0.000	1.060	1.170	216	1.107	0.000	1.072	1.143	1.090	0.000	1.046	1.140
Treatment	SBRT	167	50	1.000				1.000				104	1.000				1.000			
	TACE	159	66	1.723	0.004	1.192	2.490	1.080	0.710	0.710	1.660	112	1.723	0.000	1.314	2.258	1.220	0.210	0.890	1.660
				LC									**HC**							
				Univariable analysis				**Multivariable analysis**					**Univariable analysis**				**Multivariable analysis**			
Factor	**Level**	***N***	***n***	**HR**	***P***	**95% CI**		**HR**	***P***	**95% CI**		***n***	**HR**	***P***	**95% CI**		**HR**	***P***	**95% CI**	
Age		326	105	0.980	0.014	0.964	0.996	0.990	0.120	0.970	1.000	167	0.977	0.000	0.965	0.990	0.990	0.104	0.970	1.000
Gender	Female	46	6	1.000				1.000				14	1.000				1.000			
	Male	280	99	3.112	0.007	1.364	7.100	2.690	0.020	1.180	6.170	153	2.102	0.008	1.215	3.636	1.840	0.031	1.060	3.210
HBV	Positive	268	95	1.000				1.000				153	1.000				0.610	0.082	0.240	1.070
	Negative	58	10	0.690	0.265	0.360	1.325	0.680	0.250	0.350	1.310	14	0.595	0.063	0.344	1.029				
AFP	0–7	93	30	1.000								42	1.000				1.000			
	>7–100	92	29	1.106	0.698	0.663	1.846					44	1.237	0.328	0.808	1.896	1.360	0.175	0.870	2.110
	>100–400	42	11	0.921	0.816	0.462	1.839					23	1.598	0.073	0.957	2.668	1.660	0.060	1.980	2.800

(Continued)

TABLE 3 | Continued

Factor	Level	N	LC							HC						
			n	Univariable analysis			Multivariable analysis			n	Univariable analysis			Multivariable analysis		
				HR	P	95% CI	HR	P	95% CI		HR	P	95% CI	HR	P	95% CI
	>400	99	35	1.542	0.084	0.944	2.517			58	1.980	0.001	1.322	2.964	1.610	0.027	1.060	2.460
PT		326	105	0.993	0.916	0.878	1.124			167	0.987	0.796	0.894	1.090				
Tbil		326	105	0.997	0.616	0.985	1.009			167	0.996	0.415	0.986	1.006				
Albumin		326	105	1.000	0.978	0.967	1.035			167	1.004	0.777	0.977	1.032				
AST		326	105	1.004	0.027	1.000	1.007			167	1.003	0.061	1.000	1.006				
ALT		326	105	1.003	0.057	1.000	1.006	1.001	0.698	0.997	1.005	167	1.004	0.004	1.001	1.006	1.001	0.644	0.998	1.004
Child–Pugh socre		326	105	1.036	0.719	0.856	1.253					167	0.948	0.520	0.804	1.117				
ALBI score		326	105	0.989	0.951	0.694	1.410	1.040	0.120	0.720	1.490	167	0.950	0.723	0.715	1.262	0.980	0.874	0.730	1.310
Tumor size		326	105	1.097	0.000	1.049	1.148	1.061	0.020	1.001	1.120	167	1.125	0.000	1.086	1.165	1.100	0.000	1.050	1.140
Treatment	SBRT	167	44	1.000				1.000				69	1.000				1.000			
	TACE	159	61	2.057	0.000	1.393	3.038	1.590	0.041	1.013	2.470	98	2.300	0.000	1.684	3.143	1.610	0.009	1.130	2.290

ALBI, albumin–bilirubin; AFP, alpha fetoprotein; TACE, transarterial chemoembolization; SBRT, stereotactic body radiation therapy; PT, prothrombin time; AST, aspartate aminotransferase; ALT, alanine aminotransferase; HBV, hepatitis b virus; n, number of events; N, number in each category.

for liver transplant with tumor necrosis at explant, and overall survival (24).

According to BCLC guidelines, liver transplantation, liver resection, and RFA were recommended as first-line potentially curative treatment options for patients with early-stage HCC, providing a long-term survival at 5 years of more than 40–70% (1). TACE is reserved for patients with intermediate-stage multinodular HCC, Child–Pugh class A or B disease, and good performance status. It can also be applied to those with BCLC stage A disease who are not considered for surgery or ablation (4, 5). Burrel et al. (4) found that the 1-, 3-, and 5-year survival for such patients ($n = 41$) treated with drug-eluting beads (DEB-TACE) was 89.7, 67.8, and 33.9%, respectively. Takayasu et al. (5) found that the 1-, 3-, 5-, and 7-year survival rates for TNM stage I patients ($n = 489$) treated with TACE were 98, 78, 52, and 38%, respectively. Takaki et al. reported that 1-, 3-, 5-, and 10-year survival rates were 93.3%, 83.2, 61.5, and 17.6% in the T1 group, and 93.5, 68.7, 43.5, and 12.2% in the T2 group, respectively. The 2-, 3-, and 5- year local recurrence rates were 46, 58, and 63% in the whole group (25). In the current study, the accumulative 1-, 3-, and 5-year OS rates were 83.6, 61.0, and 50.4%, local recurrence rates were 30.7, 46.7, 63.4%, and intrahepatic recurrence rates were 42.7, 65.9, and 82.3%, respectively, in the TACE group after propensity score matching. Some retrospective studies showed that SBRT for primary HCC provides high rates of durable local control (80–100%) (7, 12, 26–28). Our LC rate in the SBRT group compared favorably to the published literature. Thus, given the agreement with previous literature, the higher rate of local and intrahepatic control after SBRT in this study is most likely due to a true difference in the treatment effectiveness, rather than an artifact from a particularly excellent SBRT or poor TACE procedures.

Tumor diameter was an independent prognostic factor of OS, PFS, and intrahepatic control in TACE group based on univariable and multivariable cox analyses. Lo et al. also reported that a tumor diameter of $\leq$5 cm was a good prognostic factor of TACE (7). Tumor control rates after TACE have varied considerably, even in prospective studies (2, 3, 29). In the use of interventional therapy to larger HCC, certain bottlenecks may be encountered. Embolization of the hepatic arteries could cause tumor necrosis because these arteries may feed nutrients to the tumor cells. However, the liver surrounding HCCs has arterial vessels and veins and, therefore, may not undergo complete necrosis due to arterial embolization alone. The long-term locoregional curative effect is unsatisfactory in cases with TACE alone, especially with large tumors, as tumor cells relapse from the intracapsular or extracapsular HCC invasion and can rarely be eradicated (30). TACE was feasible and associated with a higher response rate than that of TAE alone (31). DEB-TACE showed a better local response, lower recurrence rates, and longer time to progression than TACE (31). DEB-TACE was associated with a significant reduction in the occurrence of serious liver toxicity (32). However, no apparent differences in OS were observed between both treatment groups. These results challenge the use of DEB-TACE in HCC (33). Y90 radioembolization led to improved time to progression compared to TACE but did not improve OS (34).

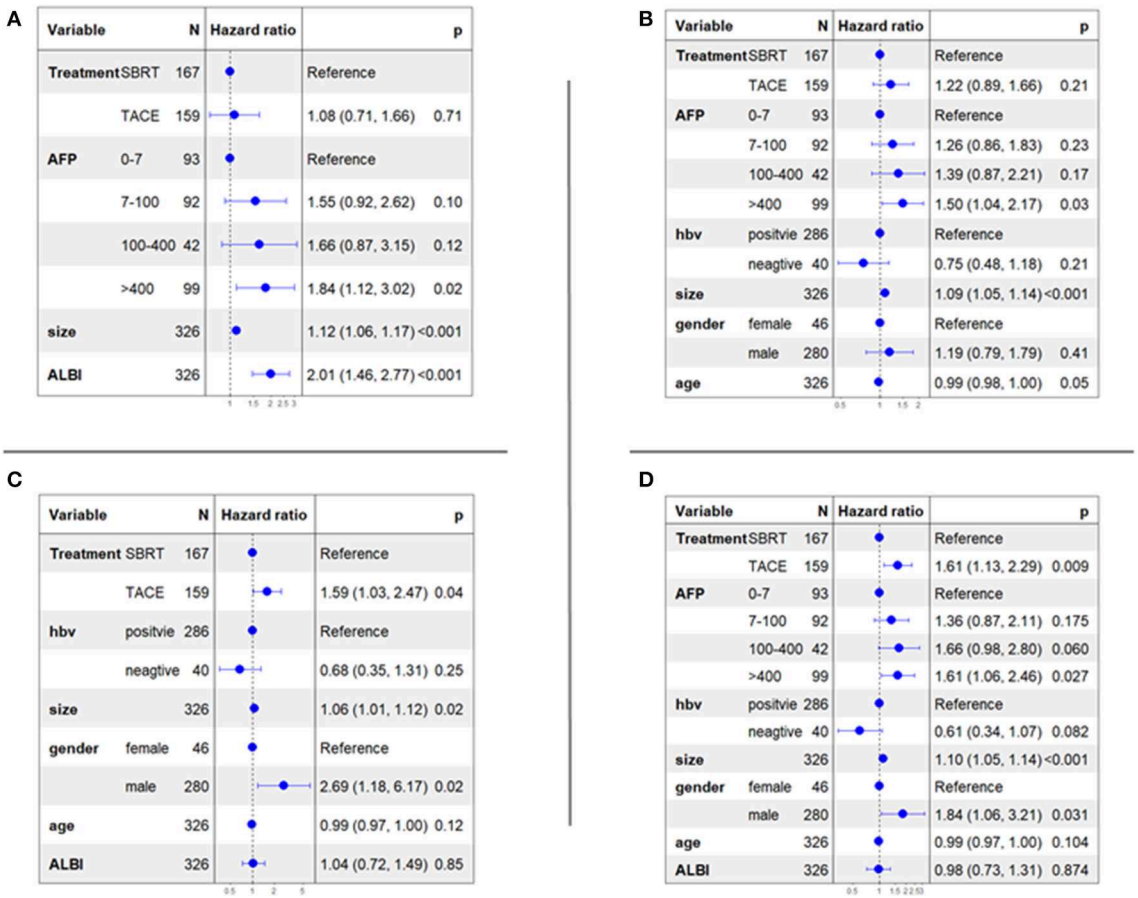

FIGURE 3 | Multivariable cox analyses of all patients. **(A)** overall survival; **(B)** progression-free survival; **(C)** local control; **(D)** intrahepatic control.

Unlike the mechanism by which TACE works, radiotherapy has the advantage of directly damaging the tumor cells. On subgroup analysis, tumor diameter has a great influence on TACE survival time and intrahepatic control, while tumor diameter has little effect on SBRT. SBRT can also provide encouraging outcomes comparable to radiofrequency ablation (12, 35, 36). In our previous study, SBRT can provide encouraging curative outcomes comparable to liver resection for small HCC. The 5-year OS rates were 70.0 and 64.4% in the SBRT and liver resection groups, respectively (11). In the current study, we found that SBRT was superior to TACE, providing better local and intrahepatic control. In recent years, there have been several reports on the combination of TACE and SBRT, suggesting that the combination may yield better outcomes than TACE alone. Jun et al. reported that SBRT-TACE is superior to TACE regarding LC in patients with one or two small HCC lesions (37). Kimura et al. found that TACE+SBRT was not better than SBRT alone in small HCC cases (38). It may be concluded that SBRT has a radical curative effect in these selected HCCs. Additional multi-institutional prospective studies are warranted for the investigation of the real effects of SBRT. The TASABR randomized controlled trial is underway and will compare SBRT vs. re-TACE for HCC patients who had an incomplete response after initial TACE (39). A randomized phase 2 trial (NCT02182687), designed to compare TACE or SBRT as a bridge to transplant with the primary outcome as time to first additional intervention, is underway. Another phase 2 trial (NCT02470533), which targets patients with one to three tumors and assesses time to any progression after SBRT or after DEB-TACE, is ongoing. Our findings also need to be verified prospectively in HCC patients with BCLC-A stage who are not considered for surgery or have refused to undergo surgery and/or local radiofrequency ablative therapies.

This study has some limitations. First, this was a retrospective, non-randomized study, and the follow-up period was not lengthy, and this could have obscured late effects. Second, it is difficult to eliminate selection bias. Some variables differed between the groups; therefore, propensity score matching was applied at a 1:1 ratio to reduce selection bias and potential confounding effects of treatment. We also used the albumin–bilirubin score instead of the Child–Pugh score to reduce subjective errors. However, the bias of selection factors cannot be completely avoided. Controlled clinical trials are recommended to evaluate the actual effects of this novel regimen adequately.

Third, we cannot account for differences between the two groups that are not known, such as the experience of institutions, patient's financial condition, and benefit of second-line treatment after recurrence.

In conclusion, SBRT was an alternative to TACE for inoperable BCLC-A stage HCC with excellent local and intrahepatic control. Controlled clinical trials are recommended to evaluate the actual effects of this novel regimen adequately.

DATA AVAILABILITY STATEMENT

The datasets analyzed in this study can be found with the corresponding author, Ting-Shi Su The statistical code and dataset are available from the author at sutingshi@163.com.

ETHICS STATEMENT

This study complied with the tenets of the Declaration of Helsinki. The study design was approved by the ethics review board of Guangxi Medical University Cancer Hospital (LW2019036). The ethics committee waived the requirement of written informed consent for participation.

AUTHOR CONTRIBUTIONS

T-SS, S-XL, and L-QL made substantial contributions to the study's conception and design. T-SS, PL, YZ, YH, TC, CZ, D-JH, SQ, LC, and B-DX made substantial contributions to the acquisition of data. T-SS made substantial contributions to the data analysis and interpretation. All authors participated in the drafting of the article or revising it critically for important intellectual content, and they provided final approval of the version to be published.

FUNDING

This research was supported by the Scientific Research and Technology Development Program of Guangxi (CN) (GuiKeGong 14124003-4), the National Natural Science Foundation of China (81903257), the National Science and Technology Major Special Project (2017ZX10203207), International Communication of Guangxi Medical University Graduate Education 2020, and Guangxi BaGui Scholars' Special Fund.

ACKNOWLEDGMENTS

We thank our colleagues and all the patients who participated in this study.

SUPPLEMENTARY MATERIAL

The Supplementary Material for this article can be found online at: https://www.frontiersin.org/articles/10.3389/fonc.2020.00347/full#supplementary-material

REFERENCES

1. European Association For The Study Of The Liver, European Organisation For Research and Treatment Of Cancer. EASL-EORTC clinical practice guidelines: management of hepatocellular carcinoma. *J Hepatol.* (2012) 56:908–43. doi: 10.1016/j.jhep.2011.12.001
2. Llovet JM, Real MI, Montana X, Planas R, Coll S, Aponte J, et al. Arterial embolisation or chemoembolisation versus symptomatic treatment in patients with unresectable hepatocellular carcinoma: a randomised controlled trial. *Lancet.* (2002) 359:1734–9. doi: 10.1016/S0140-6736(02)08649-X
3. Lo CM, Ngan H, Tso WK, Liu CL, Lam CM, Poon RT, et al. Randomized controlled trial of transarterial lipiodol chemoembolization for unresectable hepatocellular carcinoma. *Hepatology.* (2002) 35:1164–71. doi: 10.1053/jhep.2002.33156
4. Burrel M, Reig M, Forner A, Barrufet M, de Lope CR, Tremosini S, et al. Survival of patients with hepatocellular carcinoma treated by transarterial chemoembolisation (TACE) using Drug Eluting Beads. Implications for clinical practice and trial design. *J Hepatol.* (2012) 56:1330–5. doi: 10.1016/j.jhep.2012.01.008
5. Takayasu K, Arii S, Ikai I, Omata M, Okita K, Ichida T, et al. Prospective cohort study of transarterial chemoembolization for unresectable hepatocellular carcinoma in 8510 patients. *Gastroenterology.* (2006) 131:461–9. doi: 10.1053/j.gastro.2006.05.021
6. Benson AB 3rd, D'Angelica MI, Abbott DE, Abrams TA, Alberts SR, Saenz DA, et al. NCCN Guidelines insights: hepatobiliary cancers, version 1. 2017. *J Natl Compr Canc Netw.* (2017) 15:563–73. doi: 10.6004/jnccn.2017.0059
7. Su TS, Liang P, Lu HZ, Liang J, Gao YC, Zhou Y, et al. Stereotactic body radiation therapy for small primary or recurrent hepatocellular carcinoma in 132 Chinese patients. *J Surg Oncol.* (2016) 113:181–7. doi: 10.1002/jso.24128
8. Kwon JH, Bae SH, Kim JY, Choi BO, Jang HS, Jang JW, et al. Long-term effect of stereotactic body radiation therapy for primary hepatocellular carcinoma ineligible for local ablation therapy or surgical resection. Stereotactic radiotherapy for liver cancer. *BMC Cancer.* (2010) 10:475. doi: 10.1186/1471-2407-10-475
9. Bujold A, Massey CA, Kim JJ, Brierley J, Cho C, Wong RK, et al. Sequential phase I and II trials of stereotactic body radiotherapy for locally advanced hepatocellular carcinoma. *J Clin Oncol.* (2013) 31:1631–9. doi: 10.1200/JCO.2012.44.1659
10. Andolino DL, Johnson CS, Maluccio M, Kwo P, Tector AJ, Zook J, et al. Stereotactic body radiotherapy for primary hepatocellular carcinoma. *Int J Radiat Oncol Biol Phys.* (2011) 81:e447–53. doi: 10.1016/j.ijrobp.2011.04.011
11. Su TS, Liang P, Liang J, Lu HZ, Jiang HY, Cheng T, et al. Long-term survival analysis of stereotactic ablative radiotherapy versus liver resection for small hepatocellular carcinoma. *Int J Radiat Oncol Biol Phys.* (2017) 98:639–46. doi: 10.1016/j.ijrobp.2017.02.095
12. Wahl DR, Stenmark MH, Tao Y, Pollom EL, Caoili EM, Lawrence TS, et al. Outcomes after stereotactic body radiotherapy or radiofrequency ablation for hepatocellular carcinoma. *J Clin Oncol.* (2016) 34:452–9. doi: 10.1200/JCO.2015.61.4925
13. Yuan Z, Tian L, Wang P, Song Y, Dong Y, Zhuang H. Comparative research on the efficacy of CyberKnife(R) and surgical excision for Stage I hepatocellular carcinoma. *Onco Targets Ther.* (2013) 6:1527–32. doi: 10.2147/OTT.S51452
14. Takeda A, Sanuki N, Tsurugai Y, Iwabuchi S, Matsunaga K, Ebinuma H, et al. Phase 2 study of stereotactic body radiotherapy and optional transarterial chemoembolization for solitary hepatocellular carcinoma not amenable to resection and radiofrequency ablation. *Cancer.* (2016) 122:2041–9. doi: 10.1002/cncr.30008
15. Su TS, Lu HZ, Cheng T, Zhou Y, Huang Y, Gao YC, et al. Long-term survival analysis in combined transarterial embolization and stereotactic body radiation therapy versus stereotactic body radiation monotherapy for unresectable hepatocellular carcinoma >5 cm. *BMC Cancer.* (2016) 16:834. doi: 10.1186/s12885-016-2894-9

16. Honda Y, Kimura T, Aikata H, Nakahara T, Naeshiro N, Tanaka M, et al. Pilot study of stereotactic body radiation therapy combined with transcatheter arterial chemoembolization for small hepatocellular carcinoma. *Hepatogastroenterology*. (2014) 61:31–6.
17. Jacob R, Turley F, Redden DT, Saddekni S, Aal AK, Keene K, et al. Adjuvant stereotactic body radiotherapy following transarterial chemoembolization in patients with non-resectable hepatocellular carcinoma tumours of >/= 3 cm. *HPB*. (2015) 17:140–9. doi: 10.1111/hpb.12331
18. Zhou J, Sun HC, Wang Z, Cong WM, Wang JH, Zeng MS, et al. Guidelines for diagnosis and treatment of primary liver cancer in China (2017 edition). *Liver Cancer*. (2018) 7:235–60. doi: 10.1159/000488035
19. Qi YP, Zhong JH, Liang ZY, Zhang J, Chen B, Chen CZ, et al. Adjuvant transarterial chemoembolization for patients with hepatocellular carcinoma involving microvascular invasion. *Am J Surg*. (2019) 217:739–44. doi: 10.1016/j.amjsurg.2018.07.054
20. Su TS, Luo R, Liang P, Cheng T, Zhou Y, Huang Y. A prospective cohort study of hepatic toxicity after stereotactic body radiation therapy for hepatocellular carcinoma. *Radiother Oncol*. (2018) 129:136–42. doi: 10.1016/j.radonc.2018.02.031
21. Lencioni R, Llovet JM. Modified RECIST (mRECIST) assessment for hepatocellular carcinoma. *Semin Liver Dis*. (2010) 30:52–60. doi: 10.1055/s-0030-1247132
22. Austin PC. Optimal caliper widths for propensity-score matching when estimating differences in means and differences in proportions in observational studies. *Pharm Stat*. (2011) 10:150–61. doi: 10.1002/pst.433
23. Sapir E, Tao Y, Schipper MJ, Bazzi L, Novelli PM, Devlin P, et al. Stereotactic body radiation therapy as an alternative to transarterial chemoembolization for hepatocellular carcinoma. *Int J Radiat Oncol Biol Phys*. (2018) 100:122–30. doi: 10.1016/j.ijrobp.2017.09.001
24. Sapisochin G, Barry A, Doherty M, Fischer S, Goldaracena N, Rosales R, et al. Stereotactic body radiotherapy vs. TACE or RFA as a bridge to transplant in patients with hepatocellular carcinoma. An intention-to-treat analysis. *J Hepatol*. (2017) 67:92–9. doi: 10.1016/j.jhep.2017.02.022
25. Takaki S, Sakaguchi H, Anai H, Tanaka T, Yamamoto K, Morimoto K, et al. Long-term outcome of transcatheter subsegmental and segmental arterial chemoemobolization using lipiodol for hepatocellular carcinoma. *Cardiovasc Intervent Radiol*. (2012) 35:544–54. doi: 10.1007/s00270-011-0224-9
26. Bibault JE, Dewas S, Vautravers-Dewas C, Hollebecque A, Jarraya H, Lacornerie T, et al. Stereotactic body radiation therapy for hepatocellular carcinoma: prognostic factors of local control, overall survival, and toxicity. *PLoS ONE*. (2013) 8:e77472. doi: 10.1371/journal.pone.0077472
27. Sanuki N, Takeda A, Oku Y, Mizuno T, Aoki Y, Eriguchi T, et al. Stereotactic body radiotherapy for small hepatocellular carcinoma: a retrospective outcome analysis in 185 patients. *Acta Oncol*. (2014) 53:399–404. doi: 10.3109/0284186X.2013.820342
28. Huertas A, Baumann AS, Saunier-Kubs F, Salleron J, Oldrini G, Croise-Laurent V, et al. Stereotactic body radiation therapy as an ablative treatment for inoperable hepatocellular carcinoma. *Radiother Oncol*. (2015) 115:211–6. doi: 10.1016/j.radonc.2015.04.006
29. Meyer T, Kirkwood A, Roughton M, Beare S, Tsochatzis E, Yu D, et al. A randomised phase II/III trial of 3-weekly cisplatin-based sequential transarterial chemoembolisation vs embolisation alone for hepatocellular carcinoma. *Br J Cancer*. (2013) 108:1252–9. doi: 10.1038/bjc.2013.85
30. Jansen MC, van Hillegersberg R, Chamuleau RA, van Delden OM, Gouma DJ, van Gulik TM. Outcome of regional and local ablative therapies for hepatocellular carcinoma: a collective review. *Eur J Surg Oncol*. (2005) 31:331–47. doi: 10.1016/j.ejso.2004.10.011
31. Malagari K, Pomoni M, Kelekis A, Pomoni A, Dourakis S, Spyridopoulos T, et al. Prospective randomized comparison of chemoembolization with doxorubicin-eluting beads and bland embolization with beadblock for hepatocellular carcinoma. *Cardiovasc Interv Radiol*. (2010) 33:541–51. doi: 10.1007/s00270-009-9750-0
32. Lammer J, Malagari K, Vogl T, Pilleul F, Denys A, Watkinson A, et al. Prospective randomized study of doxorubicin-eluting-bead embolization in the treatment of hepatocellular carcinoma: results of the PRECISION V study. *Cardiovasc Interv Radiol*. (2010) 33:41–52. doi: 10.1007/s00270-009-9711-7
33. Brown KT, Do RK, Gonen M, Covey AM, Getrajdman GI, Sofocleous CT, et al. Randomized trial of hepatic artery embolization for hepatocellular carcinoma using doxorubicin-eluting microspheres compared with embolization with microspheres alone. *J Clin Oncol*. (2016) 34:2046–53. doi: 10.1200/JCO.2015.64.0821
34. Salem R, Gordon AC, Mouli S, Hickey R, Kallini J, Gabr A, et al. Y90 radioembolization significantly prolongs time to progression compared with chemoembolization in patients with hepatocellular carcinoma. *Gastroenterology*. (2016) 151:1155–63. doi: 10.1053/j.gastro.2016.08.029
35. Kim N, Kim HJ, Won JY, Kim DY, Han KH, Jung I, et al. Retrospective analysis of stereotactic body radiation therapy efficacy over radiofrequency ablation for hepatocellular carcinoma. *Radiother Oncol*. (2019) 131:81–7. doi: 10.1016/j.radonc.2018.12.013
36. Hara K, Takeda A, Tsurugai Y, Saigusa Y, Sanuki N, Eriguchi T, et al. Radiotherapy for hepatocellular carcinoma results in comparable survival to radiofrequency ablation: a propensity score analysis. *Hepatology*. (2019) 69:2533–45. doi: 10.1002/hep.30591
37. Jun BG, Kim SG, Kim YD, Cheon GJ, Han KH, Yoo JJ, et al. Combined therapy of transarterial chemoembolization and stereotactic body radiation therapy versus transarterial chemoembolization for </=5cm hepatocellular carcinoma: propensity score matching analysis. *PLoS ONE*. (2018) 13:e0206381. doi: 10.1371/journal.pone.0206381
38. Kimura T, Aikata H, Doi Y, Imano N, Takeuchi Y, Takahashi I, et al. Comparison of stereotactic body radiation therapy combined with or without transcatheter arterial chemoembolization for patients with small hepatocellular carcinoma ineligible for resection or ablation therapies. *Technol Cancer Res Treat*. (2018) 17:1533033818783450. doi: 10.1177/1533033818783450
39. Chen LC, Chiou WY, Lin HY, Lee MS, Lo YC, Huang LW, et al. Comparing stereotactic ablative radiotherapy (SABR) versus re-trans-catheter arterial chemoembolization (re-TACE) for hepatocellular carcinoma patients who had incomplete response after initial TACE (TASABR): a randomized controlled trial. *BMC Cancer*. (2019) 19:275. doi: 10.1186/s12885-019-5461-3

Conflict of Interest: The authors declare that the research was conducted in the absence of any commercial or financial relationships that could be construed as a potential conflict of interest.

frontiers in Oncology

ORIGINAL RESEARCH
published: 29 July 2020
doi: 10.3389/fonc.2020.01170

Which Is Better for Liver SBRT: Dosimetric Comparison Between DCAT and VMAT for Liver Tumors

*Young Min Moon, Wan Jeon, Tosol Yu, Sang Il Bae, Jin Young Kim, Jin-Kyu Kang and Chul Won Choi**

Department of Radiation Oncology, Dongnam Institute of Radiological and Medical Science, Busan, South Korea

Stereotactic body radiotherapy (SBRT) is currently well-adopted as a curative treatment for primary and metastatic liver tumors. Among SBRT methods, dynamic conformal arc therapy (DCAT) and volumetric-modulated arc therapy (VMAT) are the most preferred methods. In this study, we report a comparison study measuring the dose distribution and delivery efficiency differences between DCAT and VMAT for liver SBRT. All patients who were treated with SBRT for primary or metastatic liver tumors with a curative aim between January 2016 and December 2017 at DIRAMS were enrolled in the study. For all patients, SBRT plans were designed using the Monte Carlo (MC) algorithm in Monaco treatment planning system (version 5.1). The planning goals were set according to the RTOG 0813, RTOG 0915, and RTOG 1112 protocols. A plan comparison was made on the metrics of dose volume histogram, planning and delivery efficiency, monitor unit (MU), and dosimetric indices. PTV coverage was evaluated using the following: D_{mean}, D95%, D98%, D2%, D50%, D_{max}, V95%, heterogeneity index (HI), and conformality index (CI). For DCAT and VMAT, respectively, the D_{mean} was 5942.8 ± 409.3 cGy and 5890.6 ± 438.8 cGy, D50% was 5968.8 ± 413.1 cGy and 5954.3 ± 405.2 cGy, and CI was 1.05 ± 0.05 and 1.03 ± 0.04. The D98% and V95% were 5580.0 ± 465.3 cGy and 20.4 ± 12.0 mL for DCAT, and 5596.0 ± 478.7 cGy and 20.5 ± 12.0 mL for VMAT, respectively. For normal liver, V40, V30, V20, V17, V5, D_{mean}, D_{max} were evaluated for comparison. The V30, V20, and V10 were significantly higher in DCAT; other parameters of normal livers showed no statistically significant differences. For evaluation of intermediate dose spillage, $D2_{cm}$(%) and R50% of DCAT and VMAT were 45.8 ± 7.9 and 5.6 ± 0.9 and 45.1 ± 6.7 and 5.5 ± 1.2, respectively. Planning and delivery efficiency were evaluated using MU, Calculation time, and Delivery time. DCAT had shorter Calculation time and Delivery time with smaller MU. MU was smaller in DCAT and the average difference was 300.1 MU. For liver SBRT, DCAT is an effective alternative to VMAT plans that could meet the planning goals proposed by the RTOG SBRT protocol and increases plan and delivery effectiveness, while also ignoring the interplay effect.

Keywords: liver cancer, SBRT (stereotactic body radiotherapy), VMAT (volumetric modulated arc therapy), Monaco TPS (treatment planning system), DCAT (dynamic conformal arc therapy)

OPEN ACCESS

Edited by:
James M. Brindle, Rhode Island Hospital, United States

Reviewed by:
Fenghong Liu, UMass Memorial Medical Center, United States
Yidong Yang, University of Science and Technology of China, China

****Correspondence:***
Chul Won Choi
drasdf19@gmail.com

Specialty section:
This article was submitted to Radiation Oncology, a section of the journal Frontiers in Oncology

Received: *02 January 2020*
Accepted: *09 June 2020*
Published: *29 July 2020*

Citation:
Moon YM, Jeon W, Yu T, Bae SI, Kim JY, Kang J-K and Choi CW (2020) Which Is Better for Liver SBRT: Dosimetric Comparison Between DCAT and VMAT for Liver Tumors. Front. Oncol. 10:1170. doi: 10.3389/fonc.2020.01170

INTRODUCTION

Stereotactic body radiotherapy (SBRT) is currently well-adopted as a curative treatment for primary and metastatic liver tumors, especially for patients who are inoperable or undergoing systemic therapy (1–4). SBRT can be performed by various methods, including 3D conformal radiotherapy (3DCRT), intensity modulated radiotherapy (IMRT), dynamic conformal arc therapy (DCAT), volumetric-modulated arc therapy (VMAT), Tomotherapy, and CyberKnife. However, VMAT and DCAT are the most preferred methods (5–7). Both VMAT and DCAT are types of rotational radiotherapy, with each system having its own advantages and disadvantages. VMAT is typically considered superior to DCAT in terms of dose distribution since it has better target coverage. However, DCAT has potential advantages over VMAT in practical use. Reasons to consider DCAT instead of VMAT (8, 11) are as follows: (1) There is a concern about missing the target when VMAT is used for a moving target. Even if DCAT does not cover all targets of irregular movement, at least DCAT might offset this concern for the effect of MLC interplay since the target remains inside the open field with minimal modulation for the entire treatment. (2) VMAT requires a higher degree of quality assurance. (3) There is less concern with calculation accuracy for DCAT in an area of variable densities. (4) DCAT offers quicker plan and delivery times. (5) DCAT demands less monitor unit (MU) to deliver the same dose as VMAT. Furthermore, segment shape optimization (SSO) could supplement DCAT to maintain its inherent advantages while achieving results similar to VMAT. SSO is offered by the Monaco treatment planning system (TPS) (IMPAC Medical Systems, Inc., Maryland Heights, MO; a subsidiary of Elekta AB, Stockholm, Sweden) to improve plan quality by smoothing and clustering segments and optimizing beam weights and shapes. If DCAT for liver tumors is not inferior with regard to dose distribution and satisfies RTOG guidelines, DCAT could be a better option for SBRT plans than VMAT. Here, we report a comparison study measuring the dose distribution and delivery efficiency differences between DCAT and VMAT. Suggestions are offered for improved plan technique in primary and metastatic liver tumor radiotherapy.

MATERIALS AND METHODS

This study was approved by the institutional review board of the Dongnam Institute of Radiological and Medical Sciences (DIRAMS).

Patient Selection

All patients who were treated with SBRT for primary or metastatic liver tumors with a curative aim between January 2016 and December 2017 at DIRAMS were enrolled in the study. Patients with palliative aims, such as SBRT for portal vein tumor thrombosis, were excluded. All plans were built based on the prescribed dose at that time of treatment.

Contouring

The target volumes and organs at risk (OARs) of all included patients were reviewed and re-contoured by one radiation oncologist. Gross target volume (GTV) was determined by merging the re-drawn tumor volumes for each phase of the four-dimensional computed tomography (4DCT). Clinical target volume was same as GTV, and plan target volume (PTV) was established with 3–8 mm expansion of the GTV. The total volume of the liver, heart, stomach, and duodenum were contoured. Other OARs were partially drawn as needed for treatment planning.

Treatment Planning

For all patients, SBRT plans were designed using the MC algorithm in Monaco TPS (version 5.1). Beam modeling of the MONACO TPS was performed by beam of Elekta Infinity linear accelerator (Elekta AB, Stockholm, Sweden). All plans were designed using a photon beam of energy 6 MV with nominal dose rate 600 MU/min. To accompany the prescription and dose criteria, constraints of the plan optimization were adjusted depending on the size and location of the tumor. However, the plans were developed with the same constraints to allow comparison of the DCAT plan with the VMAT plan for each patient. After planning optimization, all plans were normalized to 95% of the PTV coverage with the prescribed dose. The physical parameters for each plan are shown in **Figure 1**. Each application of DCAT was planned as a single arc with non-constant dose rate and SSO applied. The VMAT plan was designed using a dual arc with a maximum 150 control points per arc and 1.0 cm minimum segment width. The arc length of both plan types was the same, with a range of 360° rotating from 180° in increments of 10° without couch rotation using fluence-smoothing parameters in medium mode. The final dose calculation was performed using a calculation grid resolution of 2.0 mm and a statistical uncertainty of 3% per control point. Physical parameters such as calculation grid resolution, statistical uncertainty, arc length, number of arcs, increment, number of control point/arc, and fluence-smoothing parameters were identical for each case in the same type of plan. The planning goals were set according to the RTOG 0813, RTOG 0915, and RTOG 1112 protocols.

Statistics

Statistical analysis was performed using the SPSS 18.0 program. Data normality was assessed using the Shapiro-Wilk test. Student's paired *t*-test and the Wilcoxon signed-rank test were used, respectively, for parametric and non-parametric data analyses (9).

RESULTS

Patient Characteristics

Twenty-five patients with a total of 31 lesions were enrolled. Two patients had 3 lesions, and 2 patients had 2 lesions, simultaneously. In one patient with 3 lesions, 2 of the lesions were located close to each other and were combined into a single PTV. Among the 25 patients, 17 had hepatocellular carcinomas (HCCs), 8 had metastatic liver cancers, and 7 had received

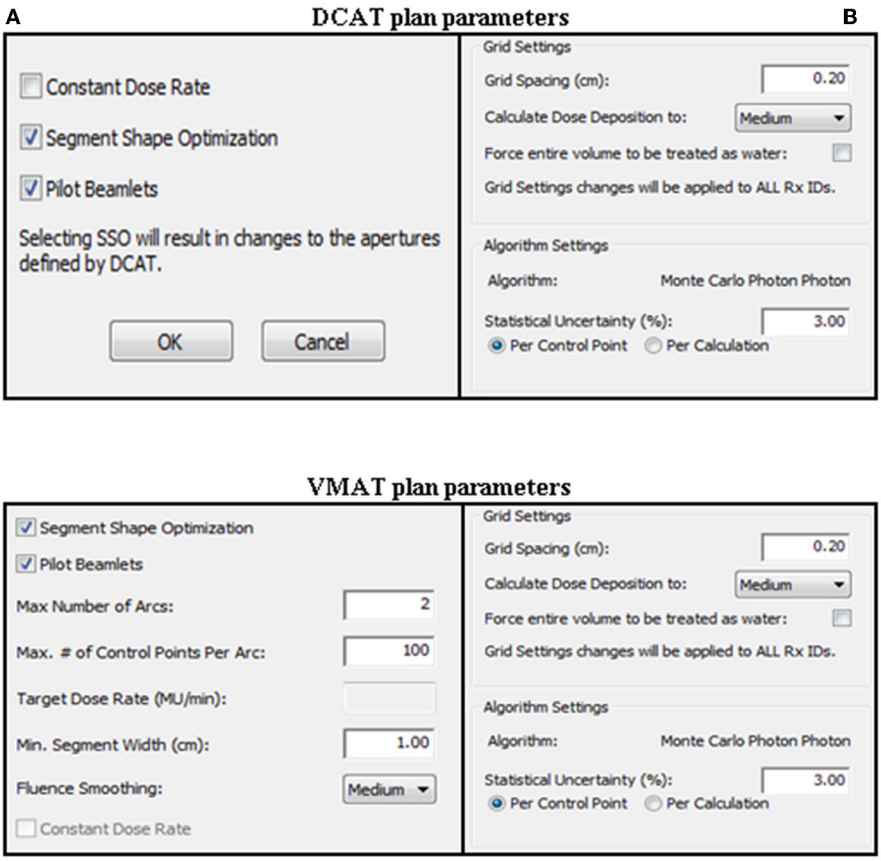

FIGURE 1 | Physical parameters for DCAT and VMAT plans. **(A)** Sequencing parameters. **(B)** Calculation parameters.

previous radiotherapy (RT). A total of 30 plans for each arm were made and evaluated for comparison. The prescribed SBRT dose was 4,800–6,000 cGy in 4 or 5 fractions. The characteristics of the patients are summarized in **Table 1**.

Dose Distribution

All DCAT and VMAT plans were optimized with an identical optimization protocol, and all except 4 patient plans achieved the planning goals. According to plan type, the dose distribution and DVH for the same patient are shown in **Figures 2**, **3**, respectively. Four patients' plans could not reach the objectives due to close proximity to OARs and some goals were compromised according to the physician's discretion to comply with the dose constraints.

PTV coverage was evaluated using the following: mean dose (D_{mean}), D95%, D98% (near-minimum absorbed dose), D2% (near-maximum absorbed dose), D50%, maximum point dose to 0.035 mL (D_{max}), V95%, heterogeneity index (HI), and conformality index (CI). Among the evaluated parameters, D_{mean}, D98%, D50%, V95%, and CI showed statistically significant differences between DCAT and VMAT. The D_{mean}, D50%, and CI were higher, and D98% and V95% were lower in DCAT than in VMAT. For DCAT and VMAT, respectively, the D_{mean} was 5942.8 ± 409.3 cGy and 5890.6 ± 438.8 cGy, D50% was 5968.8 ± 413.1 cGy and 5954.3 ± 405.2 cGy, and CI was 1.05 ± 0.05 and 1.03 ± 0.04. The D98% and V95% were 5580.0 ± 465.3 cGy and 20.4 ± 12.0 mL for DCAT, and 5596.0 ± 478.7 cGy and 20.5 ± 12.0 mL for VMAT, respectively. The data for PTV dose distribution are presented in **Table 2**.

For normal livers (liver volume minus GTV), V40, V30, V20, V17, V5, D_{mean}, D_{max} were evaluated for comparison. The V30, V20, and V10 were significantly higher in DCAT; other parameters of normal livers showed no statistically significant differences. D_{max}, maximum dose to 1 mL (D_{1mL}), maximum dose to 2 mL (D_{2mL}), and D_{mean} were assessed for OARs such as the duodenum, stomach, small bowel, large bowel, spinal cord, heart, and esophagus. For the duodenum, all assessed parameters show statistically significant differences. D_{max}, D_{1mL}, and D_{2mL} were higher in DCAT, but the D_{mean} was lower than in VMAT. For both the stomach and heart, D_{max}, D_{1mL}, D_{2mL} were significantly higher in DCAT. The dose data for OARs that show statistically significant differences are listed in **Table 3** and entire data in **Supplementary Table 1**.

The maximum dose to any point ≥2 cm away from the PTV in any direction (D_{2cm}) and the ratio of the volume of 50% of the prescription dose isodose to the volume of the PTV ($R_{50\%}$) are reported for evaluation of intermediate dose spillage and to

TABLE 1 | Patient characteristics.

Patient no.	Lesions	Primary cancer	Previous RT to Liver	Location	GTV (mL)	PTV (mL)	Prescribed dose (cGy)	Fractions
1	1	HCC	−	S4	5.1	20.1	5,200	4
2	1	HCC	−	S7	1.0	14.0	6,000	4
3	1	HCC	+	S7	5.4	19.2	5,400	4
4	1	HCC	+	S8	4.2	16.0	5,000	5
5	1	Cervix	−	S6	1.9	10.8	4,800	4
6	1	HCC	−	S5	7.7	15.9	6,000	4
7	1	HCC	−	S7/8	7.1	24.5	6,000	4
8	1	HCC	−	S7/8	10.6	31.4	6,000	4
9	1	HCC	−	S7	22.1	53.5	6,000	4
10	1	HCC	−	S7	8.7	31.9	6,000	4
11	3	Pancreas	−	S8, S4, S6	3.5, 6.9, 3.1	23.3, 23.2, 14.1	5,400	4
12	3	HCC	−	LLS, S4/8	1.1, 1.2, 2.1	24.3, 19.4	5,400	4
13	1	HCC	+	S8	7.9	14.3	6,000	4
14	1	HCC	−	S6	6.2	22.7	6,000	4
15	1	HCC	−	S8	11.5	37.4	6,000	4
16	1	HCC	−	S7	1.6	11.6	6,000	4
17	1	HCC	+	S4	3.7	15.5	6,000	4
18	1	Rectum	−	S7	0.4	6.4	6,000	4
19	1	Cervix	−	S4	7.6	22.9	6,000	5
20	1	Rectosigmoid	+	S4/8	24.0	58.7	5,000	4
21	2	Rectosigmoid	−	S8, S6	2.0, 1.2	10.9, 7.7	6,000	4
22	2	Colon	+	S5, S5	1.6, 1.7	11.4, 11.5	6,000	4
23	1	HCC	−	S5	4.0	11.5	6,000	4
24	1	HCC	−	S4	4.2	15.7	5,000	5
25	1	Rectosigmoid	+	S8	3.0	14.9	6,000	4

No., number; RT, radiotherapy; GTV, gross target volume; PTV, planning target volume.

scrutinize the fall-off gradient beyond the PTV extending into normal tissue structures. The D_{2cm}(%) and $R_{50\%}$ of DCAT and VMAT were 45.8 ± 7.9 and 5.6 ± 0.9, and 45.1 ± 6.7 and 5.5 ± 1.2, respectively. The differences were not statistically significant. The D_{2cm}(%) and $R_{50\%}$ data for all patients are shown in **Table 4**.

Efficiency

We also evaluated plan and delivery efficiency using MU, the elapsed time to make a plan (Calculation time), and the estimated delivery time (Delivery time). The MU of DCAT and VMAT were 2440.5 ± 346.5 and 2741.4 ± 417.5, respectively, and the average difference was 300.9 ± 340.4. Calculation time for DCAT and VMAT was 14.4 ± 7.5 min and 29.0 ± 14.2 min, and delivery time was 3.6 ± 0.5 min and 4.5 ± 0.7 min, respectively. All efficiency parameters analyzed showed statistically significant differences (**Table 5**).

DISCUSSION

For plan comparison, we used 1 arc for DCAT and 2 arcs for VMAT. One-arc and 2-arc plans with both DCAT and VMAT were used for some patients to verify the ideal number of arcs for each method. Dose distribution in DCAT showed little improvement from increment of arc numbers. In contrast, VMAT showed better results with 2 arcs than with 1 arc. For comparison with the best plans, 1 arc in DCAT and 2 arcs in VMAT were used.

In this study, couch rotation was not used due to disadvantages of couch rotation. Even though the use of couch rotation can help improve dosimetric parameters, couch rotation should be used with caution because the theoretical advantage could be offset by errors caused by an increase in treatment time and position changes.

As expected, VMAT was superior to DCAT to build SBRT plan with better plan quality. However, although there were some statistically significant differences between DCAT and VMAT plans, we could not assert if VMAT was better than DCAT with only dose distribution in the absence of consideration for actual use. As mentioned above, DCAT has several advantages over VMAT that could offset the better dose-distribution of VMAT. Unless the differences of dose distribution and plan quality are substantial, DCAT could be reckoned prior to VMAT for SBRT in some specific cases. There are concerns regarding missing the targets in highly modulated treatment plan for moving targets such as liver tumors. Liver tumors might not only move up and down but also move sideways and twist. Moreover, liver tumors tend to grow in a relatively circular shape and this suggests that DCAT would be as appropriate as VMAT to achieve adequate target coverage in liver tumors. That is the one of reason why we should consider DCAT for

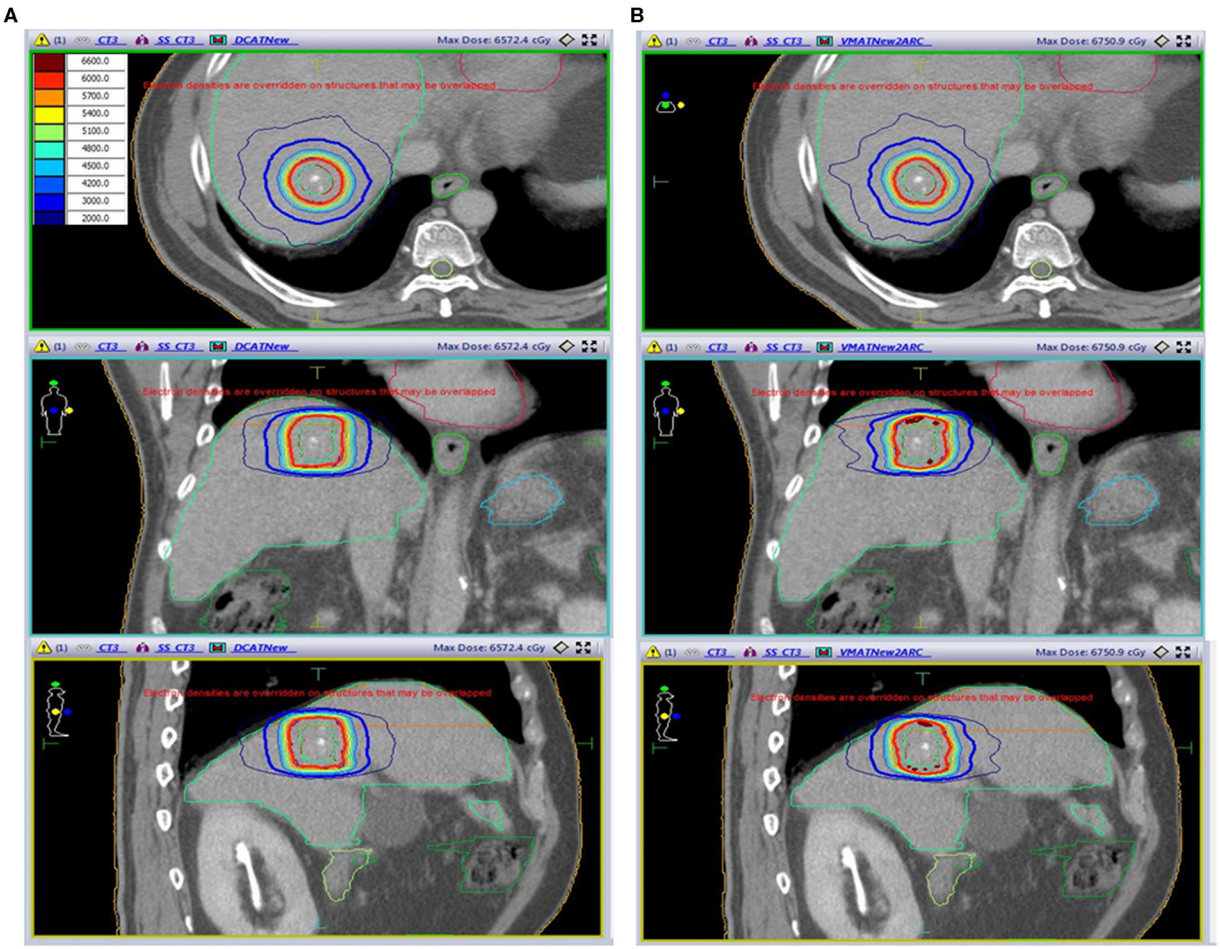

FIGURE 2 | The dose distribution for the same patient was shown in axial, coronal and sagittal planes according to the plan type. **(A)** DCAT. **(B)** VMAT.

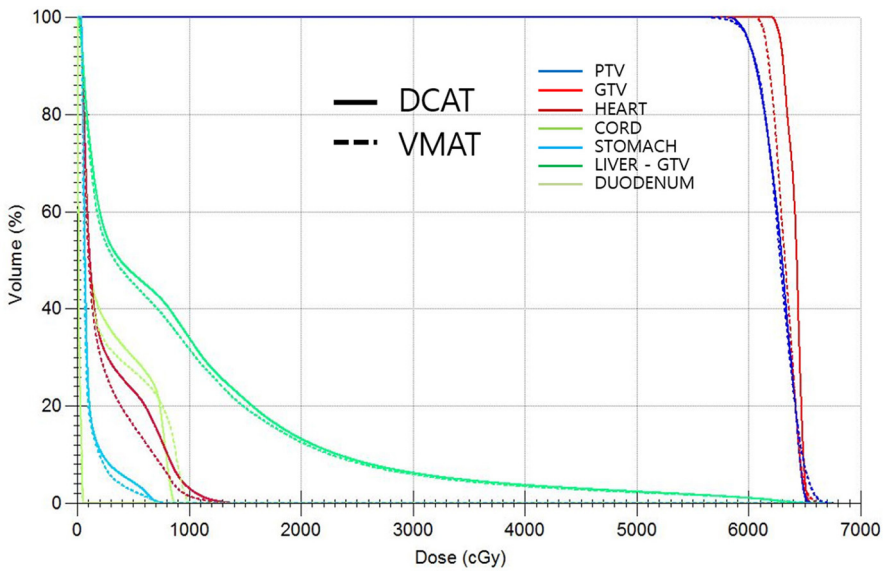

FIGURE 3 | Comparison of DVHs between DCAT and VMAT plan for the same patient.

TABLE 2 | PTV coverage.

	DCAT	VAMT	Avg. difference (DCAT – VMAT)	*p*–value
D_{max} (cGy)	6199.1 ± 419.1	6177.7 ± 428.4	21.4 ± 95.9	0.231
D_{mean} (cGy)	5942.7 ± 409.3	5890.6 ± 438.8	52.2 ± 194.3	0.015
D95% (cGy)	5678.4 ± 425.2	5680.9 ± 421.3	−2.5 ± 12.6	0.050
D98% (cGy)	5580.0 ± 465.2	5596.0 ± 478.7	−16.1 ± 44.9	0.005
D2% (cGy)	5981.1 ± 1100.8	6126.0 ± 434.2	−145.0 ± 960.2	0.289
D50% (cGy)	5968.8 ± 413.1	5954.3 ± 405.2	14.5 ± 73.6	0.042
V95% (mL)	23.5 ± 18.6	23.5 ± 18.6	−0.1 ± 0.7	0.022
HI	1.08 ± 0.04	1.07 ± 0.04	0.01 ± 0.02	0.062
CI	1.05 ± 0.05	1.03 ± 0.04	0.02 ± 0.03	0.003

Avg., average; CI, conformality index; HI, heterogeneity index; PTV, planning target volume.

TABLE 3 | Statistically significant differences in OARs.

	DCAT	VMAT	Avg. difference (DCAT – VMAT)
V30 (mL)	65.9 ± 34.4	62.1 ± 29.8	3.8 ± 9.2
V20 (mL)	133.7 ± 65.4	125.6 ± 65.4	8.1 ± 17.2
V10 (mL)	346.2 ± 196.7	318.9 ± 165.3	27.3 ± 48.4
Duodenum D_{max} (cGy)	627.6 ± 1065.3	615.82 ± 1046.7	11.8 ± 119.1
Duodenum D_{1mL} (cGy)	478.9 ± 757.1	461.7 ± 724.1	17.2 ± 123.6
Duodenum D_{2mL} (cGy)	395.3 ± 620.4	378.5 ± 581.6	16.8 ± 136.1
Duodenum D_{mean} (cGy)	85.6 ± 118.8	88.2 ± 130.3	−2.6 ± 56.7
Stomach D_{max} (cGy)	1057.2 ± 1042.6	968.0 ± 1046.4	89.1 ± 191.3
Stomach D_{1mL} (cGy)	913.3 ± 829.5	826.6 ± 796.0	86.7 ± 178.4
Stomach D_{2mL} (cGy)	855.9 ± 755.8	775.0 ± 708.4	80.9 ± 176.9
Heart D_{max} (cGy)	1439.7 ± 1589.5	1361.8 ± 1553.6	77.9 ± 185.2
Heart D_{1mL} (cGy)	1250.4 ± 1354.3	1175.3 ± 1326.4	75.1 ± 176.8
Heart D_{2mL} (cGy)	1167.8 ± 1233.6	1095.0 ± 1214.6	72.8 ± 174.0

Avg., average; D_{mean}, mean dose; D_{max}, maximum dose.

TABLE 4 | $D_{2cm(\%)}$ and $R_{50\%}$ for all cases.

Case No.	PTV (mL)	$D_{2cm(\%)}$		$R_{50\%}$	
		DCAT	VMAT	DCAT	VMAT
1	20.1	43.3	45.9	4.7	4.3
2	14.0	41.8	43.2	5.3	4.9
3	19.2	42.3	42.6	4.5	4.6
4	16.0	42.2	44.5	5.8	5.6
5	10.8	42.5	42.3	5.8	5.3
6	15.9	43.1	42.5	5.7	5.0
7	24.5	43.1	43.9	4.6	4.4
8	31.4	45.9	43.4	5.1	4.2
9	53.5	49.1	48.1	4.3	4.0
10	31.9	44.8	46.5	4.5	4.5
11	23.3	43.8	44.3	5.3	4.9
12	23.2	41.8	42.0	4.8	5.1
13	14.1	50.5	49.7	5.8	6.2
14	24.3.	51.0	51.2	5.6	6.0
15	19.4	46.2	42.7	5.6	4.5
16	14.3	41.0	41.6	5.9	6.0
17	22.7	42.6	43.2	5.0	4.8
18	37.4	44.3	45.0	4.2	4.1
19	11.6	41.4	41.3	6.2	6.4
20	15.5	41.6	41.5	5.6	5.7
21	6.4	40.6	40.0	8.0	8.8
22	22.9	83.8	76.7	7.4	6.0
23	58.7	52.1	50.0	5.5	4.7
24	10.9	48.1	45.8	6.8	7.2
25	7.7	47.6	47.3	7.7	8.1
26	11.4	42.5	39.7	5.8	6.2
27	11.5	42.0	40.2	5.7	6.5
28	15.7	44.4	42.4	5.5	5.4
29	14.9	47.4	44.7	5.8	6.0
30	13.9	41.9	41.7	5.9	6.1

No., number; PTV, planning target volume.

TABLE 5 | Calculation time, Delivery time, and MU.

	DCAT	VMAT	Avg. difference (DCAT – VMAT)
Calculation time (min)	14.4 ± 7.5	29.0 ± 14.2	−14.6 ± 15.2
Delivery time (min)	3.6 ± 0.5	4.5 ± 0.7	−0.9 ± 0.6
MU	2440.5 ± 340.4	2741.4 ± 417.5	−300.9 ± 340.4

Delivery time and MU for 1 fraction of stereotactic body radiotherapy.
Avg., average; MU, monitor unit.

liver tumors during SBRT if the differences between DCAT and VMAT are comparable. In addition, complex interplay between MLC motion, jaw movement, gantry rotation, and target motion during free-breathing treatments with VMAT could cause considerable dose discrepancies (7, 10). Our results indicated that several dosimetric parameters were significantly better in VMAT plans. However, DCAT also met the plan goals proposed by the RTOG SBRT protocol and the dose distribution differences were small enough to accept DCAT as a method of SBRT instead of VMAT.

$D_{2cm}(\%)$ and $R_{50\%}$ values are originally proposed for lung SBRT but not for the liver. However, we wanted to manage and minimize spillage dose and hence, $D_{2cm(\%)}$ and $R_{50\%}$ were evaluated. $D_{2cm(\%)}$ achieved the suggested goal except in 1 case. In this 1 case where the $D_{2cm(\%)}$ was not achieved, the tumor was located near the duodenum and $D_{2cm(\%)}$ was compromised to obtain acceptable dose distribution to the duodenum. Meanwhile, $R_{50\%}$ failed to meet the goal in 12 cases. This might be due to the different prescription goals for liver and lung PTV in RTOG protocols. To clarify the reason why $R_{50\%}$ is hard to achieve, we tested dose spillage through CT scans with lung and liver density and there was no significant difference according to tissue densities. Stathakis et al. recently published the study of dosimetric comparison between VMAT and DCAT in SBRT for the lung and liver (10). In that study, $R_{50\%}$ seemed to

reach the desired goal; however, there appeared to be calculation errors in their R50 values. Though differences in protocols make it difficult to achieve R50 in the liver, there is still a need to evaluate controlling dose spillage outside the PTV.

In terms of efficiency, DCAT had shorter calculation times and delivery times with smaller MU. Since calculation time changes variably depending on the number of programs running on the TPS at the same time, measurement of accurate time for planning is not available. Nevertheless, calculation time is generally 2–3 times longer in VMAT, and DCAT could allow for quicker plans. Shorter delivery times would help patients maintain treatment postures and to control breathing which would reduce target misses during RT. Therefore, DCAT should be considered preferential to VMAT in patients with poor breathing or poor coordination. MU was smaller in DCAT; the average difference was 300.1 MU. The use of smaller MU would reduce both the load on the LINAC machine and concerns about leakage through the multi-leaf collimator. In addition, DCAT could help conserve resources, which might be important to institutions with many patients but limited resources.

Before SBRT, some patients receive prior surgery or RT and would need stricter dose control to avoid severe toxicities. VMAT would be more appropriate in such patients for minimizing the dose to OARs, although the dose differences are small. Moreover, since DCAT is not recommended for constructing plans for multiple lesions, VMAT should be considered when SBRT is administered for multiple lesions simultaneously. However, if multiple lesions are treated separately, DCAT should be given the priority.

As noted above, DCAT might be more advantageous than VMAT for liver SBRT with exception to specific cases. Although the method of treatment is at the physician's discretion, the physician needs to understand the pros and cons of each treatment prior to choosing a treatment method. We hope this study will help radiation oncologists make better decisions for selection of SBRT methods.

DATA AVAILABILITY STATEMENT

All datasets generated for this study are included in the article/**Supplementary Material**.

ETHICS STATEMENT

This study was retrospective and exempted from obtaining written informed consent. The study was also approved by the Institutional Review Board of the Dongnam Institute of Radiological and Medical Sciences (DIRAMS).

AUTHOR CONTRIBUTIONS

All authors listed have made a substantial, direct and intellectual contribution to the work, and approved it for publication.

FUNDING

This research was supported by National R&D Program through the Dongnam Institute of Radiological & Medical Sciences (DIRAMS) funded by the Ministry of Education, Science and Technology (50602-2019).

SUPPLEMENTARY MATERIAL

The Supplementary Material for this article can be found online at: https://www.frontiersin.org/articles/10.3389/fonc.2020.01170/full#supplementary-material

REFERENCES

1. Jang WI, Bae SH, Kim M-S, Han CJ, Park SC, Kim SB, et al. A phase 2 multicenter study of stereotactic body radiotherapy for hepatocellular carcinoma: safety and efficacy. *Cancer*. (2020) 126:363–72. doi: 10.1002/cncr.32502
2. Doi H, Beppu N, Kitajima K, Kuribayashi K. Stereotactic body radiation therapy for liver tumors: current status and perspectives. *Anticancer Res.* (2018) 38:591–9. doi: 10.21873/anticanres.12263
3. Mahadevan A, Blanck O, Lanciano R, Peddada A, Sundararaman S, D'Ambrosio D, et al. Stereotactic Body Radiotherapy (SBRT) for liver metastasis - clinical outcomes from the international multi-institutional RSSearch(R) Patient Registry. *Radiat Oncol.* (2018) 13:26. doi: 10.1186/s13014-018-0969-2
4. Scorsetti M, Comito T, Clerici E, Franzese C, Tozzi A, Iftode C, et al. Phase II trial on SBRT for unresectable liver metastases: long-term outcome and prognostic factors of survival after 5 years of follow-up. *Radiat Oncol.* (2018) 13:234. doi: 10.1186/s13014-018-1185-9
5. Otto K. Volumetric modulated arc therapy: IMRT in a single gantry arc. *Med Phys.* (2008) 35:310–7. doi: 10.1118/1.2818738
6. Poon DM, Kam M, Leung CM, Chau R, Wong S, Lee WY, et al. Dosimetric advantages and superior treatment delivery efficiency of RapidArc over conventional intensity-modulated radiotherapy in high-risk prostate cancer involving seminal vesicles and pelvic nodes. *Clin Oncol.* (2013) 25:706–12. doi: 10.1016/j.clon.2013.07.010
7. Rauschenbach BM, Mackowiak L, Malhotra HK. A dosimetric comparison of three-dimensional conformal radiotherapy, volumetric-modulated arc therapy, and dynamic conformal arc therapy in the treatment of non-small cell lung cancer using stereotactic body radiotherapy. *J Appl Clin Med Phys.* (2014) 15:4898. doi: 10.1120/jacmp.v15i5.4898
8. Stathakis S. *Optimized DCAT for Lung and Liver SBRT Rapid and Accurate Delivery of Lung and Liver SBRT Using Optimized Dynamic Conformal Arc Treatment (DCAT) With Monaco® Treatment Planning System and Versa HD™*. San Antonio, TX: University of Texas Health San Antonio Cancer Center (2018).
9. Chaikh A, Giraud J-Y, Perrin E, Bresciani J-P, Balosso J. The choice of statistical methods for comparisons of dosimetric data in radiotherapy. *Radiat Oncol.* (2014) 9:205. doi: 10.1186/1748-717X-9-205
10. Stathakis S, Narayanasamy G, Licon AL, Myers P, Li Y, Crownover R, et al. A dosimetric comparison between volumetric-modulated arc therapy and dynamic conformal arc therapy in SBRT. *J Buon.* (2019) 24:838–43.
11. Stathakis S. Evaluation of dynamic conformal arc therapy for treatment of lung and liver. In: *AAMD 43rd Annual Meeting*. Austin, TX (2018).

Conflict of Interest: The authors declare that the research was conducted in the absence of any commercial or financial relationships that could be construed as a potential conflict of interest.

frontiers in Oncology

SYSTEMATIC REVIEW
published: 17 November 2020
doi: 10.3389/fonc.2020.561669

Can Radiofrequency Ablation Replace Liver Resection for Solitary Colorectal Liver Metastasis? A Systemic Review and Meta-Analysis

*Wu Hao, Jiang Binbin, Yang Wei and Yan Kun**

Key Laboratory of Carcinogenesis and Translational Research (Ministry of Education/Beijing), Department of Ultrasound, Peking University Cancer Hospital and Institute, Beijing, China

Radiofrequency ablation (RFA) can be a favorable option for patients with colorectal liver metastasis (CRLM). However, current reports about the therapeutic efficacy of liver resection (LR) and RFA for colorectal liver metastasis (CRLM) still remain controversial, especially for solitary CRLM. Therefore, this meta-analysis was performed to evaluate the therapeutic efficacy between LR and RFA for solitary CRLM. First, a comprehensive search for published studies was conducted using PubMed, the Cochrane Library Central, and Web of Science. Each study was reviewed and data extracted. In this meta-analysis, 10 studies (11 study arms) were finally included. The meta-analysis was performed using risk ratio (RR) and random effect model or fixed effect model, in which 95% confidence intervals (95% CI) for RR were calculated. The primary outcomes were disease-free survival (DFS) and overall survival (OS) at 1, 3, or 5 years plus complication rate. The results showed that patients treated by LR achieved better PFS and OS than those by RFA, but subgroup analysis and meta-regression displayed that the efficacy of RFA was equivalent to that of LR in solitary CRLM, when conditions were limited to tumors of $\leq$3 cm and fewer synchronous metastasis in the publication years 2011–2018. Meanwhile, RFA achieved lower complication rates when compared with LR. In conclusion, although patients treated by RFA cannot achieve better PFS and OS than those by LR, RFA can be considered a viable treatment option for solitary CRLM, with potentially lower complication rates.

Keywords: liver resection, radiofrequency ablation, colorectal liver metastasis, therapeutic efficacy, meta-analysis

OPEN ACCESS

Edited by:
Aditya Juloori, University of Chicago Medical Center, United States

Reviewed by:
Bilgin Kadri Aribas, Bülent Ecevit University, Turkey
Sergio Jaramillo, Willis-Knighton Cancer Center, United States

****Correspondence:***
Yan Kun
ydbz@vip.sina.com

Specialty section:
This article was submitted to Radiation Oncology, a section of the journal Frontiers in Oncology

Received: *25 June 2020*
Accepted: *24 August 2020*
Published: *17 November 2020*

Citation:
Hao W, Binbin J, Wei Y and Kun Y (2020) Can Radiofrequency Ablation Replace Liver Resection for Solitary Colorectal Liver Metastasis? A Systemic Review and Meta-Analysis. Front. Oncol. 10:561669. doi: 10.3389/fonc.2020.561669

INTRODUCTION

Colorectal cancer has become one of the most common human malignancies, affecting nearly 1 million individuals in the world every year (1, 2). When the colorectal cancer was diagnosed, up to half of the patients developed colorectal liver metastases (CRLM) (3). Colorectal liver metastasis significantly affects overall survival (OS), which has become the leading cause of cancer-related mortality in patients with colorectal cancer; the median OS for patients with untreated CRLM is 4.5–12 months (4, 5). Currently, liver resection (LR) is considered as the most effective treatment approach for CRLMs. However, only 10–30% of the cases are considered eligible for surgical resection because of general health status, anatomical location, disease extent, hepatic function reservation, or comorbidities (6–8).

Radiofrequency ablation (RFA), as a common minimally invasive treatment modality, has been widely used in clinical practice for the local control of liver tumors, and previous reports have demonstrated that thermal ablation had an advantage over surgical resection in being less invasive for hepatocellular carcinoma (HCC) ($\leq$3 cm); therefore, it can also be an alternative option for patients with unresectable CRLM (9–14). Although RFA has established its role in the management of HCC as a safe, well-tolerated, and less invasive procedure, there has been no consensus on the therapeutic efficacy of RFA for those patients with CRLM, especially for solitary lesions (15–18).

In recent years, several studies about solitary CRLM reported a comparable OS and complication rates for RFA vs. LR. These results have led to the discussion that RFA should be favored over LR due to its less invasive and easily repeated procedure, yet RFA for patients with unresectable CRLM has been labeled inferior to LR for patients with resectable CRLM according to previous studies (17, 19). However, these results should be interpreted with caution because of the apparent selection bias.

Along this line, this study analyzed the existing literature comparing the therapeutic efficacy and safety of RFA and LR for patients with solitary CRLM by conducting a meta-analysis and analyzed the factors influencing prognosis to evaluate noninferiority or inferiority of RFA for patients with unresectable CRLM.

METHODS

Literature Search

The QUOROM guidelines were followed for conducting the meta-analysis. The systematic literature search was performed independently by two of the authors using PubMed, Web of Science, and the Cochrane Library Central. No restriction was set for the date of publication. Only studies on humans and in the English language were considered for inclusion. The following Medical Subject Heading terms (MeSH) search headings were used: "radiofrequency ablation," "resection," "surgical treatment," "surgery," "hepatectomy," "colorectal tumor," "colorectal neoplasm," "colorectal cancer," "liver," "hepatic," "metastases," and "metastasis." The computer program Endnote X7 was used for reference management.

Inclusion Criteria

For inclusion in the meta-analysis, the study had to fulfill the following criteria: (1) the comparative studies of clinical outcomes between RFA and LR for solitary CRLM; (2) the studies reporting at least 1-year disease-free survival and 3- or 5-year overall survival of each treatment group; (3) the studies clearly document indications for RFA and HR; (4) when more than one study were reported by the same research, the one of higher quality or the most recent publication was included.

Exclusion Criteria

The following studies (cohorts) were excluded: (1) the original studies lacking the comparative results about the clinical outcomes of RFA and LR; (2) those studies published in the form of review articles (including meta-analysis), abstracts, comments, letters, editorials, and case reports.

Data Extraction

Data extraction was performed independently by Wu Hao and Jiang Binbin, and in the case of discrepancy, the decision was made by a discussion with a third author (Yan Kun). For literatures with no clear survival data, data extraction was performed in the survival curve from primary literature by the Engauge digitizer software. The following parameters from each study were extracted: (1) the first author, the year of publication, study design; (2) the baseline oncological characteristics of patients including tumor size, tumor count, study period, primary lymph nodes, adjuvant chemotherapy, timing of metastasis; and (3) the outcome of the trials including 1-year disease-free survival (DFS), 3- and 5-year overall survival (OS), and complications.

Statistical Analysis

All analyses were performed using the STATA statistical software package version 12.0 (STATA Corp., College Station, Texas, USA). Calculation for dichotomous variables was carried out using the estimation of risk ratio (RR) with a 95% confidence interval (95% CI). The pooled effect was calculated using either the fixed effects model or the random effects model. The heterogeneity among the included studies was evaluated by the I2 statistics and Chi-squared test. In addition, the heterogeneity was considered to be present if the I2 was more than 50%. Sensitivity analysis was performed to evaluate the stability of the results by subgroup analysis and meta-regression analysis. Evidence of publication bias was evaluated using the Begg's test. Two-sided $P < 0.05$ was considered statistically significant.

RESULTS

Selection of Trials

After initial screening, 11 potentially relevant clinical study cohorts were identified. Of them, two study cohorts were from the same medical center, the latest one with the most comprehensive information was enrolled. Thus, a total of 10 study cohorts (11 study arms) with sample size ranging from 29 to 226 have been enrolled (**Figure 1**) (2, 15–18, 20–24). Among them, 690 patients underwent LR, and 347 patients underwent RFA. A detailed information of the included studies is summarized in **Table 1**.

Efficacy

With observable interstudy heterogeneity, patients in the RFA group had slightly inferior 1-year PFS (RR: 0.77, 95% CI: 0.630–0.940, $P = 0.009$, $I^2 = 86.0\%$, Ph = 0.000) (**Figure 2A**, **Table 2**), 3-year OS (RR: 0.860, 95% CI: 0.760–0.980, $P = 0.021$, $I^2 = 40.6\%$, Ph = 0.078) (**Figure 2B**, **Table 2**), and 5-year OS (RR: 0.66, 95% CI:0.52–0.85, $P = 0.001$, $I^2 = 55.7\%$, Ph = 0.012) (**Figure 2C**, **Table 2**) when compared with patients in the LR group.

Complications

Eight of the included studies compared the complications between the RFA group and the LR group. The incidence of postoperative complication was significantly lower in the RFA group than that in the LR group (RR: 0.340, 95% CI: 0.230–0.510, $P = 0.000$, $I^2 = 32.4\%$, Ph < 0.170) (**Figure 2D**, **Table 2**).

Subgroup Analysis and Meta-Regression

Considering an existing difference among the studies and the differences among participants could contribute to overall heterogeneity among the included studies; the subgroup analysis was used to examine possible relationships between the study characteristics and 1-year PFS, 3-year OS, and 5-year OS. The subgroup analysis underlined several variables that could

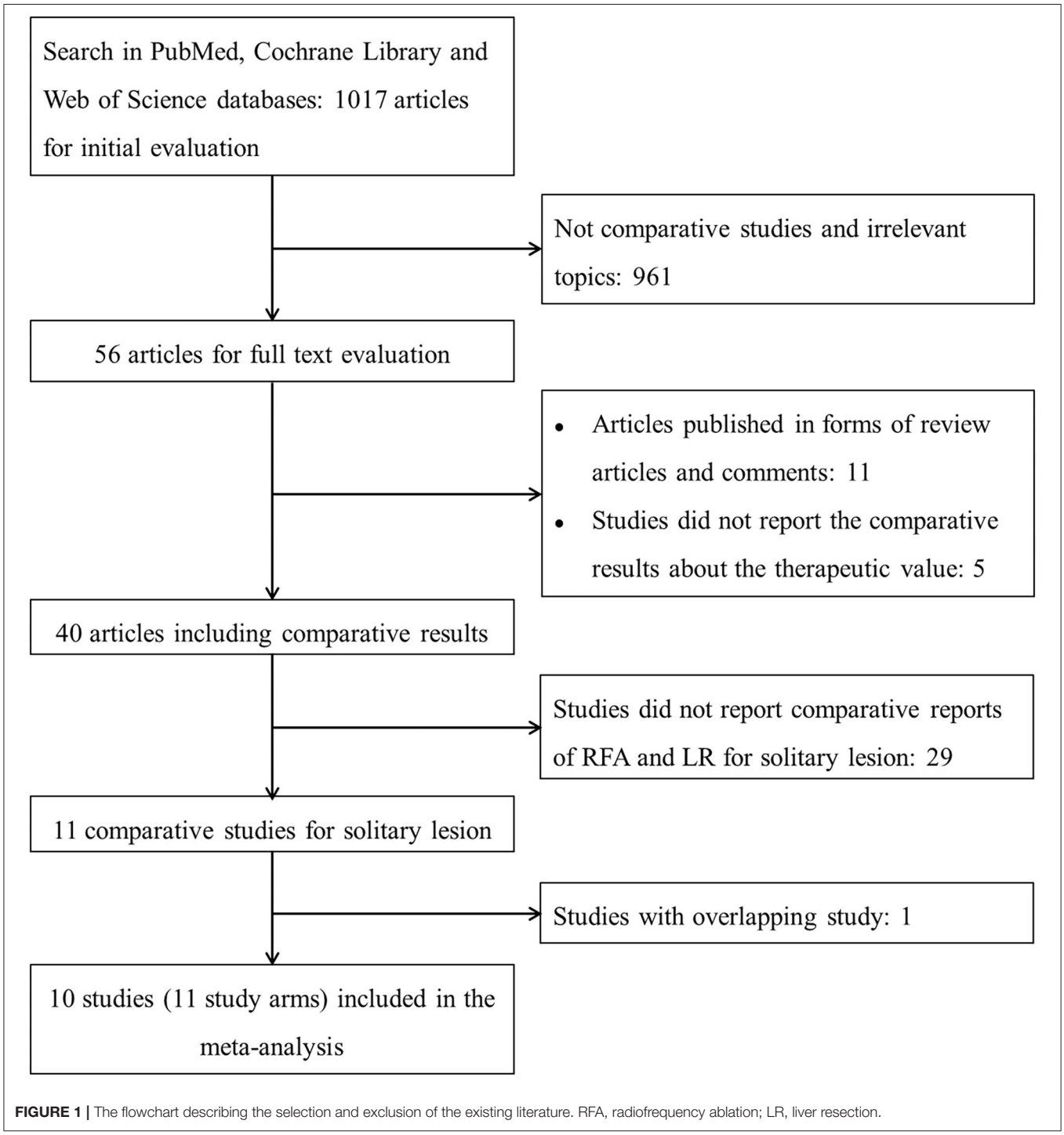

FIGURE 1 | The flowchart describing the selection and exclusion of the existing literature. RFA, radiofrequency ablation; LR, liver resection.

TABLE 1 | Characteristics of the included studies.

References	Publication year	Geographic location	Tumor size (RFA/LR, cm)	RFA method	AC (RFA/LR)	SM (RFA/LR)	Complications (RFA/LR)	Sample size (RFA/LR)	Reason of (RFA/LR)
Oshowo et al. (15)	2003	European	3/4	perc	23/17	14/4	1/2	25/20	1,2,4
Aloia et al. (25)	2006	American	3/3.5	intra	24/99	18/74	NA/NA	30/150	2,3
Berber et al. (26)	2008	American	3.7/3.8	intra	30/63	5/15	2/28	42/90	2,4
Hur et al. (17)	2009	Asian	2.5/2.8	NA	22/37	7/24	0/6	25/42	1,2,3
Kim et al. (21)	2011	Asian	1.7/1.4	NA	90/114	9/104	4/26	99/127	5,6,7
Kim et al. (21)	2011	Asian	3.6/4.8	NA	14/50	1/34	1/3	14/56	5,6,7
Ko et al. (22)	2014	Asian	2.02/3.59	perc	8/6	5/3	NA/NA	17/12	4,6
Lee et al. (27)	2015	Asian	1.8/1.7	intra	26/52	19/47	5/28	29/63	2,3
McKay et al. (24)	2009	American	3.0/4.1	intra	NA/NA	NA/NA	8/22	19/37	2,8
Takahashi et al. (28)	2018	American	1.81/1.91	intra	NA/NA	NA/NA	NA/NA	25/63	3
White et al. (29)	2007	American	2.4/2.7	perc	11/20	5/17	1/4	22/30	9

RFA, radiofrequency ablation; LR, liver resection; AC, adjuvant chemotherapy; SM, synchronous metastasis; Perc, percutaneous RFA; Intra, intraoperative RFA.
Reason of RFA: 1, close to major vessel; 2, prohibitive comorbidity; 3, inadequate liver remnant; 4, extrahepatic disease; 5, difficult anatomical location; 6, multiple metastasis; 7, severe cardiovascular or pulmonary disease; 8, proximity to critical structures; 9,other reasons with no eligible for liver resection.

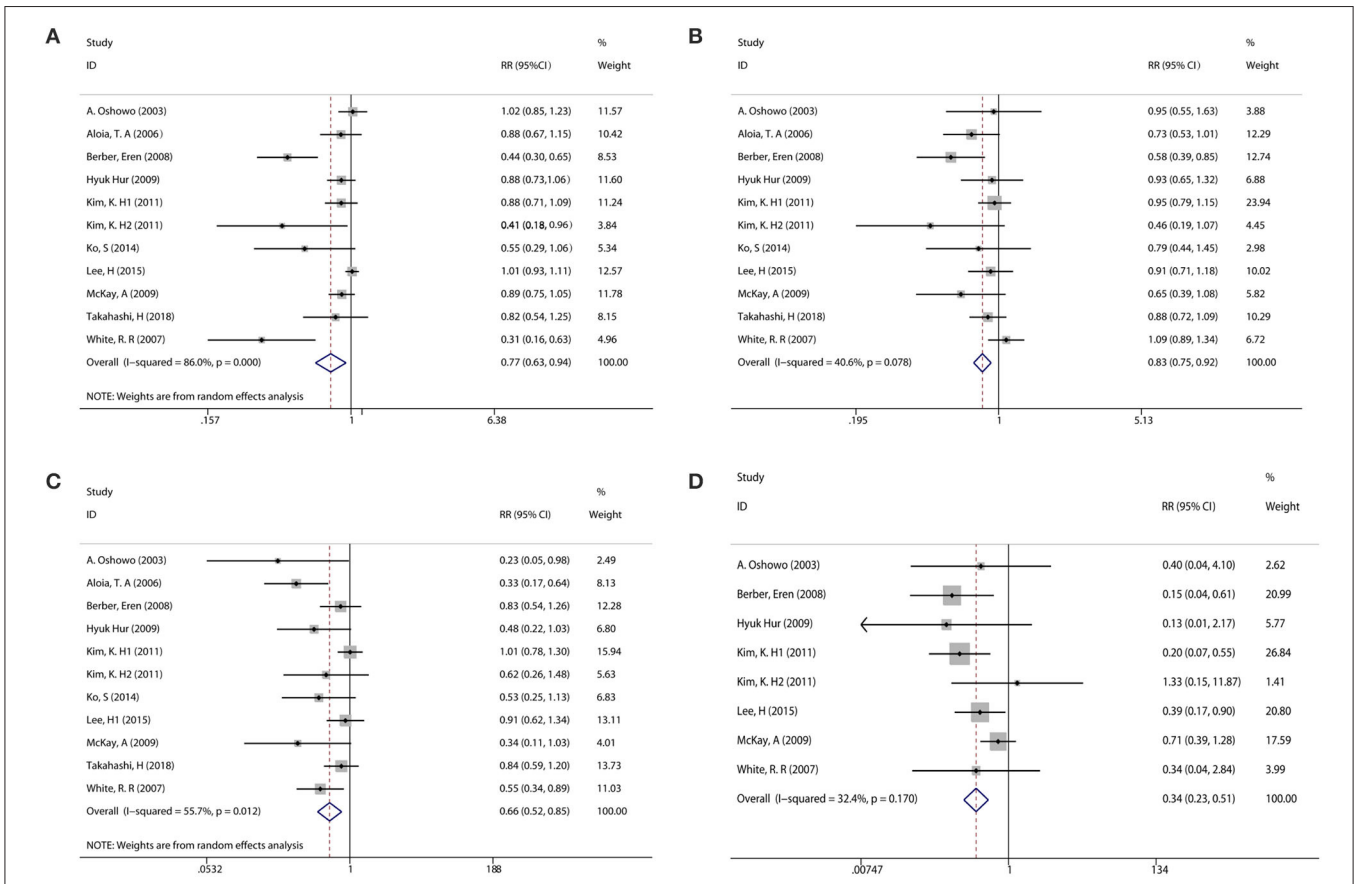

FIGURE 2 | Pooled analysis comparing the survival rate between RFA and LR groups. **(A)** Pooled analysis comparing the 1-year PFS rate. **(B)** Pooled analysis comparing the 3-year overall survival (OS) rate. **(C)** Pooled analysis comparing the 5-year OS rate. **(D)** Pooled analysis comparing the complication rate.

affect overall heterogeneity and influence the results of this meta-analysis. Namely, these were the publication years 2011–2018, geographic location (Asian), tumor size for RFA ($\leq$3 cm), and adjuvant chemotherapy [the percentage of patients with adjuvant chemotherapy (PAC); $PAC_{RFA} > PAC_{LR}$] in 1-year PFS; the geographic location (Asian), tumor size for RFA ($\leq$3 cm), and adjuvant chemotherapy ($PAC_{RFA} \leq PAC_{LR}$) in 3-year OS; the publication years 2011–2018, geographic location

TABLE 2 | Subgroup analysis and meta-regression.

Analysis	*n*	*Weight*	*HR (95%CI)*	*P*	*I2*	*Ph*	*Pr*
1-y PFS	11	100%	0.77 (0.63–0.94)	0.009	86.0%	0.000	
Publication year							0.823
Year (2003–2010)	6	41.87%	0.86 (0.79–0.95)	0.002	77.9%	0.000	
Year (2011–2018)	5	58.13%	0.97 (0.90–1.05)	0.453	56.8%	0.055	
Geographic location							0.902
Asian	5	66.80%	0.96 (0.89–1.03)	0.283	58.3%	0.048	
American	5	22.76%	0.79 (0.70–0.90)	0.000	77.3%	0.001	
European	1	10.45%	1.02 (0.85–1.23)	0.817	–	–	
Tumor size for RFA							0.014
≤3 cm	9	97.16%	0.95 (0.89–1.00)	0.071	54.5%	0.025	
>3 cm	2	2.84%	0.43 (0.30–0.62)	0.000	0.0%	0.885	
RFA methods							0.517*
Percutaneous	3	14.93%	0.91 (0.76–1.08)	0.285	84.3%	0.002	
Intraoperative	5	85.07%	0.95 (0.88–1.02)	0.129	78.0%	0.001	
Adjuvant chemotherapy							0.406*
$PAC_{RFA} > PAC_{LR}$	6	85.58%	0.96 (0.89–1.03)	0.224	77.2%	0.001	
$PAC_{RFA} \leq PAC_{LR}$	3	14.42%	0.80 (0.68–0.95)	0.012	78.4%	0.010	
Synchronous metastasis							0.485*
$PSM_{RFA} > PSM_{LR}$	3	19.12%	0.94 (0.81–1.10)	0.451	44.7%	0.164	
$PSM_{RFA} \leq PSM_{LR}$	6	80.88%	0.93 (0.87–1.00)	0.051	83.9%	0.000	
3-y OS	11	100%	0.86 (0.76–0.98)	0.021	40.6%	0.078	
Publication year							0.710
Year (2003–2010)	6	43.8%	0.88 (0.77–1.01)	0.065	55.6%	0.046	
Year (2011–2018)	5	56.2%	0.90 (0.80–1.02)	0.093	0.0%	0.558	
Geographic location							0.781
Asian	5	44.52%	0.91 (0.80–1.05)	0.187	0.0%	0.565	
American	5	52.78%	0.87 (0.77–0.99)	0.031	64.0%	0.025	
European	1	2.7%	0.95 (0.55–1.63)	0.841	–	–	
Tumor size for RFA							**0.024**
≤3 cm	9	93.6%	0.92 (0.84–1.01)	0.086	0.0%	0.561	
>3 cm	2	6.4%	0.56 (0.39–0.79)	0.001	0.0%	0.623	
RFA methods							0.101*
Percutaneous	3	33.89%	1.04 (0.87–1.25)	0.666	0.0%	0.579	
Intraoperative	5	66.11%	0.81 (0.71–0.92)	0.001	26.1%	0.247	
Adjuvant chemotherapy							0.210*
$PAC_{RFA} > PAC_{LR}$	6	65.38%	0.85 (0.75–0.96)	0.10	40.9%	0.133	
$PAC_{RFA} \leq PAC_{LR}$	3	34.62%	1.02 (0.86–1.22)	0.791	0.0%	0.511	
Synchronous metastasis							0.516*
$PSM_{RFA} > PSM_{LR}$	3	15.96%	0.79 (0.61–1.01)	0.061	0.0%	0.734	
$PSM_{RFA} \leq PSM_{LR}$	6	84.04%	0.93 (0.83–1.04)	0.200	53.3%	0.057	
5-y OS	11	100%	0.66 (0.52–0.85)	0.001	55.7%	0.012	
Publication year							**0.031**
Year (2003–2010)	6	31.52%	0.55 (0.43–0.75)	0.000	37.8%	0.154	
Year (2011–2018)	5	68.48%	0.90 (0.75–1.07)	0.217	0.0%	0.479	
Geographic location							0.183
Asian	5	55.71%	0.88 (0.72–1.06)	0.184	32.3%	0.206	
American	5	43.31%	0.67 (0.64–0.83)	0.000	55.4%	0.062	
European	1	0.98%	0.23 (0.05–0.98)	0.047	–	–	
Tumor size for RFA							0.631
≤3 cm	9	85.7%	0.77 (0.66–0.90)	0.001	61.1%	0.008	
>3 cm	2	14.3%	0.78 (0.53–1.15)	0.207	0.0%	0.550	

(Continued)

TABLE 2 | Continued

Analysis	n	Weight	HR (95%CI)	P	I2	Ph	Pr
RFA methods							0.323*
Percutaneous	3	21.66%	0.51 (0.34'0.75)	0.001	0.0%	0.536	
Intraoperative	5	78.34%	0.76 (0.62–0.93)	0.009	57.5%	0.052	
Adjuvant chemotherapy							0.296*
$PAC_{RFA} > PAC_{LR}$	6	78.34%	0.84 (0.71–1.01)	0.059	62.3%	0.021	
$PAC_{RFA} \leq PAC_{LR}$	3	21.66%	0.53 (0.37–0.75)	0.000	0.0%	0.962	
Synchronous metastasis							**0.039***
$PSM_{RFA} > PSM_{LR}$	3	11.47%	0.38 (0.24–0.61)	0.000	0.0%	0.508	
$PSM_{RFA} \leq PSM_{LR}$	6	88.53%	0.84 (0.71–1.00)	0.050	35.3%	0.172	
Complications	8	100%	0.34 (0.23–0.51)	0.000	32.4%	0.170	

PAC, the percentage of patients received with adjuvant chemotherapy in RFA group or LR group; PSM, the percentage of patients with synchronous metastasis in RFA group or LR group; HR, hazard ratio; CI, confidence interval; Ph, P value of Q-test for heterogeneity test; Pr, P-value of meta regression analysis; (*) refer to the subgroup analysis and meta-regression analysis for patients reported relevant results; the influencing factors marked by the bold values in Pr column were regarded as the reason of heterogeneity by meta-regression analysis.

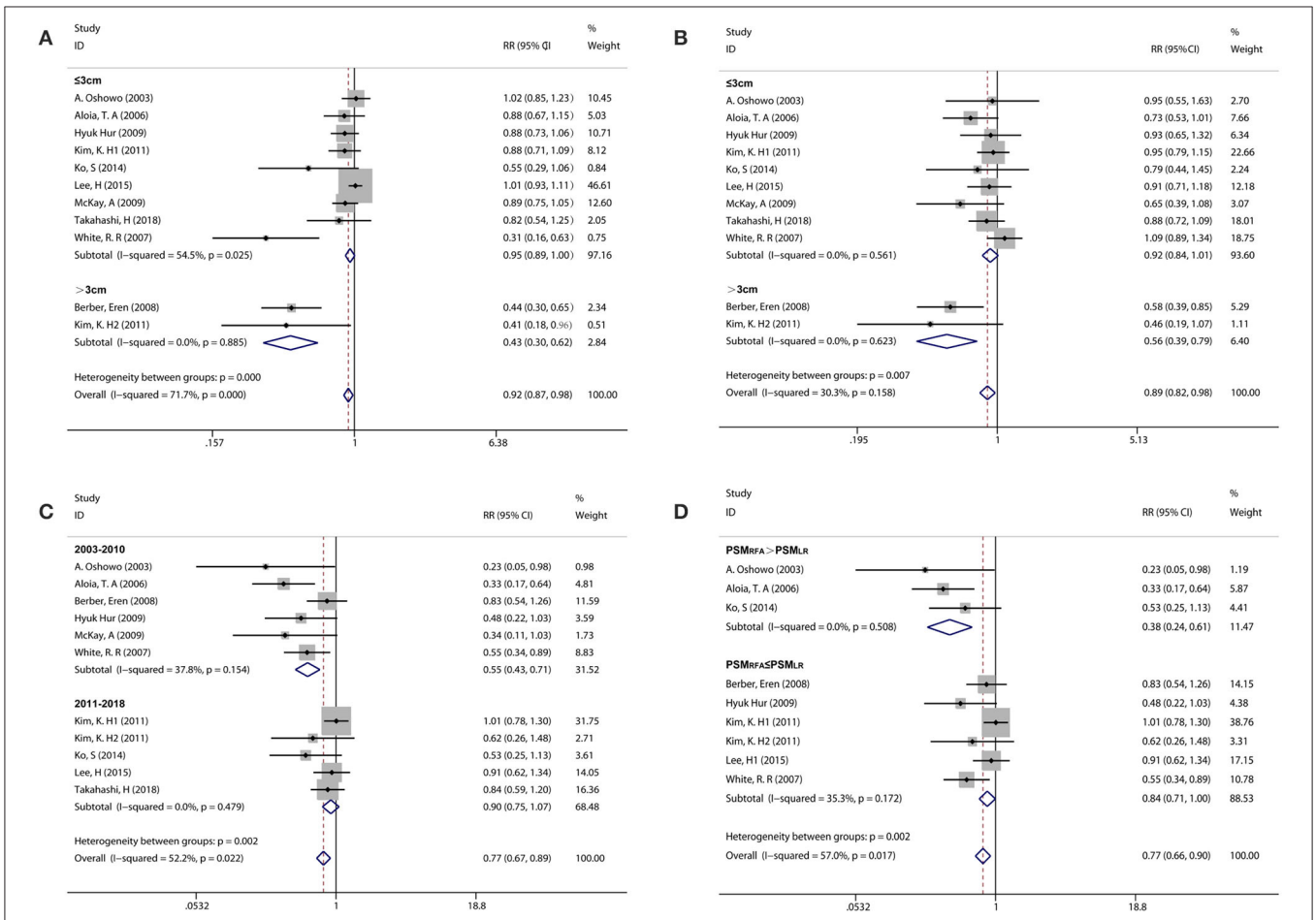

FIGURE 3 | Subgroup analysis comparing the survival rate between RFA and LR groups. **(A)** Subgroup analysis for tumor size in the 1-year PFS. **(B)** Subgroup analysis for tumor size in the 3-year OS. **(C)** Subgroup analysis for publication year in the 5-year OS. **(D)** Subgroup analysis for the percentage of patients with synchronous metastasis in the 5-year OS.

(Asian), tumor size for RFA (>3 cm), adjuvant chemotherapy ($PAC_{RFA} > PAC_{LR}$), and synchronous metastasis (the percentage of patients with synchronous metastasis, PSM; $PSM_{RFA} > PSM_{LR}$) in 5-year OS (**Figures 3A–D**, **Table 2**). In addition, to further confirm the reason of heterogeneity, a meta-regression analysis was performed with predefined variables.

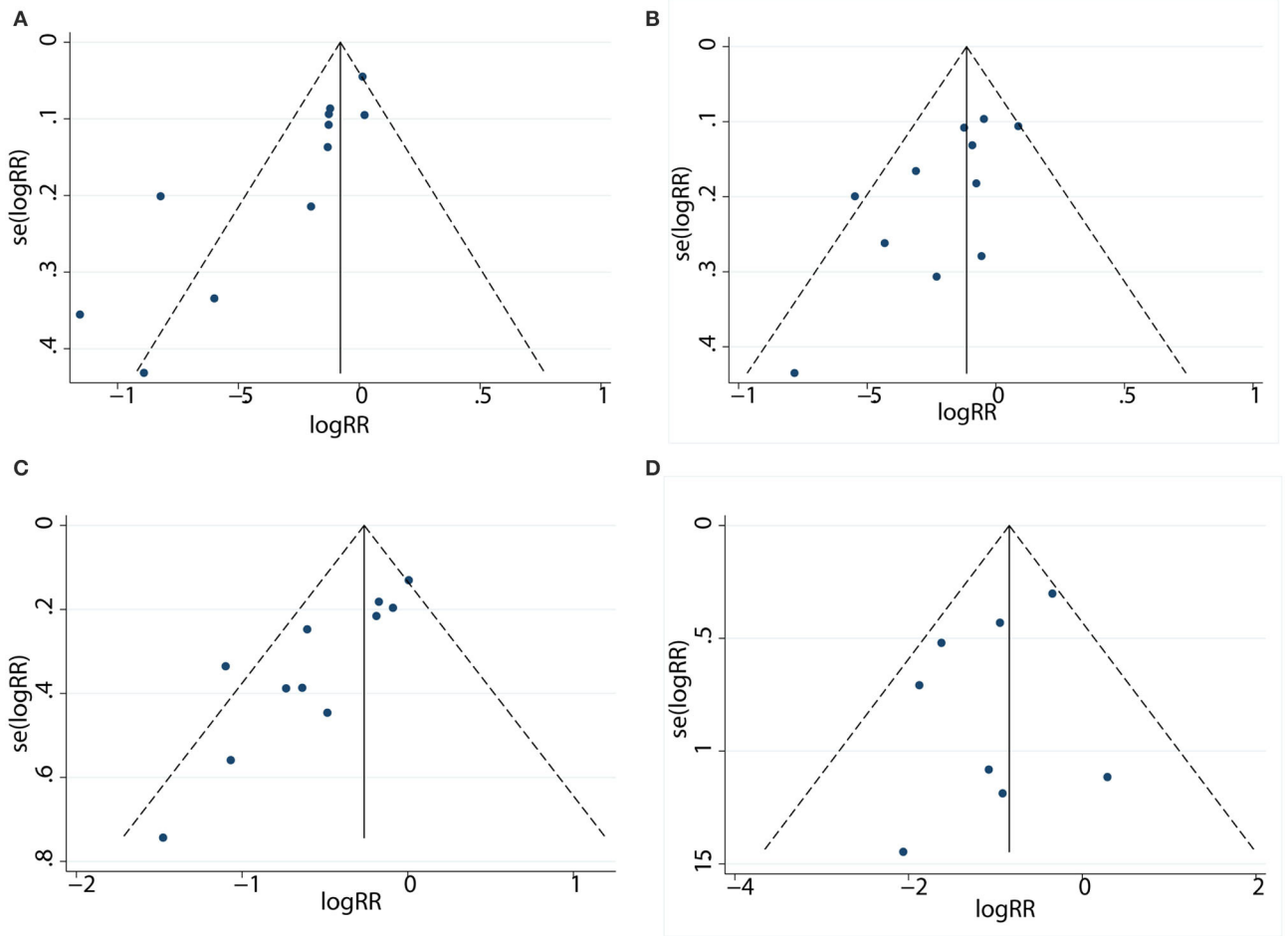

FIGURE 4 | Funnel plot to detect publication bias between patients in the LR and RFA. **(A)** Funnel plot describing the comparative analysis of 1-year PFS rate. **(B)** Funnel plot describing the comparative analysis of 3-year OS rate. **(C)** Funnel plot describing the comparative analysis of 5-year OS rate. **(D)** Funnel plot describing the comparative analysis of complication rate.

The results of the meta-regression analysis also confirmed the obtained clarification of heterogeneity proposed by the subgroup analysis at several aspects, such as tumor size for RFA (**Figures 3A,B**, **Table 2**), publication year (**Figure 3C**, **Table 2**), and the percentage of patients with synchronous metastasis (**Figure 3D**, **Table 2**).

Publication Bias

The funnel plot did not show significant asymmetry by the Begg's test in 1-year PFS ($Pr > |z| = 0.016$) (**Figure 4A**), 3-year OS ($Pr > |z| = 0.073$) (**Figure 4B**), 5-year OS ($Pr > |z| = 0.016$) (**Figure 4C**), and complication rates ($Pr > |z| = 1.000$) (**Figure 4D**).

DISCUSSION

This meta-analysis examined published data and evidence obtained from relevant clinical trials to provide pooled estimates regarding the treatment efficacy between RFA and LR in CRLMs. In the present meta-analysis, the results found that patients with CRLMs who were treated by LR achieved better survival outcomes than those who were treated by RFA. However, RFA outperformed LR in terms of fewer perioperative complication rates.

In the meta-analysis, the inferior survival outcomes of RFA could be explained as follows. First, RFA patients in the included studies were not eligible for liver resection because of poor health status, prohibitive comorbidity, extrahepatic disease, multiple metastasis, inadequate liver remnant, etc. The poor basic condition may shorten the overall survival for patients with CRLMs. Second, there were several complex characteristics for tumors treated with RFA, such as close to the major vessel, larger lesion size, and difficult anatomical location. These characteristics increased the possibility of incomplete ablation for tumors, which would further accelerate the risk of tumor recurrence after RFA.

Because of the significant heterogeneity among the included studies, subgroup analysis and meta-regression were carried on. Considering the previously mentioned fact that incomplete

ablation resulting from larger tumor size induced the expansion of tumor-initiating cells (16, 30), a subgroup analysis was performed for the influence of tumor size on RFA outcomes. The results showed that RFA patients with no more than a 3-cm tumor can achieve equivalent outcomes when compared with LR patients. In addition, the data from the meta-regression also displayed that the tumor size had an obvious influence on the significant heterogeneity in 1-year PFS and 3-year OS. According to the influence of tumor size on HCC outcomes, the reason for this may be explained by patients with smaller lesions achieving a higher ablation success rate, which can reduce the tumor recurrence attributed to hypoxia-driven acceleration of tumor growth occurring in the transition zone and the stimulated outgrowth of perilesional micrometastases (31, 32).

In contrast to the previous meta-analysis, this study also added the subgroup analysis about the publication year. Subgroup analysis showed that RFA patients in the publication years 2011–2018 had better survival than that in the publication years 2003–2010 and was identical when compared with LR patients in publication years 2011–2018. In addition, the meta-regression process in 5-year OS also further confirmed the subgroup analysis results. The results, to some extent, may be due to continuous improvement in the technical accuracy and performance of RFA in accordance with the learning curve for the treatment of CRLM, and the improvement process may be consistent with that in HCC treatment. In the past decades, RFA techniques have rapidly worked their way into clinical guidelines for the treatment of HCC, especially solitary small HCC. The international guidelines have shifted from surgical resection to minimally invasive percutaneous local ablation for small HCC (14, 33–35). Taken together, it will be possible that the therapeutic efficacy in the future will be better with the maturity of RFA technology in CRLM.

Meanwhile, to validate the effect of synchronous liver metastases on RFA therapeutic efficacy, this study also created an additional subgroup analysis and meta-regression. The results showed that synchronous liver metastases had a negative effect on the RFA therapeutic efficacy through subgroup analysis and meta-regression, which may be explained by cancer biology. According to the previous studies, the results showed that synchronous liver metastases have less favorable cancer biology and expected survival, and data from the corresponding registry showed that 5-year survival rates were shorter with synchronous than with metachronous CRLMs (36, 37). Yet, no biological marker has been identified that distinguishes synchronous metastases from metachronous metastases. Therefore, further research for biological markers is of significant importance for achieving better outcomes.

In addition, one of the results worth considering in the subgroup analysis was the finding that the Asian population can achieve better outcomes than the western population for RFA patients. Although, to the best of our knowledge, no exact evidence could be found to explain this, considering this observation, we propose the existence of a certain genetic variation among different ethnic groups. This was consistent with the fact that genome-wide polymorphism data have clearly established differences in allele frequency among continental regions (38). For the influence of gene mutation on CRLM, previous studies had demonstrated that KRAS mutation was associated with worse disease-free and overall survival following CRLM resection (39–41). However, previous reports showed that CRLM patients in Asian countries have similar KRAS mutation frequency when compared with those in western countries, and the morbidity and mortality of colorectal cancer in Asian countries were different from those in Western countries (42–44). Considering these facts, the result related to certain ethnic groups should only be used to generate a hypothesis that other genes, except the KRAS gene, may affect the outcomes for CRLM patients, which will be investigated in future research.

Of course, this meta-analysis has several limitations. First, all the included studies were retrospectively performed, which were susceptible to several biases. Second, significant heterogeneity was noticed, although the random effect model was used to compensate for part of the interstudy heterogeneity. In addition, the subgroup analysis in the adjuvant chemotherapy and RFA route should be interpreted with caution, which was mainly due to the failure of the meta-regression process to confirm the subgroup analysis results. In addition, the high-quality randomized controlled trails should be needed to resolve this problem and provide us with much more sound clinical evidences. Finally, publication bias remains to be a main concern; the Begg rank correlation for studies that involved comparative studies about therapeutic efficacy between RFA and LR suggested the presence of publication bias in 1-year PFS and 5-year OS. As we all know, articles with negative results were much more difficult to be published, and the majority of the included studies were from the surgery department; thus, the therapeutic efficacy of LR may be overvalued to some extent. In addition, although we tried to search for more relevant studies, the included number of studies may still be insufficient.

In conclusion, although LR was superior to RFA in the treatment of solitary CRLM in the meta-analysis, the subgroup analysis and meta-regression showed that the therapeutic efficacy of RFA was equivalent to that of LR in solitary CRLM, even when conditions were limited to tumors of $\leq$3 cm and fewer synchronous metastases in the publication year 2011–2018. Meanwhile, RFA provided lower rates of morbidities when compared with LR. In addition, further explanation should be interpreted through high-quality RCTs.

DATA AVAILABILITY STATEMENT

All datasets generated for this study are included in the article/supplementary material.

AUTHOR CONTRIBUTIONS

The authors were responsible for the study design, data collection and analysis, preparation of the manuscript,

and the final publishing decision. YK and YW designed the study, made a critical assessment, and had overall responsibility for this study. WH and JB conducted the literature review and data extraction, performed the statistical analysis, interpreted the statistical results, and wrote the manuscript. All authors read and approved the final manuscript.

FUNDING

This research was supported by Beijing Municipal Science & Technology Commission (Grant no. Z151100004015186), the Capital Health Research and Development of Special (Grant no. 2020-2-2152), and the Fellowship of China postdoctoral science Foundation (Grant no. 2020M670065).

REFERENCES

1. Torre LA, Bray F, Siegel RL, Ferlay J, Lortet-Tieulent J, Jemal A. Global cancer statistics, 2012. *Cancer J Clin.* (2015) 65:87–108. doi: 10.3322/caac.21262
2. Bray F, Ferlay J, Soerjomataram I, Siegel RL, Torre LA, Jemal A. Global cancer statistics 2018: GLOBOCAN estimates of incidence and mortality worldwide for 36 cancers in 185 countries. *Cancer J Clin.* (2018) 68:394–424. doi: 10.3322/caac.21492
3. Ruers T, Van Coevorden F, Punt CJA, Pierie J-PEN, Borel-Rinkes I, Ledermann JA, et al. Local treatment of unresectable colorectal liver metastases: results of a randomized phase II trial. *J Natl Cancer Inst.* (2017) 109:15. doi: 10.1093/jnci/djx015
4. Adam R, Yi B, Innominato PF, Barroso E, Laurent C, Giuliante F, et al. Resection of colorectal liver metastases after second-line chemotherapy: is it worthwhile? A LiverMetSurvey analysis of 6415 patients. *Eur J Cancer.* (2017) 78:7–15. doi: 10.1016/j.ejca.2017.03.009
5. Bengmark S, Hafstrom L. The natural history of primary and secondary malignant tumors of the liver. I. The prognosis for patients with hepatic metastases from colonic and rectal carcinoma by laparotomy. *Cancer.* (1969) 23:198–202. doi: 10.1002/1097-0142(196901)23:1<198::aid-cncr2820230126>3.0.co;2-j
6. Adam R, Hoti E, Folprecht G, Benson AB. Accomplishments in 2008 in the management of curable metastatic colorectal cancer. *Gastrointest Cancer Res.* (2009) 3:S15–22.
7. Ruers T, Punt C, Van Coevorden F, Pierie JP, Borel-Rinkes I, Ledermann JA, et al. Radiofrequency ablation combined with systemic treatment versus systemic treatment alone in patients with non-resectable colorectal liver metastases: a randomized EORTC Intergroup phase II study (EORTC 40004). *Ann Oncol.* (2012) 23:2619–26. doi: 10.1093/annonc/mds053
8. Song KD, Lim HK, Rhim H, Lee MW, Kim YS, Lee WJ, et al. Repeated hepatic resection versus radiofrequency ablation for recurrent hepatocellular carcinoma after hepatic resection: a propensity score matching study. *Radiology.* (2015) 275:599–608. doi: 10.1148/radiol.14141568
9. Ahmed M, Brace CL, Lee FT Jr, Goldberg SN. Principles of and advances in percutaneous ablation. *Radiology.* (2011) 258:351–69. doi: 10.1148/radiol.10081634
10. Gervais DA, McGovern FJ, Arellano RS, McDougal WS, Mueller PR. Renal cell carcinoma: clinical experience and technical success with radio-frequency ablation of 42 tumors. *Radiology.* (2003) 226:417–24. doi: 10.1148/radiol.2262012062
11. Frericks BB, Ritz JP, Roggan A, Wolf KJ, Albrecht T. Multipolar radiofrequency ablation of hepatic tumors: initial experience. *Radiology.* (2005) 237:1056–62. doi: 10.1148/radiol.2373041104
12. Chen MH, Yang W, Yan K, Zou MW, Solbiati L, Liu JB, et al. Large liver tumors: protocol for radiofrequency ablation and its clinical application in 110 patients–mathematic model, overlapping mode, and electrode placement process. *Radiology.* (2004) 232:260–71. doi: 10.1148/radiol.2321030821
13. Chen MS, Li JQ, Zheng Y, Guo RP, Liang HH, Zhang YQ, et al. A prospective randomized trial comparing percutaneous local ablative therapy and partial hepatectomy for small hepatocellular carcinoma. *Ann Surg.* (2006) 243:321–8. doi: 10.1097/01.sla.0000201480.65519.b8
14. Forner A, Llovet JM, Bruix J. Hepatocellular carcinoma. *Lancet.* (2012) 379:1245–55. doi: 10.1016/S0140-6736(11)61347-0
15. Oshowo A, Gillams A, Harrison E, Lees WR, Taylor I. Comparison of resection and radiofrequency ablation for treatment of solitary colorectal liver metastases. *Br J Surg.* (2003) 90:1240–3. doi: 10.1002/bjs.4264
16. Zhao W, Wang L, Han H, Jin K, Lin N, Guo T, et al. 1B50-1, a mAb raised against recurrent tumor cells, targets liver tumor-initiating cells by binding to the calcium channel alpha2delta1 subunit. *Cancer Cell.* (2013) 23:541–56. doi: 10.1016/j.ccr.2013.02.025
17. Hur H, Ko YT, Min BS, Kim KS, Choi JS, Sohn SK, et al. Comparative study of resection and radiofrequency ablation in the treatment of solitary colorectal liver metastases. *Am J Surg.* (2009) 197:728–36. doi: 10.1016/j.amjsurg.2008.04.013
18. Ricci-Vitiani L, Lombardi DG, Pilozzi E, Biffoni M, Todaro M, Peschle C, et al. Identification and expansion of human colon-cancer-initiating cells. *Nature.* (2007) 445:111–5. doi: 10.1038/nature05384
19. Abdalla EK, Vauthey JN, Ellis LM, Ellis V, Pollock R, Broglio KR, et al. Recurrence and outcomes following hepatic resection, radiofrequency ablation, and combined resection/ablation for colorectal liver metastases. *Ann Surg.* (2004) 239:818–25; discussion 25–7. doi: 10.1097/01.sla.0000128305.90650.71
20. Pattabiraman DR, Bierie B, Kober KI, Thiru P, Krall JA, Zill C, et al. Activation of PKA leads to mesenchymal-to-epithelial transition and loss of tumor-initiating ability. *Science.* (2016) 351:aad3680. doi: 10.1126/science.aad3680
21. Kim KH, Yoon YS, Yu CS, Kim TW, Kim HJ, Kim PN, et al. Comparative analysis of radiofrequency ablation and surgical resection for colorectal liver metastases. *J Korean Surg Soc.* (2011) 81:25–34. doi: 10.4174/jkss.2011.81.1.25
22. Ko S, Jo H, Yun S, Park E, Kim S, Seo HI. Comparative analysis of radiofrequency ablation and resection for resectable colorectal liver metastases. *World J Gastroenterol.* (2014) 20:525–31. doi: 10.3748/wjg.v20.i2.525
23. Li N, Zhu Y. Targeting liver cancer stem cells for the treatment of hepatocellular carcinoma. *Therap Adv Gastroenterol.* (2019) 12:1756284818821560. doi: 10.1177/1756284818821560
24. McKay A, Fradette K, Lipschitz J. Long-term outcomes following hepatic resection and radiofrequency ablation of colorectal liver metastases. *HPB Surg.* (2009) 2009:346863. doi: 10.1155/2009/346863
25. Aloia TA, Vauthey JN, Loyer EM, Ribero D, Pawlik TM, Wei SH, et al. Solitary colorectal liver metastasis: resection determines outcome. *Arch Surg.* (2006) 141:460–6; discussion 6–7. doi: 10.1001/archsurg.141.5.460
26. Berber E, Tsinberg M, Tellioglu G, Simpfendorfer CH, Siperstein AE. Resection versus laparoscopic radiofrequency thermal ablation of solitary colorectal liver metastasis. *J Gastrointest Surg.* (2008) 12:1967–72. doi: 10.1007/s11605–008-0622–8
27. Lee H, Heo JS, Cho YB, Yun SH, Kim HC, Lee WY, et al. Hepatectomy vs radiofrequency ablation for colorectal liver metastasis: a propensity score analysis. *World J Gastroenterol.* (2015) 21:3300–7. doi: 10.3748/wjg.v21.i11.3300
28. Takahashi H, Akyuz M, Kahramangil B, Kose E, Aucejo F, Fung J, et al. A comparison of the initial cost associated with resection versus laparoscopic radiofrequency ablation of small solitary colorectal liver metastasis. *Surg Laparosc Endosc Percutan Tech.* (2018) 28:371–4. doi: 10.1097/sle.0000000000000577
29. White RR, Avital I, Sofocleous CT, Brown KT, Brody LA, Covey A, et al. Rates and patterns of recurrence for percutaneous radiofrequency ablation and open wedge resection for solitary colorectal liver metastasis. *J Gastrointest Surg.* (2007) 11:256–63. doi: 10.1007/s11605-007-0100-8
30. Han Y, Yan D, Xu F, Li X, Cai JQ. Radiofrequency ablation versus liver resection for colorectal cancer liver metastasis: an updated systematic review and meta-analysis. *Chin Med J.* (2016) 129:2983–90. doi: 10.4103/0366-6999.195470

31. Nijkamp MW, van der Bilt JD, de Bruijn MT, Molenaar IQ, Voest EE, van Diest PJ, et al. Accelerated perinecrotic outgrowth of colorectal liver metastases following radiofrequency ablation is a hypoxia-driven phenomenon. *Ann Surg.* (2009) 249:814–23. doi: 10.1097/SLA.0b013e3181a38ef5
32. von Breitenbuch P, Kohl G, Guba M, Geissler E, Jauch KW, Steinbauer M. Thermoablation of colorectal liver metastases promotes proliferation of residual intrahepatic neoplastic cells. *Surgery.* (2005) 138:882–7. doi: 10.1016/j.surg.2005.05.006
33. European Association for the Study of the Liver. Electronic address eee, European Association for the Study of the L. EASL clinical practice guidelines: management of hepatocellular carcinoma. *J Hepatol.* (2018) 69:182–236. doi: 10.1016/j.jhep.2018.03.019
34. Omata M, Cheng AL, Kokudo N, Kudo M, Lee JM, Jia J, et al. Asia-Pacific clinical practice guidelines on the management of hepatocellular carcinoma: a 2017 update. *Hepatol Int.* (2017) 11:317–70. doi: 10.1007/s12072-017-9799-9
35. Song P, Cai Y, Tang H, Li C, Huang J. The clinical management of hepatocellular carcinoma worldwide: a concise review and comparison of current guidelines from 2001 to 2017. *Biosci Trends.* (2017) 11:389–98. doi: 10.5582/bst.2017.01202
36. Manfredi S, Lepage C, Hatem C, Coatmeur O, Faivre J, Bouvier AM. Epidemiology and management of liver metastases from colorectal cancer. *Ann Surg.* (2006) 244:254–9. doi: 10.1097/01.sla.0000217629.94941.cf
37. Adam R, de Gramont A, Figueras J, Kokudo N, Kunstlinger F, Loyer E, et al. Managing synchronous liver metastases from colorectal cancer: a multidisciplinary international consensus. *Cancer Treat Rev.* (2015) 41:729–41. doi: 10.1016/j.ctrv.2015.06.006
38. Henn BM, Gravel S, Moreno-Estrada A, Acevedo-Acevedo S, Bustamante CD. Fine-scale population structure and the era of next-generation sequencing. *Hum Mol Genet.* (2010) 19:R221–6. doi: 10.1093/hmg/ddq403
39. Stremitzer S, Stift J, Gruenberger B, Tamandl D, Aschacher T, Wolf B, et al. KRAS status and outcome of liver resection after neoadjuvant chemotherapy including bevacizumab. *Br J Surg.* (2012) 99:1575–82. doi: 10.1002/bjs.8909
40. Karagkounis G, Torbenson MS, Daniel HD, Azad NS, Diaz LA, Jr., et al. Incidence and prognostic impact of KRAS and BRAF mutation in patients undergoing liver surgery for colorectal metastases. *Cancer.* (2013) 119:4137–44. doi: 10.1002/cncr.28347
41. Vauthey JN, Zimmitti G, Kopetz SE, Shindoh J, Chen SS, Andreou A, et al. RAS mutation status predicts survival and patterns of recurrence in patients undergoing hepatectomy for colorectal liver metastases. *Ann Surg.* (2013) 258:619–26; discussion 26–7. doi: 10.1097/SLA.0b013e3182a5025a
42. Favoriti P, Carbone G, Greco M, Pirozzi F, Pirozzi RE, Corcione F. Worldwide burden of colorectal cancer: a review. *Updates Surg.* (2016) 68:7–11. doi: 10.1007/s13304-016-0359-y
43. Li ZZ, Wang F, Zhang ZC, Wang F, Zhao Q, Zhang DS, et al. Mutation profiling in chinese patients with metastatic colorectal cancer and its correlation with clinicopathological features and anti-EGFR treatment response. *Oncotarget.* (2016) 7:28356–68. doi: 10.18632/oncotarget.8541
44. Modest DP, Ricard I, Heinemann V, Hegewisch-Becker S, Schmiegel W, Porschen R, et al. Outcome according to KRAS-, NRAS- and BRAF-mutation as well as KRAS mutation variants: pooled analysis of five randomized trials in metastatic colorectal cancer by the AIO colorectal cancer study group. *Ann Oncol.* (2016) 27:1746–53. doi: 10.1093/annonc/mdw261

Conflict of Interest: The authors declare that the research was conducted in the absence of any commercial or financial relationships that could be construed as a potential conflict of interest.

frontiers in Oncology

MINI REVIEW
published: 25 January 2021
doi: 10.3389/fonc.2020.551622

Diagnostic Performance of Theranostic Radionuclides Used in Transarterial Radioembolization for Liver Cancer

Rou Li[1,2], *Danni Li*[1], *Guorong Jia*[1], *Xiao Li*[1], *Gaofeng Sun*[1]* *and Changjing Zuo*[1,2]*

[1] Department of Nuclear Medicine, Shanghai Changhai Hospital, Shanghai, China, [2] School of Medical Imaging, Xuzhou Medical University, Xuzhou, China

Primary liver tumor with hepatocellular carcinoma accounting for 75–80% of all such tumors, is one of the global leading causes of cancer-related death, especially in cirrhotic patients. Liver tumors are highly hypervascularized *via* the hepatic artery, while normal liver tissues are mainly supplied by the portal vein; consequently, intra-arterially delivered treatment, which includes transarterial chemoembolization (TACE) and transarterial radioembolization (TARE), is deemed as a palliative treatment. With the development of nuclear technology and radiochemistry, TARE has become an alternative for patients with hepatic cancer, especially for patients who failed other therapies, or for patients who need tumor downstaging treatment. In practice, some radionuclides have suitable physicochemical characteristics to act as radioactive embolism agents. Among them, ^{90}Y emits β rays only and is suitable for bremsstrahlung single photon emission computed tomography (BS SPECT) and positron emission tomography (PET); meanwhile, some others, such as ^{131}I, ^{153}Sm, ^{166}Ho, ^{177}Lu, ^{186}Re, and ^{188}Re, emit both β and γ rays, enabling embolism beads to play a role in both therapy and single photon emission computed tomography (SPECT) imaging. During TARE, concomitant imaging provide additive diagnostic information and help to guide the course of liver cancer treatment. Therefore, we review the theranostic radionuclides that have been used or could potentially be used in TARE for liver cancer and focus on the clinical benefits of diagnostic applications, including real-time monitoring of embolism beads, evaluating irradiation dose, predicting therapy effects, and corresponding adjustments to TARE.

Keywords: liver cancer, diagnostic performance, theranostic radionuclides, transarterial radioembolization, nuclear imaging

OPEN ACCESS

Edited by:
An Liu,
City of Hope National Medical Center, United States

Reviewed by:
Bilgin Kadri Aribas,
Bülent Ecevit University, Turkey
Ning Wen,
Henry Ford Health System, United States

***Correspondence:**
Gaofeng Sun
sgf1256@163.com
Changjing Zuo
changjing.zuo@qq.com

Specialty section:
This article was submitted to Radiation Oncology, a section of the journal Frontiers in Oncology

Received: *14 April 2020*
Accepted: *07 December 2020*
Published: *25 January 2021*

Citation:
Li R, Li D, Jia G, Li X, Sun G and Zuo C (2021) Diagnostic Performance of Theranostic Radionuclides Used in Transarterial Radioembolization for Liver Cancer. Front. Oncol. 10:551622. doi: 10.3389/fonc.2020.551622

INTRODUCTION

The primary liver tumor often occurs in patients with liver cirrhosis, with hepatitis virus being the most common risk factor for liver cirrhosis (1). As the most common type of liver cancer, hepatocellular carcinoma (HCC) is the fifth most common cancer worldwide and the second leading cause of cancer-related mortality (2).

Nowadays, there are many options for the treatment of liver cancer according to the guidelines in the Barcelona Clinic Liver Cancer (BCLC) algorithm (3). However, because of the underlying liver dysfunction and its often-late diagnosis, only approximately 30% of patients when initially diagnosed are eligible for curative treatments (resection, percutaneous ablation, etc). Additionally, due to locally advanced diseases, poor liver function, or additional comorbidities, recurrence or metastasis are common after major curative treatment. Hence, various palliative treatments are considered for intermediate-advanced stage liver cancer, especially in inoperable cases. Taking advantage of the fact that the tumor is supplied by the hepatic artery while the surrounding normal liver tissue is mainly supplied by the portal system, transarterial radioembolization (TARE) appears as one of the attractive treatment options.

TARE intra-arterially delivers therapeutic radioactive agents to the tumor, which can achieve embolization of the feeding artery and radiation killing effect on tumor cells simultaneously during the treatment of liver cancer. Different from external radiotherapy, TARE limits systemic irradiation and preserves the healthy liver to a maximum extent. Additionally, the incidence of postembolization syndrome in TARE is relatively rare and mild compared to TACE (transarterial chemoembolization). TARE has been demonstrated to be feasible in treating patients at different stages or with postoperative recurrence, and serves as a downstaging strategy prior or as a bridge to transplantation (4). Meanwhile, TARE is an alternative treatment for those may be contraindication to other treatments.

Prior to TARE, structural imaging, such as computed tomography (CT) or magnetic resonance (MR), shows the size and location of the tumor and its relationship with the surrounding tissue. Besides, x-ray angiography is also vital before TARE, which can provide the blood supply of the tumor and the travel, distribution and variation of blood vessels. Single photon emission computed tomography/computed tomography (SPECT/CT) is also common imaging method during TARE. All these imaging technologies are helpful to guide treatment planning (e.g., the method of delivery, suitable treatment dose) and even predict treatment efficacy. After injecting the theranostic radionuclide into the hepatic artery, therapeutic effect is achieved by internal exposure around the tumor. Meanwhile, real-time or post-therapeutic nuclear imaging, such as SPECT/CT, provides information on verification of treatment delivery, the biodistribution of radioconjugates, integral radiation dose at tumor site and organs of interest (lung, liver, thyroid gland, etc) and prediction of treatment outcome. Later post-therapeutic imaging mainly observes the therapeutic effect on the tumor and monitors other organs for complications. Furthermore, positron emission tomography/computed tomography (PET/CT) is also a potential imaging modality for TARE. It realizes functional imaging before and after treatment by showing the glucose metabolism of the tumor and sensitively finding metastasis. Hence, imaging plays a key role in drug development and clinical evaluation, and is conducive to developing adaptive TARE plans according to the metabolic mode.

Theranostic radionuclides integrating imaging and treatment during radioembolization are the most important component of TARE for liver cancer. Based on how TARE works, radionuclides that emit α rays are not suitable because of their pathlengths are relatively short and thus have a limited range in tissue. Radionuclides emiting β rays can provide substantial radiation therapy for liver tumors due to their pathlengths ranging from millimeters to centimeters. Meanwhile, emitted γ rays are helpful in monitoring embolization beads using nuclear imaging. Considering the therapeutic purpose, the half-life of nuclides ranging from one to several days is suitable, allowing the tumor to be exposed to sufficient radiation while avoiding radiation damage in the process of excretion. Thus far, only two ^{90}Y based microspheres (MSs) and ^{131}I-lipiodol are approved for clinical use, while many others are still in the pre-clinical or basic research stage. Recently, the use of additional theranostic nuclides in TARE has been explored. **Table 1** summarizes the critical characteristics (nuclear property and imaging type) of theranostic nuclides that have been used and those that have shown potential in TARE for hepatic cancer. At the same time, the theranostic effects, especially the diagnostic performance of those theranostic radionuclides will be summarized by nuclides and presented here. Among them, ^{90}Y is the most important.

YTTRIUM-90

Yttrium-90, which has favorable physicochemical characteristics, is presently the most widely used nuclide for TARE of liver cancer clinically. Yttrium-90 is a pure β emitter and has a half-life of 64.2 h. The average energy of β emission is 0.937 MeV with a mean tissue penetration of 2.5 mm. High energy, short tissue penetration distance and relatively short half-life make ^{90}Y a suitable nuclide in TARE. Compared with other radionuclide compounds, ^{90}Y-labeled MSs (^{90}Y-MSs) are already clinically available for liver cancer in some countries. The two currently commercially available ^{90}Y-MS products are glass MSs (TheraSphere) and resin MSs (SIR-Spheres). Because of the different physical and chemical properties, the treatment dose calculation for ^{90}Y-MS TARE differs significantly according to the MS type (5).

Blood supply and hepatic collateral circulation of tumor are essential for the efficacy and safety of treatment. Current clinical ^{90}Y-MS BS SPECT (bremsstrahlung single photon emission computed tomography) is hindered by image quality, while ^{90}Y-MS PET is extremely challenging due to low activity concentrations in the lungs and the low positron yield of ^{90}Y. Hence, ^{99m}Tc-MAA (Technetium-99m macroaggregated albumin) is a surrogate of ^{90}Y for pre-treatment imaging. Intra-arterially delivery of ^{99m}Tc-MAA is able to simulate the distribution of therapeutic drugs in the liver, by measuring the radiation intensity of cancerous and non-cancerous liver tissue respectively, the ratio of tumor/non-tumor (T/NT) can be calculated more accurately (6). That provides a quantitative index for evaluating the abundance of tumor blood supply and the ability of cancer tissue to absorb therapeutic drugs through hepatic artery. Patients should undergo ^{99m}Tc-MAA examination before ^{90}Y-MS TARE, which offers important preprocedural information. In ^{99m}Tc-MAA SPECT/CT, ^{99m}Tc-MAA (4–5 mCi) is injected into the hepatic artery to assess extra-hepatic depositions and lung shunting, and can provide the calculation of the lung shunt

TABLE 1 | Major radionuclides used for radioembolization of hepatocellular carcinoma.

Radionuclides	Emission and energy (MeV)	Half-life	Maximum tissue penetration (mm)	Imaging type
^{90}Y	β 2.28 (100%) γ/	2.7 d	12	BS SPECT/ PET
^{32}P	β 1.71 (100%) γ/	14.3 d	7.9	BS SPECT/ PET
^{131}I	β 0.607 (99%) γ 0.364 (1%)	8.04 d	2	SPECT
^{188}Re	β 2.12 (71.6%) 1.96 (25.1%) γ 0.155 (15%)	16.9 h	11	SPECT
^{166}Ho	β 1.84 (50.5%) 1.74 (48.7%) γ 0.081 (6.2%) 0.00138(0.93%)	1.1 d	8.7	SPECT/MR
^{177}Lu	β 0.176 (12.2%) 0.497 (78.6%) 0.384 (9.1%) γ 0.113 (6.4%) 0.208 (11%)	6.7 d	2.2	SPECT
^{153}Sm	β 0.81 (20%) 0.71 (30%) 0.64 (50%) γ 0.103 (28%)	46.3 h	3	SPECT
^{186}Re	β 2.13 (70%) 1.98 (26%) γ 0.155 (16.2%) 0.633 (1.6%)	3.8 d	4.5	SPECT

absorbed dose, which guides dosimetry to avoid radiation pneumonitis. Moreover, accurate superselective angiography should be performed to evaluate the targeted vascular territory and anatomic variants or extra-hepatic vessels should accept prophylactic embolization, which can avoid ectopic embolization of non-targeted organs. However, the concordance between ^{99m}Tc-MAA and ^{90}Y-MSs remains controversial. Many studies have reported both similarity (7) and differences (8) between ^{99m}Tc-MAA and ^{90}Y-MSs uptake. The inconsistent concordance may be due to several factors (the different size, shape, and number of MAA relative to microspheres, flow dynamics during delivery, etc), for which the post-therapy images of ^{90}Y-activity distribution is considered appropriate to determine the tumor dose-response. Apart from SPECT/CT, CT or MR imaging are also be used to assess the volume, location, and relationship with surrounding hepatic tissues of the tumor before TARE.

^{99m}Tc-MAA scanning and superselective angiography are often performed before ^{90}Y-MS TARE to guide dosimetry, although accumulating evidence has improved the safety and efficacy of using radioembolization with ^{90}Y-labeled resin or glass MSs for the management of hepatic tumors (9). A study of 1,652 patients (1,124 TACE, 528 ^{90}Y-TARE) showed that ^{90}Y-MS TARE increased the 2-year overall survival (OS) rates relative to the observational subgroup and resulted in better objective response (OR) rates than treatment with TACE. Furthermore, a lower risk of adverse events was observed in ^{90}Y-TARE than in TACE (10). Many studies have demonstrated that ^{90}Y-MS TARE is an effective choice and results in significantly fewer severe adverse events when treating HCC patients with portal vein thrombosis (PVT), which is a contraindication for most traditional therapies (11).

For post-treatment imaging, compared with the majority of the radionuclides used in TARE, ^{90}Y is a pure β emitter and lacks discrete-energy photon emissions, such as γ rays and/or characteristic fluorescence x-rays (12). The β particles emitted by ^{90}Y produce secondary bremsstrahlung radiation, which may be imaged to locate the ^{90}Y-MSs. Commonly, BS SPECT is used after radioembolization to exclude extra-hepatic activity deposition and to assess intra-hepatic MSs distribution. Ahmadzadehfar et al. performed BS SPECT/CT imaging on 188 patients who accepted ^{90}Y-MS TARE 24 h prior, to assess the capability of BS SPECT/CT in detecting and positioning of extrahepatic accumulation (gastrointestinal complications). Gastroduodenoscopy served as reference standards. The results showed that the positive predictive values, sensitivity, specificity and the accuracy of BS SPECT/CT were 100, 87, 100, and 99%, respectively (13). Furthermore, BS SPECT/CT after radioembolization is beneficial to evaluate tumor dose-response characteristics and predict treatment response for the management of patients (14). Potrebko et al. demonstrated that voxel-based dosimetry for ^{90}Y microsphere therapy allows for quantitative quality assurance of the delivered treatment using deformable image registration, calculated isodose distributions, and dose-volume histograms (DVHs). Since β-radiation emitted by ^{90}Y interacts with body tissues resulting in bremsstrahlung radiation, SPECT/CT has traditionally been regarded as the gold-standard modality to image the biodistribution of this radionuclide. However, the limitations of the BS SPECT image are poor spatial resolution (11–15 mm) and limited quantitative accuracy because of the low photon yield and continuous nature of the BS X-ray spectrum. The absence of some correction techniques leads to a further reduction in the image contrast. Many efforts have been

made to improve BS SPECT/CT imaging qualitatively and quantitatively, in which Monte Carlo simulation is frequently accepted. However, it is not commercially available and cannot be easily implemented clinically (15).

Interestingly, the ^{90}Y decay process is of a very small branching to the excited state of stable ^{90}Zr. The internal pair production (positron) generated during the decay scheme of ^{90}Y allows quantitative monitoring on itself *via* PET (16, 17). Compared with BS SPECT, ^{90}Y PET imaging provides better image quality in contrast and resolution (4–5 mm). Elschot et al. quantitatively demonstrated that the image quality of PET was superior to that of BS SPECT for the assessment of ^{90}Y-MS distribution after radioembolization in a study of estimated liver dose distributions in 5 patients (18) (**Figure 1B**). The **Figure 1A** showed that the PET-based CDVH (cumulative dose-volume histograms) of the spherical region-of-interest followed the true CDVH more closely than the SPECT-based CDVH. Moreover, calculating the tumor dose on imaging may predict the response to the treatment. A study published in 2013 demonstrated that tumor and non-target tissue absorbed dose quantification using ^{90}Y PET was accurate and yielded radiobiologically meaningful dose-response information to guide adjuvant or mitigative action (23). The true definitions of the minimal effective tumor dose and maximum tolerated non-tumor dose remain challenges for each tumor and MS type, and ^{90}Y PET may be a potential solution.

Undoubtedly, ^{90}Y is the most suitable theranostic radionuclide for TARE of liver cancer so far. ^{90}Y, as a pure β emitter, has high energy and relatively small radiation range, which can effectively kill tumor cells while avoiding damage to surrounding healthy tissue, and no requiring subsequent isolation of patients is needed. Although BS SPECT and PET can match the imaging requirements, there are still many unsolved technological issues restricting the accuracy of images and widespread clinical use. For example, low true-coincidence count-rate for positron emission results in relatively longer acquisition times for ^{90}Y PET imaging. Besides, standardization and uniform implementation of reconstruction and correction techniques are urgently needed. The necessity of specialized nuclear reactors and relatively long transportation times to each hospital limit the use of ^{90}Y. Importantly, ^{90}Y is still not be approved and available in many countries, such as in China. Serious complications caused by ectopic embolization of ^{90}Y-MS may also occur, which needs high attention in clinical application.

IODINE-131

The nuclide ^{131}I ($T_{1/2}$ = 8.04d) emits both β and γ rays. Its β particles have a maximum energy of 0.6 MeV and a maximum path length in tissue of 2.3 mm. Utilizing the characteristics of iodine lipiodol, which selectively deposits in nodules of hepatocellular carcinoma, radioactive lipiodol accumulates in cancer tissues and decreases irradiation damage to non-cancer tissues. Hence, ^{131}I-lipiodol was often studied for TARE of liver cancer before. In a representative clinical study of 50 patients, the median survival of patients treated with ^{131}I-lipiodol was 24 weeks longer than that of the untreated group and no radiotoxic effect was found, especially interstitial pneumonia (19) (**Figure 1C**).

In addition to lipiodol, ^{131}I can also be used to label embolism beads, normally in the form of MSs, which are often prepared in stepwise procedures for multiple theranostic applications. Liu et al. incorporated hollow CuS nanoparticles into PLGA (poly lactic-co-glycolic acid) MSs to produce HCuSNPs-loaded MSs, which were then labeled with ^{131}I to form ^{131}I-HCuSNPs-MSs (24). After the intra-arterial embolization with ^{131}I-HCuSNPs-MSs delivered into the hepatic artery of liver tumor-bearing rats, SPECT imaging confirmed that MSs were mainly located in liver tumor and only minimal accumulation was detected in other organs, particularly in the lungs. SPECT imaging findings qualitatively manifested the success of TARE operation and avoidance of damage potentially resulting from the leakage of embolism beads. The follow-up SPECT scan proved that effective embolization lasted for up to 48 h. The predictive results aided understanding of the entire treatment process and prognosis, which was more timely to figure out the primary outcome than traditional follow-up diagnosis, such as blood tests and CT.

Regarding diagnostic performance, ^{131}I-based imaging provides qualitative information on whole-body distribution, including tumor accumulation, and even permits semi-quantitative analysis (25). Becker et al. reported that 7 days after the injection, 61% of ^{131}I-lipiodol was distributed in the liver tumor, 23% was distributed in non-tumoral liver, and 16% was distributed in the lungs, which highlighted that the clinical toxicities of ^{131}I-lipiodol were more commonly affected the lungs (20). More importantly, tumor radioactivity dosimetry helps to define an absorbed dose threshold, especially when the accumulation of the radioactive embolism agent was recorded dynamically (**Figure 1D**). That would predict a therapeutic effect, thus providing guidance for the subsequent therapeutic approach and optimizing the activity to be injected.

There are still some deficiencies in the TARE transformation of ^{131}I. Compared to ^{90}Y, possible extra managements are needed for the patient's excreta (such as urine) due to the longer half-life of ^{131}I. Besides, non-therapeutic rays (γ rays) with high energy and long path length probably damage the surrounding normal tissue. In addition, too many scattered rays produced by ^{131}I lead to relatively low contrast and resolution of SPECT image that are not conducive to quantitative analysis and barely suitable for qualitative analysis. Moreover, defects in terms of *in vivo* stability still exist in ^{131}I compounds produced using iodized oil replacement or labeling methods.

OTHER POTENTIAL THERANOSTIC RADIONUCLIDES FOR TARE

Rhenium-188

^{188}Re is obtained from ^{188}W/^{188}Re generators in a convenient and comparatively cheap way, and its radioactivity yield can recover to 80% at 40 h postelution. The product of ^{188}Re is ^{188}Os by β decay, with a half-life of 16.9 h. ^{188}Re with a shorter half-life and similar energy of β rays compared ^{90}Y, is a promising radionuclide proposed for TARE of hepatic tumors. Similar to

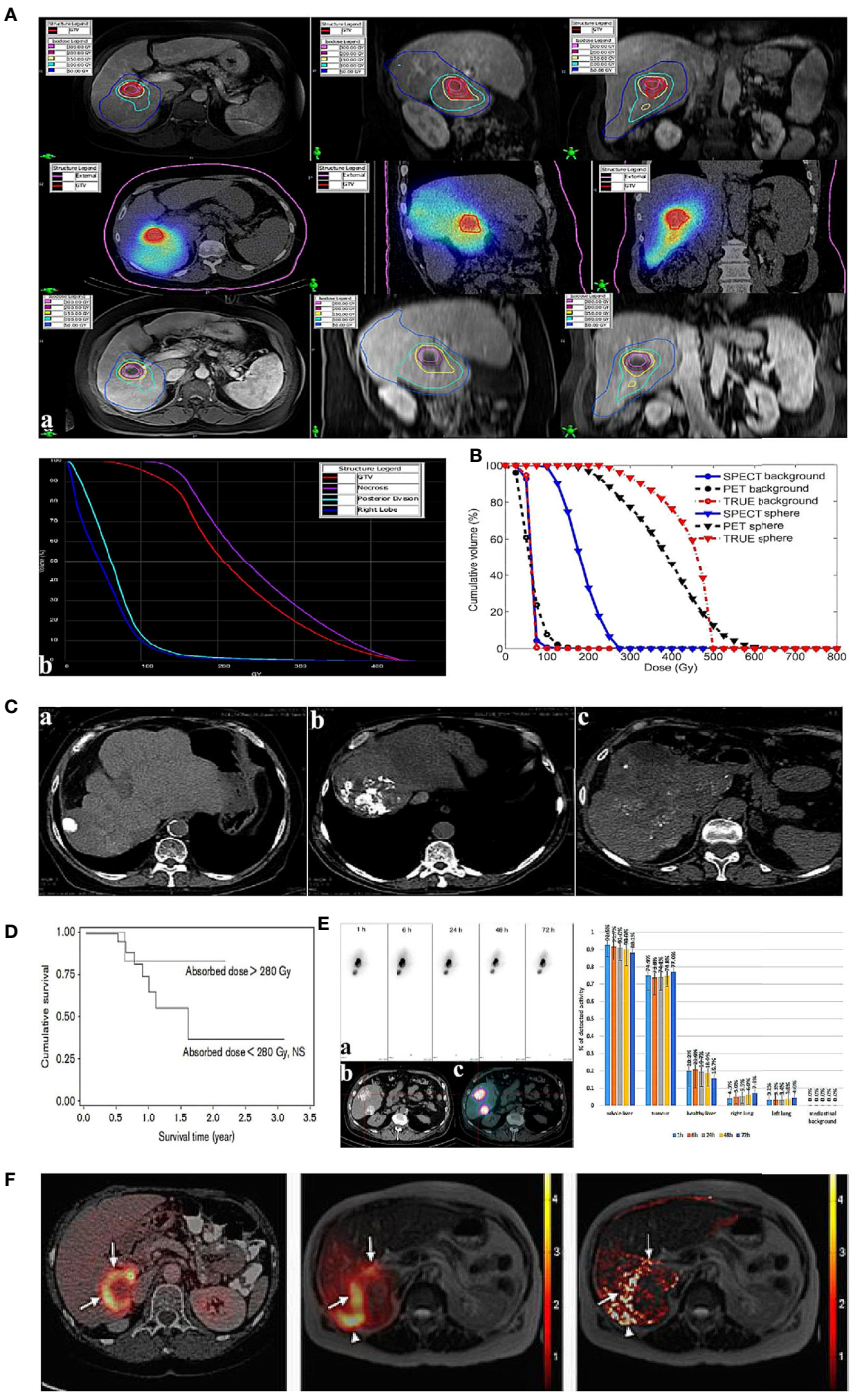

FIGURE 1 | Examples of post-therapeutic imaging of liver tumor. **(A)** The dose of each ROI (regions of interest) in pre-treatment diagnostic MR (top), post-treatment SPECT/CT (middle), and 5-week follow-up MR (bottom) for one patient with HCC (a). Dose-volume histograms of the GTV (gross target volume), necrotic region, posterior division, and right lobe (on the right) (b). Adapted from Potrebko et al. (14). **(B)** CDVH of the phantom (a method of image reconstruction) background ROI and the ROI of the 37-mm diameter sphere. Adapted from Elschot et al. (18). **(C)** Lipiodol tumor accretion at 1 month after intra-arterial injection: complete accretion (49 patients): (a) complete accumulation in 5 patients (10%), (b) partial defect in 15 (31%), (c) faint accumulation in 29 patients (59%). Adapted from Gaultier et al. (19). **(D)** Survival in terms of tumoural absorbed dose (threshold=280 Gy) calculated in tomographic mode. Adapted from Becker et al. (20). **(E)** Intra-arterial injection of ^{188}Re-SSS Lipiodol on hepatocellular carcinoma patients. Adapted from Delaunay et al. (21). The left shows whole-body scintigraphic studies (mean geometric) of patient by (a) SPECT, (b) CT, (c) fused SPECT/CT. The right is the average biodistribution profile of patients treated ^{188}Re-SSS lipiodol by SPECT/CT image. **(F)** The picture shows intrahepatic biodistribution of ^{166}Ho-microspheres on liver tumor patient by ^{18}F-FDG PET/CT, SPECT and MR imaging (from left to right). Adapted from Smits et al. (22).

^{131}I, the γ ray emission of ^{188}Re allows post-therapeutic SPECT imaging.

Early available ^{188}Re embolism agents were the lipiodol conjugates as well. ^{188}Re-chelator mixed with lipiodol, such as ^{188}Re-HDD/lipiodol, ^{188}Re-DEDC/lipiodol, and ^{188}Re-SSS/lipiodol, has been tested in humans to date. Some studies showed that TARE with ^{188}Re-HDD/lipiodol is a safe, effective, and promising method. Meanwhile, ^{188}Re was also used to label MSs as embolism beads. A study of 10 patients (3 patients with unresectable colorectal liver metastases and 7 patients with hepatocellular cancer), who received treatment with ^{188}Re-human serum albumin MSs, displayed considerable survival rates and tolerable toxicity (26). Other reported ^{188}Re-MSs include ^{188}Re-PLGA (27), ^{188}Re-poly(L-lactic acid) (PLLA) (28), ^{188}Re-glass-MSs, and ^{188}Re-resin-MSs.

Regarding diagnostic performance, embolization evaluation and related dosimetry in nuclear imaging are helpful for the treatment plan. In a study of 6 patients with unresectable HCC who accepted intra-arterial ^{188}Re-SSS/lipiodol, whole-body planar scintigraphy and SPECT were used during therapy (21) and revealed curative hepatic uptake; 90.7 ± 1.6% of radioactivity was detected in the liver with 74.9 ± 1.8% of detected radioactivity in the tumor and 9.3 ± 1.6% of radioactivity was detected in the lungs (**Figure 1E**). The average T/NT uptake ratio was 42.7 ± 7.8 on SPECT. These quantitative data provided a definite diagnosis to conclude that ^{188}Re-SSS/lipiodol had satisfactory embolization characteristics, guaranteeing *in vivo* therapeutic application.

Because of its short half-life, much more activities are needed for ^{188}Re than ^{90}Y to achieve a comparable therapeutic effect, which may produce acute radiation damage to normal tissue. Notably, ^{188}Re labeling relies on a relatively complicated reaction, which partially restricts the synthesis of the ^{188}Re embolism agents and clinical transformation.

Holmium-166

^{166}Ho emits high-energy β rays, with a comparatively short half-life (1.1 days) (29). Due to its short half-life, ^{166}Ho is suitable for patients in urgent need of downstaging treatment compared to the longer radiation therapy time of ^{90}Y. ^{166}Ho can be produced by two methods, in a nuclear reactor or by neutron activation of ^{164}Dy; hence its production is both fast and relatively cheap. Additionally, its outstanding advantage over ^{90}Y, ^{131}I, and ^{188}Re is that ^{166}Ho is paramagnetic and emits low-energy γ radiation, which enables the dual MR and SPECT imaging.

^{166}Ho-labeled lipiodol has rarely been reported. Das et al. prepared radiolabeled lipiodol by dispersing ^{166}Ho-oxine complex in lipiodol (30). For *in vivo* evaluation, the imaging studies of ^{166}Ho-lipiodol revealed satisfactory hepatic retention and insignificant uptake was detected in other major organs or tissues except skeleton. ^{166}Ho-MSs were extensively studied. Several ^{166}Ho-MSs have been prepared so far, including glass, resin, phosphate, and polymer MSs, and all of them have shown good prospects for TARE, especially polymer MSs, due to the advantage of near-plasma density, biodegradability, and biocompatibility (31). In a phase I trial including 15 patients with an unresectable and chemorefractory liver tumor, ^{166}Ho-PLLA-MS TARE was implemented in four cohorts of three to six patients, injecting 20 Gy, 40 Gy, 60 Gy, and 80 Gy, respectively. At 6 weeks, treatment response was one patient with partial response, seven with stable disease and seven with disease progression (32). Similarly, ^{166}Ho-chitosan MSs and ^{166}Ho-alginate MSs (33) that were prepared for radioembolization behaved feasibly and safely.

What is noteworthy is that, due to favorable nuclear imaging characteristics of ^{166}Ho, a scout dose (250 MBq) of ^{166}Ho is used as an alternative before ^{166}Ho-MS TARE, which is superior in calculating the lung shunt fraction compared to ^{99m}Tc MAA (34). Considering controversy over the concordance of ^{99m}Tc MAA and ^{90}Y-MSs, ^{166}Ho itself can be used in pre-treatment imaging, for which pre-treatment imaging planning dosimetry could potentially be more accurate. Regarding diagnostic performance, taking advantage of both SPECT and MR imaging, the estimated radiation absorbed dose could be evaluated more precisely in ^{166}Ho-complex liver radioembolization. In 2013, Smits et al. performed a phase I clinical trial to investigate the feasibility of quantitative imaging of ^{166}Ho radioembolization in 15 patients with unresectable liver cancer based on SPECT and MR imaging (22). The gross comparison yielded a strong correlation between MR and SPECT imaging and moderate agreement between the absorbed dose in each segment as evaluated based on MR and SPECT imaging (**Figure 1F**). The median overall T/NT ratio was 1.4 based on SPECT (range, 0.9–2.8) and 1.4 based on MR imaging (range, 1.1–3.1). In 40% patients (6/15), all T/NT ratios ≥1, indicating that dosimetry based on ^{166}Ho-MS SPECT and MR correlated well for the dose in liver segments and tumor tissue. There is no doubt that the use of two imaging modalities allows more informed decision making regarding treatment.

Due to the shorter half-life and lower energy of β rays of ^{166}Ho compared to ^{90}Y, similar to ^{188}Re, a larger administered doses are needed to achieve the dosimetry equivalent to that of ^{90}Y for treatment, which potentially cause acute damage to the surrounding normal tissue.

Lutecium-177

^{177}Lu, a popular theranostic nuclide in clinical studies and recently applied in many contexts, may also be the promising radionuclide in TARE for liver cancer treatment. ^{177}Lu has a similar half-life to ^{90}Y but emits relatively low energy β rays, which limits the radiation exposure to surrounding tissues. Regarding diagnostic performance, emitted γ rays are convenient for positioning observation and radiation dosimetry. As a potential theranostic radionuclide, ^{177}Lu has shown to be advantageous in peptide receptor radionuclide therapy (PRRT) of neuroendocrine tumors and peptide radioligand therapy (PRLT) of prostate cancers (35). As a source for TARE, ^{177}Lu still has many issues that need to be addressed in future studies. ^{177}Lu is produced using reactor irradiation, but few sources of supply and relatively high cost limit its broad application now.

Samarium-153

^{153}Sm emits both β and γ rays, meeting the requirements for theranostic radionuclides. Recent studies have shown that the absorbed doses of ^{153}Sm-labeled MSs in all organs can be

controlled below 1 Gy and are safe for surrounding healthy tissues (36). Due to limited reports, its therapeutic potential in cancer treatment has not been widely studied, and its diagnostic performance is still not clear.

Rhenium-186

^{186}Re has an appropriate half-life and emits both β and γ rays. At present, ^{186}Re is clinically used to treat bone metastases caused by prostate cancer, rarely used in TARE for liver cancer. Due to its shared chemical properties and referential experience in embolism agent development with ^{188}Re, ^{186}Re is likely to be an ideal nuclide for TARE.

CONCLUSION

The incidence of liver cancer is increasing worldwide; nevertheless, effective therapeutic options are limited, and recurrence is common after preferred suitable treatment. Although TARE is not included in the BCLC staging system guidelines, current ongoing randomized clinical trials suggest that TARE is a safe, feasible, and palliative treatment for liver cancer, especially when other conventional treatments have failed. In some cases, where there may be contraindications for other treatments, TARE will be a safe and effective choice. It can achieve a similar or higher overall survival rate and slow down the progression of the disease compared to other routine treatments in the reported literature. Theranostic radionuclides in TARE allow for controlled high radiation doses to be supplied to hepatic tumors while the adjacent liver is relatively spared. In the meantime, diagnostic performance is attractive in the course of treatment. The qualitative or quantitative detection of effective embolization promotes the development of radioactive embolic agents, and assessment of the accumulated dose can guide the course of treatment using post-treatment partial or full body scan. In fact, due to the differences in the supply of nuclides around the world, the current status of clinical application of each radionuclide is not the same. In future, technical improvements and clinical studies are needed to promote the use of radionuclides in TARE. In terms of technology, the technique of radionuclide labeling, efficiency and technology of the acquisition of β and γ rays, and technology of image reconstruction all could be improved and developed for better diagnostic and therapeutic effect. In addition, besides ^{90}Y, other potential nuclides (^{166}Ho, ^{177}Lu, etc) still lack adequate clinical studies and applications for TARE.

Furthermore, except for theranostic radionuclides, embolism agents are also being widely developed and studied. Various new drug-eluting beads (such as, HepaSpheres, CalliSpheres, TANDEM, etc) have obtained certain verification in clinical trials. Natural biological materials, silk fibroin, is proposed to become a potential embolism agent for the treatment of liver cancer and still in basic research stage. In a word, future efforts should be aimed at personalizing TARE therapy depending on the characteristics of different theranostic radionuclides and embolism agents, which making TARE a more effective and safe treatment for liver cancer.

AUTHOR CONTRIBUTIONS

RL wrote the manuscript. RL, DL and GJ were responsible for searching related literature. XL, GS, and CZ were involved in revisions and proof-reading. All authors contributed to the article and approved the submitted version.

FUNDING

This work was funded by the National Natural Science Foundation of China (81471714 and 81871390) and National Natural Science Foundation Youth Project (81701761).

REFERENCES

1. Gomaa AI, Khan SA, Toledano MB, Waked I, Taylor-Robinson SD. Hepatocellular carcinoma: epidemiology, risk factors and pathogenesis. *World J Gastroenterol* (2008) 14(27):4300–8. doi: 10.3748/wjg.14.4300
2. Ferlay J, Soerjomataram I, Dikshit R, Eser S, Mathers C, Rebelo M, et al. Cancer incidence and mortality worldwide: sources, methods and major patterns in GLOBOCAN 2012. *Int J Cancer* (2015) 136(5):E359–86. doi: 10.1002/ijc.29210
3. Bruix J, Sherman M. Management of hepatocellular carcinoma: an update. *Hepatology* (2011) 53(3):1020–2. doi: 10.1002/hep.24199
4. Woodall CE, Scoggins CR, Ellis SF, Tatum CM, Hahl MJ, Ravindraet KV, et al. Is selective internal radioembolization safe and effective for patients with inoperable hepatocellular carcinoma and venous thrombosis? *J Am Coll Surg* (2009) 208(3):375–82. doi: 10.1016/j.jamcollsurg.2008.12.009
5. Saini A, Wallace A, Alzubaidi S, Knuttinen MG, Naidu S, Sheth R, et al. History and Evolution of Yttrium-90 Radioembolization for Hepatocellular Carcinoma. *J Clin Med* (2019) 8(1):55. doi: 10.3390/jcm8010055
6. Camacho JC, Kokabi N, Xing M, Schuster DM, Kim HS. PET Response Criteria for Solid Tumors Predict Survival at Three Months After Intra-Arterial Resin-Based ^{90}Yttrium Radioembolization Therapy for Unresectable Intrahepatic Cholangiocarcinoma. *Clin Nucl Med* (2014) 39:944–50. doi: 10.1097/RLU.0000000000000557
7. Chiesa C, Mira M, Maccauro M, Spreafico C, Romito R, Morosi C, et al. Radioembolization of hepatocarcinoma with ^{90}Y glass microspheres: development of an individualized treatment planning strategy based on dosimetry and radiobiology. *Eur J Nucl Med Mol Imaging* (2015) 42 (11):1718–38. doi: 10.1007/s00259-015-3068-8
8. Haste P, Tann M, Persohn S, LaRoche T, Aaron V, Mauxion T, et al. Correlation of Technetium-99m Macroaggregated Albumin and Yttrium-90 Glass Microsphere Biodistribution in Hepatocellular Carcinoma: A Retrospective Review of Pretreatment Single Photon Emission CT and Posttreatment Positron Emission Tomography/CT. *J Vasc Interv Radiol* (2017) 28(5):722–30. doi: 10.1016/j.jvir.2016.12.1221
9. Raoul JL, Boucher E, Rolland Y, Garin E. Treatment of hepatocellular carcinoma with intra-arterial injection of radionuclides. *Nat Rev Gastro Hepat* (2010) 7(1):41–9. doi: 10.1038/nrgastro.2009.202
10. Yang Y, Si T. Yttrium-90 transarterial radioembolization versus conventional transarterial chemoembolization for patients with hepatocellular carcinoma: a systematic review and meta-analysis. *Cancer Biol Med* (2018) 15(3):299–310. doi: 10.20892/j.issn.2095-3941.2017.0177

11. Cho YY, Lee M, Kim HC, Chung JW, Kim YH, Gwak GY, et al. Radioembolization Is a Safe and Effective Treatment for Hepatocellular Carcinoma with Portal Vein Thrombosis: A Propensity Score Analysis. *PloS One* (2016) 11(5):e0154986. doi: 10.1371/journal.pone.0154986
12. Siman W, Mikell JK, Kappadath SC. Practical reconstruction protocol for quantitative ^{90}Y bremsstrahlung SPECT/CT. *Med Phys* (2016) 43(9):5093–103. doi: 10.1118/1.4960629
13. Ahmadzadehfar H, Muckle M, Sabet A, Wilhelm K, Kuhl C, Biermann K, et al. The significance of bremsstrahlung SPECT/CT after yttrium-90 radioembolization treatment in the prediction of extrahepatic side effects. *Eur J Nucl Med Mol Imaging* (2012) 39:309–15. doi: 10.1007/s00259-011-1940-8
14. Potrebko PS, Shridhar R, Biagioli MC, Sensakovic WF, Andl G, Poleszczuk J, et al. SPECT/CT image-based dosimetry for Yttrium-90 radionuclide therapy: Application to treatment response. *J Appl Clin Med Phys* (2018) 19(5):435–43. doi: 10.1002/acm2.12400
15. Du XRY, Ljungberg M, Rault E, Vandenberghe S, Frey EC. Development and evaluation of an improved quantitative ^{90}Y bremsstrahlung SPECT method. *Med Phys* (2012) 39(5):2346–58. doi: 10.1118/1.3700174
16. Kallini JR, Gabr A, Salem R, Lewandowski RJ. Transarterial Radioembolization with Yttrium-90 for the Treatment of Hepatocellular Carcinoma. *Adv Ther* (2016) 33(5):699–714. doi: 10.1007/s12325-016-0324-7
17. Kao YH, Tan EH, Lim KY, Ng CE, Goh SW. Yttrium-90 internal pair production imaging using first generation PET/CT provides high-resolution images for qualitative diagnostic purposes. *Br J Radiol* (1015) 2012) 85:1018–9. doi: 10.1259/bjr/33524085
18. Elschot M, Vermolen BJ, Lam MG, de Keizer B, van den Bosch MAAJ, de Jong HWAM. Quantitative Comparison of PET and Bremsstrahlung SPECT for Imaging the In Vivo Yttrium-90 Microsphere Distribution after Liver Radioembolization. *PloS One* (2013) 8(2):e55742. doi: 10.1371/journal.pone.0055742
19. Gaultier AL, Perret C, Ansquer C, Euge`nec T, Bode´re FK, Frampas E. Intra-arterial injection of ^{131}I-labeled Lipiodol for advanced hepatocellular carcinoma: a 7 years' experience. *Nucl Med Commun* (2013) 34(7):674–81. doi: 10.1097/MNM.0b013e32836141a0
20. Becker S, Laffonta S, Vitry F, Rolland Y, Lecloirec J, Boucher E, et al. Dosimetric evaluation and therapeutic response to internal radiation therapy of hepatocarcinomas using iodine-131-labelled lipiodol. *Nucl Med Commun* (2008) 29(9):815–25. doi: 10.1097/MNM.0b013e32830439c6
21. Delaunay K, Edeline J, Rolland Y, Lepareur N, Laffont S, Palard X, et al. Preliminary results of the Phase 1 Lip-Re I clinical trial: biodistribution and dosimetry assessments in hepatocellular carcinoma patients treated with ^{188}Re-SSS Lipiodol radioembolization. *Eur J Nucl Med Mol I* (2019) 46(7):1506–17. doi: 10.1007/s00259-019-04277-9
22. Smits ML, Elschot M, van den Bosch MA, van de Maat GH, van het Schip AD, Zonnenberg BA, et al. In Vivo Dosimetry Based on SPECT and MR Imaging of ^{166}Ho-Microspheres for Treatment of Liver Malignancies. *J Nucl Med* (2013) 54(12):2093–100. doi: 10.2967/j.113.119768
23. Kao YH, Steinberg JD, Tay YS, Lim GK, Yan J, Townsend DW, et al. Post-radioembolization yttrium-90 PET/CT-part 2: dose-response and tumor predictive dosimetry for resin microspheres. *EJNMMI Res* (2013) 3(1):57. doi: 10.1186/2191-219X-3-57
24. Liu QF, Qian YY, Li PL, Zhang SH, Liu JJ, Sun XG, et al. ^{131}I-labeled copper sulfide-loaded microspheres to treat hepatic tumors via hepatic artery embolization. *Theranostics* (2018) 8(3):785–99. doi: 10.7150/thno.21491
25. Lambert B, Van de Wiele C. Treatment of hepatocellular carcinoma by means of radiopharmaceuticals. *Eur J Nucl Med Mol Imaging* (2005) 32(8):980–9. doi: 10.1007/s00259-005-1859-z
26. Liepe, Brogsitter C, Leonhard J, Wunderlich G, Hliscs R, Pinkert J, et al. Feasibility of High Activity Rhenium-188-Microsphere in Hepatic Radioembolization. *JPN J Clin Oncol* (2007) 37(12):942–50. doi: 10.1093/jjco/hym137
27. Vega JCDL, Esquinas PL, Rodríguez-Rodríguez C, Bokharaei M, Moskalev I, Liu D, et al. Radioembolization of Hepatocellular Carcinoma with Built-In Dosimetry: First in vivo Results with Uniformly-Sized, Biodegradable Microspheres Labeled with ^{188}Re. *Theranostics* (2019) 9(3):868–83. doi: 10.7150/thno.29381
28. Jamre M, Shamsaei M, Erfani M, Sadjadi S, Ghannadi Maragheh M. Preparation and evaluation of ^{188}Re sulfide colloidal nanoparticles loaded biodegradable poly (L-lactic acid) microspheres for radio-embolization therapy. *J Labelled Compd Rad* (2018) 61(8):586–94. doi: 10.1002/jlcr.3627
29. Reinders MTM, Smits MLJ, Roekel CV, Braat AJAT. Holmium-166 Microsphere Radioembolization of Hepatic Malignancies. *Semin Nucl Med* (2019) 49(3):237–43. doi: 10.1053/j.semnuclmed.2019.01.008
30. Das T, Chakraborty S, Sarma HD, Venkatesh M, Banerjee S. Preparation of ^{166}Ho-oxine-lipiodol and its preliminary bioevaluation for the potential application in therapy of liver cancer. *Nucl Med Commun* (2009) 30(5):362–7. doi: 10.1097/MNM.0b013e328329981a
31. Bouvry C, Palard X, Edeline J, Ardisson V, Loyer P, Garin E, et al. Transarterial Radioembolization (TARE) Agents beyond ^{90}Y-Microspheres. *BioMed Res Int* (2018) 2018:1–14. doi: 10.1155/2018/1435302
32. Smits ML, Nijsen JF, van den Bosch MA, Lam MG, Vente MD, Huijbregts JE, et al. Holmium-166 radioembolization for the treatment of patients with liver metastases: design of the phase I HEPAR trial. *J Exp Clin Canc Res* (2010) 29(1):70. doi: 10.1186/1756-9966-29-70
33. Zielhuis SW, Seppenwoolde JH, Bakker CJ, Jahnz U, Zonnenberg BA, van het Schip AD, et al. Characterization of holmium loaded alginate microspheres for multimodality imaging and therapeutic applications. *J BioMed Mater Res* (2007) 82A(4):892–8. doi: 10.1002/jbm.a.31183
34. Prince JF, Rooij RV, Bol GH, de Jong HW, van den Bosch MAJ, Lam MEH. Safety of a Scout Dose Preceding Hepatic Radioembolization with ^{166}Ho Microspheres. *J Nucl Med* (2015) 56:817–23. doi: 10.2967/jnumed.115.155564
35. Ceci F, Castellucci P, Cerci JJ, Fanti S. New Aspects of Molecular Imaging in Prostate Cancer. *Methods* (2017) 130:36–41. doi: 10.1016/j.ymeth.2017.07.009
36. Aziz Hashikin1 NA, Yeong CH, Abdullah BJ, Ng KH, Chung LY, Dahalan R, et al. Neutron Activated Samarium-153 Microparticles for Transarterial Radioembolization of Liver Tumour with Post-Procedure Imaging Capabilities. *PloS One* (2015) 10(9):e0138106. doi: 10.1371/journal.pone.0138106

Conflict of Interest: The authors declare that the research was conducted in the absence of any commercial or financial relationships that could be construed as a potential conflict of interest.

frontiers in Oncology

ORIGINAL RESEARCH
published: 09 June 2021
doi: 10.3389/fonc.2021.610637

Magnetic Resonance-Guided Stereotactic Body Radiotherapy of Liver Tumors: Initial Clinical Experience and Patient-Reported Outcomes

Fabian Weykamp[1,2,3], *Philipp Hoegen*[1,2,3], *Sebastian Klüter*[1,2,3], *C. Katharina Spindeldreier*[1,2,3], *Laila König*[1,2,3], *Katharina Seidensaal*[1,2,3], *Sebastian Regnery*[1,2,3], *Jakob Liermann*[1,2,3], *Carolin Rippke*[1,2,3], *Stefan A. Koerber*[1,2,3], *Carolin Buchele*[1,2,3], *Jürgen Debus*[1,2,3,4,5,6] *and Juliane Hörner-Rieber*[1,2,3,5]*

[1] *Department of Radiation Oncology, Heidelberg University Hospital, Heidelberg, Germany,* [2] *Heidelberg Institute of Radiation Oncology (HIRO), Heidelberg, Germany,* [3] *National Center for Tumor Diseases (NCT), Heidelberg, Germany,* [4] *Heidelberg Ion-Beam Therapy Center (HIT), Department of Radiation Oncology, Heidelberg University Hospital, Heidelberg, Germany,* [5] *Clinical Cooperation Unit Radiation Oncology, German Cancer Research Center (DKFZ), Heidelberg, Germany,* [6] *German Cancer Consortium (DKTK), Heidelberg, Germany*

OPEN ACCESS

Edited by:
Brian Timothy Collins, Georgetown University, United States

Reviewed by:
Michael David Chuong, Baptist Health South Florida, United States
Simon Boeke, Tübingen University Hospital, Germany

***Correspondence:**
Juliane Hörner-Rieber
juliane.hoerner-rieber@med.uni-heidelberg.de

Specialty section:
This article was submitted to Radiation Oncology, a section of the journal Frontiers in Oncology

Received: *26 September 2020*
Accepted: *17 May 2021*
Published: *09 June 2021*

Citation:
Weykamp F, Hoegen P, Klüter S, Spindeldreier CK, König L, Seidensaal K, Regnery S, Liermann J, Rippke C, Koerber SA, Buchele C, Debus J and Hörner-Rieber J (2021) Magnetic Resonance-Guided Stereotactic Body Radiotherapy of Liver Tumors: Initial Clinical Experience and Patient-Reported Outcomes. Front. Oncol. 11:610637. doi: 10.3389/fonc.2021.610637

Purpose/Objective: Stereotactic body radiation therapy (SBRT) has emerged as a valid treatment alternative for non-resectable liver metastases or hepatocellular carcinomas (HCC). Magnetic resonance (MR) guided SBRT has a high potential of further improving treatment quality, allowing for higher, tumoricidal irradiation doses whilst simultaneously sparing organs at risk. However, data on treatment outcome and patient acceptance is still limited.

Material/Methods: We performed a subgroup analysis of an ongoing prospective observational study comprising patients with liver metastases or HCC. Patients were treated with ablative MR-guided SBRT at the MRIdian Linac in the Department of Radiation Oncology at Heidelberg University Hospital between January 2019 and February 2020. Local control (LC) and overall survival (OS) analysis was performed using the Kaplan–Meier method. An in-house designed patient-reported outcome questionnaire was used to measure patients' experience with the MR-Linac treatment. Toxicity was evaluated using the Common Terminology Criteria for Adverse Events (CTCAE v. 5.0).

Results: Twenty patients (with n = 18 metastases; n = 2 HCC) received MR-guided SBRT for in total 26 malignant liver lesions. Median biologically effective dose (BED at α/β = 10) was 105.0 Gy (range: 67.2–112.5 Gy) and median planning target volume was 57.20 ml (range: 17.4–445.0 ml). Median treatment time was 39.0 min (range: 26.0–67.0 min). At 1-year, LC was 88.1% and OS was 84.0%. Grade I° gastrointestinal toxicity °occurred in 30.0% and grade II° in 5.0% of the patients with no grade III° or higher toxicity. Overall treatment experience was rated positively, with items scoring MR-Linac staff's

performance and items concerning the breath hold process being among the top positively rated elements. Worst scored items were treatment duration, positioning and low temperature.

Conclusion: MR-guided SBRT of liver tumors is a well-tolerated and well-accepted treatment modality. Initial results are promising with excellent local control and only mildest toxicity. However, prospective studies are warranted to truly assess the potential of MR-guided liver SBRT and to identify which patients profit most from this new versatile technology.

Keywords: stereotactic body radiotherapy, liver metastases, MR-guided, hepatocellular carcinoma, patient reported outcomes

BACKGROUND AND PURPOSE

Surgical resection was one of the first local ablative treatment options for selected patients with hepatic oligometastases (1). In a retrospective cohort of 612 patients, resection of colorectal liver metastases led to a remarkable long-term survival of 17% after 10 years (2). However, only up to 20% of patients with hepatic oligometastases are initially amenable for surgery (3, 4). In case of reduced general condition, insufficient liver function or critical localization of the liver tumor, cryoablation, radiofrequency- and microwave ablation as well as transarterial chemoembolization are treatment alternatives for local therapy of both hepatic metastases and also primary liver tumors (5, 6). Lately, stereotactic body radiotherapy (SBRT) has been proven as a further safe and effective non-invasive treatment option (7–10).

In case of limited tumor burden, modern radiotherapy evolved from treatment of a whole organ to targeting specific lesions within the organ. In the last century, irradiation of the liver was therefore predominantly used to for palliation, due to dose limiting toxicity together with the fear of radiation-induced liver disease (RILD) (11–14). Nowadays, SBRT offers application of highly conformal tumoricidal irradiation doses whilst sparing surrounding organs at risk (OAR) due to a steep dose gradient. However, adjacent stomach, duodenum and small bowel still represent dose limiting OAR, which impede the goal of achieving ablative irradiation doses (15–18). Standard image guidance with cone beam CT scans only offers a limited soft tissue contrast impairing differentiation between tumor lesions and surrounding radiosensitive OAR (19). Additionally, respiratory motion of the liver causes anatomic changes of up to several centimeters, which can lead to inferior local control, if not adequately accounted for (20–23). Traditionally, motion management includes the usage of an internal target volume (ITV) concept resulting in larger, unnecessary target volumes which might further harm OAR (24). Advanced motion management strategies comprise gating and tracking of the target lesion: surface-guided (SG) SBRT uses the body surface as a surrogate structure for image guidance including patient positioning, intra-fraction motion monitoring and respiratory gating (25–28), while the Cyberknife system can track invasively implanted fiducials using frequent noncoplanar X-ray scans (29). MR-guided radiotherapy has recently become clinically available offering additional superior soft-tissue contrast for precise identification of liver lesions and adjacent OAR. Furthermore, some MR-Linac systems also enable gated dose delivery which offers the possibility to further reduce safety margins (30). Available literature on MR-guided SBRT for malignant liver lesions is growing, but still limited. Especially, patient acceptance needs to be evaluated, considering the long treatment time of MR-guided irradiation of the liver, which is further prolonged through online treatment adaptation (31, 32).

METHODS

The presented study is a subgroup analysis from a prospective observational trial comprising cancer patients with liver metastases or primary hepatocellular carcinoma (HCC), who were referred to our institution because they were deemed medically or functional inoperable or refused resection. Patients were treated with ablative MR-guided SBRT at the MRIdian Linac (ViewRay Inc., Mountain View, CA) in the Department of Radiation Oncology at Heidelberg University Hospital between January 2019 and February 2020. According to the guideline of the working group "Stereotactic Radiotherapy" of the German Society of Radiation Oncology (DEGRO), SBRT was defined as single fraction doses ≥ 4 Gy and number of fractions ≤12 (33).

Treatment Characteristics

A detailed description of our treatment simulation and planning has been published previously (31). Four of our analyzed patients had already been previously included and published in this referenced study. In short, treatment simulation at the MR-Linac was performed to both acquire MR image data and to check for patients' compliance. Three-dimensional (3D) simulation MR images, using the TrueFISP sequence (a steady-state coherent MRI sequence) with an acquisition time of 17 to 25 s were obtained in deep inspiration breath-hold, followed by planar cine-MRI in a sagittal plane to evaluate target motion characteristics (34). For the 3D simulation MRI, in-plane resolutions of either 1.5×1.5 mm^2 or 1.6×1.6 mm^2 and slice thicknesses of 3 mm with varying fields-of-view were used. No MR contrast fluid was administered. The acquired MR image data was used as the primary image set for treatment planning.

All patients received additional diagnostic, contrast-enhanced MRIs for treatment planning. Furthermore, a planning CT scan with and without contrast enhancement was performed to also obtain data on electron density information for dose calculation. The gross tumor volume (GTV) was delineated as the macroscopic tumor volume on all available co-registered planning imaging modalities, with a clinical target volume (CTV) expansion of 5 mm and additional 3 mm for creating the planning target volume (PTV) due to technical uncertainties.

Daily image guidance was performed for each fraction by onboard 3D MRI using identical settings (field of view, duration, pulse sequence, breathing instructions) as during MR simulation. Soft-tissue based registration with the reference MR scan was applied, always registered directly on the GTV.

Gated dose delivery in breath hold was performed. The TrueFISP sequence was applied for real time MR-gating (cine-MRI scan) within one sagittal slice and four frames per second. If the liver lesion was visible on the TrueFISP sequence, the lesion was used as the gating structure (region of interest; ROI). This was the case in 14 of the 20 analyzed patients. Otherwise, an anatomical surrogate structure in proximity of the target lesion was defined as the gating target. In five patients, the nearest surface of the respective liver segment was used for this purpose. In one patient, a prominent adjacent liver vessel was defined as the surrogate structure. The predefined ROI (either the GTV or the surrogate structure) was expanded by 3 mm in every direction, which formed the gating boundary. The irradiation beam was automatically shut off, if the target structure (usually the GTV) left the gating boundary, including a tolerance threshold of mostly 3%, with a maximum of 7% in very rare cases. During gated dose delivery, patients were offered visual guidance *via* an in-room monitor displaying the live sagittal cine-MR image with an overlay of the gating target and the boundary. A video of this process can be found in the supplementary material section. If an intrafractional GTV deviation occurred and the patient could therefore no longer keep the ROI within the boundary, a table correction including a subsequent new MRI scan had to be performed. This procedure was mandatory to allow for a 3D table correction, since the cine-MRI only provides a 2D image control (in the sagittal plane). No online treatment adaptation was performed, as this technique had not yet been implemented, when the patients were treated.

Doses and fractionation schemes depended on the size and localization of the hepatic lesion as well as patients' breath holding capability. In general, small and centrally located lesions were treated with three fractions of 15 Gy, prescribed to the conformally enclosing 65% isodose, while larger lesions (>5 cm) were irradiated with eight fractions of 7.5 Gy or five fractions of 10Gy prescribed to the conformally enclosing 80% isodose. Hepatic lesions in close proximity to radiosensitive OAR were usually treated with ten fractions of 5 Gy prescribed to the conformally enclosing 80%-isodose. One hepatic metastasis was treated with twelve fractions of 4 Gy prescribed to the conformally enclosing 95% isodose as the patient had been treated with prior hemihepatectomy and the lesion was diagnosed at the liver margin which had been sutured to the small bowel.

Target coverage was comprised if required OAR dose constraints could not be met. Applied dose constraints were the following (for five fractions):

–esophagus: 0.5 cc <34 Gy
–stomach/intestine: 0.5 cc <35 Gy
–liver minus CTV: ≥700 cc <24 Gy
–kidney: mean dose <10 Gy
–spinal cord 0.1 cc <27 Gy
–heart: 0.5 cc <29 Gy.

An in-house designed patient-reported outcome questionnaire (PRO-Q) was used to measure patients' experience with the MR-Linac treatment (grades from 1–5, where 1 represents a completely positive and 5 a completely negative experience) (31). Patients were additionally asked, how many minutes it took to fully mentally and physically recover after their effort during the respective treatment session. Furthermore, our staff was surveyed about their opinion on each patient's treatment performance (grades from 1–10, where 1 represents a completely easy and 10 an almost inacceptable expenditure).

Endpoints and Statistical Methods

LC and OS were estimated starting from the first day of the SBRT. LC was calculated based on each lesion, whereas OS was calculated per patient. The Response Evaluation Criteria in Solid Tumors (RECIST 1.1) was used to asses tumor response. Toxicity was described using the Common Terminology Criteria for Adverse Events (CTCAE v. 5.0).

In accordance with the study protocol, each patient was specifically assessed for presence of fatigue, nausea, vomiting, diarrhea, constipation, dyspnea, cough, skin disorder and pain. This evaluation was performed before irradiation, at the last treatment day and at first follow-up. Follow-up consisted of a contrast fluid enhanced MRI or CT scan of the liver, performed six to eight weeks after completion of the SBRT together with a clinical examination. Further imaging follow-up was performed every three months afterwards and consisted of a contrast fluid enhanced CT of the thorax and the abdomen or a contrast-enhanced MRI, but was not part of the prospective study. The Child–Pugh score was assessed within four weeks prior to the SBRT and at the first follow-up examination.

LC and OS were estimated using the Kaplan–Meier method. The biologically effective dose (BED) was calculated applying the linear-quadratic model (35). An α/β ratio of 10 was assumed for liver metastases and HCC.

$$BED(Gy) = \text{single } dose \times number \text{ of } fractions\left(1 + \frac{\text{single } dose}{\alpha/\beta}\right)$$

All statistical analyses were performed with SPSS software (IBM SPSS Version 24.0). A p-value of <0.05 was defined significant. The MR-Linac observational study was approved by the Ethics committee of the University Hospital Heidelberg (S-543/2018). Written informed consent was obtained from all patients included into the study.

Two Selected Cases From Daily Routine

For providing detailed clinical inside into treatment reality at the MR-Linac, two characteristic patients were selected for in-detail description. Since gated dose delivery in breath hold is challenging, as it demands a certain amount of treatment compliance and the bore of the MR-Linac is relatively narrow (70 cm), the oldest patient and the patient with the highest body mass index were selected for further description.

RESULTS

Patient characteristics are described in **Table 1**. Median age of the 20 patients was 61 years. Most patients had a very good performance status and a non-obese body mass index. Most irradiated liver lesions were metastases from colorectal carcinoma. Two patients suffered from HCC. Systemic therapy was administered in most patients before (75%) and after (55%) radiotherapy. One patient underwent hemihepatectomy prior to radiotherapy. Twelve patients had already complained of grades I–II° adverse events before starting hepatic SBRT, mostly grade I° fatigue.

Most patients were treated with hepatic SBRT for one single liver lesion (n = 18), while two patients had four lesions irradiated. Median PTV size was 57.2 ml (17.4–445.0 ml). Median dose was 50 Gy (45–60 Gy) with a calculated BED of 105.0 Gy (67.2–112.5 Gy).

Further treatment characteristics are listed in **Table 2**. **Figure 1** shows a characteristic treatment plan, where maximum sparing of the neighboring small bowl and stomach could be achieved.

TABLE 1 | Patient characteristics (n = 20).

median age	61 years	range 37–78 years
median Karnofsky Score	90%	range 70–100%
median Body Mass Index	23.8 kg/m²	range 18.0–42.3 kg/m²
female/male	10/10	50.0%/50.0%
Hepatocellular Carcinoma	2	10.0%
Metastases	18	90.0%
n = 5 colorectal carcinoma; n = 4 breast cancer; n = 3 malignant melanoma; n = 1 adenoid cystic carcinoma; n = 1 cholangiocellular carcinoma; n = 1 urinary bladder carcinoma; n = 1 papillary carcinoma; n = 1 pancreatic cancer; n = 1 prostate cancer.		
distant metastases present (apart from the irradiated liver metastases)		
n = 0	9	45.0%
n = 1–5	5	25.0%
n > 5	6	30.0%
prior hemihepatectomy	1	4.7%
median Child–Pugh-Score[1]	5	range 5–7
extrahepatic disease progression within four weeks before irradiation	2	10.0%
systemic therapy within 4 weeks before irradiation	15	75.0%
n = 10 chemotherapy; n = 3 checkpoint inhibition; n = 2 hormonal therapy		
systemic therapy within 4 weeks after irradiation	11	55.0%
n = 5 chemotherapy; n = 3 checkpoint inhibition; n = 2 hormonal therapy; n = 1 targeted therapy		
Adverse events before radiotherapy		
I°	10	50.0%
n = 6 fatigue; n = 2 fatigue + diarrhea; n = 2 pain + cough		
II°	2	10.0%
n = 1 nausea; n = 1 fatigue		
≥III°	0	0
Adverse events at last treatment day		
I°	12	60.0%
n = 5 fatigue; n = 1 nausea; n = 1 diarrhea + nausea + fatigue; n = 1 fatigue + dysphagia +erythema; n = 1 flatulence + fatigue; n = 1 fatigue + dyspepsia; n = 1 fatigue + nausea; n = 1 fatigue + dizziness		
II°	1	5.0%
n = 1 fatigue + diarrhea		
≥III°	0	0
Adverse events at first follow-up		
I°	8	40.0%
n = 3 fatigue; n = 1 pain; n = 1 fatigue + nausea; n = 1 nausea + diarrhea; n = 1 nausea + dyspepsia; n = 1 fatigue + pain		
II°	0	0
≥III°	0	0

[1]*available data for n = 15 patients.*

Outcome

Median follow-up was 9.4 months. Estimated local control was 88.1% at 12 months (**Figure 2A**). All irradiated liver lesions were stable or had a decrease in size at first follow-up (**Table 2**). Two patients (10%) died during follow-up time. Estimated OS at 12 months was 84.0% (**Figure 2B**). Child–Pugh score (available for n = 15 patients) did not decrease after irradiation. **Figure 3** illustrates a representative patient case, where additional pre-

TABLE 2 | Irradiation treatment characteristics.

total number of irradiated liver targets per patient		
n = 1	18	90.0%
n = 4	2	10.0%
localization of liver targets	Segment I (7.7%) II (23.1%) III (0%) IV (15.3%) V (7.7%) VI (7.7%) VII (23.1%) VIII (15.4%)	
response to irradiation in first follow-up examination		
partial remission	15	57.6%
stable disease	11	42.4%
	median	range
largest axial diameter	21 mm	8–77 mm
GTV	15.5 mL	1.4–255.0 mL
CTV	36.4 mL	6.4–349.3 mL
PTV	57.2 mL	17.4–445.0 mL
prescribed total dose	50 Gy	45–60 Gy
fractions	8	3–12
dose inhomogeneity	80%	65–80%
EQD2(α/β = 10)	87.5 Gy	56.0–93.8 Gy
BED (α/β = 10)	105.0 Gy	67.2–112.5 Gy
monitor units per fraction	2,403.9	1,155.4–6,309.7
number of beams that are on	11	7–15
duration of the session ("on table")	39.0 min	26.0–67.0 min
-radiation time	15.8 min	10.3–38.2 min
-pure beam on time	3.8 min	1.83–10.0 min

BED, biologically effective dose; CTV, clinical target volume; EQD2, equivalent dose at 2 Gy; GTV, gross tumor volume; PTV, planning target volume.

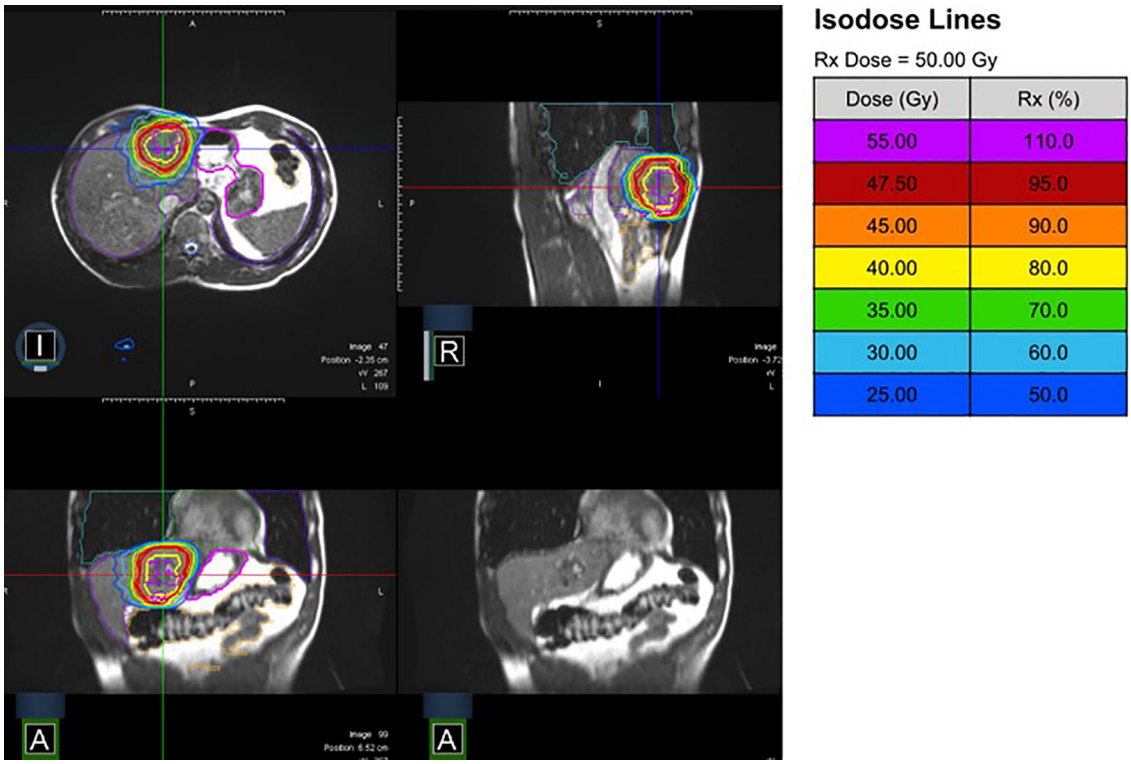

FIGURE 1 | MR-Linac treatment plan (10 fractions of 5 Gy prescribed to the conformally enclosing 80%-isodose) from different perspectives (I, inferior; A, anterior; R, right) with and without isodose lines.

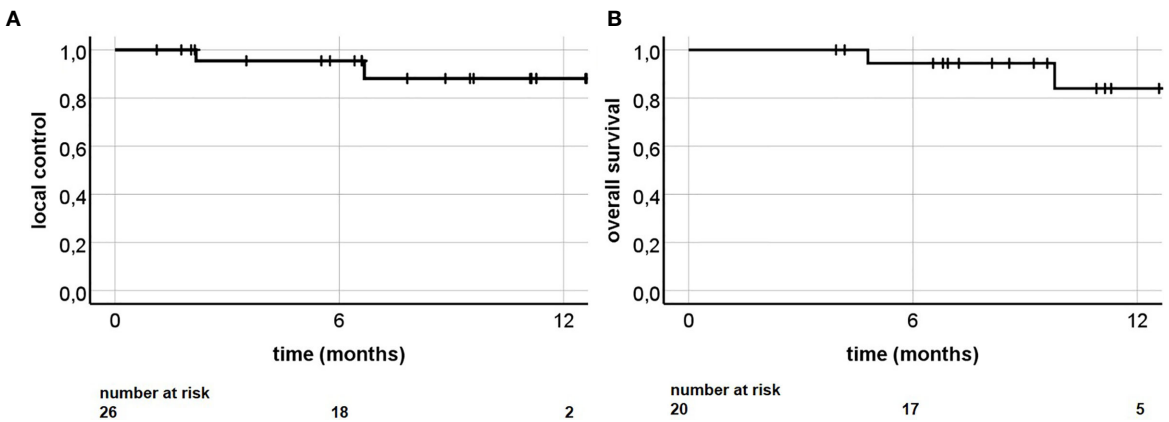

FIGURE 2 | **(A)** Local control and **(B)** overall survival following MR-guided liver SBRT.

and post-radiotherapy FDG PET-CT scans were performed, which revealed only residual activity of the liver metastasis after MR-guided hepatic SBRT. Later hemihepatectomy due to disease progression in the right liver lobe outside the irradiated area revealed complete pathological remission of the irradiated lesion.

Toxicity

Acute toxicity was mild with thirteen patients describing grades I–II° adverse events on the last day of radiotherapy, including mostly grade I° fatigue. Six patients suffered from grade I° gastrointestinal side effects and one patient was diagnosed with grade II° gastrointestinal side effects (diarrhea). Eight patients

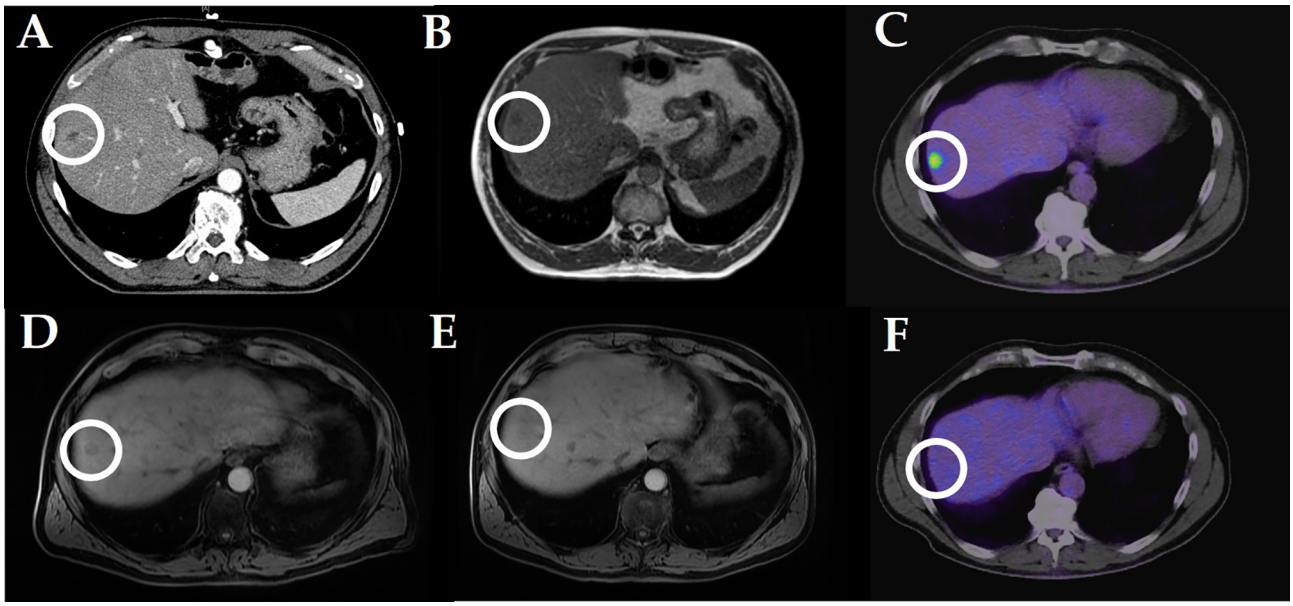

FIGURE 3 | Stereotactic MR guided radiotherapy of a hepatic metastasis in a patient with pancreatic cancer (10 × 5 Gy): **(A)** planning CT scan (portal venous phase); **(B)** online liver simulation at the MR-Linac; **(C)** pre-radiotherapy FDG-PET CT scan; **(D)** first (3 months after radiotherapy) post-radiotherapy MRI scan (liver imaging with volume acceleration-flexible MRI); **(E)** second (4 months) post-radiotherapy MRI (liver imaging with volume acceleration-flexible MRI); **(F)** post-radiotherapy (4 months) FDG-PET CT scan. Comment: later hemihepatectomy revealed complete remission of the radiated liver metastasis.

complained of grade I° adverse events at first follow-up examination, mainly fatigue. No grade III° adverse event ore higher was reported at any time.

Patient and Staff Reported Outcome

Table 3 displays the personal subjective experience of the treated patients. Overall treatment experience was rated positively, with items scoring MR-Linac staff's performance and items concerning the breath hold process being among the top positively rated items (each median 1 point). Worst scored elements were treatment duration, positioning and temperature of body parts (each median 3 points). The whole treatment processes, including breathing instructions, were challenging for some patients, both mentally and physically. Median time to full mental and physical recovery after the first treatment session was 20 min (range 0–360 min). Median complexity of radiotherapy at the MR-Linac was rated as average by the staff (**Table 3**).

Two Selected Cases From Daily Routine

The most obese patient (187 cm, 148 kg, body mass index = 42 kg/m²; ventrodorsal abdominal diameter = 35 cm; 52 years, Karnofsky Performance Score 70%) was treated for a single liver metastasis of a rectum carcinoma (three fractions of 15 Gy). The duration of the treatment session (40 min; "on table", including patient positioning), was comparable to the study median (39 min). Mere radiation time (16 min) was below the median of the study cohort (22 min). Recovery time after radiotherapy (10 min) was below the study median of 20 min. No patient reported outcome item was rated worse than average. MR-Linac staff documented average complexity of the irradiation process.

The oldest patient (78 years; Karnofsky Performance Score 80%; body mass index = 30 kg/m², no reported lung disease) was treated for a single liver metastasis of a cholangiocellular carcinoma (three fractions of 15 Gy). Duration of the treatment session (38 min) and pure radiation time (21 min) were comparable to the median of the study cohort (39 and 22 min). Recovery time after radiotherapy (90 min) was more than four times the study median of 20 min. Patient reported outcome items were among the worst of the study population (treatment duration rated with 5; breath holding rated with 4). MR-Linac staff documented maximum complexity of the irradiation process.

DISCUSSION

In this subgroup analysis of a prospective observational study, 20 patients received MR-guided SBRT for in total 26 malignant liver lesions at Heidelberg University Hospital from January 2019 to February 2020. MR-guided SBRT for tumors in the abdomen was described to be safe in a phase-I study as well as in a study by Hal et al. with no higher-grade toxicities (36, 37). However, these studies included patients with different abdominal malignancies. Experience with MR-guided radiotherapy of malignant lesions of the liver is growing, yet still scarce (**Table 4**). Gani et al. published one of the first prospective studies investigating the MR-guided liver SBRT using a high-field MR-Linac (32). Patient acceptance was high with very low toxicity burden. As far as

TABLE 3 | Patient (positions 1–18) and staff (position 19) reported outcome (available for n = 18 patients).

	categorical point scale form 1–5, where 1 equals very positive and 5 equals very negative	
	median	range
1. Overall treatment experience	2	1–5
2. Information provided by the staff	1	1–5
3. Friendliness of the staff	1	1–5
4. Duration of the treatment	3	1–5
5. Size of the MRI bore	2	1–5
6. Positioning during radiotherapy	3	1–5
7. Having to lie still	3	1–5
8. Noise in the MR-Linac	2	1–4
9. Temperature in the MR-Linac	3	1–5
10. Local temperature of body parts	3	1–5
11. Tingling sensations in fingers and toes	2	1–5
12. Breathing instructions	1	1–5
13. Breath holding	2	1–5
14. Anxiousness during treatment session	1	1–5
15. Reported time until full mental and physical recovery after the radiotherapy session	20 min	0–360 min
16. Difficulty to hold the target with one´s own breath	1	1–4
17. Ability to watch one´s own treatment *via* monitor	1	1–2
18. Feeling of having active control over the treatment duration	1	1–3
19. Treatment complexity from the perspective of the staff	categorical point scale form 1–10, where 1 equals very positive and 10 equals very negative	
	5	2–10

described, treatment toxicity was rather low in all larger studies in the field. Only two grade III° toxicities were described by Rosenberg and colleagues (40). No grade III° toxicity was reported in our study cohort, even though patients were prospectively evaluated for side effects.

The higher proportion of patients with HCC in the two US-American studies can be explained by epidemiology as well as the higher prevalence of viral hepatitis and obesity compared to Germany (38, 40, 42). Furthermore, in our study, estimated LC was excellent, with 88% at 1 year. However, with a median of 9.4 months, follow-up of our cohort is still rather short. One of the previously mentioned US-American studies provided data on treatment outcome: Rosenberg et al. reported a LC of 80% at the median follow-up of 21.2 months (40). Furthermore, Rogowski et al. described a local control rate of 100%, however with a median follow-up of 5 months (41). Preliminary LC results are therefore so far comparable to non-MRI-guided liver SBRT, as recently described in a systematic review by Ohri et al. with a LC after 1- and 2-years of 90 and 79% (43). Our estimated 1-year OS was higher than described by Rosenberg et al. (84% *vs.* 69%) and might be explained by the younger median age in our cohort (61 years *vs.* 70 years). The proportion of different primary tumors (mainly colorectal) was comparable as well as the median prescribed irradiation dose (**Table 4**). Nonetheless, Rosenberg et al. used cobalt sources instead of a linear accelerator. Furthermore, median PTV was nearly half the size as in our study cohort (38). Future follow-up will show, whether these circumstances will lead to a differing LC or OS.

An essential part of improving treatment quality at the MR-Linac is to assess patients' perspectives. Wearing headphones in an MRI scanner is a common and easy procedure to cope for the operating noise. This procedure seems to be sufficient in our study cohort as reflected by the positive patient reported outcome, in contrast to the room temperature. For optimal functionality of both MRI scanner and linear accelerator, the room temperature is leveled down. Moreover, to reduce the risk of metal items being accidentally taken into the vicinity of the magnetic field, patients wear hospital provided medical scrubs during the irradiation sessions, which are rather thin. Both circumstances explain the negative patient reported results concerning the temperature. As a reaction to our study results, we began to ask patients immediately before the irradiation session, whether they tend to feel cold easily. If so, patients are provided with additional blankets.

Surprisingly, patients were not disturbed by their own tumor being displayed on a monitor. Correspondingly, our data reveal that the breath hold procedure as a whole is perceived very positively by the patients. A more difficult terrain for improvement is patient positioning, treatment duration and the fact that patients have to lie still on the treatment couch for a relatively long time. Devices for patient immobilization are more challenging to be developed for the MR-Linac because they have to be both non-magnetic and adequate for the rather small bore (44). Treatment duration and not being allowed to move were perceived rather negative. Our practice to play radio music to the patients *via* headphones seems not to be sufficient to guarantee full patient comfort. One must keep in mind, that our presented patient cohort had been treated before daily online plan adaption was implemented at our MR-Linac, which surely further prolongs treatment duration. Patient positioning and MR-imaging procedure consume a large amount of time. Less than half of the treatment session is used for the irradiation process itself (including the gating procedure). Beam-on time even accounts for less than a tenth of the treatment duration (**Table 2**).

Based on the benefits mentioned above, The Lancet Oncology recently dedicated a whole review to the high capability of MR-guided liver SBRT. Witt and colleagues emphasized the potential of MR-guided adaptive SBRT to become a practice changing technology for irradiation of the liver (44). However, radiotherapy with the MR-Linac is resource intensive in terms of personnel, time, money and required patient compliance. Hence, it is of the utmost importance to identify the ideal patients for receiving MR-guided SBRT. To date, three prospective trials are going to investigate the potential of online adaptation in SBRT for liver malignancies. An US-American phase-I study aims to reveal the safe maximum tolerated dose for MR-guided SBRT treatment liver metastases through real time adaptation (45). The French phase-II RASTAF study will investigate Adaptative MR-Guided Stereotactic Body Radiotherapy of Liver Tumors (46). Our planned phase-II MAESTRO trial (magnetic resonance-guided stereotactic radiotherapy for hepatic metastases) is going to evaluate, if a higher proportion of liver lesions can be treated with locally

TABLE 4 | Studies on radiotherapy of liver lesions with a magnetic resonance imaging linear accelerator.

	patients, characteristics, design	radiation technique	Toxicity	LC	OS
Feldman et al. (38)	patients: n = 29 (n = 26 HCC, n = 2 cholangiocarcinoma, n = 1 metastatic colon cancer) irradiated lesions n = 34 median age: NA gender: NA Child–Pugh-Class: NA retrospective design	MRIdian Linac (ViewRay, Oakwood Village, OH) 0.35 T step-and-shoot IMRT; utilization of gating 27–50 Gy prescribed to at least 95% of the PTV in three or five fractions PTV margin: 5 mm mean number of beams: 10.8 (range 6–16) adaptive technique: n = 1 (3.4%) average treatment time: 34 min beam-on time: NA mean monitor units per fraction: 2,538.9 (range 1,549.1–5,737.4) median PTV volume: NA	constraints: American Association of Physicists in Medicine Task Group 101 (39) general toxicity: n = 1 nausea and vomiting n = 1 abdominal pain with bloody diarrhea (n = 4 deaths due to liver cirrhosis, unrelated to radiation effect)	–	–
Rosenberg et al. (40)	patients: n = 26 (n = 8 colorectal adenocarcinoma, n = 6 HCC, n = 3 lung, n = 2 cholangiocellular, n = 1 pancreas, n = 1 sarcoma, n = 1 head and neck, n = 4 others) liver lesions present: 1–3 per patient median age: 70 y (30–90 y) female: n = 9 (35%) Child–Pugh-Class: A (76,9%); NA (23,1%) retrospective design	MRIdian System (ViewRay Inc., Mountain View, CA) 0.35 T MRI scanner combined with 3 co-planar cobalt sources; utilization of gating median dose 50 Gy (range 30–60 Gy) in five fractions (6–12 Gy/fraction) PTV margin: 2–5 mm number of beams: 12–15 adaptive technique: no range of treatment time: 40–60 min range of beam-on time: 20–30 min occasional use of gadoxetic acid 20 min before treatment as contrast fluid median PTV volume: 98.2 cm^3 (13–2,034 cm^3)	constraints: –mean liver dose: <13 to 15 Gy, >700 cm^3 of liver receiving less than 15 Gy (liver-GTV), –stomach and bowel: V32–33 <0.5 cm^3 gastrointestinal toxicity: I–II°: NA III°: 7.7% ≥IV°: 0% n = 2 decrease in Child–Pugh-Class n = 1 significant hilar stricture n = 1 portal hypertension	80,4%@21m (100% in case of HCC)	69.0% @ 1 y
Gani et al. (32)	Patients: n = 10 (metastases of n = 5 colorectal adenocarcinoma, n = 1 esophageal, n = 1 melanoma, n = 1 cystic duct, n = 1 GIST, n = 1 ACC) no patients with Child B or Child C cirrhotic liver disease median age: 68 y (48–86 y) female: n = 5 (50%) sub-study of a basket phase 2 feasibility trial (NCT04172753)	1.5 T MR-Linac (Unity, Elekta, Crawley, UK) median dose 38.5 Gy to 98% of the GTV internal target volume concept PTV margin: 3–6 mm adaptive technique: yes range of treatment time: 26 -36min median beam-on time: 9.6min median PTV volume: 96.2 cm^3 (11.3-399.5cm^3)	constraints: based on the UKSABR guidelines (Version 6.1) no increase in transaminases >I° or gastrointestinal toxicity with the necessity of medical intervention	–	–
Rogowski et al. (41)	Patients: n = 11 Lesions: n = 15 (n = 2 Cholangiocarcinoma; metastases of n = 6 neuroendocrine tumor, n = 4 colorectal adenocarcinoma, n = 2 sarcoma, n = 1 GIST)	0.35T hybrid MR-Linac (Viewray Inc., Mountain View, CA, USA) mainly 12.5 Gy in three fractions PTV margin: 3–5 mm adaptive technique: yes	toxicity: I°: 55% ≥II°: 0%	100% @me-dian follow-up of 5 m	–

(Continued)

TABLE 4 | Continued

	patients, characteristics, design	radiation technique	Toxicity	LC	OS
	median age 66 y (47–86 y) female: n = 5 (46%) prospective observational clinical trial	median treatment time: 53 min median beam-on time: 10 min median PTV volume: 39.1 cm^3 (8.3–411.3 cm^3)			
Weykamp et al. (present study)	Patients: n = 20 (n = 2 HCC; metastases of: n = 5 colorectal, n = 4 breast cancer, n = 3 melanoma, n = 1 adenoid cystic carcinoma, n = 1 cholangiocellular carcinoma, n = 1 urinary bladder, n = 1 papillary carcinoma, n = 1 pancreatic cancer, n = 1 prostate cancer) median age: 61 y (37–78 y) female: n = 10 (50%) Child–Pugh-Class: A (70.0%); B (5%); NA (25.0%) subgroup analysis of a prospective observational study	MRIdian Linac (ViewRay, Oakwood Village, OH) 0.35 T step-and-shoot IMRT; utilization of gating median dose 50 Gy (range 45–60Gy) in eight fractions (3–12 Gy/fraction) CTV margin 5 mm PTV margin: 3 mm number of beams: 7–15 adaptive technique: no median duration of the session ("on table"): 39.0 min (26.0–67.0 min) median radiation time: 15.8 min (10.3–38.2 min) median monitor units per fraction: 2,403.9 (1,155.4–6,309.7) no MRI contrast fluid median PTV volume: 57.2 cm^3 (17.4–445.0 cm^3) median liver dose: 12.7 Gy (3.2–21.9 Gy)	constraints (for five fractions): –esophagus: 0.5 cc <34 Gy –stomach/intestine: 0.5 cc <35 Gy –liver minus CTV: ≥700 cc <24 Gy –kidney: mean dose <10 Gy –spinal cord 0.1 cc <27 Gy –heart: 0.5 cc <29 Gy gastrointestinal toxicity: I°: 30.0% II°: 5.0% ≥III°: 0% n = 0 decrease in Child–Pugh-Class	88.1% @ 1y	84.0% @ 1y

ACC, adenoid cystic carcinoma; GIST, gastrointestinal stroma tumor; HCC, hepatocellular carcinoma; m, months; min, minute; mm, millimeter; MRI, magnetic resonance imaging; NA, not available; y, years.

ablative doses of a biologic effective dose ≥100 Gy when applying MR-guided adaptive compared to standard ITV-based-SBRT.

The main limitation of the presented study is its small sample size. It was statistically not possible to detect factors which estimate patient acceptance. Instead, we provided a detailed description of the oldest patient and the patient with the highest body mass index. Obesity led to average treatment expenditure as rated by patient and staff. On the contrary, the oldest patient reported the worst negative scores, which was in accordance with the judgement by the staff. This might be explained by the exhausting breathing commands while observing the monitor carefully, leading to a demanding multitasking treatment environment. As a rule of thumb, patients at our clinic are asked if they can hold their breath for at least 25 s and whether they can picture themselves repeating this breath-holding several times whilst lying on a non-padded surface for about an hour. The evaluation of both the friendliness of our staff and the treatment expenditure appear to be highly subjective question items. However, since treatment at the MR-Linac is complex and demanding for the patient, guaranteeing an environment of thrust is highly important to ensure compliance, especially when breathing instructions are involved. Furthermore, the subjective rating of the treatment expenditure will help to identify patient characteristics, which may disqualify patients for treatment at the MR-Linac in the first place. Follow-up was rather short. Since the majority of radiation-induced liver diseases occur within the first three to four months after treatment, long-term toxicity might be underestimated to a certain degree (12).

We demonstrated that MR-guided SBRT of liver malignancies is a resource intensive treatment method both for the patient and the radio-oncology department. Further follow-up will reveal whether MR-guided SBRT will significantly improve clinical results compared to conventional techniques. Using the body surface as a surrogate parameter for image guidance, SG-SBRT might be even faster and more convenient than MR-guided SBRT. Albeit, the movement of the liver is not directly monitored (25–27) and the correlation of skin to tumor is not always constant especially for liver and pancreatic tumors (47, 48). Furthermore, Stick et al. investigated intrafractional fiducial marker position variations during visually guided, deep-inspiration breathhold (DIBH) SBRT of liver metastases and reported deviations of up to 10 mm. Based on those findings, the colleagues concluded that for ensuring accurate dose delivery real-time monitoring during treatment, e.g. MR-guided SBRT, is necessary and now apply MR-guided radiotherapy for liver metastases (49). Another option might be the additional application of ultrasound monitoring applied during SBRT with active breathhold control, which has been reported to reduce residual motion to <5 mm in most cases (50). Fiducials enable the Cyberknife system to directly track the immediate treatment area, however fiducial placement is an invasive procedure, which can cause liver trauma, bleedings or a pneumothorax (51, 52). Furthermore, treatment duration of hepatic SBRT applying tumor tracking at the Cyberknife might also easily exceed 30 min. MR-guided hepatic SBRT offers a non-invasive treatment alternative with direct intrafractional visualization of the tumor hereby ensuring optimal target coverage.

Since late February 2020, our clinic has been using online adaptation. Daily SBRT treatment can now be prescribed to the anatomy of the day, taking into account interfractional and even intrafractional changes, due to organ motion (53–56). Therefore, OAR can be superiorly spared and higher irradiation doses can be achieved (36, 40, 54). However, online adaptation further prolongs the duration of the treatment session and has already needed to be omitted in a few cases during our first clinical experience to secure compliance.

We showed that MR-guided SBRT is safe and effective, even without online adaptation. It might be especially adequate for selected patients with liver malignancies very close to OAR who refuse the invasive placement of fiducials.

CONCLUSION

We demonstrated that MR-guided SBRT of malignant liver lesions is a well-tolerated and well-accepted non-invasive treatment modality with only mild toxicity. Moreover, we provided insights into patient reported outcomes, which might support patient selection for this highly promising but nonetheless resource intensive treatment modality.

DATA AVAILABILITY STATEMENT

The datasets generated for this study are available on request to the corresponding author.

ETHICS STATEMENT

The studies involving human participants were reviewed and approved by the Ethics Committee of the University Hospital Heidelberg (S-543/2018). The patients/participants provided their written informed consent to participate in this study.

AUTHOR CONTRIBUTIONS

FW performed the data collection and the statistical analysis and drafted the manuscript. SAK, PH, LK, KS, SR, JL, and SK helped with data collection as well as figure and table preparation. SK, CS, CR, and CB performed treatment planning and contributed the medical physicist expertise. JH-R and JD participated in the study design and helped to draft the manuscript. All authors contributed to the article and approved the submitted version.

FUNDING

SR and JL are funded by the Physician-Scientist Program of Heidelberg University, Faculty of Medicine.

SUPPLEMENTARY MATERIAL

The Supplementary Material for this article can be found online at: https://www.frontiersin.org/articles/10.3389/fonc.2021.610637/full#supplementary-material

REFERENCES

1. Bartlett EK, Simmons KD, Wachtel H, Roses RE, Fraker DL, Kelz RR, et al. The Rise in Metastasectomy Across Cancer Types Over the Past Decade. *Cancer* (2015) 121(5):747–57. doi: 10.1002/cncr.29134
2. Tomlinson JS, Jarnagin WR, DeMatteo RP, Fong Y, Kornprat P, Gonen M, et al. Actual 10-Year Survival After Resection of Colorectal Liver Metastases Defines Cure. *ASCO Publication - JCO* (2007) 25(29):4575–80. doi: 10.1200/JCO.2007.11.0833
3. Smith JJ, D'Angelica MI. Surgical Management of Hepatic Metastases of Colorectal Cancer. *Hematol Oncol Clinics North Am* (2015) 29(1):61–84. doi: 10.1016/j.hoc.2014.09.003
4. Cummings LC, Payes JD, Cooper GS. Survival After Hepatic Resection in Metastatic Colorectal Cancer: A Population-Based Study. *Cancer* (2007) 109 (4):718–26. doi: 10.1002/cncr.22448
5. Izzo F, Granata V, Grassi R, Fusco R, Palaia R, Delrio P, et al. Radiofrequency Ablation and Microwave Ablation in Liver Tumors: An Update. *Oncologist* (2019) 24(10):e990–1005. doi: 10.1634/theoncologist.2018-0337
6. Sim H-W, Knox J, Dawson LA. An Update on Randomized Clinical Trials in Hepatocellular Carcinoma. *Surg Oncol Clinics North Am* (2017) 26(4):647–66. doi: 10.1016/j.soc.2017.05.006
7. Goodman BD, Mannina EM, Althouse SK, Maluccio MA, Cárdenes HR. Long-Term Safety and Efficacy of Stereotactic Body Radiation Therapy for Hepatic Oligometastases. *Pract Radiat Oncol* (2016) 6(2):86–95. doi: 10.1016/j.prro.2015.10.011
8. Andratschke N, Alheid H, Allgäuer M, Becker G, Blanck O, Boda-Heggemann J, et al. The SBRT Database Initiative of the German Society for Radiation Oncology (DEGRO): Patterns of Care and Outcome Analysis of Stereotactic Body Radiotherapy (SBRT) for Liver Oligometastases in 474 Patients With 623 Metastases. *BMC Cancer* (2018) 18(1):283. doi: 10.1186/s12885-018-4191-2
9. Joo JH, Park J-H, Kim JC, Yu CS, Lim S-B, Park IJ, et al. Local Control Outcomes Using Stereotactic Body Radiation Therapy for Liver Metastases From Colorectal Cancer. *Int J Radiat Oncol Biol Phys* (2017) 99(4):876–83. doi: 10.1016/j.ijrobp.2017.07.030
10. Zeng Z-C, Fan J, Tang Z-Y, Zhou J, Qin L-X, Wang J-H, et al. A Comparison of Treatment Combinations With and Without Radiotherapy for Hepatocellular Carcinoma With Portal Vein and/or Inferior Vena Cava Tumor Thrombus. *Int J Radiat Oncol Biol Phys* (2005) 61(2):432–43. doi: 10.1016/j.ijrobp.2004.05.025
11. Munoz-Schuffenegger P, Ng S, Dawson LA. Radiation-Induced Liver Toxicity. *Semin Radiat Oncol* (2017) 27(4):350–7. doi: 10.1016/j.semradonc.2017.04.002
12. Pan CC, Kavanagh BD, Dawson LA, Li XA, Das SK, Miften M, et al. Radiation-Associated Liver Injury. *Int J Radiat Oncol Biol Phys* (2010) 76(3 Suppl):S94–100. doi: 10.1016/j.ijrobp.2009.06.092
13. Greco C, Catalano G, Di Grazia A, Orecchia RJTJ. Radiotherapy of Liver Malignancies. From Whole Liver Irradiation to Stereotactic Hypofractionated Radiotherapy. *Tumori J* (2004) 90(1):73–9. doi: 10.1177/030089160409000116
14. Dawson LA, Normolle D, Balter JM, McGinn CJ, Lawrence TS, Ten Haken RK. Analysis of Radiation-Induced Liver Disease Using the Lyman NTCP Model. *Int J Radiat Oncol Biol Phys* (2002) 53(4):810–21. doi: 10.1016/S0360-3016(02)02846-8
15. Doi H, Shiomi H, Masai N, Tatsumi D, Igura T, Imai Y, et al. Threshold Doses and Prediction of Visually Apparent Liver Dysfunction After Stereotactic Body Radiation Therapy in Cirrhotic and Normal Livers Using Magnetic Resonance Imaging. *J Radiat Res* (2016) 57(3):294–300. doi: 10.1093/jrr/rrw008

16. Kavanagh BD, Pan CC, Dawson LA, Das SK, Li XA, Ten Haken RK, et al. Radiation Dose-Volume Effects in the Stomach and Small Bowel. *Int J Radiat Oncol Biol Phys* (2010) 76(3 Suppl):S101–7. doi: 10.1016/j.ijrobp.2009.05.071
17. Miften M, Vinogradskiy Y, Moiseenko V, Grimm J, Yorke E, Jackson A, et al. Radiation Dose-Volume Effects for Liver Sbrt. *Int J Radiat Oncol Biol Phys* (2021) 17(1):196–205. doi: 10.1016/j.ijrobp.2017.12.290
18. Bae SH, Kim M-S, Cho CK, Kang J-K, Lee SY, Lee K-N, et al. Predictor of Severe Gastroduodenal Toxicity After Stereotactic Body Radiotherapy for Abdominopelvic Malignancies. *Int J Radiat Oncol Biol Phys* (2012) 84(4): e469–74. doi: 10.1016/j.ijrobp.2012.06.005
19. Noel CE, Parikh PJ, Spencer CR, Green OL, Hu Y, Mutic S, et al. Comparison of Onboard Low-Field Magnetic Resonance Imaging Versus Onboard Computed Tomography for Anatomy Visualization in Radiotherapy. *Acta Oncol* (2015) 54(9):1474–82. doi: 10.3109/0284186X.2015.1062541
20. Van den Begin R, Engels B, Gevaert T, Duchateau M, Tournel K, Verellen D, et al. Impact of Inadequate Respiratory Motion Management in SBRT for Oligometastatic Colorectal Cancer. *Radiother Oncol* (2014) 113(2):235–9. doi: 10.1016/j.radonc.2014.11.005
21. Bertholet J, Worm ES, Fledelius W, Hoyer M, Poulsen PR. Time-Resolved Intrafraction Target Translations and Rotations During Stereotactic Liver Radiation Therapy: Implications for Marker-based Localization Accuracy. *Int J Radiat Oncol Biol Phys* (2016) 95(2):802–9. doi: 10.1016/j.ijrobp.2016.01.033
22. Poulsen PR, Worm ES, Petersen JB, Grau C, Fledelius W, Hoyer M. Kilovoltage Intrafraction Motion Monitoring and Target Dose Reconstruction for Stereotactic Volumetric Modulated Arc Therapy of Tumors in the Liver. *Radiother Oncol: J Eur Soc Ther Radiol Oncol* (2014) 111(3):424–30. doi: 10.1016/j.radonc.2014.05.007
23. Worm ES, Hoyer M, Fledelius W, Hansen AT, Poulsen PR. Variations in Magnitude and Directionality of Respiratory Target Motion Throughout Full Treatment Courses of Stereotactic Body Radiotherapy for Tumors in the Liver. *Acta Oncol* (2013) 52(7):1437–44. doi: 10.3109/0284186X.2013.813638
24. Sterzing F, Brunner TB, Ernst I, Baus WW, Greve B, Herfarth K, et al. Stereotactic Body Radiotherapy for Liver Tumors. *Strahlenther und Onkol* (2014) 190(10):872–81. doi: 10.1007/s00066-014-0714-1
25. Boda-Heggemann J, Knopf AC, Simeonova-Chergou A, Wertz H, Stieler F, Jahnke A, et al. Deep Inspiration Breath Hold-Based Radiation Therapy: A Clinical Review. *Int J Radiat Oncol Biol Phys* (2016) 94(3):478–92. doi: 10.1016/j.ijrobp.2015.11.049
26. Alderliesten T, Sonke JJ, Betgen A, van Vliet-Vroegindeweij C, Remeijer P. 3D Surface Imaging for Monitoring Intrafraction Motion in Frameless Stereotactic Body Radiotherapy of Lung Cancer. *Radiother Oncol: J Eur Soc Ther Radiol Oncol* (2012) 105(2):155–60. doi: 10.1016/j.radonc.2012.08.016
27. Hughes S, McClelland J, Tarte S, Lawrence D, Ahmad S, Hawkes D, et al. Assessment of Two Novel Ventilatory Surrogates for Use in the Delivery of Gated/Tracked Radiotherapy for non-Small Cell Lung Cancer. *Radiother Oncol: J Eur Soc Ther Radiol Oncol* (2009) 91(3):336–41. doi: 10.1016/j.radonc.2009.03.016
28. Freislederer P, Kügele M, Öllers M, Swinnen A, Sauer TO, Bert C, et al. Recent Advances in Surface Guided Radiation Therapy. *Radiat Oncol* (2020) 15 (1):187. doi: 10.1186/s13014-020-01629-w
29. Brock KK, Dawson LA. Adaptive Management of Liver Cancer Radiotherapy. *Semin Radiat Oncol* (2010) 20(2):107–15. doi: 10.1016/j.semradonc.2009.11.004
30. van Sörnsen de Koste JR, Palacios MA, Bruynzeel AME, Slotman BJ, Senan S, Lagerwaard FJ. MR-Guided Gated Stereotactic Radiation Therapy Delivery for Lung, Adrenal, and Pancreatic Tumors: A Geometric Analysis. *Int J Radiat Oncol Biol Phys* (2018) 102(4):858–66. doi: 10.1016/j.ijrobp.2018.05.048
31. Klüter S, Katayama S, Spindeldreier CK, Koerber SA, Major G, Alber M, et al. First Prospective Clinical Evaluation of Feasibility and Patient Acceptance of Magnetic Resonance-Guided Radiotherapy in Germany. *Strahlenther und Onkol* (2020) 196:691–8.
32. Gani C, Boeke S, McNair H, Ehlers J, Nachbar M, Mönnich D, et al. Marker-Less Online MR-Guided Stereotactic Body Radiotherapy of Liver Metastases at a 1.5 T MR-Linac – Feasibility, Workflow Data and Patient Acceptance. *Clin Trans Radiat Oncol* (2021) 26:55–61. doi: 10.1016/j.ctro.2020.11.014
33. Guckenberger M, Baus WW, Blanck O, Combs SE, Debus J, Engenhart-Cabillic R, et al. Definition and Quality Requirements for Stereotactic Radiotherapy: Consensus Statement From the DEGRO/DGMP Working Group Stereotactic Radiotherapy and Radiosurgery. *Strahlenther und Onkol* (2020) 196(5):417–20. doi: 10.1007/s00066-020-01603-1
34. Klüter S. Technical Design and Concept of a 0.35 T Mr-Linac. *Clin Trans Radiat Oncol* (2019) 18:98–101. doi: 10.1016/j.ctro.2019.04.007
35. Park C, Papiez L, Zhang S, Story M, Timmerman RD. Universal Survival Curve and Single Fraction Equivalent Dose: Useful Tools in Understanding Potency of Ablative Radiotherapy. *Int J Radiat Oncol Biol Phys* (2008) 70 (3):847–52. doi: 10.1016/j.ijrobp.2007.10.059
36. Henke L, Kashani R, Robinson C, Curcuru A, DeWees T, Bradley J, et al. Phase I Trial of Stereotactic MR-guided Online Adaptive Radiation Therapy (SMART) for the Treatment of Oligometastatic or Unresectable Primary Malignancies of the Abdomen. *Radiother Oncol* (2018) 126(3):519–26. doi: 10.1016/j.radonc.2017.11.032
37. Hal WA, Straza MW, Chen X, Mickevicius N, Erickson B, Schultz C, et al. Initial Clinical Experience of Stereotactic Body Radiation Therapy (SBRT) for Liver Metastases, Primary Liver Malignancy, and Pancreatic Cancer With 4D-MRI Based Online Adaptation and Real-Time MRI Monitoring Using a 1.5 Tesla Mr-Linac. *PLOS ONE* (2020) 15(8):e0236570. doi: 10.1371/journal.pone.0236570
38. Feldman AM, Modh A, Glide-Hurst C, Chetty IJ, Movsas B. Real-Time Magnetic Resonance-Guided Liver Stereotactic Body Radiation Therapy: An Institutional Report Using a Magnetic Resonance-Linac System. *Cureus* (2019) 11(9):e5774. doi: 10.7759/cureus.5774
39. Benedict SH, Yenice KM, Followill D, Galvin JM, Hinson W, Kavanagh B, et al. Stereotactic Body Radiation Therapy: The Report of AAPM Task Group 101. *Med Phys* (2010) 37(8):4078–101. doi: 10.1118/1.3438081
40. Rosenberg SA, Henke LE, Shaverdian N, Mittauer K, Wojcieszynski AP, Hullett CR, et al. A Multi-Institutional Experience of MR-Guided Liver Stereotactic Body Radiation Therapy. *Adv Radiat Oncol* (2019) 4(1):142–9. doi: 10.1016/j.adro.2018.08.005
41. Rogowski P, von Bestenbostel R, Walter F, Straub K, Nierer L, Kurz C, et al. Feasibility and Early Clinical Experience of Online Adaptive MR-Guided Radiotherapy of Liver Tumors. *Cancers* (2021) 13(7):1523. doi: 10.3390/cancers13071523
42. Mittal S. El-Serag Hbjjocg. *Epidemiol HCC: Consider Popul* (2013) 47:S2. doi: 10.1097/MCG.0b013e3182872f29
43. Ohri N, Tome WA, Mendez Romero A, Miften M, Ten Haken RK, Dawson LA, et al. Local Control After Stereotactic Body Radiation Therapy for Liver Tumors. *Int J Radiat Oncol Biol Phys* (2018) 21(2):e74–82. doi: 10.1016/S1470-2045(20)30034-6
44. Witt JS, Rosenberg SA, Bassetti MF. MRI-Guided Adaptive Radiotherapy for Liver Tumours: Visualising the Future. *Lancet Oncol* (2020) 21(2):e74–82. doi: 10.1016/S1470-2045(20)30034-6
45. University of Wisconsin M. *OAR-Based, Dose Escalated SBRT With Real Time Adaptive MRI Guidance for Liver Metastases ClinicalTrials.gov* (2020). Available at: https://clinicaltrials.gov/ct2/show/NCT04020276.
46. Leclerc CGF. *Adaptative MR-Guided Stereotactic Body Radiotherapy of Liver Tumors (RASTAF) ClinicalTrials.gov* (2020). Available at: https://clinicaltrials.gov/ct2/show/NCT04242342.
47. Velec M, Moseley JL, Craig T, Dawson LA, Brock K. Accumulated Dose in Liver Stereotactic Body Radiotherapy: Positioning, Breathing, and Deformation Effects. *Int J Radiat Oncol Biol Phys* (2012) 83(4):1132–40. doi: 10.1016/j.ijrobp.2011.09.045
48. Minn AY, Schellenberg D, Maxim P, Suh Y, McKenna S, Cox B, et al. Pancreatic Tumor Motion on a Single Planning 4D-CT Does Not Correlate With Intrafraction Tumor Motion During Treatment. *Am J Clin Oncol* (2009) 32(4):364–8. doi: 10.1097/COC.0b013e31818da9e0
49. Stick LB, Vogelius IR, Risum S, Josipovic M. Intrafractional Fiducial Marker Position Variations in Stereotactic Liver Radiotherapy During Voluntary Deep Inspiration Breath-Hold. *Br J Radiol* (2020) 93(1116):20200859. doi: 10.1259/bjr.20200859
50. Vogel L, Sihono DSK, Weiss C, Lohr F, Stieler F, Wertz H, et al. Intra-Breath-Hold Residual Motion of Image-Guided DIBH Liver-SBRT: An Estimation by Ultrasound-Based Monitoring Correlated With Diaphragm Position in CBCT. *Radiother Oncol* (2018) 129(3):441–8. doi: 10.1016/j.radonc.2018.07.007
51. Wurm RE, Gum F, Erbel S, Schlenger L, Scheffler D, Agaoglu D, et al. Image Guided Respiratory Gated Hypofractionated Stereotactic Body Radiation Therapy

(H-SBRT) for Liver and Lung Tumors: Initial Experience. *Acta Oncol (Stockholm Sweden)* (2006) 45(7):881–9. doi: 10.1080/02841860600919233

52. Bahig H, Campeau M-P, Vu T, Doucet R, Nadeau DB, Fortin B, et al. Predictive Parameters of CyberKnife Fiducial-Less (Xsight Lung) Applicability for Treatment of Early Non-Small Cell Lung Cancer: A Single-Center Experience. *Int J Radiat Oncol Biol Phys* (2013) 87(3):583–9. doi: 10.1016/j.ijrobp.2013.06.2048
53. Henke LE, Olsen JR, Contreras JA, Curcuru A, DeWees TA, Green OL, et al. Stereotactic MR-Guided Online Adaptive Radiation Therapy (SMART) for Ultracentral Thorax Malignancies: Results of a Phase 1 Trial. *Adv Radiat Oncol* (2019) 4(1):201–9. doi: 10.1016/j.adro.2018.10.003
54. Bohoudi O, Bruynzeel AME, Senan S, Cuijpers JP, Slotman BJ, Lagerwaard FJ, et al. Fast and Robust Online Adaptive Planning in Stereotactic MR-guided Adaptive Radiation Therapy (SMART) for Pancreatic Cancer. *Radiother Oncol* (2017) 125(3):439–44. doi: 10.1016/j.radonc.2017.07.028
55. Acharya S, Fischer-Valuck BW, Kashani R, Parikh P, Yang D, Zhao T, et al. Online Magnetic Resonance Image Guided Adaptive Radiation Therapy: First Clinical Applications. *Int J Radiat Oncol Biol Phys* (2016) 94(2):394–403. doi: 10.1016/j.ijrobp.2015.10.015
56. Henke LE, Contreras JA, Green OL, Cai B, Kim H, Roach MC, et al. Magnetic Resonance Image-Guided Radiotherapy (Mrigrt): A 4.5-Year Clinical Experience. *Clin Oncol* (2018) 30(11):720–7. doi: 10.1016/j.clon.2018.08.010

Conflict of Interest: JH-R received speaker fees and travel reimbursement from ViewRay Inc., as well as travel reimbursement form IntraOP Medical and Elekta Instrument AB outside the submitted work. JD received grants from CRI—The Clinical Research Institute GmbH, View Ray Inc., Accuray International, Accuray Incorporated, RaySearch Laboratories AB, Vision RT limited, Astellas Pharma GmbH, Merck Serono GmbH, Astra Zeneca GmbH, Solution Akademie GmbH, Ergomed PLC Surrey Research Park, Siemens Healthcare GmbH, Quintiles GmbH, Pharmaceutical Research Associates GmbH, Boehringer Ingelheim Pharma GmbH Co, PTW-Freiburg Dr. Pychlau GmbH, Nanobiotix A.A. as well as IntraOP Medical outside the submitted work. SK has received personal fees and travel reimbursement from Viewray.

The remaining authors declare that the research was conducted in the absence of any commercial or financial relationships that could be construed as a potential conflict of interest.

frontiers in Oncology

ORIGINAL RESEARCH
published: 28 July 2021
doi: 10.3389/fonc.2021.658152

Prognostic Factors of Survival of Advanced Liver Cancer Patients Treated With Palliative Radiotherapy: A Retrospective Study

Qingling Hua[1†], Dejun Zhang[1†], Yunqiao Li[2†], Yue Hu[1], Pian Liu[1], Guangqin Xiao[1], Tao Zhang[1] and Jun Xue[1*]*

[1] Cancer Center, Union Hospital, Tongji Medical college, Huazhong University of Science and Technology, Wuhan, China, [2] Department of Geriatrics, Union Hospital, Tongji Medical College, Huazhong University of Science and Technology, Wuhan, China

OPEN ACCESS

Edited by:
Thomas DiPetrillo, Tufts University School of Medicine, United States

Reviewed by:
Vinay Sharma, University of the Witwatersrand, South Africa
Linghui Zhou, Zhejiang University, China

***Correspondence:**
Jun Xue
xjunion@126.com
Tao Zhang
taozhangxh@hust.edu.cn

[†]These authors have contributed equally to this work

Specialty section:
This article was submitted to Radiation Oncology, a section of the journal Frontiers in Oncology

Received: 25 January 2021
Accepted: 14 July 2021
Published: 28 July 2021

Citation:
Hua Q, Zhang D, Li Y, Hu Y, Liu P, Xiao G, Zhang T and Xue J (2021) Prognostic Factors of Survival of Advanced Liver Cancer Patients Treated With Palliative Radiotherapy: A Retrospective Study. Front. Oncol. 11:658152. doi: 10.3389/fonc.2021.658152

Aims: Survival benefit of liver cancer patients who undergo palliative radiotherapy varies from person to person. The present study aims to identify indicators of survival of advanced liver cancer patients receiving palliative radiotherapy.

Patients and Methods: One hundred and fifty-nine patients treated with palliative radiotherapy for advanced liver cancer were retrospectively assessed. Of the 159 patients, 103 patients were included for prediction model construction in training phase, while other 56 patients were analyzed for external validation in validation phase. In model training phase, clinical characteristics of included patients were evaluated by Kaplan-Meier curves and log-rank test. Thereafter, multivariable Cox analysis was taken to further identify characteristics with potential for prediction. In validation phase, a separate dataset including 56 patients was used for external validation. Harrell's C-index and calibration curve were used for model evaluation. Nomograms were plotted based on the model of multivariable Cox analysis.

Results: Thirty-one characteristics of patients were investigated in model training phase. Based on the results of Kaplan-Meier plots and log-rank tests, 6 factors were considered statistically significant. On multivariable Cox regression analysis, bone metastasis (HR = 1.781, $P = 0.026$), portal vein tumor thrombus (HR = 2.078, $P = 0.015$), alpha-fetoprotein (HR = 2.098, $P = 0.007$), and radiation dose (HR = 0.535, $P = 0.023$) show significant potential to predict the survival of advanced liver cancer patients treated with palliative radiotherapy. Moreover, nomograms predicting median overall survival, 1- and 2-year survival probability were plotted. The Harrell's C-index of the predictive model is 0.709 (95%CI, 0.649-0.769) and 0.735 (95%CI, 0.666-0.804) for training model and validation model respectively. Calibration curves of the 1- and 2-year overall survival of the predictive model indicate that the predicted probabilities of OS are very close to the actual observed outcomes both in training and validation phase.

Conclusion: Bone metastasis, portal vein tumor thrombus, alpha-fetoprotein and radiation dose are independent prognostic factors for the survival of advanced liver cancer patients treated with palliative radiotherapy.

Keywords: liver cancer, palliative radiotherapy, prognostic factors, nomograms, multivariable Cox regression

INTRODUCTION

Liver cancer (LC) is one of the most common malignancies and the fourth leading cause of cancer-related death worldwide (1). When diagnosed with LC, about 70% patients are in advanced stage, resulting in a poor five year overall survival (OS) rate (approximately 5%) (2). Most advanced LC patients are incurable (3), thereafter it is important to provide beneficial non-curative therapies for those patients (4, 5).

Palliative radiotherapy is one of the non-curative treatments for LC, which mainly aims to alleviate symptoms and improve the quality of life (QoL) (3, 6). Interestingly, occasional success of survival prolongation can be seen in patients receiving palliative radiation. More intensive treatment regimens should be recommended if those patients who will benefit from palliative radiotherapy can be identified. Inversely, patients with poor prognosis should not receive too much radiation treatment (7, 8). Therefore, it is essential to identify predictive indicators for the survival of advanced LC patients treated with radiation, which will be convenient for clinicians to distinguish those patients who will benefit from palliative radiotherapy.

We performed a retrospective study to develop several predictive factors and construct a predictive model by analyzing the characteristics of LC patients receiving palliative radiation. Nomograms for the survival prediction of cancer patients have been widely used. It can help clinicians to predict the prognosis of cancer patients by using a convenient numerical estimation model instead of complex statistical models. In this study, nomograms were also plotted based on the identified predictive factors and model.

METHODS

Patient Selection

We retrospectively evaluated LC patients treated with palliative radiotherapy in our hospital between January 2017 and July 2020 following inclusion criteria: 1) age ≥ 18 years; 2) diagnosed by pathology or clinical evidences; 3) palliative radiotherapy for tumor in liver or distant metastatic sites; 4) stage IIIB-IV according to Chinese stage system of LC. The exclusion criteria consist of 1) curative radiotherapy; 2) metastatic tumor in liver from other cancers. The most recent follow-up date was July 26, 2020. Included patients were divided to be analyzed in model training phase and external validation phase. The training set comprised 103 advanced LC patients receiving palliative radiotherapy between November 2017 and July 2020. The external validation set comprised 56 similar patients treated between January 2017 and July 2020.

Clinical characteristics such as age, sex, stage, metastasis, radiation techniques, radiation dose, toxicity and other 25 variables were collected. Toxicities were recorded in accordance with the CTCAE (version 5.0). The primary end point was OS that was calculated from the time of palliative radiation to the time of death, or last follow-up (July 26, 2020). The requirement for informed consent from the patients was waived since this study is retrospective.

Statistical Analysis

Statistical analysis was performed by using R software packages (version 3.6). Median follow-up time was estimated by reverse Kaplan-Meier curves. Kaplan-Meier curves and log-rank test were used to identify the factors associated with OS, and statistically potential factors were confirmed by multivariable Cox regression analysis. Proportional hazards (PH) assumption of multivariable Cox regression analysis was checked by Kaplan-Meier plot for category variables, while schoenfeld residuals were calculated for continuous variables (9). To confirm the assumption of proportionality, time-dependent covariate analysis was used. Martingale residual was calculated to assess nonlinearity of continuous variables. The continuous variables will be converted to category variables if they have no linearity. Variables with high co-linearity were not included in the same regression model. Hazards ratio (HR) and 95% confidence interval (CI) were calculated for each of the variables. Then, predictive model for OS was developed by using multivariable Cox regression analysis. After that, nomograms were constructed based on the predictive model (10). Harrell's C-index and calibration curves were used to assess the feasibility of the predictive model (11). A two-tailed P value of <0.05 was considered statistically significant.

RESULTS

Clinical Characteristics of Included Patients

The detailed patients inclusion process was illustrated in **Figure 1**. Briefly, 159 patients who met the inclusion criteria were finally included, with a median age of 55 years (range, 24-84 years). Men accounted for 85.5% and women accounted for 14.5%. All patients were diagnosed by pathology. One hundred and three patients were included for predictive model training, while other 56 patients treated with palliative radiotherapy in the same time-period were used for external validation. The median follow-up time was 13.7 months (range: 0.7-64.2 months). The baseline demographic characteristics of the patients were shown in **Table 1**. Most patients have evident symptoms including pain,

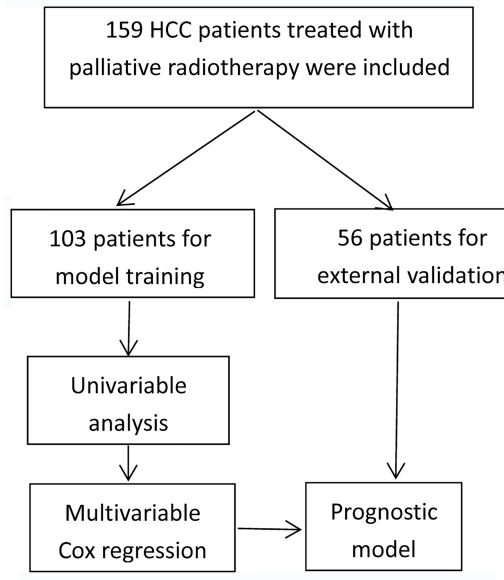

FIGURE 1 | Flowchart of patients inclusion.

shortness of breath, abdominal discomfort, nausea, or fatigue. After palliative radiation treatment, about half of patients have improvement in symptoms. Most patients have no or grade I-II toxicity. Grade III blood toxicity was recorded in 2 patients and no patients have grade IV toxicity.

Univariable Cox Regression Analyses

The median OS of LC patients receiving palliative radiotherapy is 14.8months (**Supplementary Figure 1**). In model training phase, thirty-one characteristics were investigated by Kaplan-Meier curves and log-rank tests. Six factors (bone metastasis, portal vein tumor thrombus, alpha-fetoprotein, radiation of tumor in liver, radiation dose and biologically effective dose) were considered potentially significant ($P < 0.05$) (**Table 2** and **Figure 2**). Patients with bone metastasis have a median OS of 9.5 months, which is shorter than patients without bone metastasis (17.1 months). Patients with portal vein tumor thrombus (PVTT) have a median OS of 6.8 months, while the median OS of patients without PVTT is 15.1 months. Patients with and without high alpha-fetoprotein (AFP) have a median OS of 9.0 and 16.4 months, respectively. Patients with low radiation dose (< 40 Gy) have a shorter median OS (6.6 months) than patients with high radiation dose (≥40 Gy) (16.8 months). Patients with radiation of tumor in liver have longer survival (30.2 months) compared to patients without radiation of tumor in liver (12.9 months). Patients with higher biologically effective dose (BED ≥ 60 Gy) have a better median OS (20.6 months) compared to patients with low BED (< 60 Gy) (10.1 months).

Multivariable Cox Regression Analyses

BED was excluded in multivariable Cox regression analysis because of the high co-linearity between BED and radiation dose ($P< 0.05$). Thereafter, the remaining five variables were included in the multivariable Cox regression model. Four factors including bone metastasis (HR = 1.781, $P = 0.026$), PVTT (HR = 2.078, $P = 0.015$), AFP (HR = 2.098, $P = 0.007$) and radiation dose (HR = 0.535, $P = 0.023$) have significant potential to predict survival (**Table 2**). Harrell's C-index of the predictive model is 0.709 (95%CI, 0.649-0.769), which indicates good discriminative ability. Additionally, calibration curves of the 1- and 2-year OS of the predictive model indicate that the predicted probabilities of OS are very close to the actual observed outcomes (**Supplementary Figure 2**). For external validation, the Harrell's C-index is 0.735 (95%CI, 0.666-0.804) and calibration curves also indicate good feasibility of the predictive model (**Supplementary Figure 3**).

Assessment of Robustness of Predictive Model by Stratified Analyses

Two radiation treatment techniques including conventional fraction and stereotactic body radiation therapy (SBRT) were used for included patients during the study period. The OS of these two groups of patients have no statistical difference (**Supplementary Figure 4**). Stratified analyses show that predictive model based on bone metastasis, PVTT, AFP, and radiation dose was robust both for patients treated with SBRT or conventional fraction radiation (**Supplementary Table 1**). Metastatic tumors in different organs including liver, lung, bone, and others were radiated. To further investigate the robustness of our predictive model for patients with metastatic tumors in different organs, stratified analyses were conducted and the results demonstrate that our predictive model perform good for all patients (**Supplementary Table 1**).

Nomograms for Survival of LC Patients

Coefficients obtained from the multivariable Cox regression model were taken to establish nomograms for median survival time and 1- and 2-year OS probability (**Figure 3**). Each variable included in the model was assigned a score by locating it to the point scale. The total score of all the variables determines the prediction of a patient's outcome by drawing a vertical line from the total score to the median survival time scale and survival probability scale, respectively. As shown in the **Figure 3**, more total score means better prognosis of patients.

DISCUSSION

To prevent LC patients receiving palliative radiation from over- or under-treatment, survival prediction of patients should be considered before decision making. In this study, 6 clinical characteristics were indicated to be associated with OS of patients according to univariable analysis, and 4 (bone metastasis, PVTT, AFP and radiation dose) of them were statistically significant in multivariable Cox regression analysis.

Bone metastasis often leads to skeletal-related events, such as severe bone pain, pathological fractures, spinal cord compression

TABLE 1 | Clinical characteristics of patients.

Clinical characteristics	Training set (n=103) N (%)	Validating set (n=56) N (%)
Sex (Male/Female)	88 (85.4%)/15 (14.6%)	48 (85.7%)/8 (14.3%)
Age at radiotherapy (< 55/≥ 55 years)	49 (47.6%)/54 (52.4%)	37 (66.1%)/19 (33.9%)
Tobacco (No/Yes)	78 (75.7%)/25 (24.3%)	37 (66.1%)/19 (33.9%)
Alcohol (No/Yes)	59 (57.3%)/44 (42.7%)	35 (62.5%)/21 (37.5%)
Viral hepatitis		
No	22 (21.4%)	15 (26.8%)
B type	76 (73.8%)	36 (64.3%)
Other types	5 (4.8%)	5 (8.9%)
Cirrhosis (No/Yes)	48 (46.6%)/55 (53.4%)	26 (46.4%)/30 (53.6%)
Chinese stage (IIIB/IV)	95 (92.2%)/8 (7.8%)	52 (92.9%)/4 (7.1%)
Tumor sites in liver		
Left lobe	17 (16.5%)	10 (17.9%)
Right lobe	52 (50.5%)	32 (57.1%)
Caudate lobe	11 (10.7%)	3 (5.4%)
≥ 2 lobes	23 (22.3%)	11 (19.6%)
Diagnostic type (Pathological/Clinical)	68 (66.0%)/35 (34.0%)	23 (41.1%)/33 (58.9%)
Metastatic sites		
Liver (No/Yes)	34 (33%)/69 (67%)	21 (37.5%)/35 (62.5%)
Bone (No/Yes)	55 (53.4%)/48 (46.6%)	34 (60.7%)/22 (39.3%)
Lung (No/Yes)	54 (52.4%)/49 (47.6%)	31 (55.4%)/25 (44.6%)
Others (No/Yes)	47 (45.6%)/56 (54.4%)	29 (51.8%)/27 (48.2%)
PVTT (No/Yes)	80 (77.7%)/23 (22.3%)	31 (55.4%)/25 (44.6%)
IVCT (No/Yes)	96 (93.2%)/7 (6.8%)	50 (89.3%)/6 (10.7%)
Tumor in liver (No/Yes)	23 (22.3%)/80 (77.7%)	10 (17.9%)/46 (82.1%)
AFP (Normal/High)	70 (68.0%)/33 (32.0%)	35 (62.5%)/21 (37.5%)
Early therapies		
Surgery (No/Yes)	47 (45.6%)/56 (54.4%)	36 (64.3%)/20 (35.7%)
Radiofrequency ablation (No/Yes)	79 (76.7%)/24 (23.3%)	46 (82.1%)/10 (17.9%)
Intervention therapy (No/Yes)	65 (63.1%)/38 (36.9%)	37 (66.1%)/19 (33.9%)
Target therapy (No/Yes)	87 (84.5%)/16 (15.5%)	51 (91.1%)/5 (8.9%)
Chemotherapy (No/Yes)	81 (78.6%)/22 (21.4%)	49 (87.5%)/7 (12.5%)
BED (< 60 Gy/≥ 60 Gy)	49 (47.6%)/54 (52.4%)	16 (28.6%)/40 (71.4%)
Radiation dose (< 40/≥ 40 Gy)	44 (42.7%)/59 (57.3%)	14 (25.0%)/42 (75.0%)
Fraction (Conventional/SBRT)	39 (37.9%)/64 (62.1%)	17 (30.4%)/39 (69.6%)
Radiation of tumor in		
Liver	28 (27.2%)	17 (30.4%)
Bone	28 (27.2%)	16 (28.6%)
Lung	26 (25.2%)	14 (25.0%)
Others	21 (20.4%)	9 (16.1%)
Target therapy combination (No/Yes)	97 (94.2%)/6 (5.8%)	53 (94.6%)/3 (5.4%)
Chemotherapy combination (No/Yes)	91 (88.3%)/12 (11.7%)	50 (89.3%)/6 (10.7%)
Toxicity		
Hepatic (No/Yes)	91 (88.3%)/12 (11.7%)	53 (94.6%)/3 (5.4%)
Gastroenterological (No/Yes)	89 (86.4%)/14 (13.6%)	53 (94.6%)/3 (5.4%)
Hematological (No/Yes)	82 (79.6%)/21 (20.4%)	52 (92.9%)/4 (7.1%)

PVTT, portal vein tumor thrombus; IVCT, inferior vena cava thrombosis; AFP, alpha-fetoprotein; BED, biologically effective dose; SBRT, stereotactic body radiation therapy.

and hypercalcemia. Habermehl et al.'s study showed that the median OS of LC patients with bone metastasis was 4.2 months after palliative radiation (range, 0.2-38.9 months) (6). In line with Habermehl et al.'s study, we found that bone metastasis can significantly reduce the OS of LC patients (HR = 1.781, P = 0.026). Moreover, about 10%-40% of LC patients have macrovascular invasion (MVI) including portal and/or hepatic veins when they were initially diagnosed (12–14). MVI is an independent predictive factor of poor OS in LC patients. The median OS of LC patients with MVI is significantly lower than those without MVI (2-4 months vs.10-24 months). Similarly, in our study, PVTT can significantly reduce survival of LC patients (HR = 2.078, P = 0.015). Patients with PVTT have a median OS of 6.8 months, which is shorter than patients without PVTT (15.1 months). Furthermore, Elevated AFP before palliative radiotherapy is associated with poor survival. Numerous studies use AFP as a biomarker to predict survival of LC patients. Czauderna et al.'s study shows that high pre-treatment AFP predicts reduced OS in LC (15). In our study, high AFP before palliative radiotherapy also can be an indicator of poor OS (HR = 1.098, P = 0.007). In addition, our study shows that high radiation dose can reduce death rate of advanced liver cancer patients (HR = 0.535, P = 0.023). Similarly, in Kong et al.'s study, the median OS of LC patients treated with high-dose radiation was better than that patients with low-dose radiotherapy (42 months vs. 19 months) (16).

TABLE 2 | Univariable and multivariable Cox regression analysis.

Characteristics	Univariable (*P* value)	Multivariable Cox regression analysis		
		HR	95%CI	*P* value
Bone metastasis (Yes)	0.000	1.781	1.070-2.966	0.026
PVTT (Yes)	0.025	2.078	1.150-3.755	0.015
AFP (High)	0.002	2.098	1.220-3.608	0.007
Radiation of tumor in liver (Yes)	0.036	1.168	0.605-2.257	0.644
Radiation dose ≥ 40 Gy	0.000	0.535	0.311 -0.919	0.023
BED ≥ 60 Gy	0.006	–	–	–

PVTT, portal vein tumor thrombus; AFP, alpha-fetoprotein; BED, biologically effective dose.

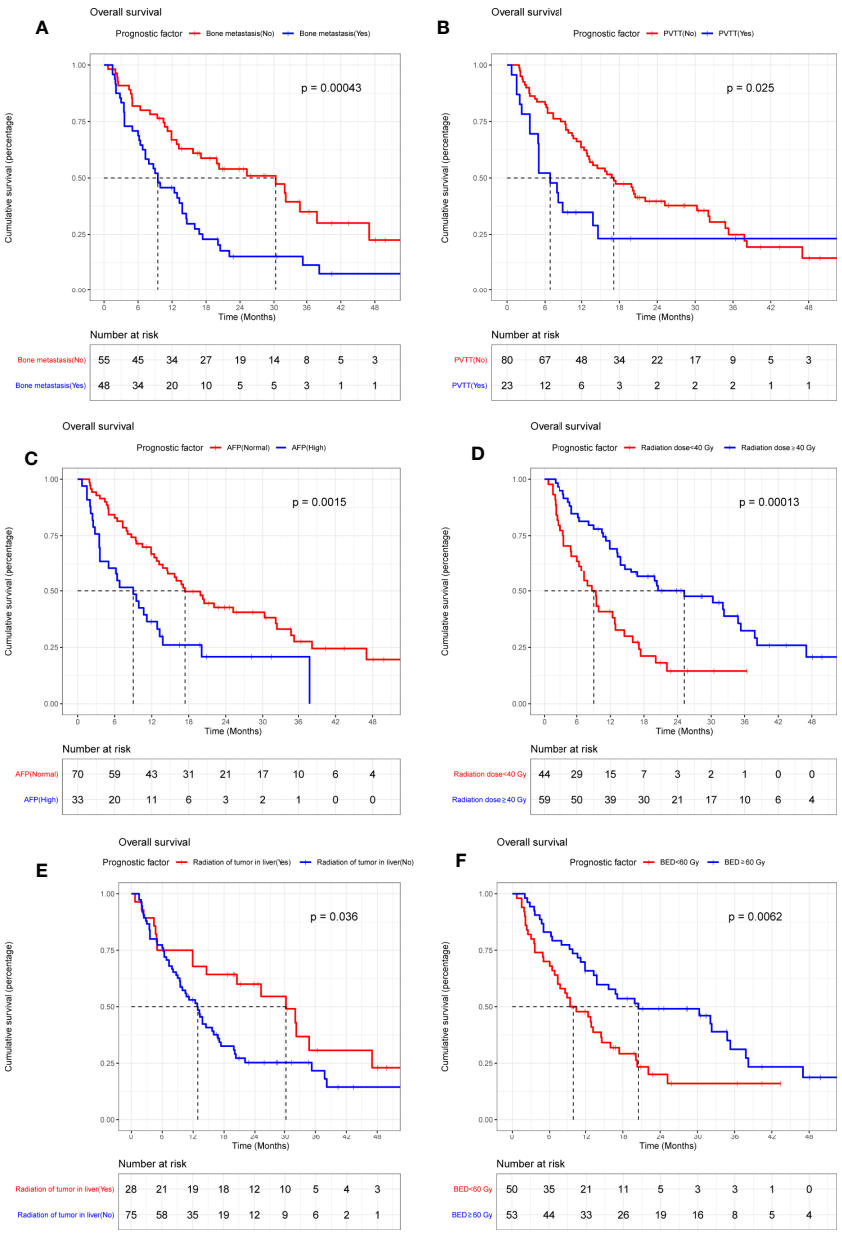

FIGURE 2 | Kaplan-Meier plots of overall survival stratified by bone metastasis **(A)**, portal vein tumor thrombus **(B)**, alpha-fetoprotein **(C)**, radiation dose **(D)**, radiation of tumor in liver **(E)**, and BED **(F)**.

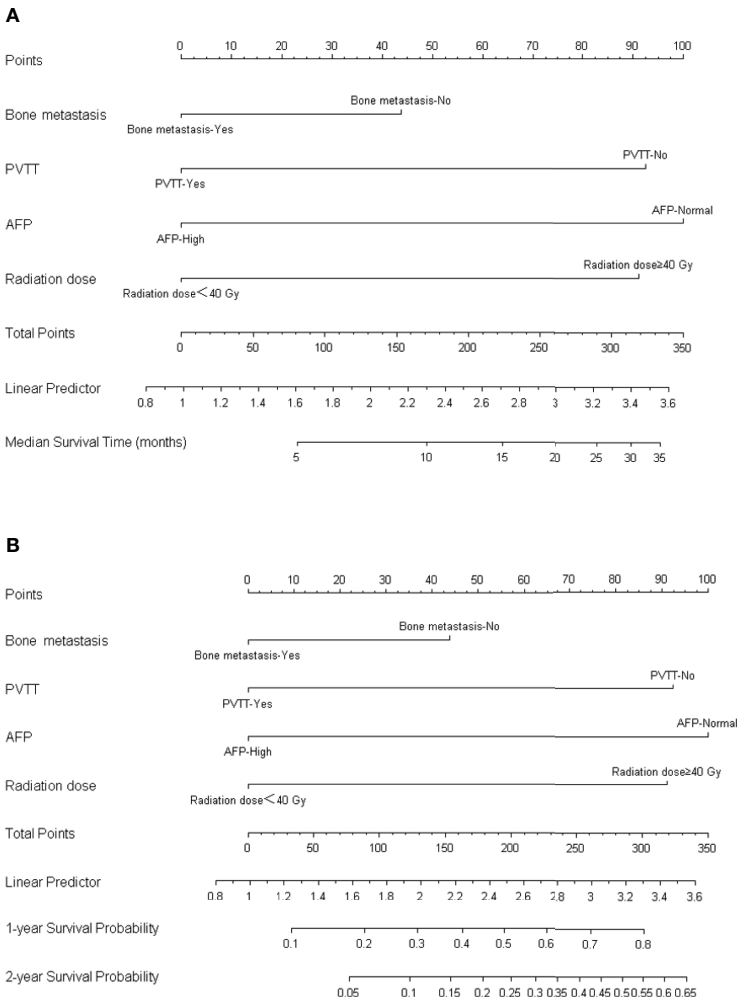

FIGURE 3 | Nomogram for predicting the median OS **(A)** and 1-year/2-year survival probability **(B)**.

There are several limitations should be stated in our article. Firstly, our findings should be interpreted with caution due to the retrospective design of our study. Moreover, all the patients included in our study were treated in a single hospital, which means that potential selection bias may diminish the accuracy of our conclusions. Secondly, different early therapies including surgery, chemotherapy, Intervention therapy and targeted therapy may increase the heterogeneity of included patients. Thirdly, different radiation techniques including SBRT and conventional radiation were taken to treat patients. Although our stratified analyses indicate that our predictive model perform good both for patients treated with conventional radiation and SBRT, our model may fail to predict the OS of patients treated with other radiation techniques. Fourthly, elaborative data of symptoms and QoL was absent, leading to absence of quantitative assessment of symptoms and QOL improvement by scale tools. Finally, several patients received both of palliative radiation and target therapy/chemotherapy during the study time period. According to our univariable analysis, target therapy or chemotherapy combined with palliative radiation have no significant effect on the OS of LC patients compared with patients received single palliative radiation. However, this conclusion should be further investigated in the future because of the small number of patients (6 patients with target therapy and 12 patients with chemotherapy).

Conclusively, four predictive factors of survival of advanced LC patients treated with palliative radiotherapy were identified. These factors were bone metastasis, PVTT, AFP and radiation dose. Recommendations for an individualized palliative radiotherapy for advanced LC patients could be made based on these four factors.

DATA AVAILABILITY STATEMENT

The raw data supporting the conclusions of this article will be made available by the authors, without undue reservation.

AUTHOR CONTRIBUTIONS

QH, DZ, and YL analyzed the data and draft the manuscript. YH, PL, and GX contributed to the collection of data. TZ and JX contributed to the design of the research. All authors contributed to the article and approved the submitted version.

FUNDING

JX is supported by research clinician grant of Tongji medical college, Huazhong university of science and technology (No. 5001530078). This work is supported by the National Natural Science Foundation of China (81903103 to DZ and 81874061 to TZ).

SUPPLEMENTARY MATERIAL

The Supplementary Material for this article can be found online at: https://www.frontiersin.org/articles/10.3389/fonc.2021.658152/full#supplementary-material

Supplementary Figure 1 | Kaplan-Meier curve of overall survival of included patients.

Supplementary Figure 2 | Calibration curves of the 1- **(A)** and 2-year **(B)** OS of the predictive model in training phase.

Supplementary Figure 3 | Calibration curves of the 1- **(A)** and 2-year **(B)** OS of the predictive model in validation phase.

Supplementary Figure 4 | Kaplan-Meier curves of overall survival of patients treated with SBRT or conventional radiation.

REFERENCES

1. Siegel RL, Miller KD, Jemal A. Cancer Statistics, 2020. *CA Cancer J Clin* (2020) 70(1):7–30. doi: 10.3322/caac.21590
2. Wu B, Zhou J, Ling G, Zhu D, Long Q. CalliSpheres Drug-Eluting Beads *Versus* Lipiodol Transarterial Chemoembolization in the Treatment of Hepatocellular Carcinoma: A Short-Term Efficacy and Safety Study. *World J Surg Oncol* (2018) 16(1):69. doi: 10.1186/s12957-018-1368-8
3. Mutsaers A, Greenspoon J, Walker-Dilks C, Swaminath A. Systematic Review of Patient Reported Quality of Life Following Stereotactic Ablative Radiotherapy for Primary and Metastatic Liver Cancer. *Radiat Oncol* (2017) 12(1):110. doi: 10.1186/s13014-017-0818-8
4. Amini A, Gamblin TC. Palliation: Treating Patients With Inoperable Biliary Tract and Primary Liver Tumors. *Surg Oncol Clin N Am* (2014) 23(2):383–7. doi: 10.1016/j.soc.2013.10.008
5. Cunningham SC, Choti MA, Bellavance EC, Pawlik TM. Palliation of Hepatic Tumors. *Surg Oncol* (2007) 16(4):277–91. doi: 10.1016/j.suronc.2007.08.010
6. Habermehl D, Haase K, Rieken S, Debus J, Combs SE. Defining the Role of Palliative Radiotherapy in Bone Metastasis From Primary Liver Cancer: An Analysis of Survival and Treatment Efficacy. *Tumori* (2011) 97(5):609–13. doi: 10.1177/030089161109700512
7. Hayashi S, Tanaka H, Hoshi H. Palliative External-Beam Radiotherapy for Bone Metastases From Hepatocellular Carcinoma. *World J Hepatol* (2014) 6 (12):923–9. doi: 10.4254/wjh.v6.i12.923
8. Zeng ZC, Tang ZY, Fan J, Zhou J, Qin LX, Ye SL, et al. Radiation Therapy for Adrenal Gland Metastases From Hepatocellular Carcinoma. *Jpn J Clin Oncol* (2005) 35(2):61–7. doi: 10.1093/jjco/hyi020
9. Rulli E, Ghilotti F, Biagioli E, Porcu L, Marabese M, D'Incalci M, et al. Assessment of Proportional Hazard Assumption in Aggregate Data: A Systematic Review on Statistical Methodology in Clinical Trials Using Time-to-Event Endpoint. *Br J Cancer* (2018) 119(12):1456–63. doi: 10.1038/s41416-018-0302-8
10. Zhang Z, Kattan MW. Drawing Nomograms With R: Applications to Categorical Outcome and Survival Data. *Ann Transl Med* (2017) 5(10):211. doi: 10.21037/atm.2017.04.01
11. Hu JQ, Yu PC, Shi X, Liu WL, Zhang TT, Lei BW, et al. Prognostic Nomograms for Predicting Overall Survival and Cancer-Specific Survival of Patients With Major Salivary Gland Mucoepidermoid Carcinoma. *J Cancer* (2019) 10(18):4380–8. doi: 10.7150/jca.27992
12. Cheung TK, Lai CL, Wong BC, Fung J, Yuen MF. Clinical Features, Biochemical Parameters, and Virological Profiles of Patients With Hepatocellular Carcinoma in Hong Kong. *Aliment Pharmacol Ther* (2006) 24(4):573–83. doi: 10.1111/j.1365-2036.2006.03029.x
13. Minagawa M, Makuuchi M. Treatment of Hepatocellular Carcinoma Accompanied by Portal Vein Tumor Thrombus. *World J Gastroenterol* (2006) 12(47):7561–7. doi: 10.3748/wjg.v12.i47.7561
14. Llovet JM, Bustamante J, Castells A, Vilana R, Ayuso Mdel C, Sala M, et al. Natural History of Untreated Nonsurgical Hepatocellular Carcinoma: Rationale for the Design and Evaluation of Therapeutic Trials. *Hepatology* (1999) 29(1):62–7. doi: 10.1002/hep.510290145
15. Czauderna C, Schmidtmann I, Koch S, Pilz L, Heinrich S, Otto G, et al. High Pre-Treatment Static and Dynamic Alpha-Fetoprotein Values Predict Reduced Overall Survival in Hepatocellular Carcinoma. *United Eur Gastroenterol J* (2021) 9(3):388–97. doi: 10.1177/2050640620972611
16. Kong XQ, Dong YP, Wu JX, He JY, Le YY, Du KX, et al. High-Biologically Effective Dose Palliative Radiotherapy for a Tumor Thrombus Might Improve the Long-Term Prognosis of Hepatocellular Carcinoma: A Retrospective Study. *Radiat Oncol* (2017) 12(1):92. doi: 10.1186/s13014-017-0831-y

Conflict of Interest: The authors declare that the research was conducted in the absence of any commercial or financial relationships that could be construed as a potential conflict of interest.

Publisher's Note: All claims expressed in this article are solely those of the authors and do not necessarily represent those of their affiliated organizations, or those of the publisher, the editors and the reviewers. Any product that may be evaluated in this article, or claim that may be made by its manufacturer, is not guaranteed or endorsed by the publisher.

frontiers in Oncology

ORIGINAL RESEARCH
published: 26 August 2021
doi: 10.3389/fonc.2021.680303

A Prospective Study of Liver Regeneration After Radiotherapy Based on a New (Su'S) Target Area Delineation

Ting-Shi Su[1†], Li-Qing Li[1†], Shi-Xiong Liang[1], Bang-De Xiang[2], Jian-Xu Li[1], Jia-Zhou Ye[2] and Le-Qun Li[2]*

[1] Department of Radiation Oncology, Guangxi Medical University Cancer Hospital, Nanning, China, [2] Department of Hepatobiliary Surgery, Guangxi Medical University Cancer Hospital, Nanning, China

OPEN ACCESS

Edited by:
John Varlotto, Marshall University, United States

Reviewed by:
Chandan Guha, Albert Einstein College of Medicine, United States
Jing Sun, Medical Center of the PLA General Hospital, China

***Correspondence:**
Ting-Shi Su
sutingshi@163.com

†These authors share first authorship

Specialty section:
This article was submitted to Radiation Oncology, a section of the journal Frontiers in Oncology

Received: *14 March 2021*
Accepted: *09 August 2021*
Published: *26 August 2021*

Citation:
Su T-S, Li L-Q, Liang S-X, Xiang B-D, Li J-X, Ye J-Z and Li L-Q (2021) A Prospective Study of Liver Regeneration After Radiotherapy Based on a New (Su'S) Target Area Delineation. Front. Oncol. 11:680303. doi: 10.3389/fonc.2021.680303

Background: In this study, we designed a new (Su'S) target area delineation to protect the normal liver during liver regeneration and prospectively evaluate liver regeneration after radiotherapy, as well as to explore the clinical factors of liver regeneration and established a model and nomogram.

Methods: Thirty patients treated with preoperative downstaging radiotherapy were prospectively included in the training cohort, and 21 patients treated with postoperative adjuvant radiotherapy were included in the validation cohort. The cut-off points of each optimal predictor were obtained using receiver-operating characteristic analysis. A model and nomogram for liver regeneration after radiotherapy were developed and validated.

Results: After radiotherapy, 12 (40%) and 13 (61.9%) patients in the training and validation cohorts experienced liver regeneration, respectively. The risk stratification model based on the cutoffs of standard residual liver volume spared from at least 20 Gy (SVs20 = 303.4 mL/m^2) and alanine aminotransferase (ALT=43 u/L) was able to effectively discriminate the probability of liver regeneration. The model and nomogram of liver regeneration based on SVs20 and ALT showed good prediction performance (AUC=0.759) in the training cohort and performed well (AUC=0.808) in the validation cohort.

Conclusions: SVs20 and ALT were optimal predictors of liver regeneration. This model may be beneficial to the constraints of the normal liver outside the radiotherapy-targeted areas.

Keywords: radiotherapy, liver regeneration, model, nomogram, hepatocellular carcinoma

INTRODUCTION

Hepatocellular carcinoma (HCC) is the fourth most common cause of cancer-related deaths worldwide (1). Advances in technology enable more accurate and effective radiotherapy (RT), while clinical exploration continues to expand the indications for radiotherapy beyond the formal paradigm of HCC. External beam radiotherapy has been used as a palliative or radical treatment depending on the stage of HCC (2–6). In the latest EASL-EORTC Clinical Practice Guidelines and National Comprehensive Cancer Network Guidelines, radiotherapy is recommended as an alternative locoregional therapy for potentially resectable and unresectable HCC (7, 8). In particular, a multidisciplinary team approach involving radiotherapy is more frequently adopted for selected patients in China and Southeast Asia (9–12).

In the past, regarding the clinical practice of radiotherapy for liver cancer, more attention has been paid to the prevention and treatment of radiation-induced liver injury (13–15), but no in-depth study on liver regeneration has been conducted. Liver regeneration after hepatectomy (16), associated with liver partition and portal vein ligation for staged hepatectomy (ALPPS) (17) and portal vein embolization (PVE) (18) were beneficial to the recovery of treatment-induced liver injury. With the gradual application of preoperative and postoperative radiotherapy for HCC (19–23), liver regeneration after radiotherapy will become a new focus of clinical attention for the prevention or recovery of radiation-induced liver damage. However, the clinical factors that influence liver regeneration after radiotherapy are poorly understood. Therefore, in this study, we designed a new target area delineation to protect the normal liver of liver regeneration and prospectively evaluate liver regeneration after preoperative and postoperative radiotherapy, and further explored the clinical factors and established a model and nomogram for liver regeneration after radiotherapy for HCC.

METHODS

Patients

Patients who underwent preoperative downstaging or postoperative radiotherapy for HCC at Guangxi Medical University Cancer Hospital were included in the study. The training cohort included 30 patients treated with radiotherapy for downstaging non-surgical locally HCC before liver resection from 2018-2019 (ChiCTR1800015350). The inclusion criteria for radiotherapy in down-staging HCC were (1): primary local unresectable HCC with macroscopic vascular tumor emboli (2); One to three lesions in a single lobe; surgical resection was expected to be performed if a descending stage of tumor or thrombolysis (3); Child-Pugh-A or B7 class; and (4) Eastern Clinical Oncology Group score 0-1. The exclusion criteria were as follows: (a) prior history of abdominal radiotherapy, (b) intrahepatic cholangiocellular carcinoma, (c) gallbladder metastases, and/or (d) liver metastases.

The validation cohort included 21 patients treated with postoperative adjuvant therapy for HCC with microvascular vascular invasion or narrow margins after hepatectomy from 2017 to 2019 (NCT 02309788). Patients received adjuvant radiotherapy according to the following criteria (1): HCC with no preoperative radiotherapy (2); resectable lesion with narrow margin (less than 1 cm), at the same time retaining a sufficient residual liver tissue to maintain adequate function (3); compensated cirrhosis or no cirrhosis (4); Child-Pugh A class (5); ECOG score 0-1. The exclusion criteria were (1): presence of distant metastasis (2), palliative resection with residual tumor, and (3) non-HCC confirmed by postoperative pathology (4). Liver failure or decompensation occurs after the surgery.

Su'S Radiotherapy Target Area Delineation Promotes Liver Regeneration

Downstaging Radiotherapy Group

Gross tumor volume (GTV) was defined as intrahepatic tumors and venous tumor thrombus. InterGTV (GTVi) was defined as a 1cm GTV retraction, with the aim of receiving a higher radiation dose to overcome the radiation tolerance caused by central tumor ischemia or hypoxia. The clinical target volume (CTV) was obtained by adding a 0.5 cm margin to the GTV. The planning target volume (PTV) was defined as the CTV and GTV expansion 0.5 cm in horizontal direction and 0.5-0.8 cm head and foot direction for setup uncertainty and respiratory motion. GTV/GTVi areas should avoid more than 1 cm when encountering gastrointestinal organs. The absolute normal liver volume was calculated as the total liver minus the GTV. Liver protected volume was defined as a normal liver segment 2.0 cm away from the CTV, and the purpose of liver protection was to promote liver regeneration (**Figure 1A**). The final radiation dose delivered to the isocentric was 66 Gy for GTVi (4.4 or 3.3 Gy/fx), 60 Gy for PGTV (4.0 or 3.0 Gy/fx), and 45–50 Gy for PCTV (3.0-2.5 Gy/fx) with 15 or 20 fractions (5 fractions per week).

Postoperative Adjuvant Radiotherapy Group

Adjuvant radiotherapy was started 4-6 weeks after surgery. The postoperative tumor bed area was designated as GTVtb. The CTV1 extends 0.5 cm on the basis of GTVtb. CTV2 extends 0.5 cm on the basis of CTV1. PTV was defined as the CTV1 and CTV2 expansion 0.5 cm in horizontal direction and 0.5-0.8 cm head and foot direction for setup uncertainty and respiratory motion. GTVtb/CTV1 areas should avoid more than 0.5-1.0 cm when encountering gastrointestinal organs. The absolute normal liver volume was calculated as the total liver minus CTV1. The liver protected volume was defined as a normal liver segment 2.0 cm away from CTV2 (**Figure 1B**), and the purpose of liver protection was to promote liver regeneration. The final radiation dose delivered to the isocentric was 50-60 Gy for PCTV1 (2.0-2.4 Gy/fx), 40-50 Gy for PCTV2 (2.0-2.25 Gy/fx) with 20 or 25 fractions (5 fractions a week).

All target areas were sketched in the MIM 6.8 system (MIM, USA). The Pinnacle 3 system (Philips, Netherlands) was used to

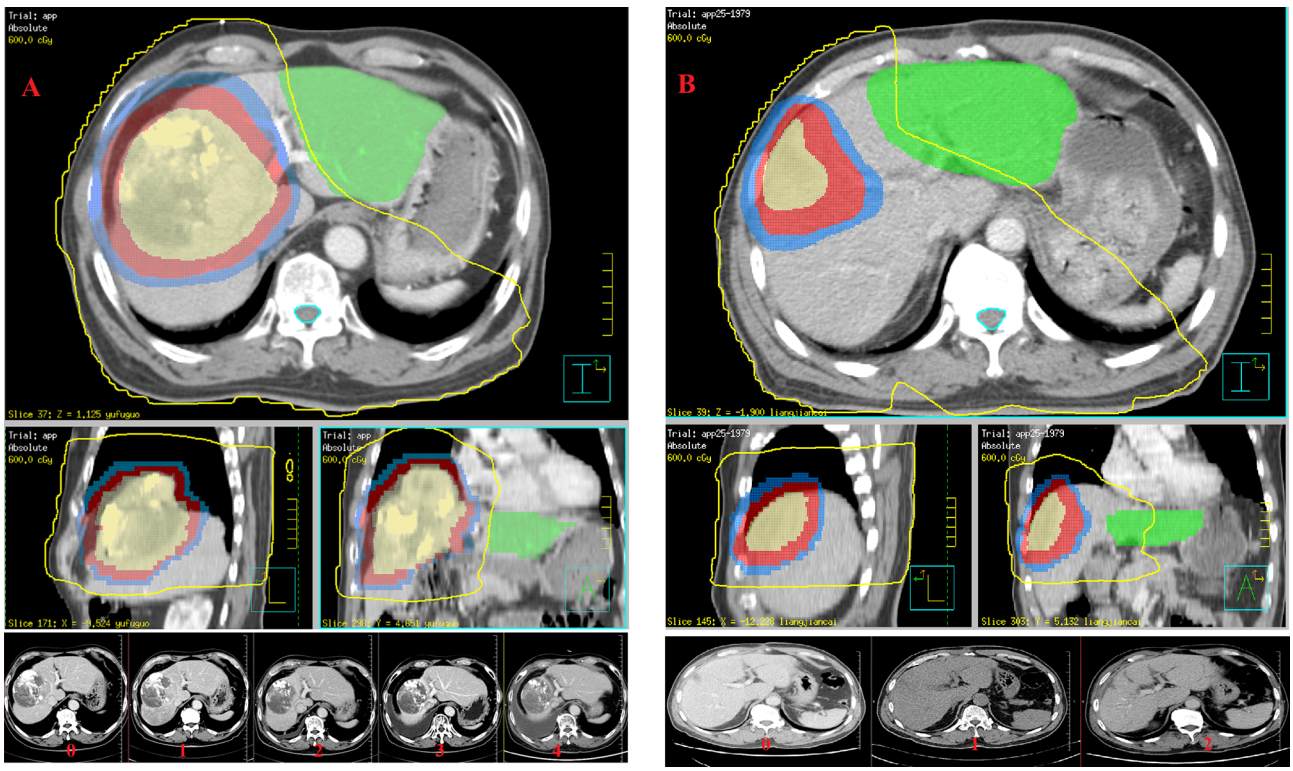

FIGURE 1 | Su'S radiotherapy target area delineation promotes liver regeneration and evaluation of liver regeneration after radiotherapy: **(A)** the training cohort (GTVi, PGTV and PCTV are shown from inside to outside, and the green part represents liver protected volume in preoperative downstaging radiotherapy plan); and **(B)** the testing cohort (GTVtb, PCTV1 and PCTV2 are shown from inside to outside, and the green part represents liver protected volume in postoperative adjuvant radiotherapy plan).

accomplish the target area dose planning (YY, USA). All patients were treated with a linear accelerator (ELEKTA Synergy, Sweden and ELEKTA VersaHD, Sweden). There were various dose–volume constraints for the organs at risk. For the liver, the normal liver volume D_{mean}< 21 Gy, and normal liver volume spared from at least 10 Gy (V_S10) was >410 mL and liver protected D_{mean} < 7 Gy. For the stomach, small bowel, and duodenum, D_{max} was < 40–45 Gy each. For the kidneys, V15 was <1/3 V. Similarly, for the spinal cord, D_{max} <40 Gy.

Liver Regeneration Ratio Assessment

Patients were re-evaluated 1 and 3 months after radiotherapy and every 3-6 months thereafter. Contrast-enhanced CT and/or MRI were performed within 2 weeks before radiotherapy and subsequently at each follow-up visit after radiotherapy. Laboratory examinations assessed the levels of aspartate transaminase (AST), alanine transaminase (ALT), prothrombin time (PT), and levels of albumin, total bilirubin, and alpha-fetoprotein (AFP).

Liver regeneration at each re-evaluation of each patient was performed for comparison. The CT or MRI images before and after radiotherapy were imported into the MIM 6.8, to delineate the hepatic parenchymal volume of the segment and lobe of interest in the same manner. Liver regeneration was defined as an increase of more than 10% of normal liver volume in the areas of the protected hepatic segment or lobe within 1 year after completion of radiotherapy compared to the volume of pre-radiotherapy, and no Child-Pugh class degradation of liver function and tumor progression was observed at the last time. If downstaging surgery or tumor progression occurs in the areas of interest, liver regeneration assessment is discontinued.

Variable Selection

We screened predictor variables for liver regeneration from the following variables: (a) clinical factors: age, sex, height, weight and hepatitis B virus (HBV) infection; (b) serum biochemical parameters: red blood cells count (RBC), white blood cells count (WBC), hemoglobin (HB), platelets (PLT), total bilirubin (Tbil), albumin, alanine aminotransferase (ALT), aspartate aminotransferase (AST), lactic dehydrogenase (LDH), activated partial thromboplastin time (APTT) and alpha-fetoprotein (AFP); (c) dose-volumetric parameters: functional liver volume, mean dose of the liver (liver-Dmean), GTV volume (the sum of all GTVs), GTV dose and fractions; (d) dosimetric Dataset 1: the percentage of normal protected liver volume (%) spared from at least x Gy (Vx); and (e) dosimetric Dataset 2: the

absolute normal liver volume (mL) spared from at least x Gy (Vsx); (f) dosimetric Dataset 3: standard residual normal liver volume (mL/m^2) spared from at least x Gy (SVsx) (formula: SVsx = Vsx/Body surface area). In the training cohort, the random forest model was applied to rank these factors in descending order of relative importance. In the preliminary screening, factors with an area under a receiver-operating characteristic (ROC) curve (AUC) greater than 0.6, were considered as potential prognostic predictors. Correlation analysis was performed to avoid overfitting. When Spearman's rho value was greater than 0.65 between the two dosimetric parameters, the one with a lower correlation with liver generation was excluded.

Calculated Values and Statistical Analysis

Continuous variables were compared using Student's t-test or the Mann–Whitney U-test, and categorical variables were compared using the chi-square test. The final nomogram was formulated to predict liver regeneration based on prognostic factors extracted from the training cohort. For internal validation, the prediction performance of the nomograms was measured using a calibration curve and concordance index (C-index) to measure internal calibration and discriminative ability. To avoid over-optimism, bootstrap resampling (1000) resamples were applied to correct the C-index for assessment of the nomogram calibration performance. The prognostic model was further validated in a postoperative adjuvant radiotherapy cohort to ascertain its feasibility. The total points of each patient in the testing cohort were calculated according to the established nomogram and used as a predictor of liver regeneration. The AUC of the ROC was used to evaluate the prediction performance of our model using external data.

For additional analyses, the optimal cut-off value for each selected factor of the models was obtained from the Youden's index in conjunction with the ROC analysis from the testing cohort. Risk stratification was then conducted according to the cut-off point in both the training and validation cohorts, as well as the entire cohort. Fisher's exact test was used to compare the proportion of patients with liver regeneration between the subgroups. All statistical analyses were completed using R version 4.0.2 (2020–06–22), and a P value less than 0.05, was considered statistically significant.

RESULTS

Baseline Characteristics

Fifty-one patients with HCC were included. The study population was predominantly male (n= 46, 90.1%), with a median age of 48 years (range, 21-70 years). Most of the patients (n=37, 72.5%) were infected with CHB.

The baseline characteristics and dosimetric data of the training (n=30) and testing cohorts (n=21) are summarized in **Table 1**. All patients in the training cohort were BCLC-C stage, including 27 patients (90%) with portal vein tumor emboli and other 3 cases with hepatic venous thrombus, while all patients in the testing cohort were BCLC-A (n=18, 86%) and B (n=3, 14%). The testing cohort was characterized by lower AFP (median 23.88 *vs.* 1436.64 ng/ml, P=0.003), AST (median 29.5 *vs.* 59 U/L, P<0.001), LDH (median 248 *vs.* 148 U/L, P<0.001) and APTT (30.5 *vs.* 34.5 s, P= 0.007), more patients infected with HBV (60% *vs.* 90%, P=0.016) while fewer patients with hypoalbuminemia (36.4 *vs.* 32.8, P=0.002). Patients in the testing cohort had lower normal liver volume (median 758.75 *vs.* 948.32 ml, P<0.001) than those in the training cohort. Dose-volumetric parameters, including the volume of GTV/CTV1 (P<0.001). Vs5 (p =0.024), Vs40 (P=0.041), SVs5 (P=0.016), SVs30 (P=0.044), SVs35 (P=0.014), and SVs40 (P=0.008) differed significantly between the two groups, with no significant difference in the remaining parameters.

Volumetric Data for Liver Regeneration

During the observation period of 1 year, a total of 25 patients (49%) experienced liver regeneration in the entire cohort. The change trends of liver regeneration after radiotherapy are shown in **Figures 2A, B**.

In the training cohort of 30 patients, 9 patients underwent surgery after radiotherapy at 3-12 months, and 5 patients at the second evaluation node (liver regeneration 2) experienced tumor progression in the area of interest, and the liver regeneration assessments were therefore stopped. The mean protected hepatic lobe and segment volume before radiotherapy was 605.2 ± 371 mL, increasing to 648.7 ± 345.6 mL after radiotherapy. Liver regeneration occurred in 12 of 30 patients, yielding a liver regeneration rate of 40%. Among them, 6, 1, 2, and 3 patients had liver regeneration rates of 10%–20%, 20–50%, 50%–100%, and greater than 100%, respectively.

In the testing cohort of 21 patients, 4 patients in the testing cohort after the first evaluation node (liver regeneration 1) experienced tumor progression in the area of interest. The mean protected hepatic lobe and segment volume before radiotherapy was 532.5 ± 450.7 mL, increasing to 578.9 ± 412.2 mL after radiotherapy. Liver regeneration occurred in 13 out of 21 patients, yielding a liver regeneration rate of 62%, which was comparable to the rate noted in the training cohort (P =0.12). Among them, 3, 8, 2, and 0 patients had liver regeneration rates of 10%–20%, 20–50%, 50%–100%, and greater than 100%, respectively.

Twenty-four cases of Child-Pugh degradation were detected within 2 weeks after radiotherapy. In the training cohort, 17 patients experienced an increase in Child-Pugh score, including 13 patients with +1 score due to decreased serum albumin levels, 3 patients with +2 scores, and 1 patient with +3 scores. In the validation cohort, 7 patients experienced an increase of one score in Child-Pugh score due to decreased serum albumin levels. There was a negative correlation between the degree of liver regeneration and the increase in Child-Pugh score (P=0.006, analysis of variance). Over a longer observation period, 13 (51.2%) patient's liver function gradually recovered with the appearance of liver regeneration. Liver regeneration did not

TABLE 1 | Information of patients in different treatment groups.

Factor	Level	Training group	Testing group	P-value
Number of patients		30	21	
liver regeneration	No	18 (60%)	8 (38%)	0.12
	Yes	12 (40%)	13 (62%)	
Gender	female	2 (7%)	3 (14%)	0.37
	male	28 (93%)	18 (86%)	
Age, median (IQR), yrs		48 (41, 58)	47 (39, 54)	0.65
Height, median (IQR), cm		165 (162, 170)	165 (160, 170)	0.66
Weight, median (IQR), kg		57.5 (51, 70)	57 (52, 62)	0.61
GTV/CTV1 dose, Gy	45	2 (6%)	0 (0%)	0.037
	50	3 (10%)	11 (52%)	
	56	2 (7%)	0 (0%)	
	60	23 (77%)	10 (48%)	
Fractions	12	1 (3%)	0 (0%)	<0.001
	15	12 (40%)	0 (0%)	
	20	17 (57%)	4 (20%)	
	25	0 (0%)	17 (80%)	
Tumor emboli	No	0 (0%)	21 (100%)	<0.001
	Yes	30 (100%)	0 (0%)	
BCLC stage	A	0 (0%)	18 (86%)	<0.001
	B	0 (0%)	3 (14%)	
	C	30 (100%)	0 (0%)	
Tumor size, median (IQR), cm		11.2 (9.3,13.7)	0 (0,0)	<0.001
Child-Pugh	A	25 (83.3%)	20 (95.2)	0.381
	B7	5 (16.7%)	1(4.8)	
hepatitis B surface antigen	positive	29 (96.7%)	19 (90%)	0.86
	negative	1 (3.3%)	2 (10%)	
AFP, median (IQR), ng/mL		1436.64 (65.67, 8446.97)	23.875 (2.9, 298.69)	0.003
RBC, median (IQR), $\times10^{12}$/L		4.385 (3.85, 4.75)	4.3 (4.04, 4.77)	0.87
HGB, median (IQR), g/L		129.5 (115, 141)	125 (121, 136)	0.86
PLT, median (IQR), $\times10^{9}$/L		186.5 (135, 252)	204 (175, 275)	0.54
Tbil, median (IQR), umol/L		15.9 (10.4, 23.2)	10.4 (7.9, 15.8)	0.053
ALT, median (IQR), u/L		46 (28, 66)	36 (24, 52)	0.31
Albumin, median (IQR), g/L		32.85 (30.5, 34.4)	36.4 (34.6, 38.2)	0.002
AST, median (IQR), u/L		59.5 (44, 97)	29 (29, 37)	<0.001
LDH, median (IQR)		248 (207, 360)	148 (139, 175)	<0.001
APTT, median (IQR)		34.5 (31, 38)	30.5 (27.4, 32.8)	0.007
GTV/CTV1 volume, median (IQR), mL		829.77 (556.25, 1395.66)	54.91 (41.82, 86.39)	<0.001
Liver volume, median (IQR), mL		758.75 (610.73, 1008.79)	943.32 (852.15, 1125.03)	0.026
Liver-Dmean, median (IQR), Gy		15.2 (12.5, 19.5)	17.6 (13.3, 20.7)	0.44
Dataset 1: Vx(%)				
V5, median (IQR)		68.07 (58.92, 82.65)	64.01 (46.97, 78.52)	0.13
V10, median (IQR)		40.99 (34.36, 53.16)	53.16 (32.51, 63.57)	0.69
V15, median (IQR)		29.095 (23.26, 45.74)	39.83 (27.6, 51.3)	0.23
V20, median (IQR)		24.08 (17.46, 38.55)	33.94 (23.91, 41.81)	0.12
V25, median (IQR)		20.71 (14.03, 29.82)	27.31 (20.95, 37.87)	0.072
V30, median (IQR)		17.445 (11.69, 25.23)	24.92 (18.03, 30.24)	0.088
V35, median (IQR)		15.16 (9.8, 19.99)	20.72 (13.51, 23.17)	0.11
V40, median (IQR)		12.51 (7.52, 16)	15.36 (11.3, 19.65)	0.15
Dataset 2: VsX(mL)				
Vs5, median (IQR)		231.281 (106.039, 340.5)	369.948 (226.726, 451.895)	0.024
Vs10, median (IQR)		440.61 (301.988, 540.796)	476.129 (328.414, 567.966)	0.24
Vs15, median (IQR)		494.219 (408.691, 660.603)	595.253 (441.678, 645.371)	0.29
Vs20, median (IQR)		576.736 (441.247, 726.929)	642.055 (500.469, 757.203)	0.23
Vs25, median (IQR)		611.642 (464.236, 768.908)	683.681 (559.181, 818.222)	0.15
Vs30, median (IQR)		626.677 (482.953, 802.44)	728.232 (615.237, 911.303)	0.085
Vs35, median (IQR)		640.942 (499.924, 855.575)	766.951 (656.837, 963.722)	0.053
Vs40, median (IQR)		658.308 (522.279, 889.097)	788.962 (686.976, 973.066)	0.041
Dataset 3: SVsX(mL/m^2)				
SVs5, median (IQR)		147.976 (55.9661, 204.89)	238.205 (137.36, 305.654)	0.016
SVs10, median (IQR)		257.066 (187.943, 305.571)	308.596 (210.072, 409.522)	0.14
SVs15, median (IQR)		298.816 (258.908, 380.281)	353.752 (277.593, 457.307)	0.13
SVs20, median (IQR)		341.586 (288.752, 428.616)	394.046 (339.95, 486.134)	0.085
SVs25, median (IQR)		354.403 (309.701, 480.15)	431.839 (350.927, 513.324)	0.056

(Continued)

TABLE 1 | Continued

Factor	Level	Training group	Testing group	P-value
SVs30, median (IQR)		361.757 (316.607, 516.365)	471.309 (384.163, 534.623)	0.044
SVs35, median (IQR)		374.189 (323.059, 528.796)	502.75 (418.129, 570.836)	0.014
SVs40, median (IQR)		385.501 (332.418, 542.123)	526.548 (440.686, 602.561)	0.008

HBV, hepatitis B virus; RBC, red blood cells count; HGB, hemoglobin; PLT, platelets; Tbil, total bilirubin; ALTa, lanine aminotransferase; AST, aspartate aminotransferase; LDH, lactic dehydrogenase; APTT, activated partial thromboplastin time ; AFP, alpha-fetoprotein. Dataset 1: the percentage of normal protected liver volume (%) spared from at least x Gy (Vx); Dataset 2: the absolute normal liver volume (mL) spared from at least x Gy (Vsx), Dataset 3: standard residual normal liver volume (mL/m2) spared from at least x Gy (SVsx).

occur in the remaining 11 cases, of which 3 patient's liver function improved spontaneously within 3 months and other 8 cases remained unimproved.

Risk Group Sub-Classification Based on ALT and SVs20

Datasets 1 and 2 had no significant correlation with liver regeneration. Dataset 3 and clinical factors were used separately for further analysis. According to the subgroup ROC analysis of ALT and SVs20 in the training cohort, the AUC of SVs20 was 0.639 (95% confidence interval [CI], 0.833–0.583) with a cut-off value of 303.4 mL (sensitivity, 65.00%; specificity, 86.15%; **Figure 3A**), and the AUC of ALT was 0.690 (95% CI, 0.722–0.667) with a cutoff value of 43 U/L (sensitivity, 65.00%; specificity, 90.77%; **Figure 3B**). Risk group sub-classification was performed according to the cutoff points. As shown in **Table 2**, a combination of ALT and SVs20 demonstrated clear differentiation in the risk of liver generation between the subgroups in the training cohort (P=0.049) and the entire cohort (P=0.032). The proportion of patients with liver regeneration decreased progressively with 88.9% in the high-probability group (ALT <43 U/L and SVs20 <303.4 mL/m^2), 60% in the high-intermediate probability group (ALT ≥43 U/L and SVs20 <303.4 mL/m^2), 43.75% in the low-intermediate probability group (ALT <43 U/L and SVs20 ≥303.4 mL/m^2), and 33% in the low-probability group (ALT≥43 U/L and SVs20≥303.4 mL/m^2), indicating that a combination of high ALT (≥43 U/L) and high SVs20 (≥303.4 mL/m^2) conferred the greatest risk of poor liver regeneration.

Establishment and Assessment of the prognostic Nomogram

To provide more convenient for clinical liver regeneration prediction and avoid overfitting, only ALT among pre-radiotherapy laboratory variables and SVs20 among dataset 3 parameters were found to be optimal predictors for liver regeneration modeling. Finally, an SVs20 based nomogram incorporating ALT and SVs20 was established (**Figure 4A**). The model and nomogram showed high predictive accuracy (C-index =0.759, **Figure 4B**) in the training cohort for predicting liver regeneration. The calibration curve confirmed the excellent calibration capability of the model, and the probability predicted by the model was in good agreement with the actual observed values of liver regeneration. The nomogram performed well in external validation (C-index = 0.808, **Figure 4C**) with high discriminatory accuracy in the testing cohort (**Supplementary Figure**).

DISCUSSION

In this study, we designed a new target area delineation to protect the normal liver for regeneration and prospectively evaluate liver regeneration after radiotherapy. After radiotherapy, 40% (12/30) of cases in the preoperative downstaging group and 61.9% (13/21) of cases in the postoperative adjuvant group experienced liver regeneration. We further found that pretreatment ALT and SVs20 were the optimal variables for liver regeneration modeling. The risk stratification model based on the cutoffs of SVs20 (303.4 mL/m^2) and ALT (43 u/L) was able to effectively discriminate the probability of liver regeneration. The model and nomogram of liver regeneration showed good prediction performance (AUC=0.759) in the training cohort and performed well (AUC=0.808) in the validation cohort, justifying its application values.

In the past decade, adjuvant radiotherapy has been confirmed to provide considerably improved treatment outcomes (19, 21–24). Neoadjuvant radiotherapy provided better overall survival and recurrence-free survival rates compared to surgery alone (20). Yeh et al. showed that 11% of HCCs could become resectable with a 2-year OS rate of 67% and a median survival of 30 months (25). Chong et al. (26) reported that 26 of 98 (26.5%) patients were downstaged after concurrent chemoradiotherapy (CCRT) followed by hepatic arterial infusion chemotherapy (HAIC) and underwent subsequent curative resection. Disease-specific survival was significantly better in the resection group after localized downstaging. Lee et al. (27) also reported that 41 (16.9%) patients underwent curative resection after CCRT followed by HAIC, and the 5-year survival rate in the curative resection group after CCRT improved significantly compared to that of the CCRT alone group (49.6%: 9.8%, P< 0.001). Preoperative downstaging radiotherapy may provide better control of the local tumor and simultaneously promote liver regeneration, creating a better opportunity for wide-margin surgery. However, the insufficient volume of the future liver remnant (FLR) remains a serious constraint that hinders R0–R1 resection (23). Inadequate functional liver volume is also a major cause of liver function deterioration after radiotherapy. Therefore, compensating for the loss of liver mass by regeneration is of great importance, especially in patients with large tumors and limited healthy livers (28). Consequently, a precise radiotherapy plan based on the accurate

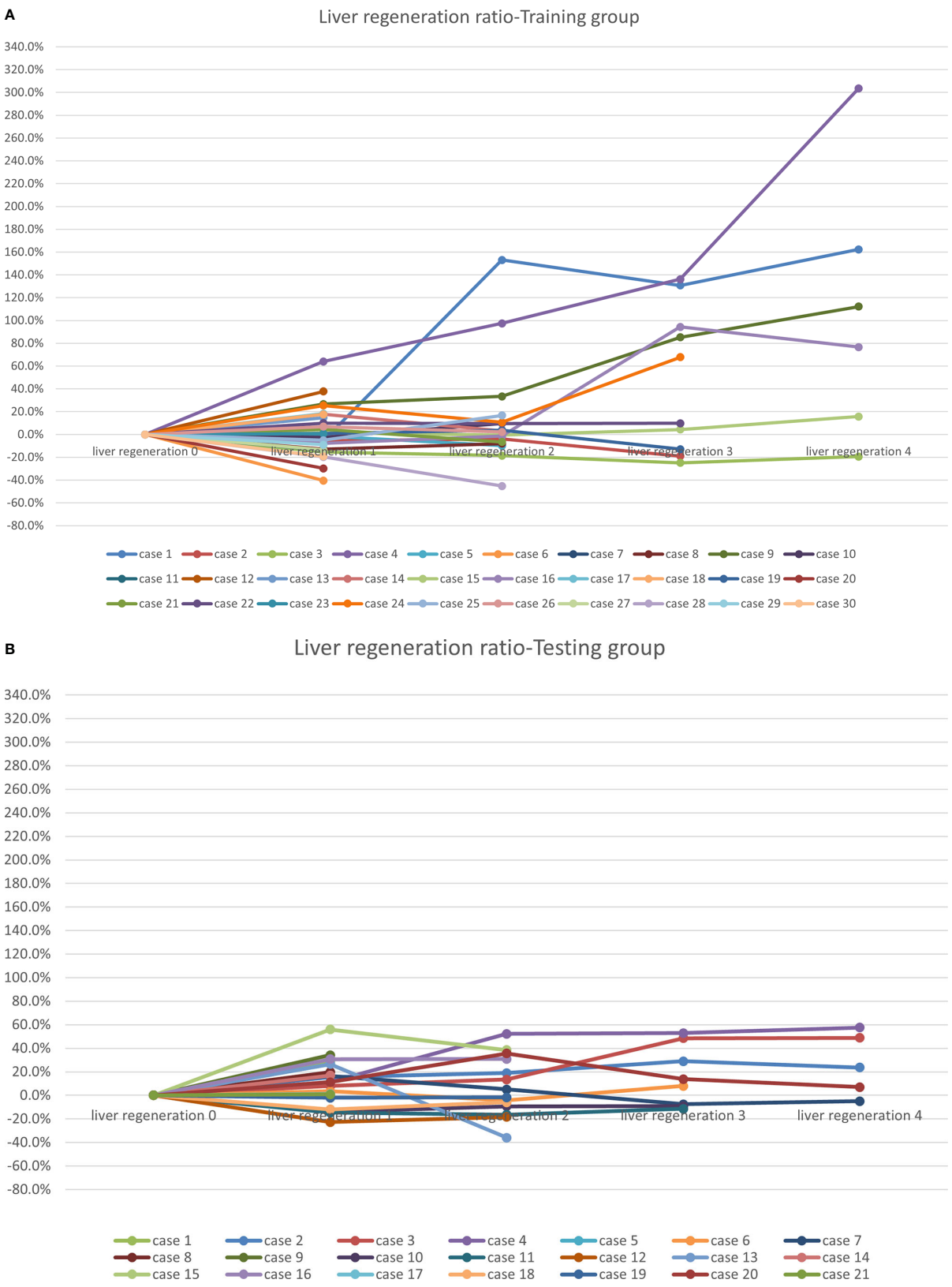

FIGURE 2 | Liver regeneration growth ratio after radiotherapy: **(A)** the training cohort; and **(B)** the testing cohort.

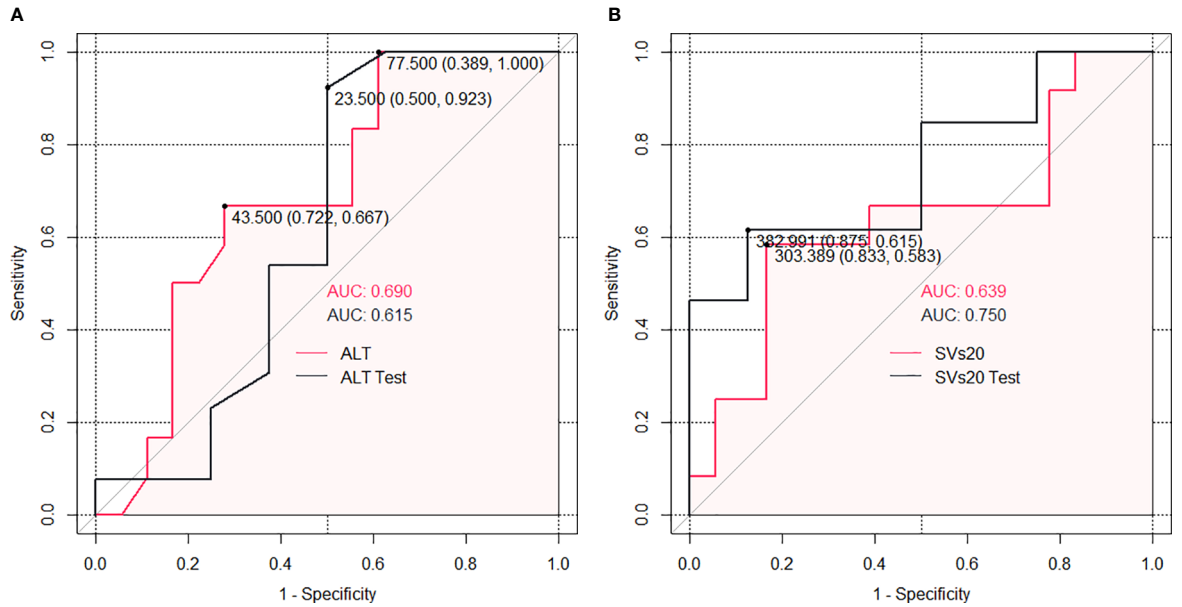

FIGURE 3 | The cut-off points and AUC of each optimal predictors by ROC analysis: **(A)** ALT; **(B)** SVs20.

prediction of liver regeneration is urgently needed in clinical practice.

Previous nomogram models based on clinical factors have focused on risk assessment, such as estimating the risk of radiation-induced liver disease (RILD) and mortality following radiotherapy (29–31). Choi et al. (32) showed that adjuvant radiotherapy with a dose of 40–50 Gy in 20-25 fractions delayed the liver regeneration process after partial hepatectomy. However, nomogram models based on dose-volume metrics for benefit assessment associated with liver regeneration in HCC patients treated with radiotherapy have never been established. We found that liver regeneration was significantly associated with domestic dataset 3(SVs, mL/m^2), but not with dataset 1 (V, %) and dataset 2 (Vs, mL). The current study identified, for the first time, SVs20 as a key predictor for liver generation following radiotherapy with an optimal cutoff of 303.4, suggesting that fewer constraints on the dose of residual liver should be taken into account to promote liver regeneration. Meanwhile, the risk of RILD following dose escalation is a major cause of liver failure after radiotherapy, and stricter dose-limiting to the functional liver should be prioritized in radiation planning. Based on our past experience of hepatic toxicity following radiotherapy, V20 (dataset 1) in normal liver volume of 48.5% as the liver tolerance predicted RILD risks well in primary liver carcinoma patients with Child–Pugh grade A cirrhosis after hypo-fractionated radiotherapy (15). We further found that Vs10 ≥416.2 mL (dataset 2) predicted a progression of at least 1 and Vs10≥621.8 mL of at least 2 points decreased in the Child–Pugh score after stereotactic body radiation therapy (14), highlighting the necessity for hepatotoxicity mitigating in high-risk functional liver areas. Functional liver avoidance with V20 <48.5% and/or Vs10 ≥416.2 mL may be used as a radiotherapy reference in clinical practice by balancing the pros and cons.

Among the pre-RT laboratory variables, ALT was found to have a significant correlation with liver regeneration. ALT is well recognized as a marker of liver injury related to liver parenchymal

TABLE 2 | Risk Group Sub-classification based on ALT and SVs20.

Sub-classification	Training cohort (n=30)			Entire cohort (n=51)		
	NLR, n (%)	LR, n (%)	P	NLR, n (%)	LR, n (%)	P
ALT<43U/L SVs20<303.4 mL/m^2	1 (16.7%)	5 (83.3%)	0.049	1 (11.1%)	8 (88.9%)	0.032
ALT≥43U/L SVs20<303.4 mL/m^2	2 (50%)	2 (50%)		2 (40%)	3 (60%)	
ALT<43U/L SVs20≥303.4 mL/m^2	5 (62.5%)	3 (37.5%)		9 (56.2%)	7 (43.8%)	
ALT≥43U/L SVs20≥303.4 mL/m^2	10 (83.3%)	2 (16.7%)		14 (66.7%)	7 (33.3%)	

LR, liver regeneration; NLR, no liver regeneration; ALT, alanine aminotransferase; SVs20, standard residual normal liver volume (mL/m2) spared from at least 20Gy.

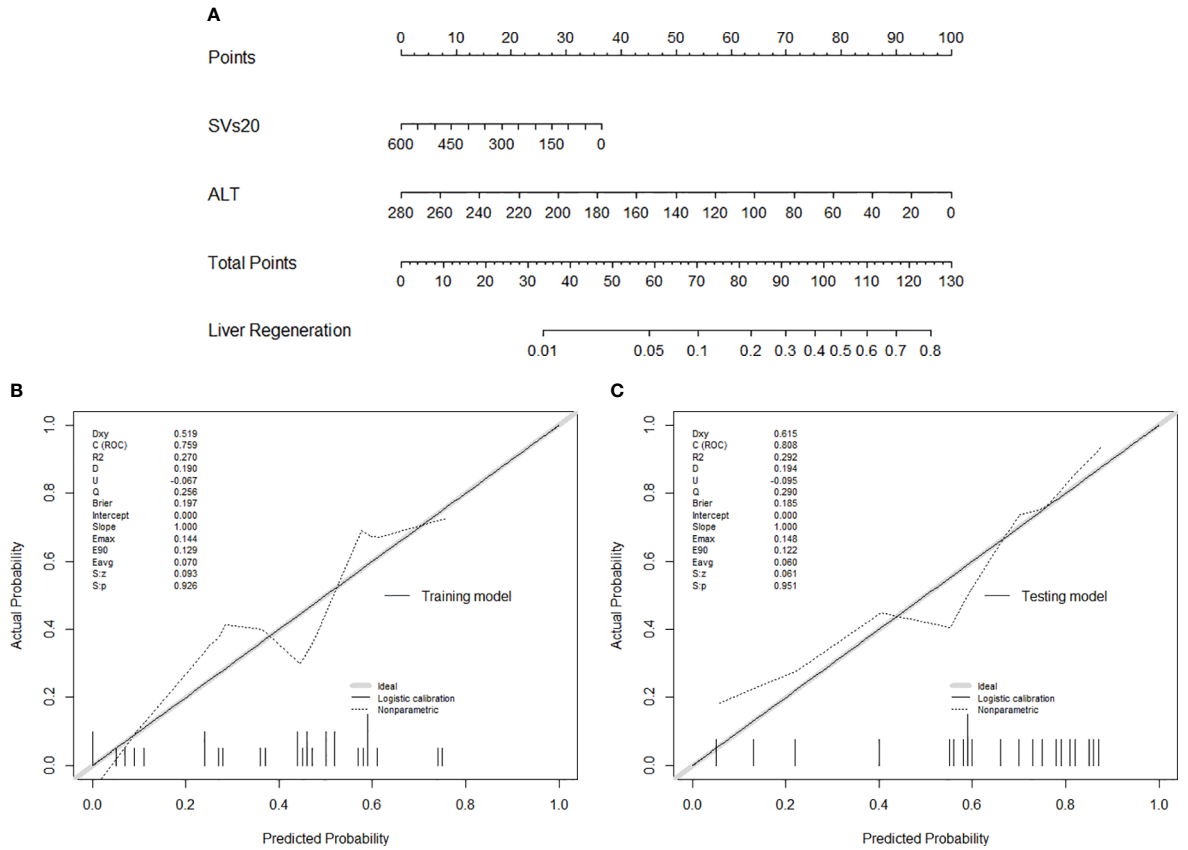

FIGURE 4 | **(A)** Nomogram of liver regeneration based on SVs20 and ALT; **(B)** The calibration curve in the training cohort; **(C)** The calibration curve in the testing cohort.

injury. In line with our current results, Mohapatra et al. (33) reported that a high level of ALT predicted poor liver regeneration following donor hepatectomy. Caldez et al. (34) showed that ALT is hyperactivated when liver cells fail to divide during liver regeneration, indicating that ALT not only acts as a signal of liver damage but is also a crucial metabolic regulator necessary to support tissue recovery. Kimura et al. (35) reported that serum ALT levels after partial liver resection are negatively correlated with L-ascorbic acid and L-ascorbic acid 2-Glucoside, which stimulates liver regeneration. Similarly, Lin et al. (36) revealed the crucial role of translationally controlled tumor protein in liver regeneration, as well as enhancing the recovery of ALT after liver resection in humans. Ito et al. (37) found that partially hepatectomized rats had lower serum ALT levels and higher recovery of remnant liver weight. Although the precise mechanisms are not fully understood, these results strongly indicate that lower ALT levels are associated with better liver regeneration. This potential mechanism requires further exploration and research.

Our study has several limitations. First, this study was conducted in China, where HBV-associated HCC rates are high. The applicability of this nomogram for patient cohorts in other areas is uncertain and requires further validation. Second, the sample size was small in this study, the reliability of the model has been verified in two different prospective studies, and it is still worth verifying with a larger sample size in the future.

In conclusion, this simple-to-use nomogram incorporating ALT and SVs20 is beneficial to the constraints of the normal liver outside the radiotherapy target area. It may provide a reference for clinicians to make prognosis-based decisions without complex calculations. Further validation with multicenter data is warranted to verify its practicability in patients with HCC who have undergone radiotherapy.

DATA AVAILABILITY STATEMENT

The datasets presented in this article are not readily available because the confidentiality rules of hospital. Requests to access the datasets should be directed to sutingshi@163.com.

ETHICS STATEMENT

The studies involving human participants were reviewed and approved by Institutional Ethics Committee of Guangxi Medical University Cancer Hospital (LW2021009). The patients/participants provided their written informed consent to participate in this study.

AUTHOR CONTRIBUTIONS

Conception and design: T-SS. Administrative support: T-SS, S-XL, and L-QuL. Provision of study materials or patients: All authors. Collection and assembly of data: L-QiL. Data analysis and interpretation: T-SS and L-QiL. Manuscript writing: T-SS and L-QiL. All authors contributed to the article and approved the submitted version.

FUNDING

This research was supported by the National Natural Science Foundation of China (81903257 and 81960534), and Guangxi Natural Science Foundation (CN) (2020GXNSFAA297171), and Cancer Precision Radiotherapy Spark Program of China International Medical Foundation (2019-N-11-01), High-level innovation team and outstanding scholar program in Guangxi Colleges and Universities, and Guangxi Medical University Training Program for Distinguished Young Scholars, and Guangxi BaGui Scholars' Special Fund.

SUPPLEMENTARY MATERIAL

The Supplementary Material for this article can be found online at: https://www.frontiersin.org/articles/10.3389/fonc.2021.680303/full#supplementary-material

Supplementary Figure | The AUC of the training and testing model using ROC analysis.

REFERENCES

1. Yang JD, Hainaut P, Gores GJ, Amadou A, Plymoth A, Roberts LR. A Global View of Hepatocellular Carcinoma: Trends, Risk, Prevention and Management. *Nat Rev Gastroenterol Hepatol* (2019) 16(10):589–604. doi: 10.1038/s41575-019-0186-y
2. Su TS, Li LQ, Meng WW, Wang YD, Chen YT, Li JX, et al. Long-Term Survival Analysis of Transarterial Chemoembolization Plus Radiotherapy *vs.* Radiotherapy for Hepatocellular Carcinoma With Macroscopic Vascular Invasion. *Front Oncol* (2020) 10:1205. doi: 10.3389/fonc.2020.01205
3. Su TS, Liang P, Liang J, Lu HZ, Jiang HY, Cheng T, et al. Long-Term Survival Analysis of Stereotactic Ablative Radiotherapy Versus Liver Resection for Small Hepatocellular Carcinoma. *Int J Radiat Oncol Biol Phys* (2017) 98 (3):639–46. doi: 10.1016/j.ijrobp.2017.02.095
4. Sun J, Wang Q, Hong ZX, Li WG, He WP, Zhang T, et al. Stereotactic Body Radiotherapy Versus Hepatic Resection for Hepatocellular Carcinoma (≤ 5 Cm): A Propensity Score Analysis. *Hepatol Int* (2020) 14(5):788–97. doi: 10.1007/s12072-020-10088-0
5. Yoon SM, Ryoo BY, Lee SJ, Kim JH, Shin JH, An JH, et al. Efficacy and Safety of Transarterial Chemoembolization Plus External Beam Radiotherapy vs Sorafenib in Hepatocellular Carcinoma With Macroscopic Vascular Invasion: A Randomized Clinical Trial. *JAMA Oncol* (2018) 4(5):661–9. doi: 10.1001/jamaoncol.2017.5847
6. Li LQ, Zhou Y, Huang Y, Liang P, Liang SX, Su TS. Stereotactic Body Radiotherapy Versus Intensity-Modulated Radiotherapy for Hepatocellular Carcinoma With Portal Vein Tumor Thrombosis. *Hepatol Int* (2021) 15 (3):630–41. doi: 10.1007/s12072-021-10173-y
7. Vogel A, Cervantes A, Chau I, Daniele B, Llovet J, Meyer T, et al. Hepatocellular Carcinoma: ESMO Clinical Practice Guidelines for Diagnosis, Treatment and Follow-Up. *Ann Oncol* (2018) 29(Supplement_4):iv238–iv55. doi: 10.1093/annonc/mdy308
8. Benson AB3rd, D'Angelica MI, Abbott DE, Abrams TA, Alberts SR, Saenz DA, et al. NCCN Guidelines Insights: Hepatobiliary Cancers, Version 1.2017. *J Natl Compr Canc Netw* (2017) 15(5):563–73. doi: 10.6004/jnccn.2017.0059
9. Lu J, Zhang XP, Zhong BY, Lau WY, Madoff DC, Davidson JC, et al. Management of Patients With Hepatocellular Carcinoma and Portal Vein Tumour Thrombosis: Comparing East and West. *Lancet Gastroenterol Hepatol* (2019) 4(9):721–30. doi: 10.1016/S2468-1253(19)30178-5
10. Korean Liver Cancer A and National Cancer Center GK. 2018 Korean Liver Cancer Association-National Cancer Center Korea Practice Guidelines for the Management of Hepatocellular Carcinoma. *Korean J Radiol* (2019) 20 (7):1042–113. doi: 10.3348/kjr.2019.0140
11. Cheng SQ, Chen MS, Cai JQ, Sun JX, Guo RP, Bi XY, et al. Chinese Expert Consensus on Multidisciplinary Diagnosis and Treatment of Hepatocellular Carcinoma With Portal Vein Tumor Thrombus (2018 Edition). *Liver Cancer* (2020) 9(1):28–40. doi: 10.1159/000503685
12. Zhou J, Sun HC, Wang Z, Cong WM, Wang JH, Zeng MS, et al. Guidelines for Diagnosis and Treatment of Primary Liver Cancer in China (2017 Edition). *Liver Cancer* (2018) 7(3):235–60. doi: 10.1159/000488035
13. Liang SX, Zhu XD, Xu ZY, Zhu J, Zhao JD, Lu HJ, et al. Radiation-Induced Liver Disease in Three-Dimensional Conformal Radiation Therapy for Primary Liver Carcinoma: The Risk Factors and Hepatic Radiation Tolerance. *Int J Radiat Oncol Biol Phys* (2006) 65(2):426–34. doi: 10.1016/j.ijrobp.2005.12.031
14. Su TS, Luo R, Liang P, Cheng T, Zhou Y, Huang Y. A Prospective Cohort Study of Hepatic Toxicity After Stereotactic Body Radiation Therapy for Hepatocellular Carcinoma. *Radiother Oncol* (2018) 129(1):136–42. doi: 10.1016/j.radonc.2018.02.031
15. Liang SX, Huang XB, Zhu XD, Zhang WD, Cai L, Huang HZ, et al. Dosimetric Predictor Identification for Radiation-Induced Liver Disease After Hypofractionated Conformal Radiotherapy for Primary Liver Carcinoma Patients With Child-Pugh Grade A Cirrhosis. *Radiother Oncol* (2011) 98 (2):265–9. doi: 10.1016/j.radonc.2010.10.014
16. Gong WF, Zhong JH, Lu Z, Zhang QM, Zhang ZY, Chen CZ, et al. Evaluation of Liver Regeneration and Post-Hepatectomy Liver Failure After Hemihepatectomy in Patients With Hepatocellular Carcinoma. *Biosci Rep* (2019) 39(8):BSR20190088. doi: 10.1042/BSR20190088
17. Wang Z, Peng Y, Hu J, Wang X, Sun H, Sun J, et al. Associating Liver Partition and Portal Vein Ligation for Staged Hepatectomy for Unresectable Hepatitis B Virus-Related Hepatocellular Carcinoma: A Single Center Study of 45 Patients. *Ann Surg* (2020) 271(3):534–41. doi: 10.1097/SLA.0000000000002942
18. Pourcher G, El-Kehdy H, Kanso F, Groyer-Picard MT, Gaillard M, Trassard O, et al. Volumetric Portal Embolization: A New Concept to Improve Liver Regeneration and Hepatocyte Engraftment. *Transplantation* (2016) 100 (2):344–54. doi: 10.1097/TP.0000000000001024
19. Bai T, Chen J, Xie ZB, Wu FX, Wang SD, Liu JJ, et al. The Efficacy and Safety of Postoperative Adjuvant Transarterial Embolization and Radiotherapy in Hepatocellular Carcinoma Patients With Portal Vein Tumor Thrombus. *Onco Targets Ther* (2016) 9:3841–8. doi: 10.2147/OTT.S104307
20. Wei X, Jiang Y, Zhang X, Feng S, Zhou B, Ye X, et al. Neoadjuvant Three-Dimensional Conformal Radiotherapy for Resectable Hepatocellular Carcinoma With Portal Vein Tumor Thrombus: A Randomized, Open-Label, Multicenter Controlled Study. *J Clin Oncol* (2019) 37(24):2141–51. doi: 10.1200/JCO.18.02184
21. Sun J, Yang L, Shi J, Liu C, Zhang X, Chai Z, et al. Postoperative Adjuvant IMRT for Patients With HCC and Portal Vein Tumor Thrombus: An Open-Label Randomized Controlled Trial. *Radiother Oncol* (2019) 140:20–5. doi: 10.1016/j.radonc.2019.05.006
22. Yu W, Wang W, Rong W, Wang L, Xu Q, Wu F, et al. Adjuvant Radiotherapy in Centrally Located Hepatocellular Carcinomas After Hepatectomy With Narrow Margin (<1 Cm): A Prospective Randomized Study. *J Am Coll Surg* (2014) 218(3):381–92. doi: 10.1016/j.jamcollsurg.2013.11.030
23. Wang WH, Wang Z, Wu JX, Zhang T, Rong WQ, Wang LM, et al. Survival Benefit With IMRT Following Narrow-Margin Hepatectomy in Patients With Hepatocellular Carcinoma Close to Major Vessels. *Liver Int* (2015) 35 (12):2603–10. doi: 10.1111/liv.12857

24. Rong W, Yu W, Wang L, Wu F, Zhang K, Chen B, et al. Adjuvant Radiotherapy in Central Hepatocellular Carcinoma After Narrow-Margin Hepatectomy: A 10-Year Real-World Evidence. *Chin J Cancer Res* (2020) 32 (5):645–53. doi: 10.21147/j.issn.1000-9604.2020.05.09
25. Yeh SA, Chen YS, Perng DS. The Role of Radiotherapy in the Treatment of Hepatocellular Carcinoma With Portal Vein Tumor Thrombus. *J Radiat Res* (2015) 56(2):325–31. doi: 10.1093/jrr/rru104
26. Chong JU, Choi GH, Han DH, Kim KS, Seong J, Han KH, et al. Downstaging With Localized Concurrent Chemoradiotherapy Can Identify Optimal Surgical Candidates in Hepatocellular Carcinoma With Portal Vein Tumor Thrombus. *Ann Surg Oncol* (2018) 25(11):3308–15. doi: 10.1245/s10434-018-6653-9
27. Lee HS, Choi GH, Choi JS, Kim KS, Han KH, Seong J, et al. Surgical Resection After Down-Staging of Locally Advanced Hepatocellular Carcinoma by Localized Concurrent Chemoradiotherapy. *Ann Surg Oncol* (2014) 21 (11):3646–53. doi: 10.1245/s10434-014-3652-3
28. Wei W, Hua C, Zhang T, Dirsch O, Gremse F, Homeyer A, et al. Size of Portally Deprived Liver Lobe After Portal Vein Ligation and Additional Partial Hepatectomy: Result of Balancing Proliferation and Apoptosis. *Sci Rep* (2020) 10(1):4893. doi: 10.1038/s41598-020-60310-0
29. Velec M, Haddad CR, Craig T, Wang L, Lindsay P, Brierley J, et al. Predictors of Liver Toxicity Following Stereotactic Body Radiation Therapy for Hepatocellular Carcinoma. *Int J Radiat Oncol Biol Phys* (2017) 97(5):939–46. doi: 10.1016/j.ijrobp.2017.01.221
30. Huang WY, Tsai CL, Que JY, Lo CH, Lin YJ, Dai YH, et al. Development and Validation of a Nomogram for Patients With Nonmetastatic BCLC Stage C Hepatocellular Carcinoma After Stereotactic Body Radiotherapy. *Liver Cancer* (2020) 9(3):326–37. doi: 10.1159/000505693
31. Zhang L, Yan L, Niu H, Ma J, Yuan BY, Chen YH, et al. A Nomogram to Predict Prognosis of Patients With Unresected Hepatocellular Carcinoma Undergoing Radiotherapy: A Population-Based Study. *J Cancer* (2019) 10 (19):4564–73. doi: 10.7150/jca.30365
32. Choi JH, Kim K, Chie EK, Jang JY, Kim SW, Oh DY, et al. Does Adjuvant Radiotherapy Suppress Liver Regeneration After Partial Hepatectomy? *Int J Radiat Oncol Biol Phys* (2009) 74(1):67–72. doi: 10.1016/j.ijrobp.2008.06.1941
33. Mohapatra N, Sinha PK, Sasturkar SV, Patidar Y, Pamecha V. Preoperative Alanine Aminotransferase and Remnant Liver Volume Predict Liver Regeneration After Live Donor Hepatectomy. *J Gastrointest Surg* (2020) 24 (8):1818–26. doi: 10.1007/s11605-019-04332-8
34. Caldez MJ, Van Hul N, Koh HWL, Teo XQ, Fan JJ, Tan PY, et al. Metabolic Remodeling During Liver Regeneration. *Dev Cell* (2018) 47(4):425–38.e5. doi: 10.1016/j.devcel.2018.09.020
35. Kimura M, Moteki H, Uchida M, Natsume H, Ogihara M. L-Ascorbic Acid- and L-Ascorbic Acid 2-Glucoside Accelerate In Vivo Liver Regeneration and Lower Serum Alanine Aminotransaminase Activity in 70% Partially Hepatectomized Rats. *Biol Pharm Bull* (2014) 37(4):597–603. doi: 10.1248/bpb.b13-00839
36. Lin Z, Zhang X, Wang J, Liu W, Liu Q, Ye Y, et al. Translationally Controlled Tumor Protein Promotes Liver Regeneration by Activating Mtorc2/AKT Signaling. *Cell Death Dis* (2020) 11(1):58. doi: 10.1038/s41419-020-2231-8
37. Ito K, Ozasa H, Noda Y, Koike Y, Arii S, Horikawa S. Splenic Artery Ligation Improves Remnant Liver Function in Partially Hepatectomized Rats With Ischemia/Reperfusion Injury. *Liver Int* (2007) 27(3):400–7. doi: 10.1111/j.1478-3231.2006.01432.x

Conflict of Interest: The authors declare that the research was conducted in the absence of any commercial or financial relationships that could be construed as a potential conflict of interest.

Publisher's Note: All claims expressed in this article are solely those of the authors and do not necessarily represent those of their affiliated organizations, or those of the publisher, the editors and the reviewers. Any product that may be evaluated in this article, or claim that may be made by its manufacturer, is not guaranteed or endorsed by the publisher.

frontiers in Oncology

ORIGINAL RESEARCH
published: 21 December 2021
doi: 10.3389/fonc.2021.801352

A Comprehensive Evaluation of ZrC Nanoparticle in Combined Photothermal and Radiation Therapy for Treatment of Triple-Negative Breast Cancer

Shan Jiang[1†], Zhao Liu[1†], Yuhang Tian[1], Ming Zhuang[2], Shiqi Piao[2], Yan Gao[3], Andrew Tam[4], Hongtao Hu[2] and Wen Cheng[1*]*

[1] Department of Ultrasound, Harbin Medical University Cancer Hospital, Harbin, China, [2] Department of Radiation Oncology, Harbin Medical University Cancer Hospital, Harbin, China, [3] School of Chemistry and Chemical Engineering, Harbin Institute of Technology, Harbin, China, [4] Department of Radiation Oncology, City of Hope National Medical Center, Duarte, CA, United States

OPEN ACCESS

Edited by:
John Varlotto,
Marshall University, United States

Reviewed by:
Chengyu Shi,
New York Proton Center, United States
Ruijie Yang,
Peking University Third Hospital, China

***Correspondence:**
Wen Cheng
hrbchengwen@163.com
Hongtao Hu
huht9099@sohu.com

[†]These authors have contributed equally to this work

Specialty section:
This article was submitted to Radiation Oncology, a section of the journal Frontiers in Oncology

Received: 25 October 2021
Accepted: 24 November 2021
Published: 21 December 2021

Citation:
Jiang S, Liu Z, Tian Y, Zhuang M, Piao S, Gao Y, Tam A, Hu H and Cheng W (2021) A Comprehensive Evaluation of ZrC Nanoparticle in Combined Photothermal and Radiation Therapy for Treatment of Triple-Negative Breast Cancer. Front. Oncol. 11:801352. doi: 10.3389/fonc.2021.801352

Because of the difficulty in treating triple-negative breast cancer (TNBC), the search for treatments has never stopped. Treatment opinions remain limited for triple-negative breast cancer (TNBC). The current treatment approach of using photothermal therapy (PTT) is often imprecise and has limited penetration below the surface of the skin. On the other hand, radiation therapy (RT) has its unavoidable disadvantages, such as side effects or ineffectiveness against hypoxic tumor microenvironment (TME). In this study, we proposed the use of ZrC nanoparticles in conjunction with RT/PTT to enhance antitumor and antimetastatic effect. We modified the ZrC nanoparticle with bovine serum albumin (BSA) and folic acid (FA), sizing desirable about 100nm. The photothermal conversion efficiency was calculated to be 40.51% and sensitizer enhancement ration (SER) was 1.8. With addition of ZrC NPs, more DNA were damaged in γ-H2AX and more ROS were detected with immunofluorescence. *In vitro* and vivo, the combined therapy with ZrC NPS showed the best effect of tumor cell inhibition and safety. Our results provide evidence that the combination of ZrC NPs, PT, and RT is effective in of TNBC, making it a great potential application for cancer therapy in clinic.

Keywords: sensitizer, PTT, RT, nanoparticle, breast cancer

INTRODUCTION

Radiation therapy (RT), combined with surgery and systemic chemotherapy, is the current standard of care treatment for breast cancer (1, 2). Using high energy radiation such as X-ray or γ-ray, RT directly ionizes DNA molecules (3), or indirectly interacts with water, to form reactive oxygen species (ROS) to induce cell apoptosis (4, 5). Compared to tumor of squamous cell origin, such as the common type of nasopharyngeal carcinoma, breast adenocarcinoma, especially for triple-negative breast cancer (TNBC), has lower sensitivity to X-ray radiation (6, 7). Techniques currently employed to maximize exposure of

target volume to radiation include intensity modulated radiation therapy and hypofractionation, but risk of acute and late adverse events still need consideration (8, 9). How to improve the efficacy of RT for triple-negative breast cancer is a question worth pondering.

Radiosensitizers are agents that increase efficacy of RT, and thereby allow for lower doses of radiation and reducing toxicity to organ at risk (10). Notably, clinical trials demonstrated the potential of high atomic number (Z) nanomaterials as enhancer of radiation to target cancer cells (e.g., gold (10–13), bismuth, wolfram (14, 15), platinum, gadolinium (16)) have been exploited. Even though developing radiosensitizers is a promising way to increase the level of efficacy, some difficulties, such as radiation resistance of hypoxic cancer cells, still limit its applications in RT (14, 17). To overcome such obstacles, combining RT with phototherapy (PT) to realize a synergistic therapy can open new potentials (18, 19). Given the limitations of RT alone, new efforts have explored the potential of combining RT with phototherapy (PT), including photothermal therapy (PTT) and photodynamic therapy (PDT), as a synergistic approach to therapy. The photothermal nanomaterial at tumor site creates local hyperthermia under external near infrared (NIR) irradiation (20, 21). The *in vivo* hyperthermia not only contributes to necrosis or apoptosis of cancer cells, but also creates an oxygen-enriched environment, and in effect reduces radiotherapy resistance (22). In combination with PT, lower dose in RT could be sufficient to kill the tumor and simultaneously enhance systemic antitumor immune response, while high dose RT cause damage to immune system (23, 24). Recent evidence has shown that radiation of X-ray and NIR can also be immunomodulatory by altering the microenvironment of the irradiated field (25, 26). Since RT and PT are both local treatments as main role, the anti-tumor immunity effects could compensate disadvantages (24, 27). Although antitumor immunity induced by RT or PT alone is rarely sufficient to activate systemic anti-tumor immune response, whether combination has the potential to extend the applications beyond a local modality is worth investigating.

It will be very significant if we can construct an ideal "all in one" nanoparticles to act as the sensitizer for both RT and PT that have the following characteristics: (1) good photo-thermal conversion behavior; (2) can act as radiosensitizers to enhance the deposition of irradiation energy; (3) can be specifically targeted to tumors; and (4) is biodegraded (28). In this work, we present a new multifunctional nano agent to be used in combined PT and RT. Using BSA to modify the nanoparticles in order to improve the biocompatibility, as well as tumor-targeted molecule FA (ZrC-BSA-FA, ZrC NPs). Detailed therapeutic strategy by using ZrC NPs was presented in **Scheme 1**. At the first part, we characteristic ZrC NPs and then tests were performed to see its excellent thermal storage, thermal stability, thermal conductivity and photo-thermal conversion feature. ZrC NPs has been an attractive candidate for PT because of its potential as a dual-modality therapy sensitizer, its efficacy as a radio-sensitizer is investigated here for the first time. At the third part we performed experiments to assess the potential to selectively treat TNBC, including vivo and vitro. To further

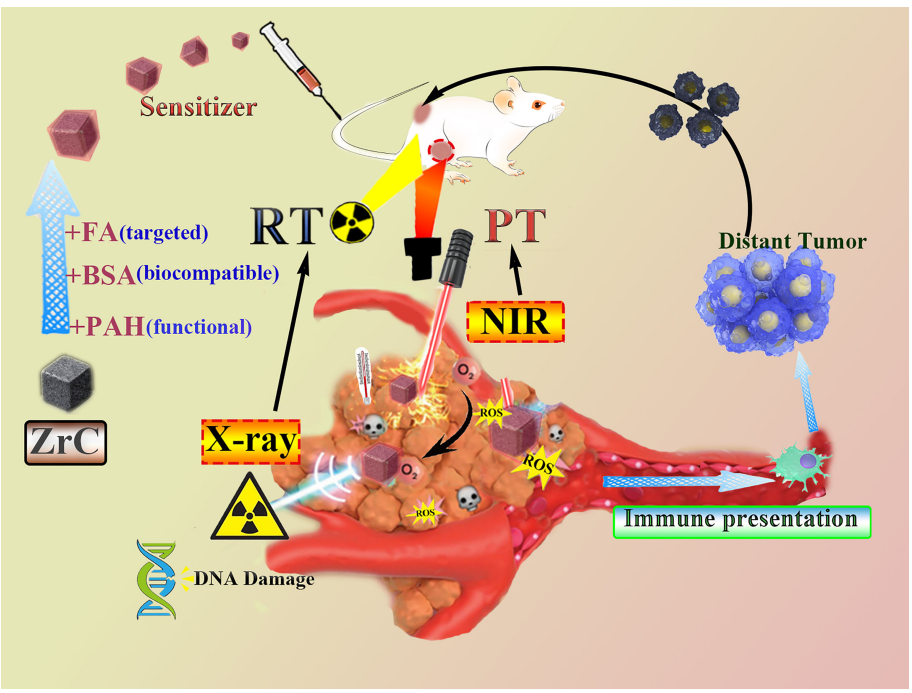

SCHEME 1 | Scheme diagram of radiation therapy combined phototherapy process of this work.

explain its mechanism, we performed the semiquantitative method to detect tumor apoptosis factors/proliferative factors of tumor. In the last part, we built tumor-bearing mouse model of double tumors to see whether ZrC NPs with PT and RT in mouse could activate immune response *in vitro*. Our results provide proof of concept evidence that the combination of ZrC NPs, PT, and RT is effective for the treatment of TNBC, making it a great potential application for cancer therapy in clinic.

MATERIALS AND CHARACTERIZATIONS

Materials

All chemicals and reagents were used as received without further purification.

ZrC nanoparticles were purchased from Shanghai Chaowei Nano Technology Co. Ltd and stored in a desiccator. Folic acid, Poly (allylamine hydrochloride) (PAH, Mw= 17 500), DCFH-DA and DPBF were purchased from Sigma-Aldrich. Bovine serum albumin (BSA), calcein-AM, propidium iodide (PI), and 3-(4,5-dimethyl-2-thiazolyl)-2,5-diphenyl-2-H-tetrazolium bromide (MTT) were obtained from Summus. All the antibodies were purchased from Abcam. The γ-H2AX antibody was purchased from Abcam. Phospho-Histone γ-H2AX (Ser139) (20E3) Rabbit mAb and Antirabbit IgG (H+L) were provided by Cell Signaling Technology.

BALB/c nude mouse and BALB/c mouse were purchased from Beijing Vital River Laboratory Animal Technology Co., Ltd. Animals are fed sterile water and unrestricted food. They were placed in mice room with standard conditions. All the experimental steps adopted in this experiment conformed to the experimental scheme approved by the Key Laboratory for Biomedical Effects of Nanomaterials and Nanosafety (Chinese Academy Sciences, CAS).

Surface Modification Process of ZrC Nanoparticles

Prior to the modification, ZrC nanocrystals were heated in NH3atmosphere at 850°C for 2 h for full nitridation. Then, the powder was dispersed in water and underwent ultrasonic dispersion for 20 min. The suspension was centrifuged at 4000 rpm for 5 min to remove bulk particles. The ZrCNPs were prepared *via* electrostatic interaction according to our previously published method with minor modifications. (51), (53) In brief, ZrC(6 mg) and PAH (4 mg) were dissolved in 2 mL NaCl solution (0.5 M) under ultrasonic dispersion for 20 min with a mass ratio of 1: 4. Then, the sample was collected by centrifugation (12 000 rpm, 5 min) and rinsed three times with NaCl solution (0.1 M) to obtain ZrC@PAH.

After that, ZrC@PAH and BSA with a mass ratio of 1: 3 were dissolved in deionized water and continuously stirred for 4 h in an ice bath. Finally, the suspension was centrifuged, washed with distilled water and freeze dried, obtaining ZrC@PAH/BSA.

After ZrC@PAH/BSA were prepared, they were mixed with 0.5% (wt/vol) of FA–gelatin solution and stirring at room temperature for 24 hours. The FA-functionalized ZrC@PAH/BSA/FA were collected by centrifugation, washed with Milli-Q water, and redispersed in Milli-Q water for further use.

Characterizations

The nanostructural features of sample were observed on a JEOL 2100 electron microscope at 200 kV (JEOL Ltd.), including transmission electron microscopy (TEM). The optical behavior of the samples was measured on a spectrophotometer (U-4100, Hitachi). TEM observation was performed using a FEI Tecnai G2 F30 system. The nanoparticles characteristics were determined by XRD (Shimadzu XD-D1). XPS spectra (PerkinElmer PHI 5600) were used to analyze the composition and chemical valence of the samples. The absorption spectra were performed by Cary Series UV-Vis-NIR Spectrophotometer. The hydrodynamic diameter was measured by a Zeta-Sizer (Malvern Nano series). FTIR was acquired by the Excalibur 3100 (Varian). Temperature monitoring was realized with an infrared camera (FLIR System i7).

Photothermal Test

To examine the photothermal performance of heterogeneous ZrCNPs, different concentrations of CSA solutions were prepared and heated with an 808 nm laser at different power. An infrared thermal imaging camera (FLIR, A65) was applied to record the change of temperature. The photothermal stability of ZrCNPs was also examined by heating and cooling for 5 cycles. For each cycle, 808 nm laser was turned on to heat the ZrCNPs solution for 10 minutes and then switched off to allow cooling to room temperature.

$$\eta = \frac{\mathrm{hS}(\mathrm{T_{max}} - \mathrm{T_{surr}}) - \mathrm{Q_d}}{\mathrm{I}(1 - 10^{-\mathrm{A}}808)} \tag{1}$$

In the equation 1, S is the surface area of the container, h is the heat transfer coefficient, Tmax and TSurr are the equilibrium temperature and ambient temperature of the surroundings, respectively. Qdis is heat dissipated from light absorbed by the quartz sample cell itself, I is the incident laser power (1.0 W cm-2) and A808 means the optical absorbance of ZrC NPs at 808 nm. Only the hS remains unknown. We introduced a dimensionless driving force temperature to obtain the value of hS.

$$\theta = \frac{\mathrm{T} - \mathrm{T_{surr}}}{\mathrm{T_{max}} - \mathrm{T_{surr}}} \tag{1.1}$$

$$\mathrm{t} = -\tau_s \ln(\theta) \tag{1.2}$$

$$hS = \frac{\Sigma m_i C_{p,I}}{\tau_s} \tag{1.3}$$

Equation 1.1 shows the cooling stage of the aqueous dispersion, the cooling time t and abide by the equation 1.1, time constant (τs) for heat transfer from the system could be determined.

Where m, Cp,I are the mass, heat capacity of water, respectively. According to Equation S1.1, Equation S1.2 and Equation 1.3, the value hS is obtained. The photothermal

conversion efficiency (η) is calculated to be 20.51% according to Equation 1.

Cell Lines and Cell Culture

4T1 cells were routinely cultured in DMEM (Corning) medium containing 10% (v/v) FBS (Gibco), and 1% antibiotics (penicillin–streptomycin) (Corning) in a humidified atmosphere at 37°C including 5% CO2.

Cytotoxicity Assay

We performed MTT method to illustrate this issue. 4T1 cells and HUVE cells were seeded into 96-well plates (1 × 104cells per well) and co-incubated with the ZrCNPs dispersion of different concentrations for 24 hours. Then, 20 μL (5 mg/mL) MTT solution was introduced into each well and incubated for another 4 hours. After that, the medium was replaced with dimethyl sulfoxide (DMSO, 150 μL per well) for 30 min. A microplate reader (SynergyTMHT, BioTek Instruments Inc., USA) was used to test the optical absorbance at 490 nm.

In Vitro Phototherapeutic Effect

To explore the optimum sensitizer dose of PTT and RT, the *in vitro* cell survival rate was evaluated on 4T1 cells using a standard MTT assay. The experiment controlled for a single variable at a time and we draw a conclusion:

For RT, cells were treated by linear accelerator of image guided radiotherapy, X-ray radiation set was 6MV, 4Gy and 300 Does Rate. The height of the liquid level from the underlying cells is 1 cm. For PTT, cells were treated by 808 nm laser at power density (2.0 W cm-2). They were divided into six groups, including control, NIR, ZrC+NIR, X-ray, ZrC+X-ray. ZrC +NIR+X-ray All the experiments were performed for three times. 4T1 cells were seeded into a 35 mm culture dish (3 × 105 cells per dish) and incubated at 37°C until being nearly 90% coverage. The culture medium containing ZrC NPs (250 μg mL-1 was added into the culture dish and incubated for 6 h). After washing with PBS for three times, the fresh culture medium was added into culture dish and the cells were treated. Afterward, the cells were stained using cell doublestaining method (calceinAM and PI) for 20 min to distinguish the living and dead cells, and then observed immediately using fluorescence microscope (Olympus BX53)

Cell Experiments (γ-H2AX Antibody Recognition Immunofluorescence)

The cells and anti-phospho-histone γ-H2AX mouse monoclonal antibody (dilution 1:1000) were incubated together overnight at 4°C. Next day, the sheep anti-mouse secondary antibody (dilution 1:1000) was incubated with the cells at room temperature for 1 h. DAPI was used to stain cells by labeling the nuclei at room temperature for 5 min. Eventually, the Leica SP5 confocal microscopy was used to observe the cells.

Detection of ROS

Intracellular ROS generation was detected using DPBF and H2DCFH-DA probe, which could be oxidized to produce fluorescent compound of DCF in the presence of ROS. 4T1 cells were seeded into a 35 mm culture dish and incubated overnight. Afterward, the medium was discarded and cells were incubated with fresh medium containing ZrC NPs (0.5mg mL-1) for 4 h. The cells were then washed with PBS. Untreated cells were used as negative control. After that, the cells were stained with H2DCFH-DA (50 μL, 10 × 10-3m) for another 1 h. Thereafter, the cells were washed with PBS and treated in 6 groups as above. The DCF fluorescence images were acquired by fluorescence microscope (Olympus BX53).

Calculation of the Sensitization Enhancement Ratio

Cell survival fraction of each group was calculated by the ratio of the seeded cells following treatments to form colonies versus the untreated cells as described above. Cell survival fraction and sensitization enhancement ratio (SER) were determined by a classical multitarget single-hit model.and the SER was expressed with the following formulas:

$$\mathrm{SER} = \frac{\mathrm{D_q(control\ group)}}{D_q(\mathrm{sensitizer\ group})}$$

$$D_q = \ln(n) \times D_0$$

$$\mathrm{S} = 1 - (1 - e^{-\frac{D}{D_0}})^n$$

where S is the survival fraction, D is the radiation dose, D_0 is the mean lethal dose, and n is the extrapolation number. Where D_{qis} the quasi-threshold dose.

In Vivo Antitumor Effect

1×10^6 4T1 cells were suspended in 100 μL PBS mixed with matrix glue 1:1 (V:V), and were inoculated at the left hind legs of female BALB/c nude mice. The tumor-bearing mice were then divided into six groups (five mice each group) when the tumor was about 200 mm^3in size: (a) control, (b) NIR alone, (c) ZrC NPs+NIR, (d) X-ray alone, (e) ZrC NPs +X-ray and (f). ZrC NPs +NIR+X-ray. The 4T1 tumor-bearing mice from groups (c), (e), and (f) were administrated nanomaterials intravenously, and the other 3 groups were injected with PBS instead as control. Immobilization scan is operated with Philips CT sim for RT. And RT for mice was performed by Varian IX medical electron linear accelerator immediately after PT. Then, mouse weight and tumor growth were measured after for 14 days. The length and width of tumor were measured with a vernier caliper daily. When the whole experiment finished, all of the mice were sacrificed according to the protocols of Harbin Medical University Cancer Hospital. The tumor and major organs were removed and weighed to calculate the therapy efficacy among six groups.

To study whether the immunity could be triggered by the treatments and how strong it could be on suppressing distant tumors, we designed two experiments to evaluate the therapeutic effect as shown in **Figures 6A, E**. Two groups of the 4T1 tumor-bearing mice were divided randomly: 1) control 2) ZrC treated (ZrC+N+X). In experiment A, we built tumor-bearing mouse

model with bilateral tumors at -13th day (n = 5 for each group), and treated primary one (left) at day 0, leaving the other side distant tumor to be untreated. Thereafter, the tumor volume changes of distant tumor were recorded. The tumor growth rate showed no significant difference between the two groups. In experiment B, we implanted the tumor seeds on the other side of mice post treatment and measured their growth rate. As be seen in **Figures 6B, F**, although the post treatment-implanted tumor grew not as fast as before, distant tumors on treated mice showed more limited tumor growth rate. The logic explanation of the study is the antitumor immune responses of host.

Immunohistochemical Examination

Immunohistochemistry (IHC) was performed according to the instructions from manufacturer to detect the antibodies, apoptotic factor, multiplication factor, and hypoxia factor in tumor. The anatomical operation of the organs according to standard histological techniques and all the tumor tissues were frozen and then made into 4 μm thick serial sections. These paraffin sections were used for IHC staining using standard method. The pathologist was blinded to the identities and analyses of the pathology slides.

Western Blot Analysis

Total protein was purified and extracted from tissues with RIPA buffer supplemented with proteinase/phosphatase inhibitors (Thermo, Cambridge, MA). Same amounts of total protein were resolved by 10% SDS-PAGE, followed by transfer onto nitrocellulose membranes (Millipore, Bedford, MA). Anti-Bax (1:500), Bcl-2 (1:500), caspase (1:500), Ki67(1:500), HIF-1α(1:500(Abcam, USA) primary antibodies were used for the detection

Flow Cytometric Analysis

Tumors and surrounding tissues were obtained after combined therapy (be specific here). Phenotyping of cells was stained with the following antibodies: FITC-CD3, PE-CD4, PC7-CD8 (BD Phar Mingen, San Diego, CA). Flow cytometric analysis was performed with FACS Calibur (BD Biosciences, Franklin Lakes, NJ)

Histology Analysis

The mice were sacrificed to collect the tumors and major organs (heart, liver, spleen, lung, and kidney), which were fixed in 4% paraformaldehyde and embedded with paraffin. The slices of the major organs and tumors of the mice were stained with H&E for histological analysis. Finally, optical microscope images were acquired by a fluorescent microscope (Olympus BX53).

Hematological Analysis

Blood (100 μL) specimen from the mice were collected and analyzed at 14th day using automatic blood analyzer (HF3800).

Statistic calculated using "Statistical Program for Social Sciences" software (SPSS, version 19.0) and graphpad Prism 8. The final survival fraction curve of each group was generated *via* a nonlinear fitting using Origin 8.0.

RESULT

Preparation and Characterization of ZrC NPs

In this work, we selected ZrC nanoparticles as the sensitizer to be used in conjunction with RT and PT. To enhance the biocompatibility of ZrC, we alternately coated polyallylamine hydrochloride (PAH, positively charged) and bovine serum albumin (BSA, negatively charged) on the surface of ZrC *via* electrostatic interactions. In addition, we used folic acid (FA) for surface modification of the nanoparticles to increase tumor targeting by enhancing the utilization of sensitizer *in vivo*. The initial zeta potential of unmodified ZrC nanoparticles is 23.8 mV, and after modification with PAH-BSA-FA, the potential changed to 8.61 mV, -12.98 mV, and 8.47 mV. The change in zeta potential indicates the successful surface modification. This is also supported by the increase of their hydrodynamic size from 95.9 nm to 121.2 nm (**Figure S1**). To determine the dimension of ZrC NPs in the aqueous solution, the hydrodynamic diameter of ZrC NPs was tested *via* dynamic light scattering (DLS) measurement and determined to be 89.6 ± 1.6 nm (**Figure S2**), which is a suitable size for further *in vivo* administration. The PDI value corresponding to the DLS result is 0.187. As shown in **Figure S3**, A is the ZrC powder dissolved in PBS and B is the solution of ZrC NPs. Both solutions were allowed to stand for six hours, and A showed observable precipitation while no obvious change in B, indicating their better stability in physiological solutions.

The TEM image of ZrC is presented in **Figures 1A** and **S4**, showing that the ZrC nanoparticles are about 35 nm in size. The high-resolution TEM (HRTEM), elemental mapping and energy dispersive spectrometer (EDS) were used to further characterize the material. The results demonstrate that the nanoparticles consist of Zr and C elements, as proven by an overlay of green (Zr) and red (C) colors in each particle. Next, the chemical valence of the as-prepared ZrC NPs was determined *via* XPS analysis **Figure 1B**. All reflective peaks are well matched with standard cubic ZrC. After deconvolution, the XPS core-level of Zr 3d orbit results disclose the presence of Zr2+, Zr3+ and Zr 4+ ions in the sample. Classically, the XRD **Figure 1C** pattern reveals that all the diffractive peaks are attributable to standard cubic ZrC (PDF#35-0784). Additionally, **Figure 1D** shows the powder UV-Vis-NIR spectra of ZrC. ZrC powder exhibits strong and broad absorption in the whole NIR window. Next, FTIR **Figure 1E** spectrum was applied to detect the chemical compositions of ZrC NPs.

Photothermal Properties of ZrC

Photothermal therapy requires photo absorption in the NIR region and the resultant photothermal properties of photoactive materials is particularly important. We first inspected the optical absorption properties of the ZrC aqueous dispersion by correlating the change in temperature with the concentration of ZrC over an irradiation time. Different concentrations of ZrC NPs (0.125, 0.25, 0.5 μg/mL) were heated by an 808 nm NIR laser with various power (0.5,1,1.5,2 W cm-2) for 10 min, and the

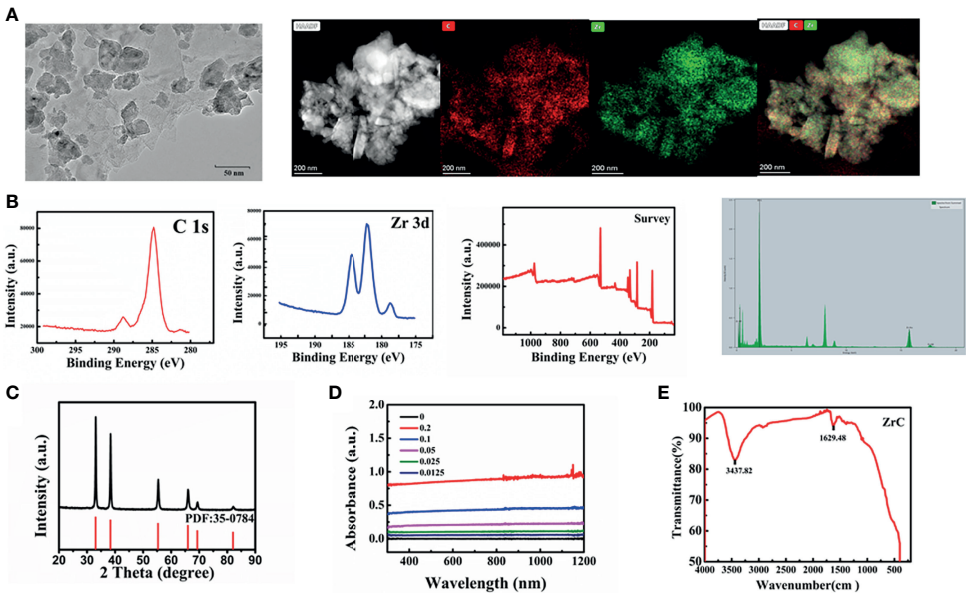

FIGURE 1 | **(A)** The TEM image and elements mappings image, **(B)** XPS, **(C)** XRD PDF:35-0784, **(D)** UV spectra: optical absorbance of ZrC dispersions with varied concentration, **(E)** the FTIR spectrums.

transformation in solution temperature was recorded by an infrared thermal imaging camera. As shown in **Figure 2A**, pure water and ZrC dispersion of 0.125 mg/mL showed no significant temperature elevation (about 10°C) after 10 min of NIR irradiation. In contrast, the temperature of the ZrC dispersion of 0.25 and 0.5mg/mL increased significantly. The curve in **Figure 2B** reveals the relationship between temperature increment on the nanoparticle concentration and power, the maximal temperature reached 42.3 and 47.6°C for 0.25 and 0.5 mg/mL ZrC dispersion, respectively. The photothermal conversion efficiency was calculated to be 40.51% (**Figure 2C**, the calculation details are presented in method and material). The optical density at 808 nm had a good linear relationship with concentration of ZrC NPs (the inset of **Figure 2C**). In addition, the temperature change of ZrC NPs solution upon NIR on/off irradiation did not change much for five rounds. Shown in **Figure 2D**, our results revealed photostability of ZrC NPs. Moreover, ZrC also has a very high absorption in the NIR region, which improves the infrared absorption value of ZrC NPs to some extent. Such photothermal production and photostability indicated that ZrC can act as an efficient photothermal conversion agents(PTA).

Inspired by the previous study of X-PDT and PDT, we investigated ROS production from ZrC NPs under NIR and X-ray irradiation by using sodium terephthalic as a probe. The 1,3-diphenylisobenzofuran (DPBF) and 2′7-dichlorofluores-cin diacetate (DCFH-DA) probes were employed to detect the extracellular and intracellular ROS production, respectively. The DPBF probe for detecting extracellular ROS production lies in its decomposition by ROS. As result, a decrement of DPBF characteristic absorption could be observed accordingly. As displayed in **Figure 2E**, the absorbance of the DPBF solution with ZrC decreased meaningfully as irradiation time and X-ray dose increased, suggesting that significant level of ROS was induced by ZrC under NIR and X-ray. In contrast, the pure water led to very limited ROS generation with the same laser irradiation.

We examined intracellular ROS production in 4T1 cells with the use of DCFH-DA probe, which would convert to green fluorescent molecules after being oxidized by ROS, to detect the presence of ROS. As shown in **Figure 2F** there was no observable green fluorescence from the negative control, while a very weak signal was observed from the NIR group and X-ray group. The fluorescence intensity of sample irradiated by both X-ray and NIR, contained ZrC NPs, increase 75% than that of the average of other 5 groups, indicating the ROS producing ability of ZrC NPs. This result is in agreement with the above-mentioned photocurrent experiment. Therefore, the as-prepared ZrC NPs have potential as both radiosensitizers and photosensitizers for tumor treatment.

In Vitro Cell Cytotoxicity and Phototherapeutic Treatment Combined Radiotherapy

To determine the optimal nanoparticle concentration for subsequent experiments, we investigated cytotoxicity towards mouse breast cancer 4T1 tumor cells and normal human umbilical vein endothelial cells (HUVECs) using standard MTT assay. was investigated. Cell viabilities are strongly dependent on the concentration of ZrC NPs. There were no significant differences within or between groups and more than 80% of the 4T1 cells, and HUVECs survived when they were

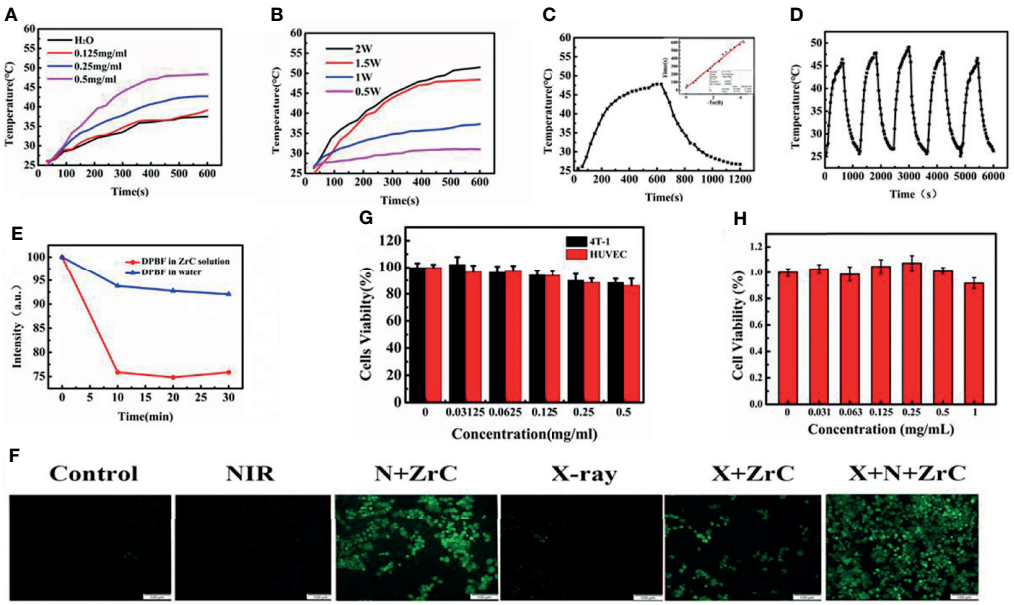

FIGURE 2 | **(A)** Photothermal temperature curves of ZrC NPs aqueous dispersions at different concentrations. **(B)** Photothermal temperature curves of ZrC NPs aqueous dispersions at different power of NIR laser. **(C)** Photothermal test of ZrC dispersion of 0.5 mg·mL-1. (NIR laser: 808 nm, 1.5 W·cm-2; inset shows plot of time versus – ln (Θ); The ZrC dispersion was irradiated with NIR for 10 min and left to natural cooling for another 10 min), **(D)**Temperature change of ZrC NPs solution at concentration of 0.5 mg·mL-1over five laser on/off cycles. (808 nm laser irradiation, with a power density of 1.5 W cm-2. **(E)** DPBF degradation behavior for ROS detection (NIR laser: 808 nm, 1.5 W·cm-2); **(F)** Confocal fluorescence images of reactive oxygen species (ROS) in 6 groups. **(G)** *In vitro* cytotoxicity of different concentrations of ZrC NPs to 4T1 cells and HUVE cells, **(H)** The biocompatibility of ZrC NPs on proliferation ability of 4T1 cells at different concentration (0, 0.03215, 0.0625, 0.125, 0.5 and 1 mg/ml) after incubation for 48 h. Error bars represent mean ± SD. **(F)** The cytotoxicity of ZrC NPs on 4T1 and HUVE cells at different concentration (0, 0.03215, 0.0625, 0.125, 0.5 and 1 mg/ml) after incubation for 24 h.

cultured with 0.5 mg/mL ZrC NPs solution (**Figure 2G**). **Figure 2H** demonstrates the effects of different concentration of solution on proliferation of 4T1 cells, and then MTT was performed in 48 hours. As shown in the histogram, there was no significant change between the groups, signifying the minimal effect of ZrC NPs on the cells' proliferation ability.

The cytotoxicity results suggest that the concentration of ZrC NPs applied to tumor cells should be no higher than 0.5 mg/ml. To detect the effective energy level of X-ray for cell experiments, 4MV, 6MV and 12MV were selected with various radiation dose (2,4,6,8Gy). The results show 6MV group had the statistically significant difference (about 43.47%) as demonstrated in **Figure S5**. From S6, based on the obvious difference of cell surviving fraction between sensitization of ZrC NPs (25.3% in 4Gy), 4Gy of RT with 6MV was used for the experiment. PT, 4min with 1.5 W cm-2 was selected, the differences of surviving fraction was 28.6%. We discovered that the final survival rate in these conditions were about 40% after sensitization. If the single treatment kills most of tumor cells, it will be meaningless to combine additional treatment. Basing on these explorations, we started to compare the killing effect of different therapeutic methods on tumor cells. As shown in **Figure 3A**, a Live/Dead kit was used to test the activity of 4T1 cells in 6 groups, in which the living cells were stained green and dead cells were stained red. Notably in **Figure 3B**, with the data analysis of MTT, ZrC NPs played an effective role in sensitization of PT (surviving rate from 109.32% to 39.01%) while RT(from 45.71% to 38.66%), and the combination therapy of PT/RT with ZrC NPs contributed to the best cancer cell killing efficiency, where the cell survival dropped to 5.16%, demonstrating the powerful synergistic PT and RT effects *in vitro*. There is a result does not seem to meet expectations that the cell surviving fraction in NIR group was higher than the control group. This is because all the groups were treated under the same conditions, and the room temperature was relatively low during radiotherapy, so cell survival rates were higher with mild PTT. The sensitizer enhancement ration (SER) in this experiment was used to evaluate the radio sensitization efficiency. The SER value of ZrC+N+X group was about 1.8 compared with X-ray group, further confirming that PT *via* ZrC NPs can promote RT function on the cancer cells. However, ZrC +X group's SER is about 1.2. Analyze from these data, we found that higher temperature around tumor induced by ZrC NPs under NIR had obvious sensitization effect on RT while ZrC NPs alone showed weak sensitization effect.

The radiation enhancement was confirmed to be attributed to the process of DNA breaking. **Figure 3C** showed there were no significant γ-H2AX fluorescent signals in control and NIR treated groups. Only limited γ-H2AX spots in fluorescent were detected in N(ZrC, X-ray, and X+ZrC groups. Comparing to other groups, a very high amount of γ-H2AX foci was detected in N+X+ZrC group, indicating significant more DNA breaking due to enhanced X-ray generation by synergistic treatment. There

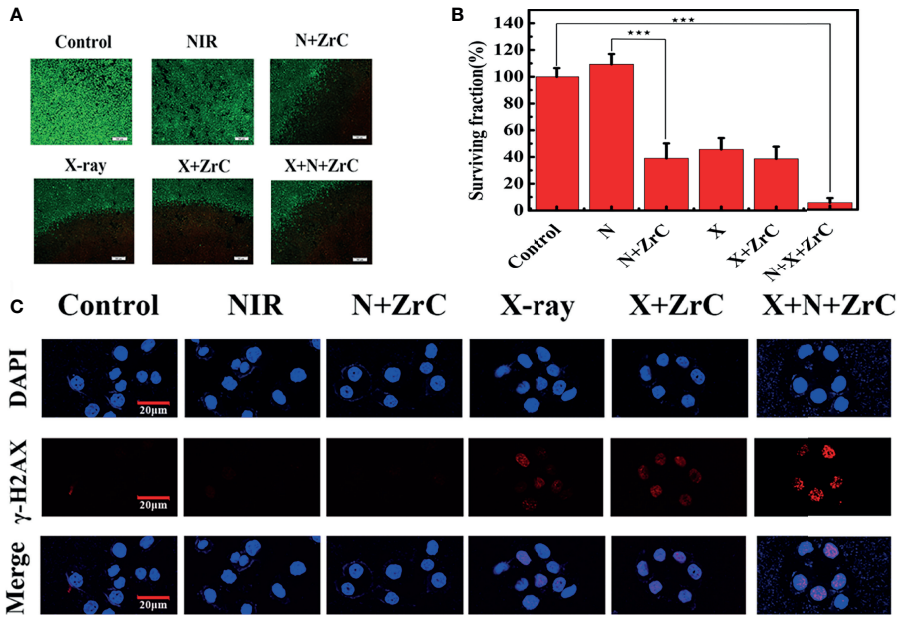

FIGURE 3 | **(A, B)** live/dead images of 4T1 cells and survival rates analysis after different type of treatment with six groups respectively: Control, NIR, N+ZrC (PT +ZrC NPs), X-ray, X+ZrC (RT+ZrC NPs), X+N+ZrC (RT+PT+ZrC NPs) in concentrations of 0.5 mg mg·mL-1and irradiated with an 808 nm laser 4min with 1.5 W cm-2, X-ray with 6MV,4Gy. Error bars represent mean ± SD. P values based on Student's t-test: ***p < 0.001. **(C)** Qualitative representation of DNA fragmentation with different treatment (scale bar: 20 μm).

results suggest that ZrC NPs mediated synergistic treatment provides an approach to kill cancer cells with high efficiency. These results were consistent and demonstrated the possibility of using sensitization of PT combined RT in tumors and leading to DNA breakdown in tumor cells.

In Vivo Investigation Anti-Cancer Efficacy

We further investigated the *in vivo* photo-therapeutic efficacy of ZrC NPs *via* a subcutaneous 4T1 tumor-bearing mice model. When the tumor volume reached≈200 mm3, 4T1 tumor-bearing mice were randomly divided into six groups (n = 5 for each group) for various treatments: group 1) Control, 2) NIR alone (PT), 3) ZrC +NIR (PT+ZrC NPs), 4) X-ray alone (RT), 5) ZrC +X-ray (RT+ZrC),6) ZrC+NIR+X-ray (RT+PT+ZrC NPs). The Balb/c nude mice were intravenously (i.v.) injected with 100 μL of PBS (group 1) or ZrC NPs (group 3, 5, 6) and then exposed to NIR irradiation (808 nm, 1.5 W cm-2 10min) or X-ray (6MV, 6Gy) at 2 h post injection for group2,3,4,5 and 6. First, the surface temperature profiles of tumor region were recorded using an infrared thermal camera during PT at specific points in time. As illustrated in **Figures 4A–B**, the temperature of tumor site with ZrC NPs administration rapidly increased to about 57.3°C within 10 min under NIR laser irradiation. However, the temperature of tumor site with only NIR laser irradiation exhibited limited temperature (from 35.5°C to 41.5°C) elevation under the same conditions. As temperature increased very limited after 6 min and this is the meaningful point to be sensitized, so PT's time is settled to be 6 min in mice treatment. Shown in **Figure 4C**, it is the RT plan for mice. 14 days post-treatment for the body weight and tumor volume. No significant difference was observed in body weight among six groups. However, groups got X-ray irradiation lose a little more weight, most likely due to intestinal mucosa injury after RT when the black mice feces were noticed for about 3 days **Figure 4D**. To evaluate tumor response, the tumor volume was measured in each group within 14 d. From the comparison of group 2 and 3, group 4 and 5, it shows stronger antitumor effect in the later groups which were injected with ZrC NPs, indicating that ZrC NPs played a sensitizer role in both PT and RT, respectively. The relative tumor volume of the mice treated with RT or PT alone was slightly smaller than that in the control group, which illustrated that RT and PT could mildly inhibit the growth of the tumors. However, the mean tumor volume of group 6 was the lowest in all six groups (**Figures 4E–G**) which indicated that the ZrC NPs as sensitization materials enhanced PT and RT efficacy and led to substantial better tumor control. Remarkably, although the tumor volume recorded after treatment showed same trend on ZrC+N group and ZrC+N+X group in the first few days after treatment, remnant tumor tissues were noticed beneath black scab in ZrC+N group as a common phenomenon and showed high local recurrence rate after a week, while in ZrC+N+X group: the interior of the tumor is dominated by residual pus and necrotic tissue.

After PT/RT treatment, the mice show the black scars at their original sites of tumor. To give a better visualization of the killing of tumor, the mice were sacrificed 14 d later after therapy and histology analysis of tumor tissues was performed *via* a typical hematoxylin and eosin (H&E) method. SI.8shows massive tumor cells necrosis in group ZrC +N and ZrC +N+X, but not in other

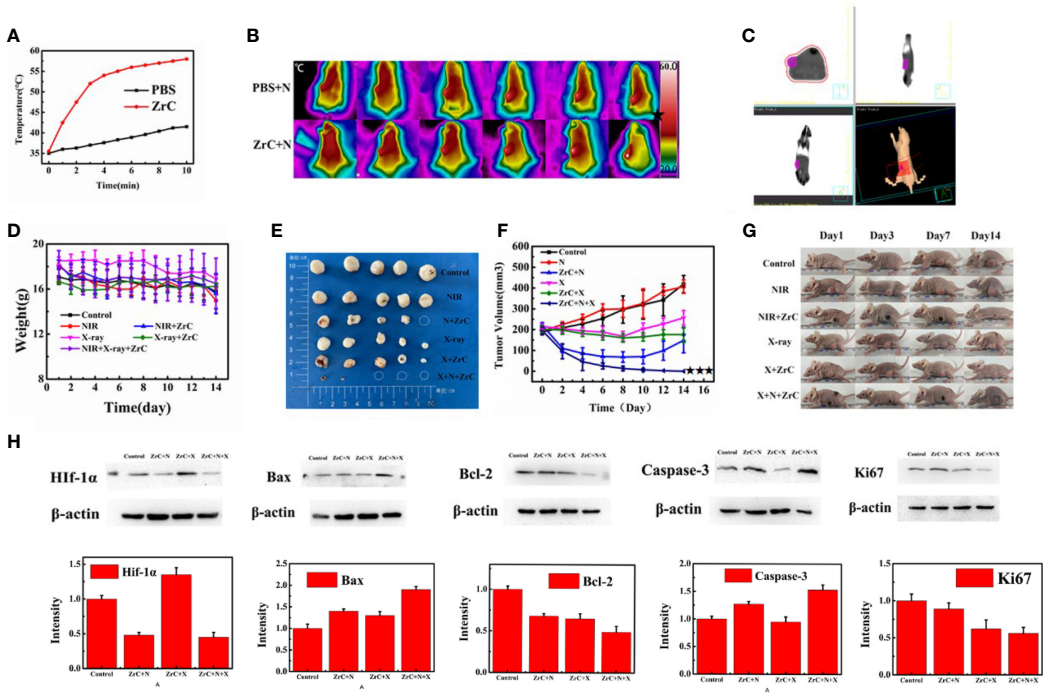

FIGURE 4 | **(A)**The temperature curves of the tumor site after they were intravenously injected with ZrC NPs (dose 0.5 mg mL-1, 200 μL) and PBS, respectively, and then exposed to an 808 nm NIR laser (1.5 W cm-2, 10 min); **(B)**Infrared thermal images of tumor-bearing mice while PT. **(C)** RT plan for mice. **(D)** The variations in weight of mice in six groups. Error bars represent mean ± SD. **(E)** Tumors were cut out at 14 days after treatment from five mice in each group. **(F)** Tumor volume in six groups were measured after treatment. Error bars represent mean ± SD. **(G)** Representative photos of tumor-bearing mice after 14 d treatment. **(H)** In control, NIR(PT), ZrC+N (PT+ZrC NPs), X-ray (RT), ZrC+X (RT+ZrC) and ZrC +N+X (RT+PT+ZrC NPs) groups, respectively. Protein expression measured by Western Blot of HIF-1a/Bax/Bcl-2/Caspase-3/Ki67 and Intensity expression level of these genes.

four control groups. To provide a deep insight into the mechanism of tumor-growth inhibition, the expression level of bax, bcl-2, caspase-3 which were associated with apoptosis, and proliferation related gene Ki67 were tested by immunohistochemical analysis of tumor tissues and western blot, respectively. As illustrated in **Figures 4H**, **5**, ZrC+N+X group had higher expression of bax and caspeas-3 and lower expression of bal-2, both associate with cell apoptosis. To evaluate the ability of tumor proliferation, the expression of Ki67, representing the proliferation ability of cells, was examined. We found that the expression level of Ki67 in the combined group was lower. Also, the ability of proliferation in tumor was not inhibited by any single treatment compared to sensitization therapy groups. From the expression of western blot, a conclusion could be drawn that in the groups with X-ray, the proliferation factors showed lower expression while apoptotic factors showed higher in PTT and combined therapy groups, owing to X-ray dose damage to the DNA double-stranded structure and local heat leads to a disruption on cell membrane permeability fist. To further verify the previous hypothesis that the combination of PT and RT could sensitize RT by improving tumor hypoxic microenvironment. Hypoxia-inducible factor 1a (Hif-1α) was tested by western blot and Immunohistochemical analysis from tumor and surrounding tissue. HIF-1α often expressed in tumors and its transcriptional activity is accurately regulated by the concentration of oxygen, meaning that the stronger Hif-1α expressed the more severe of hypoxia is. In, it showed that the protein expression of Hif-1α in group ZrC+N was the lowest, and slightly higher in group ZrC+N +X while high in control/X-ray alone/ZrC NPs+X groups. The expression in group ZrC+N+X was the highest, meaning the RT consumes oxygen in tumor microenvironment produced by PT. The same expression trend of Hif-1α showed up in immunohistochemical analysis. As the tumor growth inhibition rates were positive correlated to absorption doses and the improvement of hypoxic environment can promote the absorption of radiotherapy (22, 29). To summarize the above experimental data *in vivo*, a conclusion can be drawn that the combination of PT and RT with ZrC NPs alleviate hypoxia induced resistance of RT and sensitizing tumor tissues to absorb more doses of PT and RT, improving cell apoptosis and tumor suppression rate.

In Vivo Evaluation of Immunoassay

Recent studies reveal that the free radicals generated by NPs, as well as necrotic tissue debris after PT, are capable of increasing tumor immunogenicity, and thus making these materials possible for cancer immunotherapy (30, 31). To study the benefits of ZrC NPs mediated PT and RT, we explored the

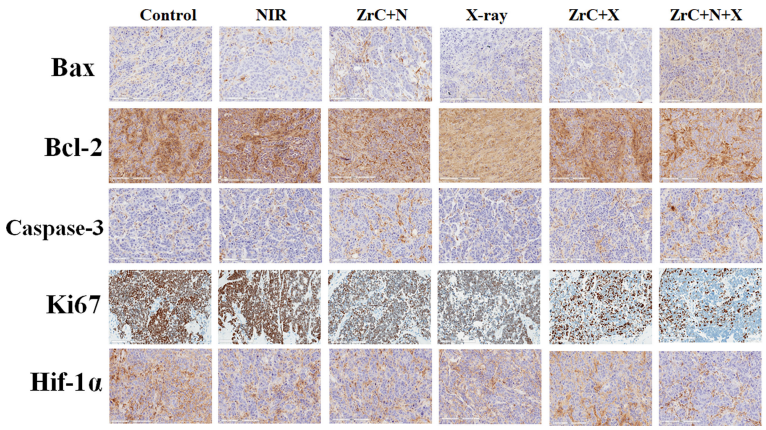

FIGURE 5 | Immunohistochemical analysis of related genes of tumor tissues from six groups of 4T1 tumor-bearing mice after treatment. Furthermore, H&E staining on the major organs, including heart, kidney, lung, liver and spleen, disclosed no notable damages (i.e., inflammation or necrosis) of all mice (S12). Because of the tumor targeting effect of ZrC NPs, the materials concentrate around the tumor. They result more energy deposition from NIR and X-ray interactions and protect normal tissues while achieving the strongest tumor killing. These results showed a very promising potential which can significantly improve the limitation of single therapy regimen by altering the tumor microenvironment, achieving a safe and efficient elimination of tumor cells.

immunity effect of the material in post treatment mice by: 1) measuring the growing rate of distant tumor on the other side of the body 2) investigating populations of T cells, analyzed with flow cytometry. 3) immunohistochemical analysis of apoptosis, and proliferation related gene of the distant tumors. The results of the distant tumor inhibition experiment showed that the immune response induced by combined therapy an inhibition effect on new metastatic tumor growth rate after treatment, but had no certain effect on existing distant tumors (32) (**Figures 6A, B, E, F**, **S9**). Besides, the first implanted tumor could stimulate some immunity *in vivo* to some extent.

In addition, we verified above assumption of immune responses further by analysis of flow cytometry. In (**Figures 6C, G**), the immune cells (tumor-infiltrating cytotoxic T lymphocytes CD8 ($CD3^+CD4^-CD8^+$) and helper T lymphocytes CD4 ($CD3^+CD4^+CD8^-$) were analyzed in untreated distant tumors from different groups. In experiment A, CD4 and CD8 raised slightly in ZrC treated group. Relatively, the proportion of CD8 raised more in experiment B while CD4 raised less.

Immunohistochemical analysis of bax, bcl-2, caspase-3 and Ki 67 were examined from distant tumor tissues. Shown in **Figures 6D, H**. there was no obvious difference between two

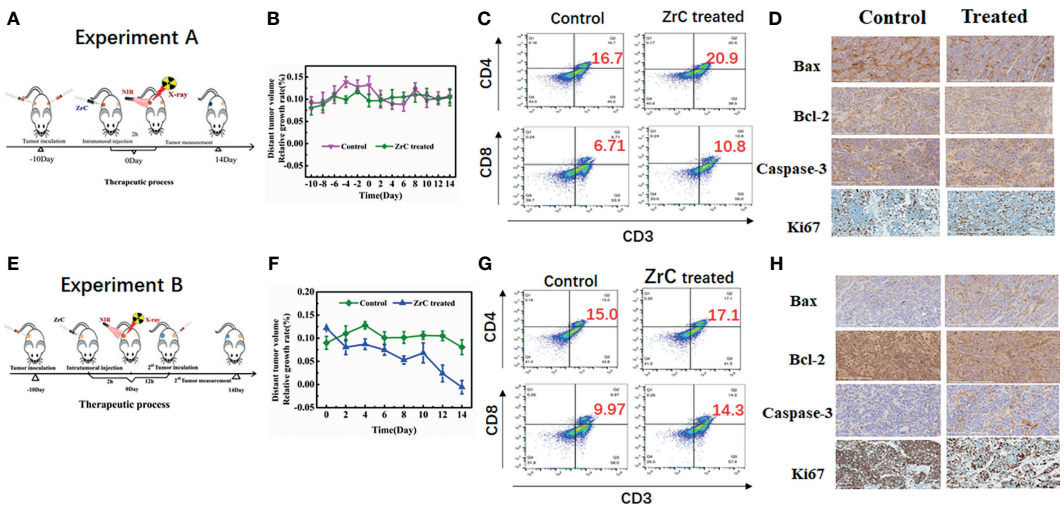

FIGURE 6 | **(A, E)** Schematic illustration of A/B experiment design and measure the distant tumor volume. **(B, F)** Relative growth rate of distant tumor volume in two groups. Error bars represent mean ± SD. **(C, G)** Representative flow cytometry plots showing different types of T cells in tumor tissue from different groups of mice. **(D, H)** Immunohistochemical analysis of tumor tissues.

groups in experiment A. However, in experiment B, similar to caspase-3, bax showed a higher expression in the treated group while bcl-2 showed a lower expression, indicating the enhanced immune system which promoted cancer cell apoptosis. Expression of Ki6 showed the following difference: higher in control group and lower in combined therapy group, confirming that combined treatment impacted the ability of distant tumor proliferation.

In Vivo Safety Evaluation of ZrC NPs

Lastly, we evaluated the safety of nanomaterials for biomedical application.

No significant abnormal behavior, such as twitching, drowsiness, hobbling, or weight loss were observed in the mice throughout the entire experiment period. No obvious difference was observed in routine blood data after treatment by nanomaterials. To further confirm the treatment safety, major organs of mice from each group were harvested and cut into slices for histochemical analysis through staining with H&E. As illustrated in S12, histological study of major organs (heart, liver, spleen, lung, kidney) showed no obvious tissue damage or side-effect in all treatment groups. As for in the blood biochemistry index, besides routine inspection, we measured the hepatic and renal function markers including ALT, AST, BUN and CREA. We separated the mice into 2 groups depending on the application of ZrC NPs or not. One group included: 1) control, 2) NIR alone, 4) X-ray alone, the other group included:3) ZrC +N,5) ZrC+X,6) ZrC+N+X. The white blood cell count increased in group with ZrC NPs and that was expected as ZrC NPs are foreign bodies in the blood that stimulate white blood cell growth. Besides, serum biochemical examination showed slightly increased in groups with ZrC NPs, corresponding no noticeable renal and hepatic dysfunction induced by the application of ZrC NPs, the results showed the slightly increase in S13-14 All results showed that ZrC NPs are safe *in vivo*.

DISCUSSION

In TNBC, RT alone has limited curative effect because of the insensitivity of cancer cells to X-ray radiation. To enhance the effect of treatment, this work is the first to present the synthesis and application of brand-new ZrC NPs as sensitization substance for PT/RT combination therapy. In this way, to kill the tumor, less does of X-ray and less time of NIR could be enough. Due to the strong photo absorption capability in the NIR region, the synthesized ZrC NPs can generate thermal energy and ROS upon NIR irradiation, simultaneously enhancing RT therapeutic effects. The combined therapy of PT and RT has shown great potential to produce excellent antitumor outcome. Immunohistochemistry, histopathological analysis and western blot were utilized to demonstrate ablation mechanism of tumor. Biocompatibility, ZrC NPs mediated therapy showed no obvious hematotoxicity and systemic toxicity. In addition, combination regimen makes it possible to deliver lower dose PT and RT, relatively, which could avoid the side effects of a single, intense treatment on patients, such as the damage for immune system from high dose RT. Without this drawback, the combination triggered the immune effect and induce tumor immunity for the treatment of metastatic tumors. The investigation attempts to provide some insight into the treatment of TNBC, not only in the sensitization of RT, but also the multiple combinations of treatment.

DATA AVAILABILITY STATEMENT

The original contributions presented in the study are included in the article/**Supplementary Material**. Further inquiries can be directed to the corresponding authors.

ETHICS STATEMENT

This study was approved by the institutional research ethics committee of Harbin Medical University. All animal experiments were performed in strict accordance with the ARRIVE guidelines and were approved by the institutional Animal Care and Use Committee of Harbin Medical University.

AUTHOR CONTRIBUTIONS

SJ and ZL worked at the sequence alignment, animal experimental, and drafted the manuscript. YT and YG carried out the immunoassays and nanomaterial characterization. SJ, MZ, and SP participated in cell experimental and performed the statistical analysis. HH carried out the plan of radiation therapy and dose calculation. HH and WC joined the study's design and performed the statistical analysis. AT participated in the article's text polish and data integration. SJ and ZL contributed equally to this study. All authors contributed to the article and approved the submitted version.

FUNDING

This work was funded by Science Foundation of Health Commission of Heilongjiang Province (2019052), Innovative scientific research funding project of Harbin Medical University (2020-KYYWF-1471), HAI YAN Science Foundation of Harbin Medical University Cancer Hospital (grant no. JJQN2018-18). HAI YAN Science Foundation of Harbin Medical University Cancer Hospital (grant no. JJQN2021-08).

SUPPLEMENTARY MATERIAL

The Supplementary Material for this article can be found online at: https://www.frontiersin.org/articles/10.3389/fonc.2021.801352/full#supplementary-material

REFERENCES

1. Hamilton S, Nichol A, Wai E, Gondara L, Velásquez García H, Speers C, et al. Local Relapse After Breast-Conserving Therapy Versus Mastectomy for Extensive Pure Ductal Carcinoma *in Situ* ≥4 Cm. *Int J Radiat Oncol Biol Phys* (2019) 103(2):381–8. doi: 10.1016/j.ijrobp.2018.09.022
2. Possanzini M, Greco C. Stereotactic Radiotherapy in Metastatic Breast Cancer. *Breast (Edinburgh Scotland)* (2018) 41:57–66. doi: 10.1016/j.breast.2018.06.011
3. Goldstein M, Kastan M. The DNA Damage Response: Implications for Tumor Responses to Radiation and Chemotherapy. *Annu Rev Med* (2015) 66:129–43. doi: 10.1146/annurev-med-081313-121208
4. Fang H, Gai Y, Wang S, Liu Q, Zhang X, Ye M, et al. Biomimetic Oxygen Delivery Nanoparticles for Enhancing Photodynamic Therapy in Triple-Negative Breast Cancer. *J Nanobiotechnol* (2021) 19(1):81. doi: 10.1186/s12951-021-00827-2
5. Gilreath C, Boerma M, Qin Z, Hudson M, Wang S. The Hypoxic Microenvironment of Breast Cancer Cells Promotes Resistance in Radiation Therapy. *Front Oncol* (2020) 10:629422. doi: 10.3389/fonc.2020.629422
6. Dubsky P, Pinker K, Cardoso F, Montagna G, Ritter M, Denkert C, et al. Breast Conservation and Axillary Management After Primary Systemic Therapy in Patients With Early-Stage Breast Cancer: The Lucerne Toolbox. *Lancet Oncol* (2021) 22(1):e18–28. doi: 10.1016/S1470-2045(20)30580-5
7. Zhong Y, Xu Y, Zhou Y, Mao F, Lin Y, Guan J, et al. Omitting Radiotherapy is Safe in Breast Cancer Patients ≥ 70 Years Old After Breast-Conserving Surgery Without Axillary Lymph Node Operation. *Sci Rep* (2020) 10(1):19481. doi: 10.1038/s41598-020-76663-5
8. Jacobs D, Horeweg N, Straver M, Roeloffzen E, Speijer G, Merkus J, et al. Health-Related Quality of Life of Breast Cancer Patients After Accelerated Partial Breast Irradiation Using Intraoperative or External Beam Radiotherapy Technique. *Breast (Edinburgh Scotland)* (2019) 46:32–9. doi: 10.1016/j.breast.2019.04.006
9. Gong L, Zhang Y, Liu C, Zhang M, Han S. Application of Radiosensitizers in Cancer Radiotherapy. *Int J Nanomed* (2021) 16:1083–102. doi: 10.2147/IJN.S290438
10. Wang H, Mu X, He H, Zhang X. Cancer Radiosensitizers. *Trends Pharmacol Sci* (2018) 39(1):24–48. doi: 10.1016/j.tips.2017.11.003
11. Yamada M, Foote M, Prow T. Therapeutic Gold, Silver, and Platinum Nanoparticles. *Wiley Interdiscip Rev Nanomed Nanobiotechnol* (2015) 7 (3):428–45. doi: 10.1002/wnan.1322
12. Guo Z, Zhu S, Yong Y, Zhang X, Dong X, Du J, et al. Synthesis of BSA-Coated Bioi@Bi s Semiconductor Heterojunction Nanoparticles and Their Applications for Radio/Photodynamic/Photothermal Synergistic Therapy of Tumor. *Adv Mater (Deerfield Beach Fla.)* (2017) 29(44):1704136.1-.12. doi: 10.1002/adma.201704136
13. Wen L, Chen L, Zheng S, Zeng J, Duan G, Wang Y, et al. Ultrasmall Biocompatible WO3- X Nanodots for Multi-Modality Imaging and Combined Therapy of Cancers. *Adv Mater (Deerfield Beach Fla.)* (2016) 28 (25):5072–9. doi: 10.1002/adma.201506428
14. Zhou R, Wang H, Yang Y, Zhang C, Dong X, Du J, et al. Tumor Microenvironment-Manipulated Radiocatalytic Sensitizer Based on Bismuth Heteropolytungstate for Radiotherapy Enhancement. *Biomaterials* (2019) 189:11–22. doi: 10.1016/j.biomaterials.2018.10.016
15. Hlouschek J, Ritter V, Wirsdörfer F, Klein D, Jendrossek V, Matschke J. Targeting SLC25A10 Alleviates Improved Antioxidant Capacity and Associated Radioresistance of Cancer Cells Induced by Chronic-Cycling Hypoxia. *Cancer Lett* (2018) 439:24–38. doi: 10.1016/j.canlet.2018.09.002
16. Liu S, Li H, Xia L, Xu P, Ding Y, Huo D, et al. Anti-Rhoj Antibody Functionalized Au@I Nanoparticles as CT-Guided Tumor Vessel-Targeting Radiosensitizers in Patient-Derived Tumor Xenograft Model. *Biomaterials* (2017) 141:1–12. doi: 10.1016/j.biomaterials.2017.06.036
17. Sadeghi N, Kok R, Bos C, Zandvliet M, Geerts W, Storm G, et al. Hyperthermia-Triggered Release of Hypoxic Cell Radiosensitizers From Temperature-Sensitive Liposomes Improves Radiotherapy Efficacy *In Vitro*. *Nanotechnology* (2019) 30(26):264001. doi: 10.1088/1361-6528/ab0ce6
18. Anand S, Chan T, Hasan T, Maytin E. Current Prospects for Treatment of Solid Tumors *via* Photodynamic, Photothermal, or Ionizing Radiation Therapies Combined With Immune Checkpoint Inhibition (a Review). *Pharm (Basel Switzerland)* (2021) 14(5):447. doi: 10.3390/ph14050447
19. Shang T, Yu X, Han S, Yang B. Nanomedicine-Based Tumor Photothermal Therapy Synergized Immunotherapy. *Biomater Sci* (2020) 8(19):5241–59. doi: 10.1039/D0BM01158D
20. Mauro N, Utzeri M, Varvarà P, Cavallaro G. Functionalization of Metal and Carbon Nanoparticles With Potential in Cancer Theranostics. *Molecules (Basel Switzerland)* (2021) 26(11):3085. doi: 10.3390/molecules26113085
21. Jiang Q, Li X, Yin C. A Study on Improving the Efficacy of Nanoparticle-Based Photothermal Therapy: From Nanoscale to Micron Scale to Millimeter Scale. *Mater (Basel Switzerland)* (2021) 14(9):2407. doi: 10.3390/ma14092407
22. Ma T, Liu Y, Wu Q, Luo L, Cui Y, Wang X, et al. Correction to Quercetin-Modified Metal-Organic Frameworks for Dual Sensitization of Radiotherapy in Tumor Tissues by Inhibiting the Carbonic Anhydrase IX. *ACS Nano* (2020) 14(2):2553. doi: 10.1021/acsnano.9b09760
23. Poleszczuk J, Enderling H. The Optimal Radiation Dose to Induce Robust Systemic Anti-Tumor Immunity. *Int J Mol Sci* (2018) 19(11):3377. doi: 10.3390/ijms19113377
24. Chen Z, Wu Z, Muluh T, Fu S, Wu J. Effect of Low-Dose Total-Body Radiotherapy on Immune Microenvironment. *Trans Oncol* (2021) 14 (8):101118. doi: 10.1016/j.tranon.2021.101118
25. Boustani J, Grapin M, Laurent P, Apetoh L, Mirjolet C. The 6th R of Radiobiology: Reactivation of Anti-Tumor Immune Response. *Cancers* (2019) 11(6). doi: 10.3390/cancers11060860
26. Li M, Xie D, Tang X, Yang C, Shen Y, Zhou H, et al. Phototherapy Facilitates Tumor Recruitment and Activation of Natural Killer T Cells for Potent Cancer Immunotherapy. *Nano Lett* (2021) 21(14):6304–13. doi: 10.1021/acs.nanolett.1c02238
27. Zhang C, Dong J, Shen T, Li Y, Yang Z, Cheng X, et al. [Comparison of the Application Among Intensity-Modulated Radiotherapy, 3D-Conformal Radiotherapy and Conventional Radiotherapy for Locally Advanced Middle-Low Rectal Cancer]. *Zhonghua wei chang wai ke za zhi = Chin J Gastrointestinal Surg* (2018) 21(12):1414–20.
28. Ma Y, Zhang Y, Li X, Zhao Y, Li M, Jiang W, et al. Near-Infrared II Phototherapy Induces Deep Tissue Immunogenic Cell Death and Potentiates Cancer Immunotherapy. *ACS Nano* (2019) 13(10):11967–80. doi: 10.1021/acsnano.9b06040
29. Wang S, You Q, Wang J, Song Y, Cheng Y, Wang Y, et al. MSOT/CT/MR Imaging-Guided and Hypoxia-Maneuvered Oxygen Self-Supply Radiotherapy Based on One-Pot Mno-Msio@Au Nanoparticles. *Nanoscale* (2019) 11 (13):6270–84. doi: 10.1039/C9NR00918C
30. Liu T, Lu T, Yang Y, Chang S, Chen H, Lu I, et al. New Combination Treatment From ROS-Induced Sensitized Radiotherapy With Nanophototherapeutics to Fully Eradicate Orthotopic Breast Cancer and Inhibit Metastasis. *Biomaterials* (2020) 257:120229. doi: 10.1016/j.biomaterials.2020.120229
31. Dos Santos M, Gouvêa A, de Moura L, Paterno L, de Souza P, Bastos A, et al. Nanographene Oxide-Methylene Blue as Phototherapies Platform for Breast Tumor Ablation and Metastasis Prevention in a Syngeneic Orthotopic Murine Model. *J Nanobiotechnol* (2018) 16(1):9. doi: 10.1186/s12951-018-0333-6
32. Han R, Xiao Y, Yang Q, Pan M, Hao Y, He X, et al. Ags Nanoparticle-Mediated Multiple Ablations Reinvigorates the Immune Response for Enhanced Cancer Photo-Immunotherapy. *Biomaterials* (2021) 264:120451. doi: 10.1016/j.biomaterials.2020.120451

Conflict of Interest: The authors declare that the research was conducted in the absence of any commercial or financial relationships that could be construed as a potential conflict of interest.

frontiers in Oncology

METHODS
published: 09 February 2022
doi: 10.3389/fonc.2022.789506

Respiratory 4D-Gating F-18 FDG PET/CT Scan for Liver Malignancies: Feasibility in Liver Cancer Patient and Tumor Quantitative Analysis

Anson H. Y. Cheung[1,2], *Vincent W. C. Wu*[1], *Andy L. Y. Cheung*[1,3] *and Jing Cai*[1]*

[1] Department of Health Technology & Informatics, The Hong Kong Polytechnic University, Hong Kong, Hong Kong SAR, China, [2] Radiotherapy and Oncology Department, Hong Kong Baptist Hospital, Hong Kong, Hong Kong SAR, China, [3] Department of Clinical Oncology, Queen Mary Hospital, Hong Kong, Hong Kong SAR, China

Purpose: To evaluate the potential clinical role and effectiveness of respiratory 4D-gating F-18 FDG PET/CT scan for liver malignancies, relative to routine (3D) F-18 FDG PET/CT scan.

Materials and Methods: This study presented a prospective clinical study of 16 patients who received F-18 FDG PET/CT scan for known or suspected malignant liver lesions. Ethics approvals were obtained from the ethics committees of the Hong Kong Baptist Hospital and The Hong Kong Polytechnic University. Liver lesions were compared between the gated and ungated image sets, in terms of 1) volume measurement of PET image, 2) accuracy of maximum standardized uptake value (SUV_{max}), mean standardized uptake value (SUV_{mean}), and 3) accuracy of total lesion glycoses (TLG). Statistical analysis was performed by using a two-tailed paired Student *t*-test and Pearson correlation test.

Results: The study population consisted of 16 patients (9 males and 7 females; mean age of 65) with a total number of 89 lesions. The SUV_{max} and SUV_{mean} measurement of the gated PET images was more accurate than that of the ungated PET images, compared to the static reference images. An average of 21.48% ($p < 0.001$) reduction of the tumor volume was also observed. The SUV_{max} and SUV_{mean} of the gated PET images were improved by 19.81% ($p < 0.001$) and 25.53% ($p < 0.001$), compared to the ungated PET images.

Conclusions: We have demonstrated the feasibility of implementing 4D PET/CT scan for liver malignancies in a prospective clinical study. The 4D PET/CT scan for liver malignancies could improve the quality of PET image by improving the SUV accuracy of the lesions and reducing image blurring. The improved accuracy in the classification and identification of liver tumors with 4D PET image would potentially lead to its increased utilization in target delineation of GTV, ITV, and PTV for liver radiotherapy treatment planning in the future.

Keywords: liver, 4D PET/CT, respiratory gated PET/CT, SUV, clinical protocol

OPEN ACCESS

Edited by:
John Varlotto,
Marshall University, United States

Reviewed by:
Jungsu S. Oh,
University of Ulsan, South Korea
Wouter van Elmpt,
Maastricht University, Netherlands

***Correspondence:**
Jing Cai
jing.cai@polyu.edu.hk

Specialty section:
This article was submitted to Radiation Oncology, a section of the journal Frontiers in Oncology

Received: *05 October 2021*
Accepted: *12 January 2022*
Published: *09 February 2022*

Citation:
Cheung AHY, Wu VWC, Cheung ALY and Cai J (2022) Respiratory 4D-Gating F-18 FDG PET/CT Scan for Liver Malignancies: Feasibility in Liver Cancer Patient and Tumor Quantitative Analysis. Front. Oncol. 12:789506. doi: 10.3389/fonc.2022.789506

INTRODUCTION

Positron emission tomography/computed tomography (PET/CT) has been proven irreplaceable in providing anatomical and functional radiological information. Fluorodeoxyglucose fluorine-18 (F-18 FDG) PET/CT has been widely utilized for modern oncology imaging and considered as a useful tool for disease staging, assessment of patients' response to drug therapy, and detection of local recurrence or metastases (1, 2). Primary and secondary liver malignancies typically show increased glucose uptake and metabolism. Tumors consume FDG as a glucose analogue and display a strong uptake in PET images (1). Studies have shown that the sensitivity of detecting liver malignancies with F-18 FDG PET image ranged from 90% to 95% (3–5). The acquisition of PET/CT images consists of two parts: first, CT data are acquired by scanning the entire patient body in a few seconds. Secondly, PET data are acquired by using PET ring detectors; a range of 6–7 bed position acquisition is typically used for an adult scan, and the acquisition time can be up to several minutes per bed.

Of note, the acquired CT and PET image data are derived from an average of multiple respiratory cycles (6). The potential deleterious impact of respiration-induced motion of the upper thorax on accurate image acquisition and target delineation for radiotherapy has been well-documented in literature (6–10). In general, respiration-induced organ motion during PET/CT image acquisitions may cause four problems: 1) motion artifact in CT images, 2) image misregistration between CT and PET image data, 3) image blurring of PET uptake images, and 4) PET reconstruction error due to CT attenuation error (9, 10). The issues of image artifacts and image blurring result in qualitative and quantitative inaccuracy in determination of tumor morphology and its uptake activity in the attenuation-corrected PET/CT images (9, 10). To improve the accuracy of CT and PET image registration and minimize the issue of image blurring, the respiratory gating method has been introduced. The PET/CT scanner is equipped with a respiratory gating system that enables image data sorting. The acquired CT and PET data are equally separated into different respiratory phases, then each phase data within specific respiratory cycles are used for image reconstruction (10). Furthermore, imaging-based prognostic markers are crucial for patients' treatment option and survival; metabolic parameters derived using standard uptake values (SUV) or total lesion glycolysis (TLG) may be beneficial for disease staging and risk stratification before surgery and radiotherapy treatment (11, 12).

Despite the recognized issues caused by the respiration-induced motion in thoracic imaging, studies on investigating the impact of patients' breathing motion in PET/CT scan for liver malignancies, especially in a prospective clinical design, are severely scarce in the body of literature. Indeed, determination of the trajectory of respiration-induced liver motion is one of the major challenges in highly precise liver radiotherapy (13). Several studies have shown that liver tumor motion occurs primarily in the superior–inferior (SI) direction, ranging from 5 to 50 mm (14, 15). This respiration-induced tumor motion had adverse influences on radiation therapy treatment planning and delivery, including inaccurate tumors and normal tissue localization (16–18), dosimetric uncertainty based on a static CT images plan (16), and the requirement of increased planning target volume (PTV) margins, potentially leading to overexposure of the surrounding normal tissues and limiting the maximum allowable dose that should be given to the tumors (19, 20). For instance, Crivellaro et al. retrospectively analyzed standard 3D-PET/CT (i.e., ungated) and liver 4D-PET/CT (i.e., gated) images of 56 patients, hoping to investigate the added diagnostic value of respiratory-gated 4D PET/CT in detecting and characterizing a total of 72 liver lesions (21). They reported that an enhanced confidence of physicians in lesion detection on the gated PET/CT was found in 51.4% of the studied lesions, compared to the ungated PET/CT. Besides, they also demonstrated a significantly higher level of the SUV_{max} value for liver lesions in the gated PET, therefore improving quantitative characterization of the lesions, in comparison to the ungated PET (21). In addition, Michael et al. conducted a retrospective analysis on 149 cancer patients to evaluate the impact of data-driven respiratory gating (DDG) on PET image quality and lesion detection (22). They reported that the issue of image blurring in PET images was significantly lower when DDG (i.e., gated) was used, compared to the PET images without DDG application (i.e., ungated). Besides, boundary of organs, including liver and spleen, was rated significantly sharper on the DDG-gated PET images than those on the ungated PET images (22). These retrospective studies have underlined the importance of 4D-gating PET images in liver lesion detection.

In this study, we attempted to perform a prospective clinical study for evaluating the potential clinical role and effectiveness of respiratory 4D-gating F-18 FDG PET/CT scan specifically for liver malignancies. Comparative analyses of the liver lesions between the gated and ungated PET images were made in aspects of 1) volume measurement of PET image, 2) accuracy of maximum standardized uptake value (SUV_{max}) and mean standardized uptake value (SUV_{mean}), and 3) accuracy of total lesion glycoses (TLG). The success of this study would not only consolidate evidence in previous retrospective studies but also promote the clinical implementation of 4D-gating FDG PET/CT scans in target delineation for liver radiotherapy treatment planning in the future.

MATERIALS AND METHODS

Study Design and Subject Recruitment

This study was a prospective study. Ethics approvals were obtained from the ethics committees of the Hong Kong Baptist Hospital and The Hong Kong Polytechnic University. Patients who received F-18 FDG PET/CT scan for known or suspected malignant liver lesions between October 1, 2017, and December 31, 2017, were consecutively recruited in this study. Patients who 1) received previous radiotherapy, 2) were diagnosed with diffused liver lesions on CT images, 3) were diagnosed with benign liver lesions, 4) failed to perform respiratory gated PET/CT scan, or 5) rejected participation of this study were excluded. Verbal and written consents for all subjects were obtained prior

to routine scans. The workflow of this study is explained and summarized in **Figure 1**.

PET/CT Image Acquisitions

All PET/CT scans were carried out on a PET/CT 710 Discovery scanner (GE Healthcare, Milwaukee, WI, USA). This scanner was equipped with time-of-flight (TOF) function, lutetium-based scintillator (LBS) PET scanner, CT detector with 64 rows, and real-time position management respiratory-gated system (RPM, version 1.7.5; Varian Medical Systems, Palo Alto, CA, USA). The RPM motion tracking was set to be three-dimensional as the same as the setup for external beam liver radiotherapy. According to the in-house clinical protocol from the Nuclear Medicine & PET Centre (NMPC), patients were fasted for more than 6 h before FDG injection. The injected dose was related to patients' body weight with 3.7 MBq per kg, and patients were required to rest for 1 h after injection prior to image acquisition. Patients were instructed to void before getting into the scan room.

The whole-body ungated CT images were acquired under the following imaging parameters: 120 kVp, automatic tube current setting (10–300 mA, noise index 12), $CTDI_{vol}$: 15.68 mGy, 0.938 pitch, 0.4-s speed of gantry rotation, and 3.75-mm thickness per slice. For the routine whole-body scan, images were obtained from the femoral heads to base of skull during a shallow-breathing condition. After whole-body ungated CT scan was obtained, an additional respiratory gating liver CT scan was acquired. The respiratory-gated CT imaging protocol was comparable to those reported by Rietzel et al. (23) and Pan et al. (24). The respiratory-gated CT images for the liver were acquired with the following image parameters: 120 kVp, low-dose mA (10–80 mA, noise index 30), $CTDI_{vol}$: 104.49 mGy, 1.675 pitch, 0.4 s gantry rotation speed, and 2.5 mm slice thickness. It is worth noting that although the CTDIvol for the gated protocol is 6.67-fold higher than that for the non-gated protocol, the maximum tube current was drastically reduced (80 vs. 300 mA) and the pitch was approximately doubled (1.675 vs. 0.938) to reduce CT radiation exposure to the patients in this study. Cine mode in axial slices was performed with continued scans at the liver position with an intervening period equal to 1–1.5 s plus the patient's mean time of each respiratory cycle. The infrared video camera detected the 3D displacement of two infrared reflective markers in a plastic box which was placed on the patient's abdomen at the level of the umbilicus. The respiration cycle of the patients was acquired using the RPM system in precise temporal correlation to CT data acquisition.

The whole-body ungated PET images were obtained after the CT scan. A total of 6–7 bed positions were required for a regular adult; all data were collected during shallow breathing for 2 min at each bed position. At the bed position during liver imaging, PET data were acquired for 5 min with respiratory gating. Similar to the respiratory gated CT image acquisition, the RPM system was used to acquire patients' breathing cycle.

4D-Gating and Ungated PET Image Reconstruction

All PET raw data obtained from respiratory gated scan and ungated scan were reconstructed using the 3D Order Subsets Expectation Maximization (3D-OSEM) iterative reconstruction algorithm (24 subsets, 4 iterations) to generate PET images. Details of the image reconstruction parameters are as follows: VUE Point

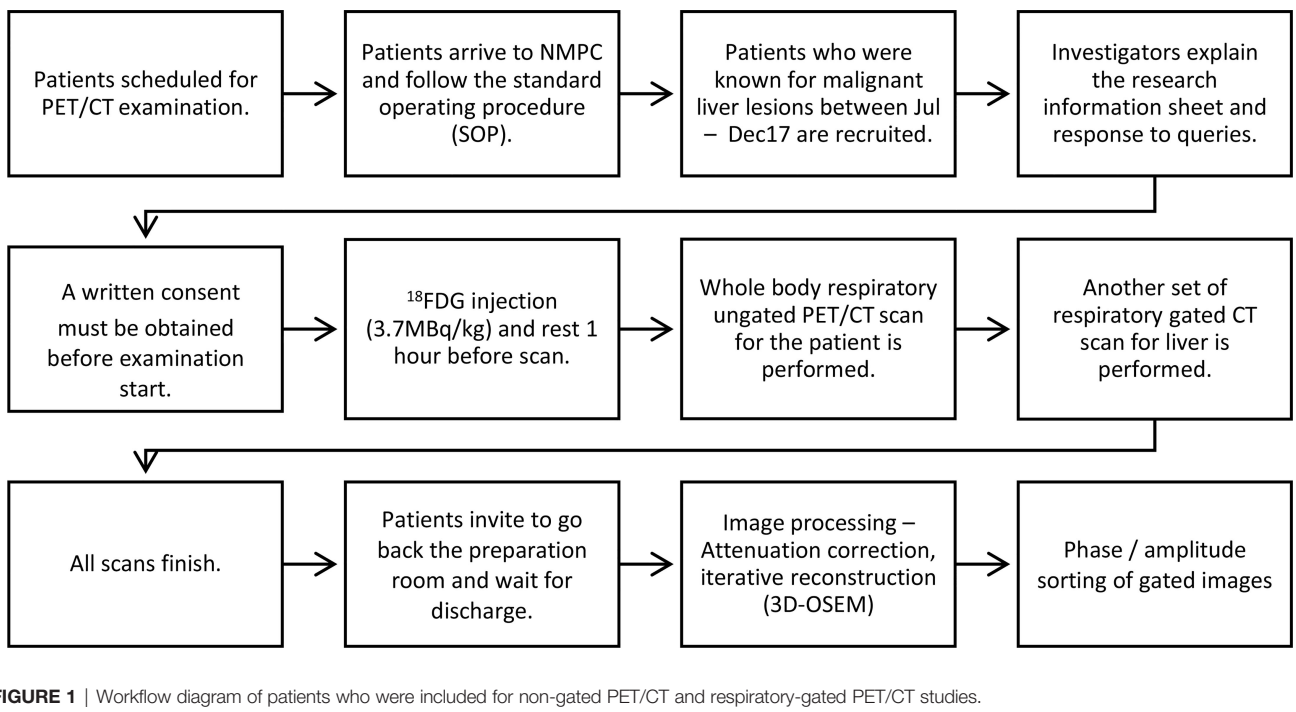

FIGURE 1 | Workflow diagram of patients who were included for non-gated PET/CT and respiratory-gated PET/CT studies.

FX reconstructed method, SharpIR quantitation method, 50.0 cm FOV, 192 × 192 matrix, Gaussian 6.0-mm filter of full width at half maximum (FWHM), 3.27-mm thickness per slice, Z-Axis Filter: Standard, and TOF reconstruction algorithm.

Phantom Validation of the Motion Correction

The QUASAR™ respiratory motion phantom with 4D PET/CT imaging insert (P/N: 500-3318) was used to validate the motion correction before clinical implementation. The PET insert was equipped with a 30-mm sphere which was filled with clinical activity concentrations (injected activity: 3.5 kBq/ml, image acquisition ~ 1 h: ~2.4 kBq/ml) of F-18 FDG (25). The sphere was animated with a 2-cm longitudinal respiratory simulated motion. The movement cycle was set to be 12 breaths per minute. The RPM system was placed on the platform of the QUASAR™ phantom to acquire the movement cycles during data acquisitions. The 4D-gating and ungated PET images were compared to static reference PET images (respiratory motion was disabled).

Individual Phase Sorting for Respiratory-Gated PET/CT Images

All image data sets were arranged into 10 phases based on the temporal correlation between data acquisition on Advantage Workstation 4.5 (GE Healthcare, Milwaukee, WI, USA) and patients' breathing displacement motion. The 10 reconstructed respiratory phase images were evenly divided from a full respiratory cycle. Each CT image set was labeled based on their phase of acquisition, e.g., CT_0%, CT_10%, CT_20%, CT_30%, CT_40%, CT_50%, CT_60%, CT_70%, CT_80%, and CT_90%. CT_0% corresponds to end of inspiration, and CT_50% is the start of inspiration or end of expiration.

Attenuation Correction for Respiratory Gated and Non-Gated PET Images

All CT images were utilized to produce an attenuation correction map that could then be utilized to correct the attenuation effect of 511-keV emission photon passing through the body (26). For PET images which are respiratory gated, phase-matched attenuation correction was carried out using the respiratory-sorted CT images. For PET images obtained from shallow-breathing whole-body scan (ungated scan), they were corrected with the corresponding shallow-breathing CT image set. The gated PET image was based on the registered (i.e., phase-matched) gating image. When the PET/CT examination was acquired based on the mentioned protocol, the examination is defined as successful. Finally, all DICOM CT images were exported to a contouring workstation (MIM Maestro™, MIM Software Inc.) for contouring and image analysis.

Generation of Gross Tumor Volume in Respiratory Gating PET/CT Images

For identification of respiration-induced liver tumors, the gated PET volume was defined as the gross tumor volume (GTV). As previously mentioned, each respiratory gated PET/CT image set was sorted into 10 phases. In each phase image, GTVs were automatically contoured based on the SUV threshold. Subsequently, all delineated GTVs were verified by an in-house radiation oncologist.

Assessment Criteria and Statistical Analysis

Two in-house experienced radiologists who are specialized in nuclear medicine were invited to perform image assessments; if there is any uncertainty, consensus between two radiologists was required. Lesions with $SUV_{max} < 1.0$ were considered as non-malignant lesions and discarded from downstream analysis; this threshold value was chosen based on previous studies (27, 28). The use of the SUV threshold in tumor volume segmentation eliminates intra-rater and inter-rater segmentation variability, and it is worth noting that all the generated segments in this study were approved by experienced medical oncologists with specialty in nuclear medicine. The respiratory gated and ungated images of liver lesions were analyzed and compared in terms of four parameters, namely, 1) percentage change in PET volume (Vp) and 2) percentage change on SUV_{max}, SUV_{mean}, and TLG values using the following equations:

$$\%\ change\ in\ PET_{vol} = \frac{(ungated\ PET_{vol} - gated\ PET_{vol})}{ungated\ PET_{vol}} \times 100 \quad (1.1)$$

$$\%\ change\ in\ SUV_{max} = \frac{(gated\ SUV_{max} - ungated\ SUV_{max})}{ungated\ SUV_{max}} \times 100 \quad (1.2)$$

$$\%\ change\ in\ SUV_{mean} = \frac{(gated\ SUV_{mean} - ungated\ SUV_{mean})}{ungated\ SUV_{mean}} \times 100 \quad (1.3)$$

$$\%\ change\ in\ TLG = \frac{(gated\ TLG - ungated\ TLG)}{ungated\ TLG} \quad (1.4)$$

Statistical Analysis

Statistical analysis was carried out by using SPSS statistics software, version 28 (IBM Corporation, Armonk, NY, USA). Mean ± standard deviation (S.D.) of measurements was reported. Variations between respiratory gated and ungated were tested using the two-sided paired Student *t*-test. A p value less than 0.05 was considered as statistically significant. The correlation between three SUV parameters and TLG were evaluated by Pearson's correlation coefficients.

RESULTS

Patient Characteristic

The summary of the study population is shown in **Figure 2**. Twenty-five patients who were scheduled for receiving F-18 FDG PET/CT scan for known or suspected liver malignant diseases were recruited. Nine subjects were excluded, and the remaining

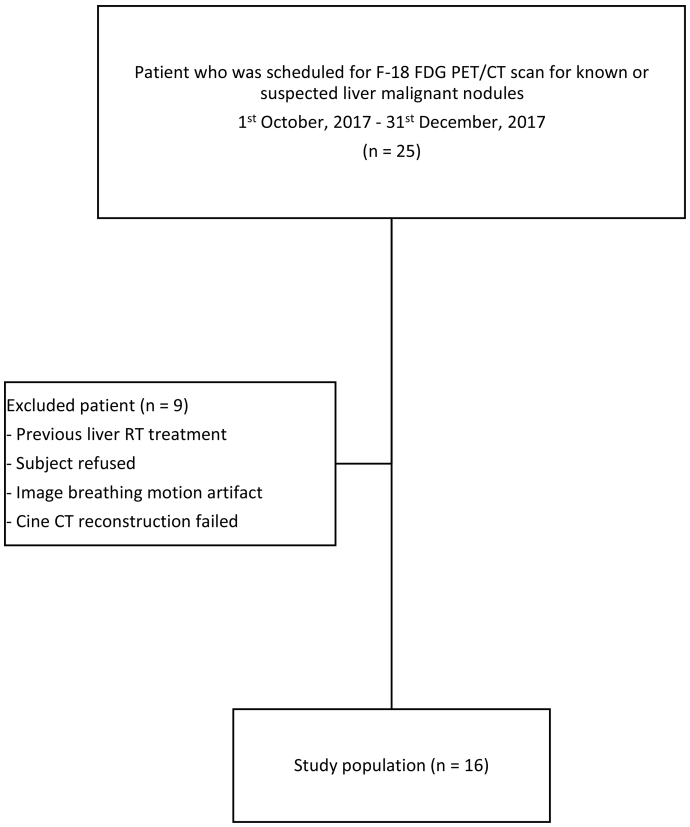

FIGURE 2 | Chart on recruitment and final study population.

study subjects (n = 16, including 9 men and 7 women) were included. The average age of the included subjects was 65 years (range: 41 to 84). The patient demographic and lesion characteristic are presented in **Table 1**. The mean total time for 4D PET/CT liver acquisition was 23 ± 2 min (range: 18.5–28.4). All successful subjects were included to perform image and uptake quantitative analyses (**Figure 3**).

Phantom Validation of the Motion Correction

From the phantom validation experiment, we observed that the SUV_{max} and SUV_{mean} values of the 4D-gating PET images were similar to the reference of static phantom images (SUV_{max}: 4.97 vs. 5.13, SUV_{mean}: 2.74 vs. 3.20), while those values of the ungated PET images were markedly decreased (SUV_{max}: 3.97 vs. 5.13, SUV_{mean}: 2.13 vs. 3.20).

The Effect of Respiratory Gated Scan on Liver Tumors Compared to Routine 3D PET/CT Scan

The effects of respiratory gated scan on PET contour volume (Vp), SUV_{max}, SUV_{mean}, and total lesion glycolysis (TLG) for the 89 lesions are presented in **Table 2**. Vp (ml) was significantly decreased by using the respiratory gating technique (from 4.22 ± 7.46 to 3.32 ± 6.78, 21.48%, $p < 0.001$). The SUV_{max} and SUV_{mean} using the respiratory gated technique were significantly improved by 19.81% and 25.53% compared to the respiratory ungated technique. The TLG was slightly reduced from 26.37 ± 47.68 to 25.12 ± 50.59 ($p = 0.1812$). Details on variations of lesion volume, SUV_{max}, SUV_{mean}, and TLG between respiratory phases are displayed as **Supplementary Tables 1–4**, respectively, in the **Supplementary Material**.

Influence of Liver Tumor's Location on the Effect of Respiratory Gating

Among the 89 studied lesions, 11 and 78 are located in the left lobe and right lobe, respectively. The average lesion size was 4.95 ± 5.69 ml for the left lobe and 4.12 ± 7.75 ml for the right lobe. The effect of respiratory gating on Vp, SUV_{max}, SUV_{mean}, and TLG in both lobes are presented in **Table 2**.

In the left lobe, the results showed a significant difference between ungated and gated images in Vp (4.95 ± 5.69 vs. 3.88 ± 5.62, $p < 0.001$), SUV_{max} (9.15 ± 3.99 vs. 10.34 ± 4.70, $p = 0.0049$), and SUV_{mean} (5.45 ± 1.67 vs. 7.03 ± 2.84, $p = 0.0034$). By contrast, ungated and gated images showed no significant difference in terms of TLG values (24.67 ± 26.72 vs. 22.28 ± 30.31, $p = 0.1161$).

TABLE 1 | The patient demographic and lesion characteristics.

Patient Demographic			
Total subjects	16	Age (mean ± S.D.)	65 ± 13 (years)
Male/female	9/7	Age (range)	41–84 (years)
Lesions characteristic		***Primary cancer site***	
Total lesions	89	Ca rectum	4
Lesion size (mean ± S.D.[a])	4.22 ± 7.46 (ml)	Ca colon	3
Lesions (range)	0.45 – 62.24 (ml)	Ca pancreas	2
Lesion location		Ca liver	2
Segment 1	2	Ca breast	1
Segment 2	8	Ca cecum	1
Segment 3	3	Ca lung	1
Segment 4	17	Ca sigmoid	1
Segment 5	15	Ca thyroid	1
Segment 6	21		
Segment 7	9		
Segment 8	14		

[a]*Standard deviation (S.D.).*

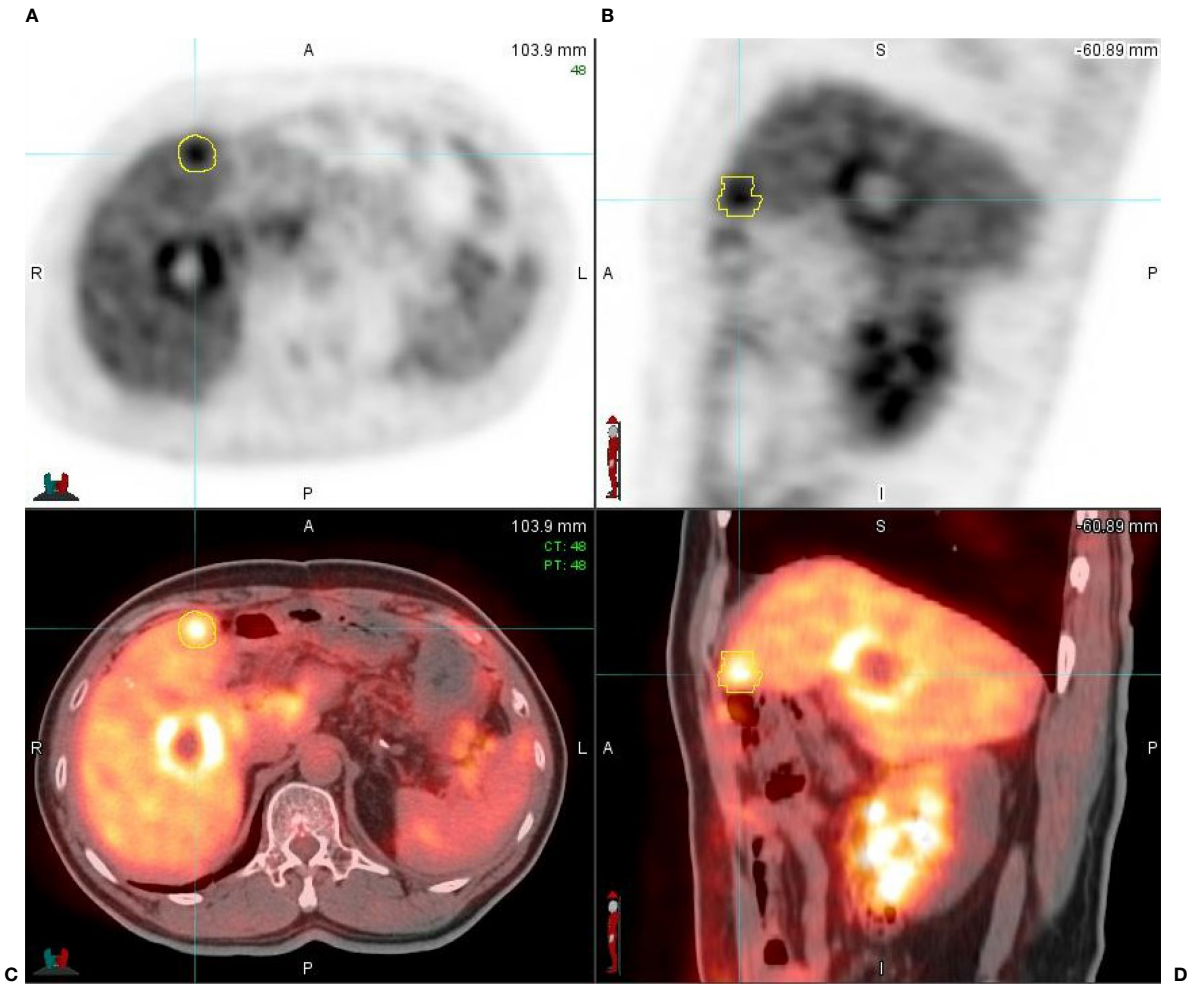

FIGURE 3 | A 65-year-old male patient with hepatic metastasis from a primary rectal cancer. **(A)** Axial respiratory gated PET image (PET_0% sorted) shows two liver lesions with an increased uptake of FDG; one of the liver lesions is contoured (in yellow), measuring 2.5 cm × 2.3 cm in diameter with SUV_{max} = 9.24, conforming to liver metastasis. **(B)** Sagittal respiratory gated PET image (PET_0% sorted); one of the lesions is contoured (in yellow), measuring 2.8 cm in diameter with SUV_{max} = 9.24. **(C, D)** The respiratory gated PET axial and sagittal images fused with respiratory gated CT images (PET/CT_0% sorted); the high FDG uptake area is presented in thermal color and CT images are in gray scale.

TABLE 2 | PET volume (Vp), and SUV_{max}, SUV_{mean}, and TLG in non-gating and gating PET/CT.

	Respiratory Ungated	Respiratory Gated	Percentage Change	p value
Total (n = 89)				
Vp (ml)	4.22 ± 7.46	3.32 ± 6.78	21.48%	<0.001
SUV_{max}	8.87 ± 4.23	10.63 ± 5.25	19.81%	<0.001
SUV_{mean}	5.56 ± 1.95	6.98 ± 2.94	25.53%	<0.001
TLG	26.37 ± 47.68	25.12 ± 50.59	-4.74%	0.1812
Lt lobe (n = 11)				
Vp (ml)	4.95 ± 5.69	3.88 ± 5.62	21.91%	<0.001
SUV_{max}	9.15 ± 3.99	10.34 ± 4.70	12.91%	0.0049
SUV_{mean}	5.45 ± 1.67	7.03 ± 2.84	29.00%	0.0034
TLG	24.67 ± 26.72	22.28 ± 30.31	-9.68%	0.1161
Rt lobe (n = 78)				
Vp (ml)	4.12 ± 7.75	3.23 ± 7.00	21.45%	<0.001
SUV_{max}	8.84 ± 4.31	10.68 ± 5.38	20.82%	<0.001
SUV_{mean}	5.57 ± 2.01	6.97 ± 3.00	25.06%	<0.001
TLG	26.61 ± 50.34	25.52 ± 53.27	-4.09%	0.2987

1) Values of respiratory ungated and gated were indicated as mean ± standard deviation.
2) Left (Lt) lobe (Segments 2 and 3).
3) Right (Rt) lobe (Segments 1, 4, 5, 6, 7, 8).

In the right lobe, ungated and gated images in Vp showed a significant difference (4.12 ± 7.75 vs. 3.23 ± 7.00, $p < 0.001$), SUV_{max} (8.84 ± 4.31 vs. 10.68 ± 5.38, $p < 0.001$), and SUV_{mean} (5.57 ± 2.01 vs. 6.97 ± 3.00, $p < 0.001$). However, there was no significant difference between ungated and gated images in terms of TLG values (26.61 ± 5034 vs. 25.52 ± 53.27, p = 0.2987).

In the comparison of lesions between both sides of liver lobes, there were no significant differences in Vp (3.88 ± 5.62 vs. 3.24 ± 7.00, p = 0.7721), SUV_{max} (10.34 ± 4.70 vs. 10.68 ± 5.38, p = 0.8426), SUV_{mean} (7.03 ± 2.84 vs. 6.97 ± 2.99, p = 0.9526), and TLG (22.28 ± 30.31 vs. 25.52 ± 53.27, p = 0.8443).

The Correlation Between % Change in SUV_{max} and 3 Quantitative Parameters on PET Image (Percentage Change in Vp, Percentage Change in SUV_{mean}, and Percentage Change in TLG)

There was a weak correlation between percentage change in SUV_{max} and percentage change Vp (r = 0.2117, p = 0.0359) (**Figure 4**), between percentage change in SUV_{max} and percentage change in SUV_{mean} (r = 0.4891, p = 0.0897) (**Figure 5**), and between percentage change in SUV_{max} and percentage change in TLG (r = 0.4522, $p < 0.0001$) (**Figure 6**).

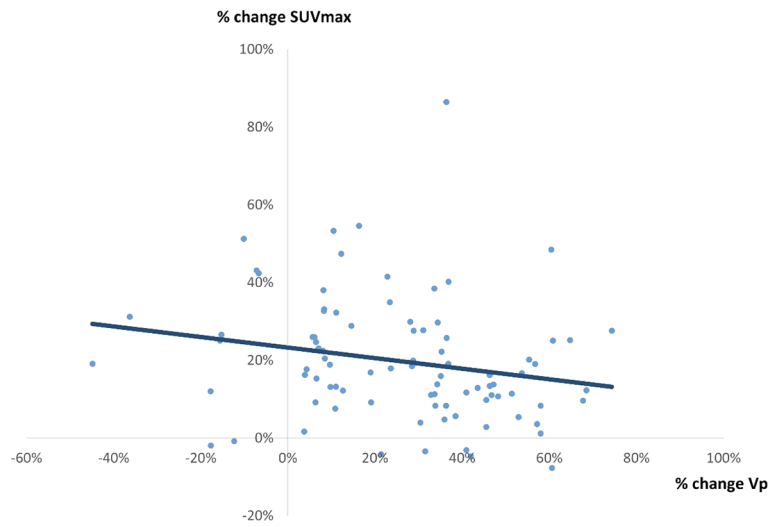

FIGURE 4 | A correlation between % change in SUV_{max} and % change in Vp by 4D PET/CT scan. A weak correlation was observed (r = 0.2117, p = 0.0359, y = -0.1356x + 0.2328).

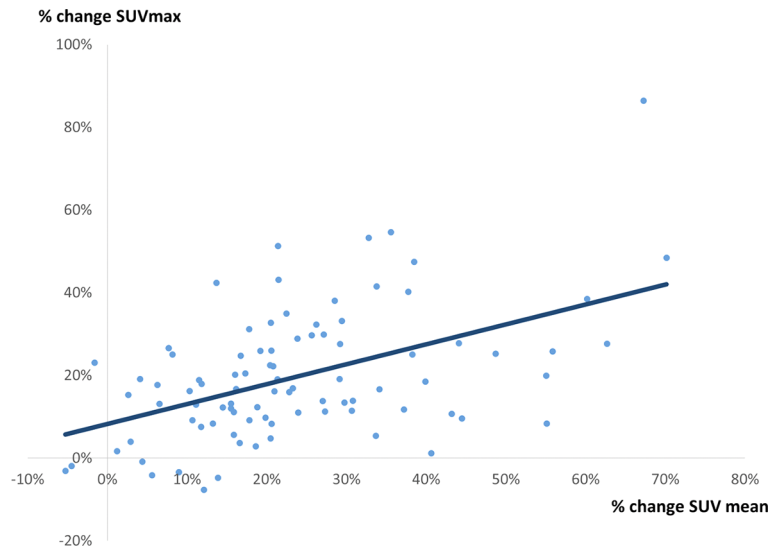

FIGURE 5 | A correlation between % change in SUV_{max} and % change in SUV_{mean}. A weak correlation was observed (r = 0.4891, p = 0.0897, y = 0.4815x + 0.0828).

DISCUSSION

The implementation of additional gated PET/CT liver scan in routine PET/CT scan was successfully (92%) achieved. The reasons for unsuccess were gated CT image motion artifact and failure in cine CT image reconstruction. In this prospective clinical study, the gated PET/CT image demonstrated a reduction of image blurring on FDG uptake lesions. There was improvement in quantitative values including Vp, SUV_{max}, and SUV_{mean}. In a gated PET/CT liver study, all scans were acquired in only one bed position and the mean gated PET/CT acquisition time was about 23 min. All patients were satisfied, and duty staff had positive feedback with the workflow (29). The potential clinical applications of the gated PET images are manifold. It would allow physicians to determine an appropriate treatment regimen on a patient basis by providing better appreciation of tumor real-time trajectory in terms of both motion speed and range. Besides, the gated PET images can be used for tumor delineation with higher accuracy by providing better visualization of tumor size and border. When registered with static planning CT images, it may also allow physicians to incorporate biologic metabolism of the tumor into target delineation, paving the way toward biologic-guided RT (30).

Respiration-induced liver motion was prominent in the cranial–caudal direction. 3D PET images were acquired during multiple respiratory cycles, causing blurring of PET images, incorrect estimation of F-18 FDG uptake volume, and inaccurate lesion size determination. In the study of a total of 89 lesions, the gated PET illustrated a significant reduction in PET volume by 21.48% compared to the ungated PET. Furthermore, the gated PET images were sharper, with a more well-defined tumor boarder. Our findings are in line with previous 4D PET/CT studies which reported a mean reduction of 11%–45% in the gated PET volume compared to the non-gated PET volume (31–33). In addition, radiological information from PET/CT images is commonly utilized in radiotherapy treatment planning, especially when radiation oncologists delineate the gross target volume (GTV) and clinical target volume (CTV) and estimate tumor motion during respiration (34). The improvement of visual diagnostic value in the gated PET/CT was also in agreement with the finding reported by Fin et al., although PET quantitative analysis was not described (35). Therefore, we believe that the gated PET images could be a routine scan when liver radiotherapy treatment is intended, especially when the treatment was determined to be respiratory-gated (36, 37). Although additional time for patient setup and scan is required, respiratory gated scan can be implemented feasibly and efficiently in clinical routines. Gated PET/CT also has a great potential for giving higher spatial resolution and motion artifact free images, which is an essence of future development of molecular imaging.

It is worth mentioning that recent advances in PET cameras and AI techniques have enabled a data-driven (i.e., device-less) approach, such as MotionFree™/data-driven gating (DDG), for respiratory gating in PET images, potentially serving as an alternative to the classical device-based gating system, such as the Varian RPM-based approach. Both approaches have been studied for gated PET imaging. For instance, Crivellaro et al. retrospectively analyzed standard 3D-PET/CT (i.e., ungated) and liver 4D-PET/CT (i.e., gated) images of 56 patients, hoping to investigate the added diagnostic value of device-based respiratory-gated 4D PET/CT in detecting and characterizing a total of 72 liver lesions (21). They reported that an enhanced confidence of physicians in lesion detection on the gated PET/CT was found in 51.4% of the studied lesions, compared to the ungated PET/CT. Besides, they also demonstrated a significantly higher level of the SUV_{max} value for liver lesions in the gated

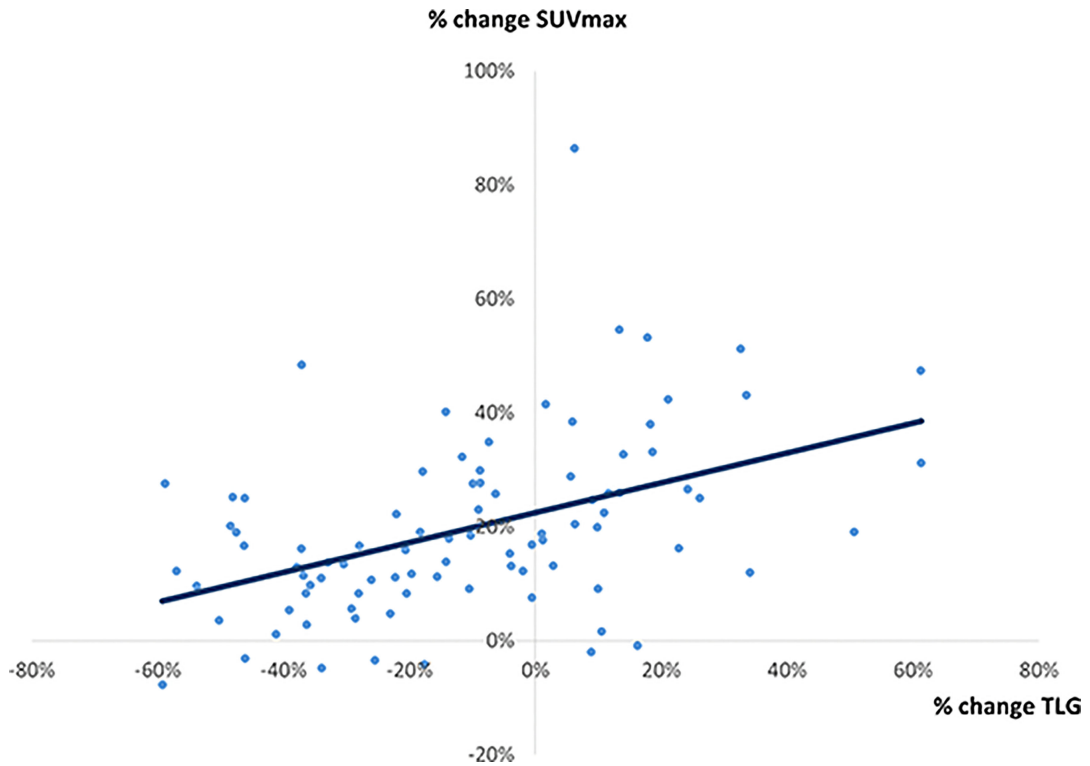

FIGURE 6 | A correlation between % change in SUV_{max} and % change in TLG. A weak correlation was observed (r = 0.4522, p < 0.0001, y = 0.262x + 0.2252).

PET, therefore improving quantitative characterization of the lesions, in comparison to the ungated PET (21). In addition, Michael et al. conducted a retrospective analysis on 149 cancer patients to evaluate the impact of device-less respiratory gating (DDG) on PET image quality and lesion detection (22). They reported that the issue of image blurring in PET images was significantly lower when DDG (i.e., gated) was used, compared to the PET images without DDG application (i.e., ungated). Besides, boundary of organs, including liver and spleen, was rated significantly sharper on the DDG-gated PET images than those on the ungated PET images (22).

Both device-based and device-less approaches have their advantages and drawbacks. Unlike the Varian RPM-based (i.e., device-based) respiratory gating technique, the device-less approach waives the requirement of setting up the respiratory gating device on the patient's body which prolongs the scanning time, making this approach appear to be more patient-friendly. Nevertheless, the device-based system has long been considered as a standard procedure for correcting respiratory motion-induced uncertainties in PET images in clinics at present, and hence, it is a more popular and widely used technique, compared to the device-less gating technique. Furthermore, the device-based system possesses a unique capability in achieving breathing-synchronized RT treatment (38), while the device-less system is not used in RT application. This feature is of high clinical value in realizing real-time tumor trajectory, and the treating oncologist can therefore be more confident in delineating the internal target volume (ITV) of the tumor, which would eventually translate to the patient's treatment outcome benefit. Besides, the information of real-time tumor trajectory also allows physicians to better appreciate the speed of the tumor motion, based on which the physicians can better determine an appropriate treatment regimen (e.g., whether to treat with SBRT or not) on a case-by-case basis. All things considered, although the device-less approach appears to be more patient-friendly, it is not presently used for radiotherapy purposes. In the context of radiotherapy, other aspects, such as reliability and treatment efficacy, are more important, and thus we believe that the Varian RPM-based respiratory gating system still plays a key role in managing liver malignancies.

Previously, gated PET/CT images were found to produce a more accurate evaluation of FDG uptake in liver tumors that may allow physicians to make better tumor characterization, more personalized treatment strategy, treatment response monitoring, and prediction of survival (9, 31, 39). In this study, respiratory gating improved PET image measurement of tumor SUV and metabolic volume. The SUV value is a sensitive indicator to represent tumor metabolism or even tumor proliferation. In our gated PET image analysis, the mean value of SUV_{max} was increased by 19.81% compared to the ungated PET image. This finding is in line with that reported by Suenaga et al., in which a 22% increase in SUV_{max} value was reported (34). However, the SUV_{max} value represents the local maximum of a region of interest, which means that it might only reflect a single

voxel value of maximum FDG uptake within the entire tumor (40, 41). By contrast, SUV_{mean} is another indictor to represent the tumor's metabolic activity as a whole. In the present study, respiratory gating improved the mean value of SUV_{mean} by 25.53%. The deviation of FDG uptake results through respiratory gating between our finding and previous studies could be related to the following two reasons. First, the FDG uptake in liver tumor may change with PET scan time; a delayed gated PET acquisition protocol could result in a higher SUV value (42, 43). In this study, all gated PET/CT acquisition was performed after routine ungated whole-body FDG scan. Second, as suggested by Guerra et al., differences in tumor type, volume, geographical region, elasticity, and motion could influence the percentage change of the respiratory gated results (42).

In previous reports, the prognostic value of TLG on preoperative F-18 FDG PET/CT has been widely studied for estimating intrahepatic recurrence-free survival (IHRFS), extrahepatic metastasis-free survival (EHMFS), and overall survival (OS) in patients with liver malignancies (44–46). Therefore, it is important for physicians to identify TLG and compare clinical findings with other pathological or histological prognostic factors. In this study, we evaluated the percentage change in TLG when the 4D PET/CT technique was introduced. The mean of the TLG value decreased by 4.74% in a total of 89 lesions, although no significant difference was observed. The decrease in the tumor's TLG values could probably be due to the reduction in PET volume in the respiratory gated scan.

On the other hand, the correlation with percentage change in SUV_{max} was stronger in percentage change in SUV_{mean} ($r = 0.49$) and TLG ($r = 0.45$) than percentage change in Vp ($r = 0.21$) in this study. These findings indicated that the 4D PET/CT scan may provide a generally higher SUV value, which has a stronger effect on the lesion's uptake improvement than the effect on the reduction of PET volume. Apart from this, we have assessed the correlation between amplitude of motion and SUV differences between gated and ungated images (**Supplementary Figures 1, 2**). It was observed that the correlation was not strong ($R = 0.4543$ for SUV_{mean} and 0.5016 for SUV_{max}). We speculated that this finding could be probably attributed to the intrinsic property of PET images. Unlike CT images where imaging voxels are characterized by a well-defined absolute value of Hounsfield unit, PET images commonly suffer from high imaging noise and is susceptible to injection dose of the radioactive agents, leading to a highly unstable imaging voxel intensity. In view of this, image normalization between patients and hence comparison of SUV values between patients are practically challenging. Therefore, it would be difficult to obtain a high correlation between the SUV differences and the motion amplitude of lesion. Although we found that the correlation was 0.4543 for SUV_{mean} and 0.5015 for SUV_{max}, we think that these values are still considered reasonable due to the intrinsic unstable property of PET images.

There were several limitations in the present study. First, the patient population was relatively small, although a total of 89 lesions were studied. Future evaluation of a large cohort is recommended to evaluate the feasibility and clinical benefits of respiratory gated PET/CT for detection of liver malignancies. Second, although the digital phantom was adopted for validation in this study because of its wide-spreading application (47, 48), further investigation on a 4D eXtended CArdiac-Torso (XCAT) phantom is warranted to yield a more validated result. Third, the choice of the SUV threshold value for lesion contouring might affect the quantitative measurements in this study, although all the final contours were verified by a nuclear medicine physician. Lastly, this work remains to be a feasibility study in nature; optimal settings of reconstruction parameters and function for PET gating were not investigated in this study. Further explorations in this regard are highly encouraged to strengthen the clinical value of the gated PET in the future.

In conclusion, we have demonstrated the feasibility of implementing 4D PET/CT scan for liver malignancies in a prospective clinical study. The 4D PET/CT was found to mitigate issues of image blurring artifact and improve the accuracy of lesion volume on PET images. The improved accuracy in the classification and identification of liver tumors with 4D PET image would potentially lead to its increased utilization in target delineation of GTV, ITV, and PTV for liver radiotherapy treatment planning in the future.

DATA AVAILABILITY STATEMENT

The original contributions presented in the study are included in the article/**Supplementary Material**. Further inquiries can be directed to the corresponding author.

ETHICS STATEMENT

The studies involving human participants were reviewed and approved by 1) the Hong Kong Polytechnic University - human subjects ethics sub-committee and 2) Hong Kong Baptist Hospital - Clinical and research ethics committee. The patients/participants provided their written informed consent to participate in this study.

AUTHOR CONTRIBUTIONS

JC was the chief supervisor in the study. AHC and VW contributed to the conception and methodology of the study. AHC and VW applied the ethical approval. AHC organized the patient recruitment and data collection process. AHC and ALC performed the data analysis. AHC wrote the first draft of the manuscript. ALC revised the content. JC revised and approved the submitted version. All authors contributed to the article and approved the submitted version.

SUPPLEMENTARY MATERIAL

The Supplementary Material for this article can be found online at: https://www.frontiersin.org/articles/10.3389/fonc.2022.789506/full#supplementary-material

REFERENCES

1. Khandani AH, Wahl RL. Applications of PET in Liver Imaging. *Radiol Clin North Am* (2005) 43(5):849–60, vii. doi: 10.1016/j.rcl.2005.05.008
2. Nahmias C, Hanna WT, Wahl LM, Long MJ, Hubner KF, Townsend DW. Time Course of Early Response to Chemotherapy in Non-Small Cell Lung Cancer Patients With 18F-FDG PET/CT. *J Nucl Med* (2007) 48(5):744–51. doi: 10.2967/jnumed.106.038513
3. Lai DT, Fulham M, Stephen MS, Chu KM, Solomon M, Thompson JF, et al. The Role of Whole-Body Positron Emission Tomography With [18F] Fluorodeoxyglucose in Identifying Operable Colorectal Cancer Metastases to the Liver. *Arch Surg* (1996) 131(7):703–7. doi: 10.1001/archsurg.1996.01430190025007
4. Kinkel K, Lu Y, Both M, Warren RS, Thoeni RF. Detection of Hepatic Metastases From Cancers of the Gastrointestinal Tract by Using Noninvasive Imaging Methods (US, CT, MR Imaging, PET): A Meta-Analysis. *Radiology* (2002) 224(3):748–56. doi: 10.1148/radiol.2243011362
5. Bipat S, van Leeuwen MS, Comans EF, Pijl ME, Bossuyt PM, Zwinderman AH, et al. Colorectal Liver Metastases: CT, MR Imaging, and PET for Diagnosis–Meta-Analysis. *Radiology* (2005) 237(1):123–31. doi: 10.1148/radiol.2371042060
6. Erdi YE, Nehmeh SA, Pan T, Pevsner A, Rosenzweig KE, Mageras G, et al. The CT Motion Quantitation of Lung Lesions and Its Impact on PET-Measured SUVs. *J Nucl Med* (2004) 45(8):1287–92.
7. Cai J, Read PW, Larner JM, Jones DR, Benedict SH, Sheng K. Reproducibility of Interfraction Lung Motion Probability Distribution Function Using Dynamic MRI: Statistical Analysis. *Int J Radiat Oncol Biol Phys* (2008) 72(4):1228–35. doi: 10.1016/j.ijrobp.2008.07.028
8. Ge H, Cai J, Kelsey CR, Yin FF. Quantification and Minimization of Uncertainties of Internal Target Volume for Stereotactic Body Radiation Therapy of Lung Cancer. *Int J Radiat Oncol Biol Phys* (2013) 85(2):438–43. doi: 10.1016/j.ijrobp.2012.04.032
9. Lupi A, Zaroccolo M, Salgarello M, Malfatti V, Zanco P. The Effect of 18F-FDG-PET/CT Respiratory Gating on Detected Metabolic Activity in Lung Lesions. *Ann Nucl Med* (2009) 23(2):191–6. doi: 10.1007/s12149-008-0225-1
10. Nehmeh SA, Erdi YE, Ling CC, Rosenzweig KE, Squire OD, Braban LE, et al. Effect of Respiratory Gating on Reducing Lung Motion Artifacts in PET Imaging of Lung Cancer. *Med Phys* (2002) 29(3):366–71. doi: 10.1118/1.1448824
11. Vesselle H, Freeman JD, Wiens L, Stern J, Nguyen HQ, Hawes SE, et al. Fluorodeoxyglucose Uptake of Primary Non-Small Cell Lung Cancer at Positron Emission Tomography: New Contrary Data on Prognostic Role. *Clin Cancer Res* (2007) 13(11):3255–63. doi: 10.1158/1078-0432.CCR-06-1128
12. Paesmans M, Berghmans T, Dusart M, Garcia C, Hossein-Foucher C, Lafitte JJ, et al. Primary Tumor Standardized Uptake Value Measured on Fluorodeoxyglucose Positron Emission Tomography Is of Prognostic Value for Survival in Non-Small Cell Lung Cancer: Update of a Systematic Review and Meta-Analysis by the European Lung Cancer Working Party for the International Association for the Study of Lung Cancer Staging Project. *J Thorac Oncol* (2010) 5(5):612–9. doi: 10.1097/JTO.0b013e3181d0a4f5
13. Eccles CL, Dawson LA, Moseley JL, Brock KK. Interfraction Liver Shape Variability and Impact on GTV Position During Liver Stereotactic Radiotherapy Using Abdominal Compression. *Int J Radiat Oncol Biol Phys* (2011) 80(3):938–46. doi: 10.1016/j.ijrobp.2010.08.003
14. Balter JM, Dawson LA, Kazanjian S, McGinn C, Brock KK, Lawrence T, et al. Determination of Ventilatory Liver Movement *via* Radiographic Evaluation of Diaphragm Position. *Int J Radiat Oncol Biol Phys* (2001) 51(1):267–70. doi: 10.1016/S0360-3016(01)01649-2
15. Davies SC, Hill AL, Holmes RB, Halliwell M, Jackson PC. Ultrasound Quantitation of Respiratory Organ Motion in the Upper Abdomen. *Br J Radiol* (1994) 67(803):1096–102. doi: 10.1259/0007-1285-67-803-1096
16. Balter JM, Lam KL, McGinn CJ, Lawrence TS, Ten Haken RK. Improvement of CT-Based Treatment-Planning Models of Abdominal Targets Using Static Exhale Imaging. *Int J Radiat Oncol Biol Phys* (1998) 41(4):939–43. doi: 10.1016/S0360-3016(98)00130-8
17. Aruga T, Itami J, Aruga M, Nakajima K, Shibata K, Nojo T, et al. Target Volume Definition for Upper Abdominal Irradiation Using CT Scans Obtained During Inhale and Exhale Phases. *Int J Radiat Oncol Biol Phys* (2000) 48(2):465–9. doi: 10.1016/S0360-3016(00)00610-6
18. Chen GT, Kung JH, Beaudette KP. Artifacts in Computed Tomography Scanning of Moving Objects. *Semin Radiat Oncol* (2004) 14(1):19–26. doi: 10.1053/j.semradonc.2003.10.004
19. Rosu M, Dawson LA, Balter JM, McShan DL, Lawrence TS, Ten Haken RK. Alterations in Normal Liver Doses Due to Organ Motion. *Int J Radiat Oncol Biol Phys* (2003) 57(5):1472–9. doi: 10.1016/j.ijrobp.2003.08.025
20. Tse RV, Hawkins M, Lockwood G, Kim JJ, Cummings B, Knox J, et al. Phase I Study of Individualized Stereotactic Body Radiotherapy for Hepatocellular Carcinoma and Intrahepatic Cholangiocarcinoma. *J Clin Oncol* (2008) 26(4):657–64. doi: 10.1200/JCO.2007.14.3529
21. Crivellaro C, De Ponti E, Elisei F, Morzenti S, Picchio M, Bettinardi V, et al. Added Diagnostic Value of Respiratory-Gated 4D 18F–FDG PET/CT in the Detection of Liver Lesions: A Multicenter Study. *Eur J Nucl Med Mol Imaging* (2018) 45:102–9. doi: 10.1007/s00259-017-3795-0
22. Messerli M, Liberini V, Grünig H, Maurer A, Skawran S, Lohaus N, et al. Clinical Evaluation of Data-Driven Respiratory Gating for PET/CT in an Oncological Cohort of 149 Patients: Impact on Image Quality and Patient Management. *Br J Radiol* (2021) 94(1126):94. doi: 10.1259/bjr.20201350
23. Rietzel E, Pan T, Chen GT. Four-Dimensional Computed Tomography: Image Formation and Clinical Protocol. *Med Phys* (2005) 32(4):874–89. doi: 10.1118/1.1869852
24. Pan T, Lee TY, Rietzel E, Chen GT. 4d-CT Imaging of a Volume Influenced by Respiratory Motion on Multi-Slice CT. *Med Phys* (2004) 31(2):333–40. doi: 10.1118/1.1639993
25. Bouyeure-Petit AC, Chastan M, Edet-Sanson A, Becker S, Thureau S, Houivet E, et al. Clinical Respiratory Motion Correction Software (Reconstruct, Register and Averaged-RRA), for (18)F-FDG-PET-CT: Phantom Validation, Practical Implications and Patient Evaluation. *Br J Radiol* (2017) 90(1070):20160549. doi: 10.1259/bjr.20160549
26. Nagel CC, Bosmans G, Dekker AL, Ollers MC, De Ruysscher DK, Lambin P, et al. Phased Attenuation Correction in Respiration Correlated Computed Tomography/Positron Emitted Tomography. *Med Phys* (2006) 33(6):1840–7. doi: 10.1118/1.2198170
27. Suzawa N, Ichikawa Y, Ishida M, Tomita Y, Nakayama R, Sakuma H. Respiratory-Gated Time-of-Flight PET/CT During Whole-Body Scan for Lung Lesions: Feasibility in a Routine Clinical Setting and Quantitative Analysis. *Ann Nucl Med* (2016) 30(10):722–30. doi: 10.1007/s12149-016-1118-3
28. Suenaga Y, Kitajima K, Aoki H, Okunaga T, Kono A, Matsumoto I, et al. Respiratory-Gated ^{18}F-FDG PET/CT for the Diagnosis of Liver Metastasis. *Eur J Radiol* (2013) 82(10):1696–701. doi: 10.1016/j.ejrad.2013.05.019
29. Von Schulthess GK, Steinert HC, Hany TF. Integrated PET/CT: Current Applications and Future Directions. *Radiology* (2006) 238(2):405–22. doi: 10.1148/radiol.2382041977
30. Sindoni A, Minutoli F, Pontoriero A, Iatì G, Baldari S, Pergolizzi S. Usefulness of Four Dimensional (4D) PET/CT Imaging in the Evaluation of Thoracic Lesions and in Radiotherapy Planning: Review of the Literature. *Lung Cancer* (2016) 96:78–86. doi: 10.1016/j.lungcan.2016.03.019
31. Werner MK, Parker JA, Kolodny GM, English JR, Palmer MR. Respiratory Gating Enhances Imaging of Pulmonary Nodules and Measurement of Tracer Uptake in FDG PET/CT. *AJR Am J Roentgenol* (2009) 193(6):1640–5. doi: 10.2214/AJR.09.2516
32. Nehmeh SA, Erdi YE, Ling CC, Rosenzweig KE, Schoder H, Larson SM, et al. Effect of Respiratory Gating on Quantifying PET Images of Lung Cancer. *J Nucl Med* (2002) 43(7):876–81.
33. Grootjans W, de Geus-Oei LF, Meeuwis AP, van der Vos CS, Gotthardt M, Oyen WJ, et al. Amplitude-Based Optimal Respiratory Gating in Positron Emission Tomography in Patients With Primary Lung Cancer. *Eur Radiol* (2014) 24(12):3242–50. doi: 10.1007/s00330-014-3362-z
34. Suenaga Y, Kitajima K, Aoki H, Okunaga T, Kono A, Matsumoto I, et al. Respiratory-Gated (1)(8)F-FDG PET/CT for the Diagnosis of Liver Metastasis. *Eur J Radiol* (2013) 82(10):1696–701. doi: 10.1016/j.ejrad.2013.05.019
35. Fin L, Daouk J, Bailly P, Slama J, Morvan J, El Esper I, et al. Improved Imaging of Intrahepatic Colorectal Metastases With 18F-Fluorodeoxyglucose Respiratory-

Gated Positron Emission Tomography. *Nucl Med Commun* (2012) 33(6):656–62. doi: 10.1097/MNM.0b013e328351fce8
36. Korreman SS, Juhler-Nottrup T, Boyer AL. Respiratory Gated Beam Delivery Cannot Facilitate Margin Reduction, Unless Combined With Respiratory Correlated Image Guidance. *Radiother Oncol* (2008) 86(1):61–8. doi: 10.1016/j.radonc.2007.10.038
37. Bundschuh RA, Andratschke N, Dinges J, Duma MN, Astner ST, Brügel M, et al. Respiratory Gated [18F]FDG PET/CT for Target Volume Delineation in Stereotactic Radiation Treatment of Liver Metastases. *Strahlenther Onkol* (2012) 188(7):592–8. doi: 10.1007/s00066-012-0094-3
38. Chang Z, Liu T, Cai J, Chen Q, Wang Z, Yin FF. Evaluation of Integrated Respiratory Gating Systems on a Novalis Tx System. *J Appl Clin Med Phys* (2011) 12(3):3495. doi: 10.1120/jacmp.v12i3.3495
39. Kasuya T, Tateishi U, Suzuki K, Daisaki H, Nishiyama Y, Hata M, et al. Role of Respiratory-Gated PET/CT for Pancreatic Tumors: A Preliminary Result. *Eur J Radiol* (2013) 82(1):69–74. doi: 10.1016/j.ejrad.2012.05.037
40. Burger IA, Huser DM, Burger C, von Schulthess GK, Buck A. Repeatability of FDG Quantification in Tumor Imaging: Averaged SUVs Are Superior to SUVmax. *Nucl Med Biol* (2012) 39(5):666–70. doi: 10.1016/j.nucmedbio.2011.11.002
41. Lodge MA, Chaudhry MA, Wahl RL. Noise Considerations for PET Quantification Using Maximum and Peak Standardized Uptake Value. *J Nucl Med* (2012) 53(7):1041–7. doi: 10.2967/jnumed.111.101733
42. Guerra L, De Ponti E, Elisei F, Bettinardi V, Landoni C, Picchio M, et al. Respiratory Gated PET/CT in a European Multicentre Retrospective Study: Added Diagnostic Value in Detection and Characterization of Lung Lesions. *Eur J Nucl Med Mol Imaging* (2012) 39(9):1381–90. doi: 10.1007/s00259-012-2148-2
43. Alkhawaldeh K, Bural G, Kumar R, Alavi A. Impact of Dual-Time-Point (18) F-FDG PET Imaging and Partial Volume Correction in the Assessment of Solitary Pulmonary Nodules. *Eur J Nucl Med Mol Imaging* (2008) 35(2):246–52. doi: 10.1007/s00259-007-0584-1
44. Hwang JP, Lim I, Byun BH, Kim BI, Choi CW, Lim SM. Prognostic Value of SUVmax Measured by Pretreatment 18F-FDG PET/CT in Patients With Primary Gastric Lymphoma. *Nucl Med Commun* (2016) 37(12):1267–72. doi: 10.1097/MNM.0000000000000579
45. Khan MA, Combs CS, Brunt EM, Lowe VJ, Wolverson MK, Solomon H, et al. Positron Emission Tomography Scanning in the Evaluation of Hepatocellular Carcinoma. *J Hepatol* (2000) 32(5):792–7. doi: 10.1016/S0168-8278(00)80248-2
46. Lee JD, Yun M, Lee JM, Choi Y, Choi YH, Kim JS, et al. Analysis of Gene Expression Profiles of Hepatocellular Carcinomas With Regard to 18F-Fluorodeoxyglucose Uptake Pattern on Positron Emission Tomography. *Eur J Nucl Med Mol Imaging* (2004) 31(12):1621–30. doi: 10.1007/s00259-004-1602-1
47. Panta RK, Segars P, Yin FF, Cai J. Establishing a Framework to Implement 4D XCAT Phantom for 4D Radiotherapy Research. *J Cancer Res Ther* (2012) 8(4):565–70. doi: 10.4103/0973-1482.106539
48. Segars WP, Tsui BMW, Cai J, Yin F-F, Fung GSK, Samei E. Application of the 4-D XCAT Phantoms in Biomedical Imaging and Beyond. *IEEE Trans Med Imagin* (2018) 37(3):680–92. doi: 10.1109/TMI.2017.2738448

Conflict of Interest: The authors declare that the research was conducted in the absence of any commercial or financial relationships that could be construed as a potential conflict of interest.

Publisher's Note: All claims expressed in this article are solely those of the authors and do not necessarily represent those of their affiliated organizations, or those of the publisher, the editors and the reviewers. Any product that may be evaluated in this article, or claim that may be made by its manufacturer, is not guaranteed or endorsed by the publisher.

frontiers in Oncology

ORIGINAL RESEARCH
published: 10 February 2022
doi: 10.3389/fonc.2022.827171

Targeted Phototherapy by Niobium Carbide for Mammalian Tumor Models Similar to Humans

*Zhao Liu[1], Shan Jiang[1], Yuhang Tian[1], Haitao Shang[1], Kexin Chen[2], Haoyan Tan[1], Lei Zhang[1], Hui Jing[1] and Wen Cheng[1]**

[1] Department of Ultrasound, Harbin Medical University Cancer Hospital, Harbin, China, [2] Department of Pathology, Harbin Medical University Cancer Hospital, Harbin, China

OPEN ACCESS

Edited by:
An Liu,
City of Hope National Medical Center, United States

Reviewed by:
Kun Qing,
City of Hope National Medical Center, United States
Chengyu Shi,
New York Proton Center, United States

***Correspondence:**
Wen Cheng
hrbchengwen@163.com

Specialty section:
This article was submitted to Radiation Oncology, a section of the journal Frontiers in Oncology

Received: *01 December 2021*
Accepted: *17 January 2022*
Published: *10 February 2022*

Citation:
Liu Z, Jiang S, Tian Y, Shang H, Chen K, Tan H, Zhang L, Jing H and Cheng W (2022) Targeted Phototherapy by Niobium Carbide for Mammalian Tumor Models Similar to Humans. Front. Oncol. 12:827171. doi: 10.3389/fonc.2022.827171

Background: In the past few decades, nanomaterial-mediated phototherapy has gained significant attention as an alternative antitumor strategy. However, its antitumor success is majorly limited to the treatment of subcutaneous tumors in nude mice. In fact, no studies have been previously conducted in this area/field on clinically-relevant big animal models. Therefore, there is an urgent need to conduct further investigation in a typical big animal model, which is more closely related to the human body.

Results: In this study, niobium carbide (NbC) was selected as a photoactive substance owing to the presence of outstanding near-infrared (NIR) absorption properties, which are responsible for the generation of NIR-triggered hyperthermia and reactive oxygen species that contribute towards synergetic photothermal and photodynamic effect. Moreover, the present study utilized macrophages as bio-carrier for the targeted delivery of NbC, wherein phagocytosis by macrophages retained the photothermal/photodynamic effect of NbC. Consequently, macrophage-loaded NbC ensured/allowed complete removal of solid tumors both in nude mice and big animal models involving rabbits. Meanwhile, two-dimensional ultrasound, shave wave elastography (SWE), and contrast-enhanced ultrasound (CEUS) were used to monitor physiological evolution in tumor *in vivo* post-treatment, which clearly revealed the occurrence of the photoablation process in tumor and provided a new strategy for the surveillance of tumor in big animal models.

Conclusion: Altogether, the use of a large animal model in this study presented higher clinical significance as compared to previous studies.

Keywords: theranostic agent, photothermal/photodynamic co-therapy, macrophage loaded NbC, orthotopic tumor model, CEUS/SWE

INTRODUCTION

Cancer is regarded as a major threat to public health worldwide. The severity of the cancer is highlighted by the absence of any global solution (1). Cancer diseases, such as liver cancer and breast cancer, are the leading causes of death or disability worldwide (2, 3). In clinical practice, the poor therapeutic efficacy of traditional antitumor therapies, like surgery, chemotherapy, or/and radiotherapy, is primarily related to associated side effects and inevitable secondary actions (4, 5). Currently, cancer research is focused on the development of a more efficient way/strategy to improve the accuracy and controllability of oncotherapy. To achieve better treatment outcomes in the patients, there is a need to develop novel therapeutic techniques to surmount the aforementioned issues (6). In recent years, phototherapy, including both photothermal therapy (PTT) and photodynamic therapy (PDT), has emerged as a promising alternative to traditional antitumor therapies, primarily owing to high Spatio-temporal selectivity, low complications, minimal damage, and deeper penetration of near-infrared (NIR) light (7–10). Phototherapy usually acts *via* light-triggered photoactive materials, resulting in the generation of local hyperthermia (PTT) or reactive oxygen species (ROS) or PDT to induce cancer cell death (11, 12). Thus, according to this modality, phototherapy could assist in achieving high spatiotemporal accuracy. Although several studies have illustrated the advantages and superiority of PTT or PDT, these two methods are still in the developing stage as the antitumor effect of these methods is restricted to the mice model (13). In a real scenario, the mice model with subcutaneous tumor is quite different from the clinical tumor, in terms of tumor size, depth, and physiological characteristics. Initially, NIR-mediated phototherapy was developed as a strategy to treat the deep-site tumor, which relied on the excellent penetration depth of NIR. However, a limited volume of mice and shallow subcutaneous tumors could not examine the true advantages of phototherapy. In fact, the subcutaneous tumor model in mice involves only a thin layer of skin, which is almost equivalent to no barrier for the arrival of NIR. Hence, the currently used mice models fail to evaluate the true efficiency/potential of phototherapy. Before clinical trials, it is important to conduct *in vivo* investigation/assessment in a big animal model, but such studies are seldom done.

Rabbits are one of the most frequently used species in big animal model studies. In fact, the subcutaneous fat layer of rabbits is quite suitable for simulating deep-site tumors. It has been previously reported that the VX2 carcinoma model in rabbits exhibited great similarities to the human tumor. In fact, VX2 carcinoma could be implanted in several tissues of rabbits and showed significant similarities to the human orthotopic tumor in several aspects, such as vascularization and histological and biological characteristics (14). Furthermore, the thick skin of rabbits and subcutaneous lipid layers are expected to simulate the treatment of deep tumors in humans, to an extreme degree. When compared with the mice model, rabbits are more suitable for the establishment of orthotopic xenograft tumors. In fact, the tumor is expected to be larger in such a case. Altogether, orthotopic tumors in rabbits appear to be more similar to the clinical human tumor (15). However, the fast development of tumors and the high rate of tumor recurrence in rabbits hinder the assessment of phototherapy in a big animal model. Consequently, no reports are currently available on big animal studies in phototherapy. To achieve success in a big animal model, there is a need to enhance antitumor outcomes. In this regard, synergetic PTT and PDT treatment could exert a dual effect on the tumor, enhancing the overall effect of phototherapy. It has been previously reported that PDT action is generally strong in the early stage and becomes weaker with oxygen depletion. In comparison to this, PTT is known to be weaker in early stage and increases with temperature elevation. Consequently, synergetic action of PTT/PDT treatment appears to be promising for effective tumor removal, especially in the case of single-matter-mediated treatment. When compared with PTT/PDT system involving multiple components, it could avoid mutual interference and absorption mismatch between photothermal agent and photosensitizer. Thus, the use of a photoactive material that behaves both as a photothermal agent and photosensitizer should be explored and used for big animal studies.

This study presented the use of a novel photoactive material of NbC, which is a NIR-harvesting material that exhibits both PTT and PDT effects. The study involved the use of cell cargo of macrophages for the loading of NbC nanoparticles. The use of macrophages could target tumors by recognizing cytokines produced/released by cancer cells. Consequently, NbC loaded macrophages (NbC@M) provided/ensured targeted delivery to the tumor site, which was mediated *via* endocytosis by macrophages. In this study, in order to verify the phototherapeutic effect of the NbC@M, we designed the experimental plan using mice with subcutaneous tumors and rabbits with breast cancer of VX2 carcinoma, as shown in **Scheme 1**. The study further used shave wave elastography (SWE) and contrast-enhanced ultrasound (CEUS) for orthotopic rabbit tumor detection, monitoring, and diagnosis, and thus provided a more convincing evaluation for the treatment outcome of PTT/PDT, which has seldom been investigated in past. Such an evaluation of PTT/PDT outcome holds great clinical significance (16, 17). We expect that NbC@M mediated treatment of the tumor in rabbits could be exploited for clinical application in humans in the future.

MATERIALS AND METHODS

Characterization of NbC Nanoparticles

Materials

NbC nanoparticles were obtained from Chaowei Company of Shanghai. The RAW264.7 macrophages, rabbit peripheral blood macrophages and HepG2 cells lines were obtained from the Institute of Cancer Research affiliated to Harbin Medical University. The dulbecco's modified eagle medium (DMEM, Corning), penicillin/streptomycin (Corning), phosphate buffer saline (PBS), fetal bovine serum (FBS, Gibco) and Trypsin-EDTA solution were purchased from Harbin Shengze Biotechnology Co. Ltd. Calcein-AM, propidium iodide (PI),

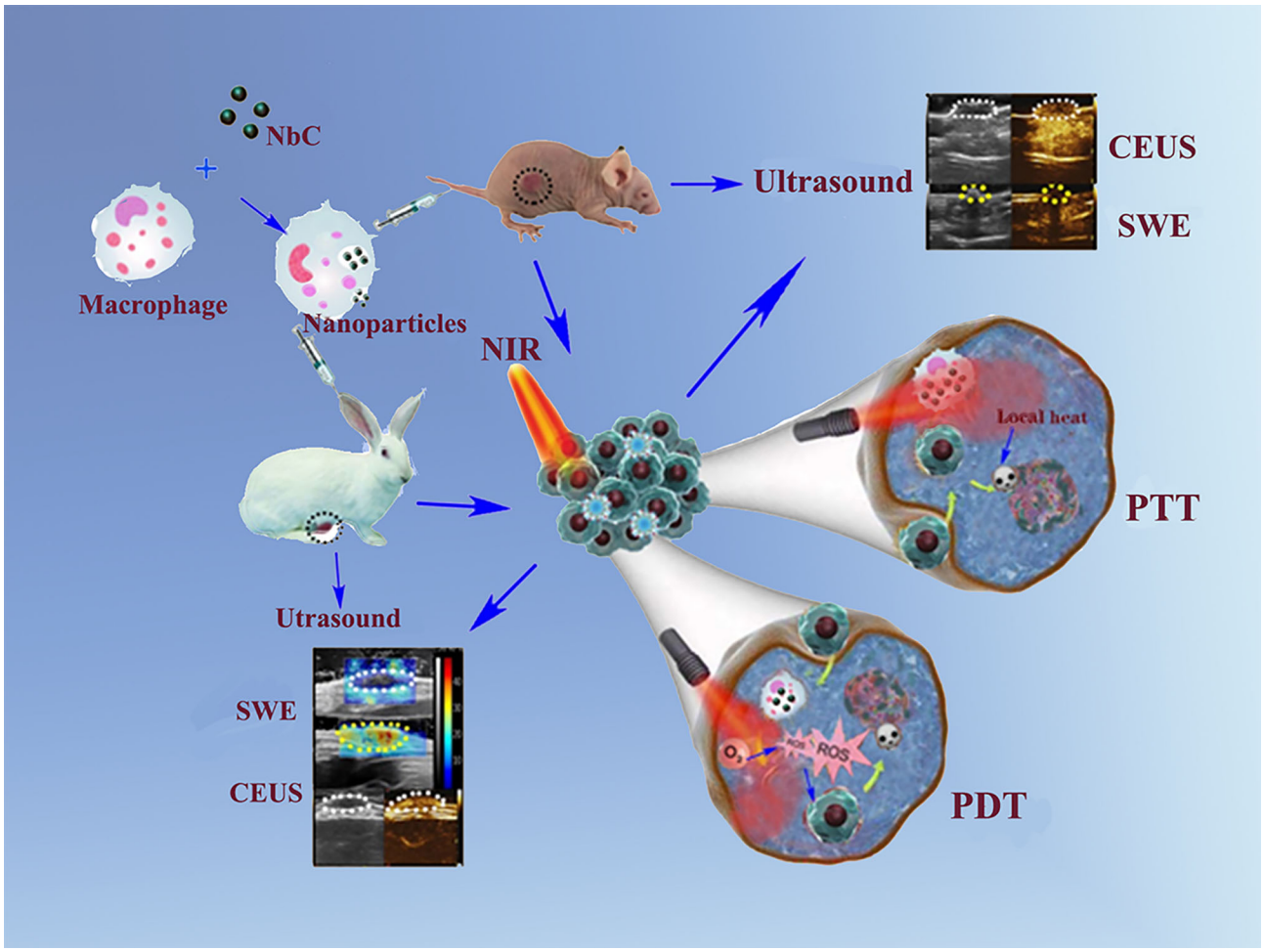

SCHEME 1 | Schematic illustration of NbC@M nanoparticles for targeted phototherapy of nude mice and rabbit VX2 tumor models.

and 2-(2-methoxy-4-nitrophenyl)-3-(4-nitrophenyl)-5-(2, 4-disulfophenyl)-2H-tetrazolium and monosodium salt (Cell Counting Kit-8, CCK-8) were purchased from Beyotime Biotechnology Co. Ltd. 1, 3- diphenylisobenzofuran (DPBF) and 2', 7'- dichlorodihydrofluorescein diacetate (DCFH-DA) were obtained from Sigma-Aldrich.

Characterization

The morphologies of NbC were observed by TEM (JEOL JEM-2100, Japan). The size distribution analysis was conducted on Zetasizer Nano S90 (Malvern Panalytical, UK). The crystal phase was tested by XRD (Shimadzu XD-D1). The composition and chemical valence of NbC were measured by XPS spectra (PerkinElmer PHI 5600). UV-vis-NIR absorptive spectra of samples were performed on a spectrophotometer (U-4100, Hitachi, Japan). The concentration of Nb element within cells was analyzed by inductively coupled plasma (ICP) atomic emission spectrometer (8300, PerkinElmer, USA). Two-dimensional ultrasound (2D US), Color Doppler Flow Imaging (CDFI) and contrast-enhanced ultrasound (CEUS) scans were performed using MyLab twice system (Esaote SpA, Florence, Italy) with LA523 probe. All the data of shave wave elastography (SWE) were recorded by a real-time US device (Aixplorer; SuperSonic Imagine, Aix-en-Provence, France) with 4-15 MHz liner transducer.

Photothermal Test

0.5 mL NbC aqueous dispersion of various concentrations was irradiated with 808 nm NIR laser (1.0 W/cm^2) for 10 minutes. The changes of solution temperature were collected by a NIR camera (E6, FL-IR Systems, Inc, USA). The photothermal conversion efficiency was calculated according to the photoheating curve of the equivalent NbC.

Characterization of NbC Loaded Macrophages

Cell Lines and Cell Culture

The RAW264.7 macrophages, rabbit peripheral blood macrophages and HepG2 cells lines were cultured in DMEM supplemented with

10% FBS and 1% penicillin/streptomycin in a humidified atmosphere of 5% CO_2 at 37°C. Hemocytometer (Bürker-Türk, Wertheim, Germany) was used for the total cell counting.

Preparation of the Macrophage-Loaded NbC Nanoparticles

The RAW264.7 macrophages and rabbit peripheral blood macrophages were incubated with DMEM until the cell coverage reached about 80% ~ 90%. Then, the stale DMEM was removed and the fresh DMEM supplemented with various concentrations of NbC (0.125, 0.25, 0.5, 1 and 2 mg/mL) and incubated for varied time (2, 4, 6, 12 and 24 h). After incubation, the supernatant was removed and macrophage-loaded NbC nanoparticles were washed with PBS twice. The macrophages were observed with inverted biological microscope (Olympus CKX41). ICP analysis was used to quantify the uptake amount of Nb content in the macrophage cells.

Detection of ROS

DPBF solution with NbC or NbC@M was respectively placed in a quartz tube, and then irradiated with 808 nm NIR laser (1 W/cm^2) for 10, 20, 40 and 60 min. Then, absorbance at 420 nm was determined by U-4100 spectrophotometer. In order to detect intracellular reactive oxygen species (ROS), HepG2 cells were divided into five groups, including untreated control (group 1), cells incubated with NbC@M (0.2 mg/mL) for 4 h (group 2), 808 nm NIR laser (1 W/cm^2) irradiated cells (group 3), positive control with H_2O_2 (200 μL, 50 × 10^{-3} M) at 37 °C for 1 h (group 4), NbC@M mediated phototherapy (group 5). After the treatments, the cells treated in different ways were stained with DCFH-DA (50 μL, 50 × 10^{-3} M) for 1 h and then imaged on inverted biological microscope.

Cytotoxicity Assay

The standard CCK-8 assay was used to evaluate the viability of cells. HepG2 cells (8×10^3 cells/well) were seeded into 96-well plates and cultured for 12 h. NbC@M solutions of different concentrations were then added into above wells and incubated for another 12 or 24 h, respectively. After washed by PBS solution for three times, 10 μL CCK-8 was added to the samples and incubated for another 1 h. The absorbance at 450 nm was then recorded on a microplate reader (BioTek, Winooski, VT, USA). The CCK-8 method was also applied for analyzing the therapeutic effect of *in vitro* PDT, PTT, and PDT +PTT experiments. Similarly, HepG2 cells (8×10^3 cells per well) in each group were cultured in 96-well plates for 12 h. Then, 100 μL NbC@M (500 μg/mL) were added into each well and incubated for another 12 h, respectively. All groups were subjected to 808 nm NIR irradiation except control group. Additional operations are needed to handle PDT and PTT group. The process of PDT should be set in an ice bath, while sodium azide (50 μL, 1×10^{-5} M) was added into the medium of PTT group before NIR irradiation.

Phototherapeutic Effects of NbC@M *In Vitro*

To evaluate the phototherapeutic effects at the cellular level, HepG2 cells (3×10^5 cell/dish) were cultured with DMEM medium containing NbC or NbC@M (2 mL, 250 μg/mL) in 35 mm culture dishes for 6 h. Redundant NbC or NbC@M was removed by washing with PBS and then 500 μL fresh DMEM medium was added into each dish. Then, above resultant cells were irradiated with 808 nm NIR laser (1 W/cm^2) for 2, 5, and 10 min. Several groups were designed as controls, including untreated cells, cells only irradiated by 808 nm NIR laser (1 W/cm^2), and incubated with NbC or NbC@M. Finally, dead and live cells were labeled by Calcein-AM (1 μg/mL, 200 μL) and PI (20 μg/mL, 200 μL) for 20 min, and then washed with PBS. The fluorescence visualization images were imaged on Olympus BX53 microscope.

Phototherapeutic Effect of NbC@M in Nude Mice and Rabbits Tumor Model

In Vivo Phototherapy on Mice

All experimental female Balb/c nude mice were purchased from Beijing Vital River Laboratory Animal Technology Co., Ltd. HepG2 cells were digested and dispersed in DMEM to form a uniform suspension, which were then injected into the subcutaneous tissue of the upper left hind leg of nude mice to establish tumor-bearing mice model (tumor size is about 150 mm^3). Then, tumor-bearing mice were randomly divided into four groups (n = 5 for each group): group 1 (100 μL PBS was injected intravenously as control), group 2 (808 nm NIR irradiation for 10 min, 1 W/cm^2), group 3 (NbC@M was injected intravenously) and group 4 (intravenous injection of NbC@M plus 808 nm NIR irradiation for 10 min). NbC@M (100 μL) was injected intravenously into nude mice at a concentration of 1 mg/mL in the group 3 and 4, respectively. In the group 2 and 4, 808 nm NIR irradiation (1 W/cm^2) was required to irradiate the tumor area for 10 min. Notably, the mice in the group 4 should be irradiated at 12 hours post injection of NbC@M. The change of temperature was monitored and recorded every 30 s by an FL-IR System E6 infrared camera. The data of tumor size and body weight of nude mice were recorded in detail for 14 days. The tumor volume was calculated as V = length × width^2/2. Relative body weight was designed as dividing instant weight by initial weight (W/W_0), and similarly relative tumor volume was defined as V/V_0. All the animal experiments were approved by the criteria of the National Regulation of China for Care and the Ethics Research Committee of Harbin Medical University Cancer Hospital.

Rabbit VX2 Breast Xenograft Model

All of the female New Zealand white rabbits (12~14 weeks old, 2.5 ~ 3.0 kg) were purchased from animal laboratory of the Second Affiliated Hospital of Harbin Medical University. The VX2 tumors were surgically implanted into the left second nipple areola edge for each rabbit. The VX2 tumor mass was obtained from the hind limb of a donor rabbit and minced approximately into 1 mm^3 fragments, which were dispersed in normal saline to form a suspension. Extract a small amount of suspension and ensure that at least two VX2 tumor fragments were injected into the designated location. Ten days after tumor implantation, the tumors should be observed until the tumors' volume reached up to about 300 ~ 500 mm^3.

In Vivo Phototherapy on Rabbits

Twelve VX2 tumor-bearing rabbits were divided into four groups randomly (n = 3 for each group), including injection of PBS (1 mL) as control, receiving only NIR irradiation, receiving only injection of NbC@M (1 mL, 1 mg/mL), and receiving NIR irradiation at 8 h post-injection of NbC@M (1mL, 1 mg/mL). For the real-time thermal imaging, tumor regions were irradiated by an 808 nm laser with a power density of 2 W/cm^2 for 20 min, and then monitored with an infrared imaging device (FL-IR System E6). All injections of PBS or NbC@M are performed through the posterior auricular vein.

Ultrasound on Mice and Rabbits

Ultrasound tests as a general term, including two-dimensional ultrasound (2D US), Color Doppler Flow Imaging (CDFI), SWE and CEUS, were completed by two radiologists with more than five years of experience. After confirming the tumor area and applying enough ultrasonic coupling gel during SWE process, the probe was kept in a stable position with no pressure for about 3 seconds and was vertical to better reduce compression artifacts. A suitable region of interest (ROI) and scale ruler were identical for the elastographic quantitative analysis (SWE_{max} and SWE_{mean}). CEUS examinations were performed with intravenous vein injection of SonoVue (Bracco SpA, Milan, Italy) followed by a saline flush. 100 μL SonoVue was injected into the caudal vein for mice, while 1 mL SonoVue was injected into the posterior auricular vein for rabbits. Video clips of the examinations, including the process of enhancement and washout, were immediately recorded over a time period of 1 min after injection of SonoVue.

Histological and Blood Biochemistry Analysis

To perform histological analysis, all the mice and rabbits were sacrificed at 14th day after treatment. Hematoxylin and eosin (H&E) staining of major organs including heart, liver, spleen, lung, kidney was done for histopathologic analysis. Slices were observed by a digital microscope (magnification: ×100; DM3000; Leica, Germany). The blood (20 μL) of mice were collected and tested at 14th day after treatment by automatic blood analyzer (HF-3800).

RESULTS AND DISCUSSION

Characterization of NbC Nanoparticles

In this study, NbC nanoparticles were employed as photoactive material for phototherapy. The morphological features of these nanoparticles were assessed using transmission electron microscopy (TEM). As shown in **Figure 1A**, TEM micrographs revealed that NbC nanoparticles were ~10–30 nm in size. However, the aggregation of particles appeared to be a concern. Dynamic light scattering (DLS) results showed that the average hydrodynamic size of NbC nanoparticle was 255 nm (**Figure 1B**), which was bigger as compared to TEM measurements. This further verified the aggregation of the nanoparticles. The crystal phase and crystallinity of the powdered sample were characterized by X-ray diffraction (XRD). As shown in **Figure 1C**, all the diffractive peaks were consistent with JCPDS No. 65-7964 of NbC species, and no impurities were reported. XPS survey on core-level of NbC's 3d orbit revealed the presence of two spin-orbit coupling doublets, corresponding to Nb^{4+} and Nb^{2+} ions, after fitting (**Figure 1D**). The aforementioned results further verified the purity of NbC nanoparticles.

Following this, the optical absorbance of NbC nanoparticles was examined. The results of the same are shown in **Figures 1E, F**. Spectroscopy measurements showed that powdered NbC exhibited strong and wide photoabsorption in the range of 300–2000 nm. Consequently, powdered NbC covered the biological window of 700–1200 nm that is normally used for phototherapy (**Figure 1E**). Meanwhile, the absorbance of an aqueous solution of NbC presented a similar wide optical absorption band, and the absorbance was positively correlated to the concentration of NbC (**Figure 1F**). Next, the photothermal conversion effect was assessed. As shown in **Figure 1G**, aqueous solution of various concentrations of NbC exhibited a sharp temperature increment under 808 nm of NIR irradiation, with a safe power density of 1 W/cm^2, when measured in contrast to deionized (DI) water control that usually involves a slight temperature elevation only. Thus, the higher the concentration of the sample, the higher was the temperature elevation. To measure photothermal conversion efficiency, the curve of temperature change was assessed for 20 min (**Figure 1H)**, which involved 808 nm (1W/cm^2) irradiation for 10 mins and natural cooling for the next 10 mins. According to the previously reported method (18, 19), the value of photothermal conversion efficiency (η) for NbC was evaluated to be 47.5% (**Figure 1I**), which was much higher as compared to the most commonly used PTT agent. This evidence indicated that NbC exhibited excellent photothermal properties, and thus could be used for PTT treatment of tumors.

Characterization of NbC Loaded Macrophages

In this study, macrophages were used as bio-cargo for targeted delivery of NbC to the tumor site. First, the payload capability of macrophages towards NbC, mediated *via* endocytosis, was assessed. Briefly, NbC nanoparticles were incubated with macrophages to form an NbC@M complex, under different incubation times and NbC concentrations. Following this, uptake of NbC by macrophages was studied as a function of incubation time and concentration of NbC using inductively coupled plasma mass spectrometry (ICP-MS) measurement. The micrographs for macrophages before and after loading of NbC are shown in **Figures 2A, B**. These micrographs clearly demonstrated the endocytosis of NbC by macrophages. The quantitative assessment further confirmed that optimal incubation conditions involved incubation time of 12 h and NbC concentration of 0.1 mg/mL (**Figures 2C, D)**, wherein macrophages exhibited the best performance in terms of endocytosis. Interestingly, when the concentration of NbC was too high, the intracellular content of NbC was significantly

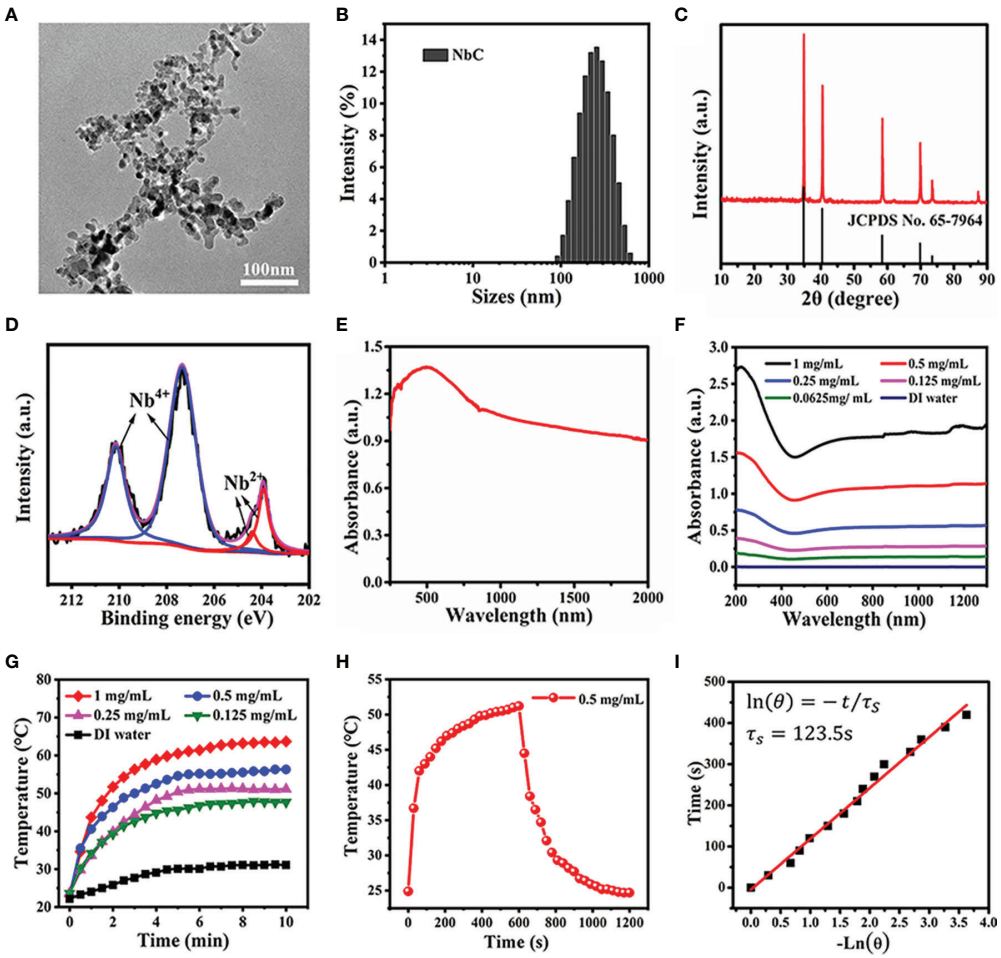

FIGURE 1 | Characterization of the NbC nanoparticles. **(A)** TEM image. **(B)** The hydrodynamic size of NbC measured by the dynamic light scattering (DLS). **(C)** X-ray diffraction pattern of NbC. **(D)** XPS spectra of Nb 3d orbit). **(E)** Powder absorbance of NbC. **(F)** Absorbance of NbC aqueous dispersion. **(G)** Photothermal heating curves of the NbC aqueous dispersion with different concentrations under NIR laser irradiation (808nm, 1W/cm^2). **(H)** Heating and cooling curves of NbC dispersion. **(I)** Plot of time versus the negative natural logarithm of the driving force temperature.

reduced, which might be contributed by surpassing the maximum amount of macrophage endocytosis that ultimately leads to cell death. Altogether, macrophages acted as an ideal drug carrier. The study next assessed whether macrophage loading affects the photothermal behavior of the nanoparticles. As shown in **Figures 2E, F**, no significant differences were recorded in the temperature rising trends for equivalent NbC and macrophage-engulfed NbC (NbC@M), which indicated that endocytosis of the nanoparticles by macrophages did not confer any effect on the photothermal capacity of NbC.

Phototherapeutic Effects of NbC@M *In Vitro*

The present study aimed to use NbC both as a photothermal agent for PTT and a photosensitizer to generate reactive oxygen species (ROS) for the PDT (20). Two methods were used to detect the production of ROS. The first method involved the use of a DPBF probe, which could be decomposed by ROS, resulting in a decrement in its typical absorption peak at 420 nm. Thus, for the evaluation of ROS levels, loss of DPBF absorption could be measured using spectrophotometry. As shown in **Figure 3A**, NbC@M, and NbC could mediate faster and higher DPBF loss as compared to the control group, which indicated significant production of ROS under the effect of 808 nm NIR irradiation. Moreover, the degradation curve of DPBF for NbC@M and NbC were nearly similar/same, which further suggested that macrophage loading conferred no detrimental effect on photosensitive properties of NbC. Following this, another probe, 2',7'-dichlorodihydrofluorescein diacetate (DCFH-DA) was employed for the detection of intracellular ROS levels. Principally, ROS can oxidize non-fluorescent DCFH-DA to produce green fluorescent 2',7'-dichlorofloresceín (DCF), which can be used to determine the levels of ROS in cells in terms of visual fluorescence. When compared with other control

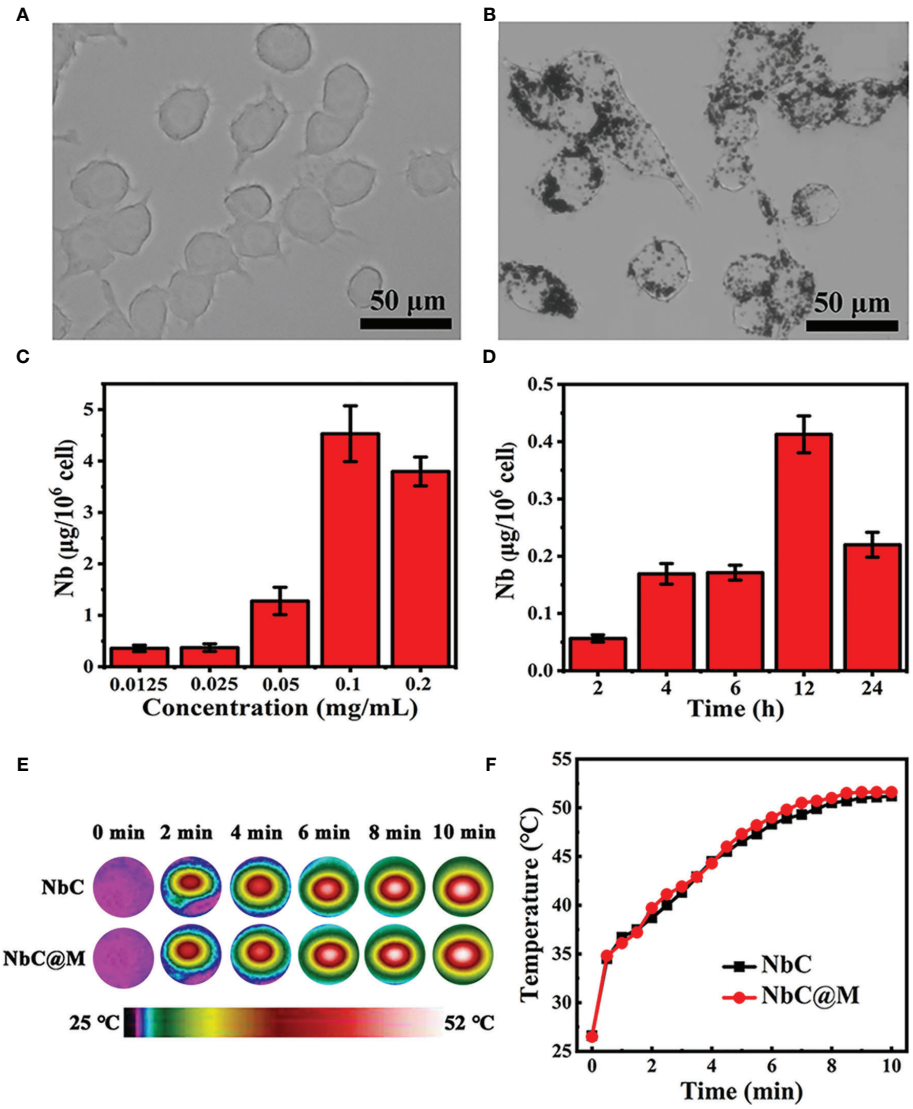

FIGURE 2 | **(A)** Micrograph of macrophages and **(B)** NbC nanoparticles loaded macrophages. The influence of **(C)** concentration and **(D)** incubation time on intracellular NbC content in macrophage by ICP-MS measurement. **(E)** Thermography image and corresponding **(F)** photo-heating curve of the equivalent NbC and macrophage-engulfed NbC (NbC@M).

groups, bright green fluorescence was observed in the NIR-excited NbC@M group, which was found to be similar to the fluorescence observed in the positive control group that comprised of H_2O_2 treated samples. These results indicated the generation of ROS within the cells (**Figures 3B–F**). Therefore, the phagocytosis by macrophages incurred no effect on PTT and PDT generated by NbC@M, under NIR irradiation.

The biocompatibility of NbC@M was examined using CCK-8 assay, wherein low cytotoxicity of NbC@M was recorded in HepG2 cells without irradiation. The cell viability was recorded to be over 85% and 80% after 12 h and 24 h of incubation, respectively, even at the concentration of 2 mg/mL (**Figures 4A, B**). Following this, *in vitro* phototherapy evaluation was performed under NIR irradiation. In the view of the dual-role of NbC that allows simultaneous generation of ROS and hyperthermia, the use of NbC nanoparticles might provide both PDT and PTT effects to the cancer cells. For investigating a single contribution from PDT or PTT, an ice bath or ROS quencher NaN_3 was introduced to eliminate heat or ROS, respectively. Following this, the CCK-8 method was used to analyze the cell viability of HepG2 after different treatments. As shown in **Figure 4C**, the single role of PDT resulted in 22% of cancer cell death, while PTT incurred 64% of cancer cell death. In comparison to this, the combination of PDT/PTT (without the introduction of NaN_3 and ice bath) showed the best cancer cell killing effect, wherein 74% cell death was recorded. At the same time, the killing effect of PTT was found to be much

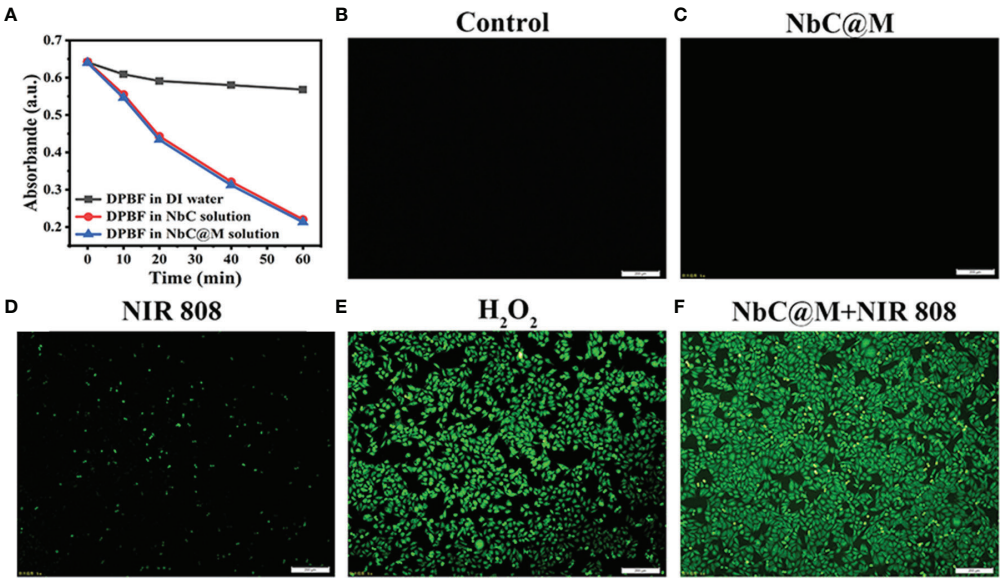

FIGURE 3 | Detection of ROS generation. **(A)** Degradation curve of DPBF. Fluorescence microscopy images of ROS level for **(B)** cells without any treatment as a negative control, **(C)** cells incubated with NbC@M, **(D)** cells received NIR irradiation, **(E)** H_2O_2 treated cells as a positive control, **(F)** cells treated with NbC@M and NIR irradiation (808 nm, 1W/cm^2, 10 min; scale bar = 200μm).

better as compared to PDT. Thus, the aforementioned results verified the synergetic action of PDT and PTT for the ablation of cancer. Besides this, a fluorescence staining method involving Calcein AM and propidium Iodide (PI) was used to visually evaluate the NbC@M-triggered phototherapy effect. In particular, live cells give green fluorescence when stained using Calcein AM, whereas PI staining results in red staining in dead cells. As shown in fluorescence microscopic images (**Figures 4D–F**, **S1A–C**), control group, NbC@M treated cells, NbC treated cells, and 808 nm NIR irradiated cells exhibited green fluorescence only, indicating that neither NIR irradiation nor NbC@M killed HepG2 cells. In comparison to this, macroscopic cancer cell death was confirmed in NbC@M or NbC meditated phototherapy groups, as indicated by the presence of distinct red fluorescence (**Figures 4G–I**, **S1D–F**). Moreover, the number of dead cells positively correlated with the duration of irradiation. In this study, NbC played a major role in the killing of tumor cells, regardless of the loading in macrophages. Altogether, these results suggested that NbC@M acted as an effective NIR-triggered synergetic PTT/PDT agent for cancer treatment.

Phototherapeutic Effect of NbC@M in Nude Mice Tumor Model

The excellent results for phototherapeutic properties of NbC@M *in vitro* encouraged the assessment of NbC@M *in vivo*, wherein HepG2 tumor-bearing nude mice were first used as a typical animal model. Briefly, 20 nude mice were randomly divided into four groups, namely the control group (PBS was only injected intravenously), mice treated with 808 nm NIR irradiation, mice treated with NbC@M injection intravenously, and mice treated with NbC@M + 808 nm NIR irradiation. An infrared thermal camera was used to record temperature changes at the tumor location. As shown in **Figure 5A**, tumor site in group 4 exhibited a rapid increase in temperature from 37.4°C to 61.7°C, while group 2 displayed only a slight increase in temperature from 38.1°C to 40.5°C (**Figure 5B**). The only difference between groups 2 and 4 was the presence or absence of NbC@M, which verified the *in vivo* photothermal ability of NbC@M. Following the application of phototherapy, vernier caliper and electronic autobalance were used to monitor changes in tumor volume and weight of mice for 14 consecutive days. Meanwhile, 2D US, CDFI, CEUS, and SWE images and photographs for mice in all groups were obtained on the 1st, 3rd, 7th, and 14th day, respectively. During this period, no significant differences were recorded in the bodyweight among different groups of mice (**Figure 5C**). Importantly, it was observed that the volume of tumors in groups 1–3 increased during the study, while the tumors in group 4 were found to shrink gradually until they completely disappeared (**Figures 5D, E**, **S2**), leaving only scars on the skin. The scabs without blood supply were observed in group 4 after treatment, while tumors in the other three groups were not destroyed and retained blood vessels, and thus high blood perfusion could be seen by CEUS (white dotted line outline, **Figure 6A**) in these three groups. In contrast to this, scabs in group 4 showed no blood perfusion area (yellow dotted line outline, **Figure 6A**). In addition to blood perfusion, SWE value for the tumor site in all groups changed continuously over time. The SWE values for tumors in group 1, group 2, and group 3 showed a continuous upward trend, both in terms of mean and maximum values. On the contrary, SWE values for scabs in group 4 increased significantly on the 3rd day, but decreased on the 7th and 14th day, as shown in **Figures 6B, C**, **S3**. These results

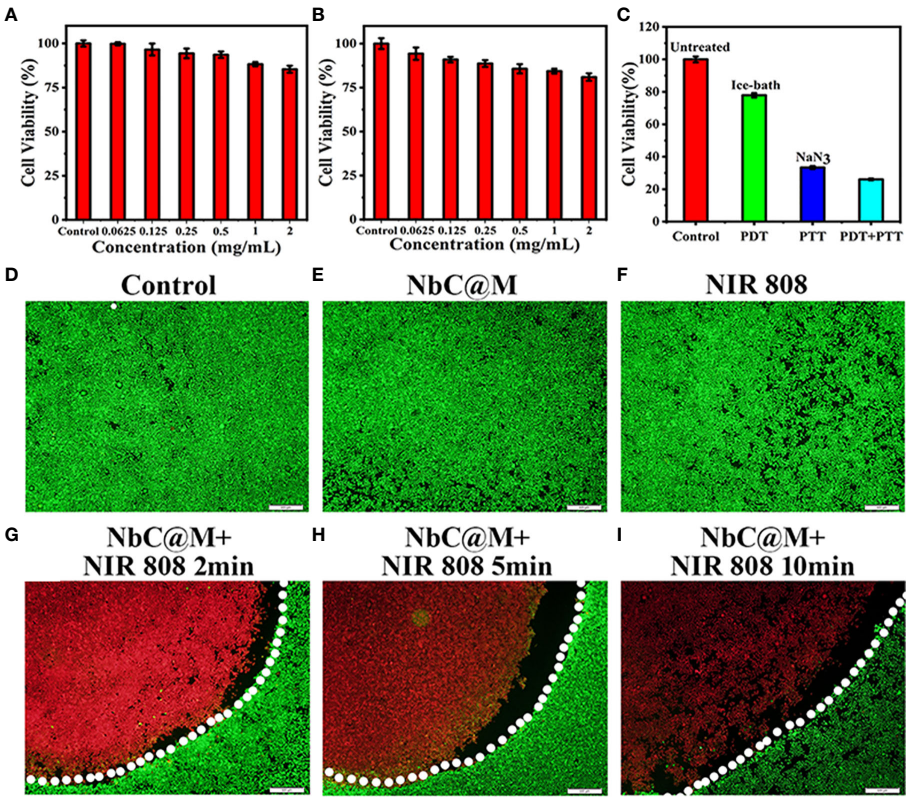

FIGURE 4 | *In vitro* cell cytotoxicity assay and phototherapeutic effect of NbC@M nanoparticles. Relative cell viability of HepG2 cells treated with different concentrations of NbC@M nanoparticles for 12h **(A)** and 24h **(B)**. **(C)** Relative cell viability after different treatments with NbC@M nanoparticles. **(D–I)** Fluorescence images of Live/dead HepG2 cells after receiving different treatments (808 nm, 1W/cm^2, 10 min; scale bar = 500μm).

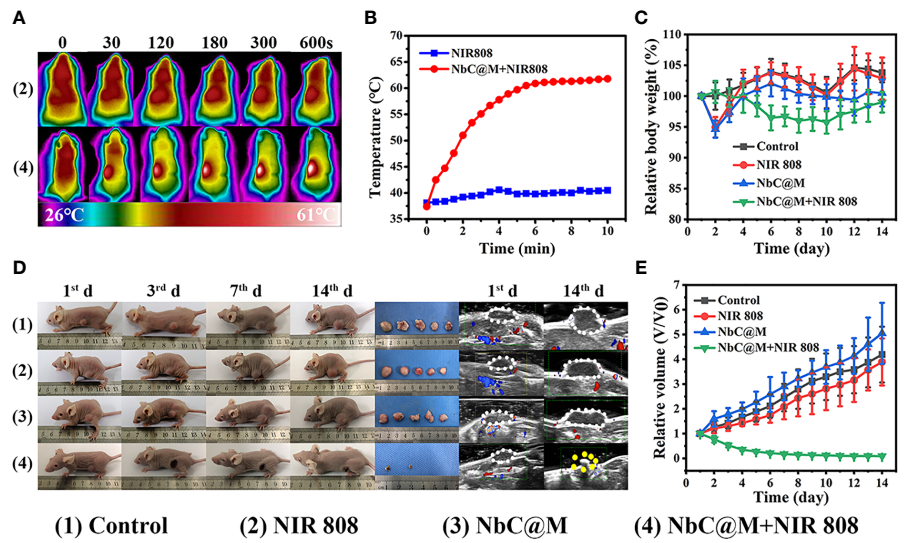

FIGURE 5 | *In vivo* phototherapy study. **(A)** Photothermal images of HepG2 tumor-bearing mice under NIR irradiation (808 nm, 1W/cm^2) and **(B)** corresponding temperature variation at tumor sites under NIR irradiation. **(C)** Quantitative measurements of relative body weight after different treatments during 14 days. **(D)** Representative photographs of mice, tumors and ultrasound image during the treatments. **(E)** Relative tumor volume after different treatments during 14 days.

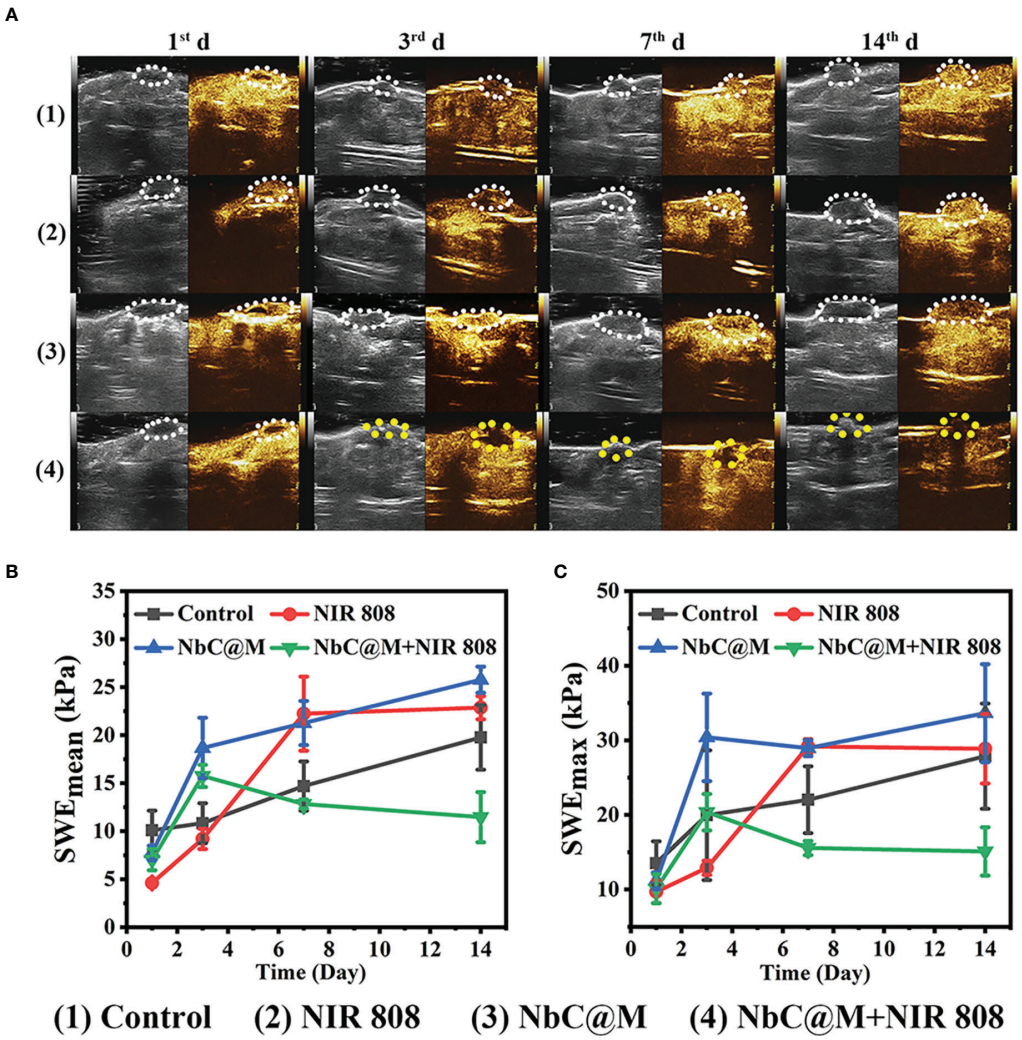

FIGURE 6 | Contrast-enhanced ultrasound (CEUS) and shave wave elastography (SWE) observation on HepG2 tumor-bearing mice after different treatments. **(A)** CEUS detection of tumor internal changes during 14 days post treatment. The changing trend in terms of mean **(B)** and maximum **(C)** values of the SWE at the tumor site during 14 days post treatment.

demonstrated that the tumors in the three control groups progressed continuously, and the use of 808 nm laser irradiation or NbC@M alone could not ablate the tumors. In comparison to this effective antitumor treatment was observed in the case of NbC@M mediated PTT/PDT. The results for CEUS and SWE showed that when compared with the control group, the tumor area got cured and scabbed, and gradually improved. In fact, no blood perfusion and low SWE value were observed in this group. To evaluate *in vivo* toxicity of NbC@M, the main organs (heart, liver, spleen, lung, and kidney) and blood were extracted from mice in groups 1–4 on the 14th day. The results for hematoxylin-eosin (H&E) staining showed no obvious pathological changes. Meanwhile, the hemanalysis indicated no blood abnormalities in groups 1–4 (**Figures S4**, **S5**), which indicated biosafety of NbC@M for phototherapy.

Phototherapeutic Effects of NbC@M in Rabbits Tumor Model

In this study, rabbit VX2 carcinoma, a squamous epithelioid carcinoma with rapid growth, was used to develop breast tumors in rabbits, primarily owing to the presence of a similar tumor microenvironment in rabbits and humans. Similar to the aforementioned nude mice experiment, rabbits were also divided into four groups. The occurrence of thicker skin in rabbits made it difficult to measure tumor volume with vernier calipers, and thus B-mode ultrasonography was used for volume measurements. As shown in **Figure 7A**, the temperature changes for NIR 808 group and NbC@M + NIR 808 group were found to be similar to that of the nude mice experiment. In sharp contrast to the control group, the temperature of the tumor area increased rapidly up to 65°C in NbC@M + NIR 808 group (**Figure 7B**).

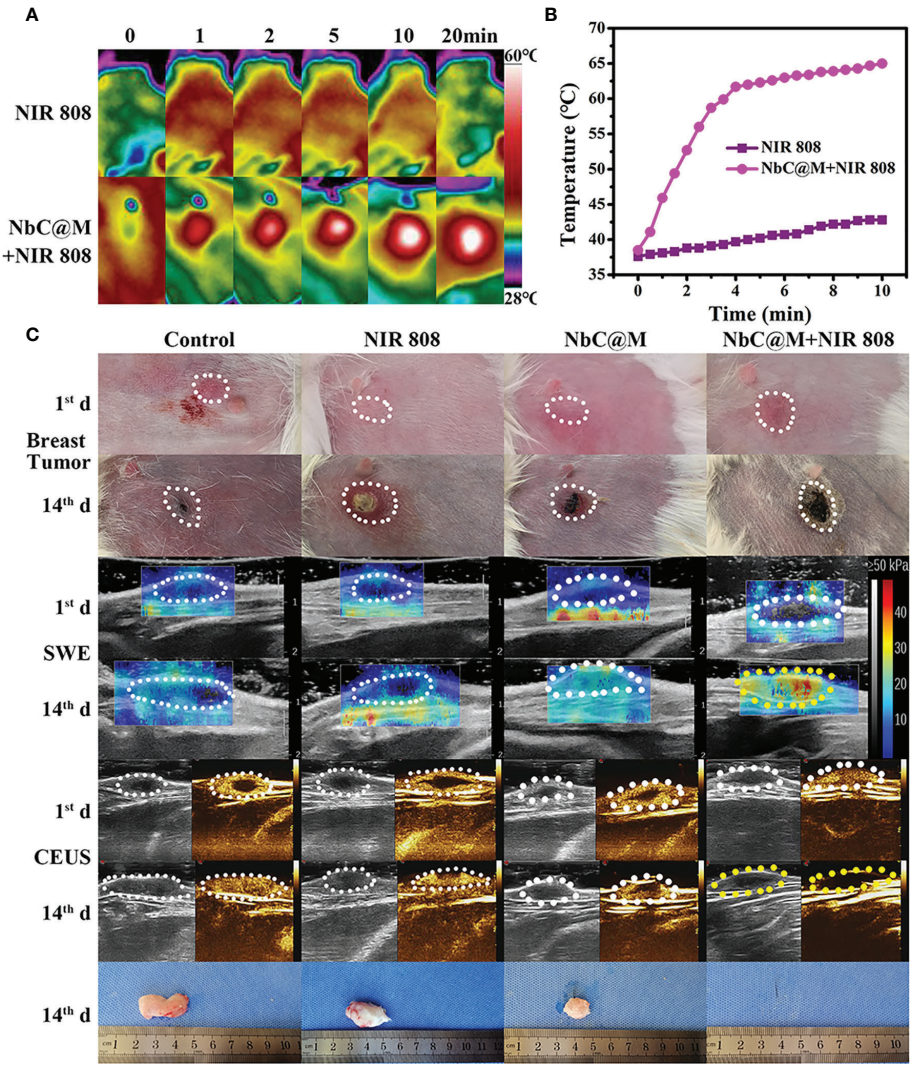

FIGURE 7 | *In vivo* phototherapy study of rabbits. **(A)** Photothermal images and corresponding **(B)** temperature variation at tumor site under NIR irradiation. **(C)** Representative photographs of tumor sites on rabbits and tumors, SWE and CEUS images of tumor site.

And the penetration distance of NIR 880 nm laser is 10mm, which can meet the needs of this study (21, 22). It is well known that insufficient internal blood supply might lead to the appearance of necrotic areas in the tumors, which could break through the skin and drain pus (**Figure 7C**). Hence, it appeared that the size of the tumors did not increase, but in reality, these tumors were rapidly progressing. Over time, SWE values for the tumors in control, NIR 808, and NbC@M groups increased only slightly, while SWE values for the tumors in NbC@M + NIR 808 group increased significantly, primarily due to the presence of scab (**Figure S6**). Moreover, the expanding necrotic areas in control, NIR 808, and NbC@M groups were characterized by abundant blood supply within the tumors and no blood supply in the necrotic areas, as observed by CEUS. The tumor areas in NbC@M + NIR 808 group were not enhanced, which was different when compared with the other three groups. The mutual confirmation of SWE and CEUS results indicated that the tumors were completely cured by the PDT/PTT effects of NbC@M. Furthermore, no significant pathological changes were observed in all groups of rabbits (**Figure S7**), indicating negligible biological toxicity of NbC@M. Thus, the present study demonstrated the successful application of phototherapy in a big animal model, involving the use of rabbits.

CONCLUSION

Altogether, this study presented the application of phototherapy, both in mice models and large animal models of rabbits, in a more clinically relevant manner. In particular, the study demonstrated that NbC photoactive material exhibited excellent NIR-harvesting performance, particularly in terms of

hyperthermia and ROS generation. In fact, significant photothermal and photodynamic capabilities of NbC were retained even after loading within macrophages, which served as a carrier for the targeted enrichment in the tumor. The SWE and CEUS results showed that the effect of the NbC@M-mediated PTT/PDT method successfully cured subcutaneous tumors in mice and orthotopic tumors in rabbits. In addition to this, NbC@M exhibited negligible hematotoxicity and systemic toxicity. Therefore, this study provided evidence for the suitability of NbC@M-mediated PTT/PDT to be explored for clinical treatment.

DATA AVAILABILITY STATEMENT

The original contributions presented in the study are included in the article/**Supplementary Material**. Further inquiries can be directed to the corresponding author.

ETHICS STATEMENT

The animal study was reviewed and approved by the institutional research ethics committee of Harbin Medical University.

AUTHOR CONTRIBUTIONS

ZL worked at concept design, experiment arrangement and manuscript drafting. YT carried out the synthesis and characterization of theranostic agent. SJ, HS, and HT participated in the cell mice and rabbit experiment. KC was responsible for diagnosis and analysis of pathological section. ZL and LZ were in charge of summarizing and analyzing experimental data. HJ and WC joined the study's design and performed review and editing. All authors read and approved the final manuscript.

FUNDING

This work was funded by the National Natural Science Foundation of China (81873900 and 81801709), Key projects of Natural Science Foundation of Heilongjiang Province (ZD2021H005), Science Foundation of Health Commission of Heilongjiang Province (2019052), Innovative scientific research funding project of Harbin Medical University (2020-KYYWF-1471), HAI YAN Science Foundation of Harbin Medical University Cancer Hospital (grant no. JJQN2018-18, JJQN2018-15, JJQN2020-21 and JJQN2021-08).

SUPPLEMENTARY MATERIAL

The Supplementary Material for this article can be found online at: https://www.frontiersin.org/articles/10.3389/fonc.2022.827171/full#supplementary-material

REFERENCES

1. Jemal A, Bray F, Center MM, Ferlay J, Ward E, Forman D. Global Cancer Statistics. *CA: Cancer J Clin* (2011) 61(2):69–90. doi: 10.3322/caac.20107
2. Fitzmaurice C, Allen C, Barber RM, Barregard L, Bhutta ZA, Brenner H, et al. Global, Regional, and National Cancer Incidence, Mortality, Years of Life Lost, Years Lived With Disability, and Disability-Adjusted Life-Years for 32 Cancer Groups, 1990 to 2015: A Systematic Analysis for the Global Burden of Disease Study. *JAMA Oncol* (2017) 3(4):524–48. doi: 10.1001/jamaoncol.2016.5688
3. Christina F, Degu A, Naghmeh A, Hedayat A, Foad AA, Omar AR, et al. Global, Regional, and National Cancer Incidence, Mortality, Years of Life Lost, Years Lived With Disability, and Disability-Adjusted Life-Years for 29 Cancer Groups, 1990 to 2017: A Systematic Analysis for the Global Burden of Disease Study. *JAMA Oncol* (2019) 5(12):1749–68. doi: 10.1001/jamaoncol.2019.2996
4. Marijnen C, Kapiteijn E, Van de Velde C, Martijn H, Steup W, Wiggers T, et al. Acute Side Effects and Complications After Short-Term Preoperative Radiotherapy Combined With Total Mesorectal Excision in Primary Rectal Cancer: Report of a Multicenter Randomized Trial. *J Clin Oncol* (2002) 20 (3):817–25. doi: 10.1200/JCO.2002.20.3.817
5. Dearnaley DP, Khoo VS, Norman AR, Meyer L, Nahum A, Tait D, et al. Comparison of Radiation Side-Effects of Conformal and Conventional Radiotherapy in Prostate Cancer: A Randomised Trial. *Lancet* (1999) 353 (9149):267–72. doi: 10.1016/S0140-6736(98)05180-0
6. Miao ZH, Lv LX, Li K, Liu PY, Li Z, Yang H, et al. Liquid Exfoliation of Colloidal Rhenium Disulfide Nanosheets as a Multifunctional Theranostic Agent for *In Vivo* Photoacoustic/CT Imaging and Photothermal Therapy. *Small* (2018) 14(14):1703789. doi: 10.1002/smll.201703789
7. Liu T, Zhang M, Liu W, Zeng X, Song X, Yang X, et al. Metal Ion/Tannic Acid Assembly as a Versatile Photothermal Platform in Engineering Multimodal Nanotheranostics for Advanced Applications. *ACS Nano* (2018) 12(4):3917–27. doi: 10.1021/acsnano.8b01456
8. Sheng D, Liu T, Deng L, Zhang L, Li X, Xu J, et al. Perfluorooctyl Bromide & Indocyanine Green Co-Loaded Nanoliposomes for Enhanced Multimodal Imaging-Guided Phototherapy. *Biomaterials* (2018) 165:1–13. doi: 10.1016/j.biomaterials.2018.02.041
9. Liu K, Xing R, Zou Q, Ma G, Möhwald H, Yan X. Simple Peptide-Tuned Self-Assembly of Photosensitizers Towards Anticancer Photodynamic Therapy. *Angewandte Chem Int Edition* (2016) 55(9):3036–9. doi: 10.1002/anie.201509810
10. Chen Q, Xu L, Liang C, Wang C, Peng R, Liu Z. Photothermal Therapy With Immune-Adjuvant Nanoparticles Together With Checkpoint Blockade for Effective Cancer Immunotherapy. *Nat Commun* (2016) 7:13193. doi: 10.1038/ncomms13193
11. Lv R, Zhong C, Li R, Yang P, He F, Gai S, et al. Multifunctional Anticancer Platform for Multimodal Imaging and Visible Light Driven Photodynamic/Photothermal Therapy. *Chem Mater* (2015) 27(5):1751–63. doi: 10.1021/cm504566f
12. Fan W, Huang P, Chen X. Overcoming the Achilles' Heel of Photodynamic Therapy. *Chem Soc Rev* (2016) 45(23):6488–519. doi: 10.1039/C6CS00616G
13. Shao Q, Ashkenazi S. Photoacoustic Lifetime Imaging for Direct *in vivo* tissue oxygen monitoring. *J Biomed Opt* (2015) 20(3):036004. doi: 10.1117/1.JBO.20.3.036004
14. Tan L, Wang S, Xu K, Liu T, Liang P, Niu M, et al. Layered MoS2 Hollow Spheres for Highly-Efficient Photothermal Therapy of Rabbit Liver Orthotopic Transplantation Tumors. *Small* (2016) 12(15):2046–55. doi: 10.1002/smll.201600191
15. Zhu M, Lin X-A, Zha X-M, Zhou W-B, Xia T-S, Wang S. Evaluation of the Therapeutic Efficacy of Sequential Therapy Involving Percutaneous Microwave Ablation in Combination With 131I-Hypericin Using the VX2 Rabbit Breast Solid Tumor Model. *PloS One* (2015) 10(3):e0120303. doi: 10.1371/journal.pone.0120303

16. Solbiati L, Ierace T, Tonolini M, Cova L. Guidance and Monitoring of Radiofrequency Liver Tumor Ablation With Contrast-Enhanced Ultrasound. *Eur J Radiol* (2004) 51:S19–23. doi: 10.1016/j.ejrad.2004.03.035
17. Liberman A, Martinez HP, Ta CN, Barback CV, Mattrey RF, Kono Y, et al. Hollow Silica and Silica-Boron Nano/Microparticles for Contrast-Enhanced Ultrasound to Detect Small Tumors. *Biomaterials* (2012) 33(20):5124–9. doi: 10.1016/j.biomaterials.2012.03.066
18. Wang M, Deng K, Lü W, Deng X, Li K, Shi Y, et al. Rational Design of Multifunctional Fe@ γ-Fe2O3@ H-TiO2 Nanocomposites With Enhanced Magnetic and Photoconversion Effects for Wide Applications: From Photocatalysis to Imaging-Guided Photothermal Cancer Therapy. *Adv Mater* (2018) 30(13):1706747. doi: 10.1002/adma.201706747
19. Leng C, Zhang X, Xu F, Yuan Y, Pei H, Sun Z, et al. Engineering Gold Nanorod–Copper Sulfide Heterostructures With Enhanced Photothermal Conversion Efficiency and Photostability. *Small* (2018) 14(12):1703077. doi: 10.1002/smll.201703077
20. Li Z, Zhang H, Han J, Chen Y, Lin H, Yang T. Surface Nanopore Engineering of 2D MXenes for Targeted and Synergistic Multitherapies of Hepatocellular Carcinoma. *Adv Mater* (2018) 30(25):1706981. doi: 10.1002/adma.201706981
21. Yang C, Huang W, Gao Y, Liu Z, Han X. Phototherapy Ablation of Rabbit Orthotopic Tumors by non-Stoichiometric BiPO4-X Nanoparticles. *Chem Eng J* (2019) 386:123961. doi: 10.1016/j.cej.2019.123961
22. Lin H, Gao S, Dai C, Chen Y, Shi J. A Two-Dimensional Biodegradable Niobium Carbide (MXene) for Photothermal Tumor Eradication in NIR-I and NIR-II Biowindows. *J Am Chem Soc* (2017) 139(45):16235–47. doi: 10.1021/jacs.7b07818

Conflict of Interest: The authors declare that the research was conducted in the absence of any commercial or financial relationships that could be construed as a potential conflict of interest.

Publisher's Note: All claims expressed in this article are solely those of the authors and do not necessarily represent those of their affiliated organizations, or those of the publisher, the editors and the reviewers. Any product that may be evaluated in this article, or claim that may be made by its manufacturer, is not guaranteed or endorsed by the publisher.

frontiers in Oncology

SYSTEMATIC REVIEW
published: 15 February 2022
doi: 10.3389/fonc.2022.829708

Comparison of External Beam Radiation Therapy Modalities for Hepatocellular Carcinoma With Macrovascular Invasion: A Meta-Analysis and Systematic Review

Guanheng Wu†, Guomin Huang†, Jianwen Huang, Ligong Lu, Shaojun Peng, Yong Li and Wei Zhao**

Zhuhai Precision Medical Center, Guangdong Provincial Key Laboratory of Tumor Interventional Diagnosis and Treatment, Zhuhai People's Hospital, Zhuhai Hospital Affiliated with Jinan University, Jinan University, Zhuhai, China

OPEN ACCESS

Edited by:
An Liu,
City of Hope National Medical Center, United States

Reviewed by:
Bin-Yan Zhong,
The First Affiliated Hospital of Soochow University, China
Chai Hong Rim,
Korea University, South Korea

***Correspondence:**
Yong Li
lorry5160@163.com
Wei Zhao
zhaoweismu@foxmail.com

†*These authors have contributed equally to this work*

Specialty section:
This article was submitted to Radiation Oncology, a section of the journal Frontiers in Oncology

Received: *06 December 2021*
Accepted: *24 January 2022*
Published: *15 February 2022*

Citation:
Wu G, Huang G, Huang J, Lu L, Peng S, Li Y and Zhao W (2022) Comparison of External Beam Radiation Therapy Modalities for Hepatocellular Carcinoma With Macrovascular Invasion: A Meta-Analysis and Systematic Review. Front. Oncol. 12:829708. doi: 10.3389/fonc.2022.829708

Purpose: We performed a systematic review and meta-analysis to compare external beam radiation therapy modalities for hepatocellular carcinoma (HCC) with macrovascular invasion (MVI).

Methods: Studies were selected from online databases from the date of inception to November 2021. The outcomes of interest were overall survival (OS), objective response rate (ORR), and local control rate (LCR).

Results: Forty-four studies (n = 3730) were selected from 1050 articles. The pooled 1-year OS were 60.9%, 45.3%, and 44.9 for particle radiotherapy (PRT) group, conventional radiotherapy (CRT), and stereotactic body radiotherapy (SBRT) group, respectively; p = 0.005 and 0.002 for PRT vs. CRT and SBRT, respectively. Both the PRT group and the SBRT group have the advantage over the CRT group in the pooled ORR. The PRT group showed significantly higher than the CRT group (p = 0.007) in LCR. For combination therapy, CRT plus transarterial chemoembolization can prolong survival than CRT alone (p = 0.006 for 1-year OS; p = 0.014 for 2-year OS). Among grade ≥ 3 complications, the most frequent type of toxicity in CRT, SBRT, PRT group was hematological toxicity, hepatotoxicity, dermatological toxicity, respectively.

Conclusions: Among patients with HCC with MVI, the 1-year OS and the 2-year OS were both higher in the PRT group than in the CRT, SBRT groups. The ORR was similar between the PRT and SBRT groups. The combination therapy based on radiotherapy is expectable. PRT is associated with less complications than photon radiotherapy.

Keywords: radiation therapy, hepatocellular carcinoma, macrovascular invasion, portal vein tumor thrombosis, conformal radiation therapy, stereotactic body radiotherapy, particle therapy

INTRODUCTION

According to the Global Cancer Statistics 2020, primary liver cancer is the sixth most common malignancy and the third leading cause of cancer-related death worldwide, with around 906,000 new cases and 830,000 deaths reported in 2020. Approximately 80% of these cases were hepatocellular carcinomas (HCCs) (1). As the clinical manifestations are not evident, most cases of HCCs only detected at the advanced stage. Microvascular invasion (MVI) is common in HCC. Portal vein tumor thrombus (PVTT) occurs in 10–40% of patients with HCC (2, 3). The median survival time is significantly lower in patients with PVTT than in those without (4). Worse outcomes are noted when inferior vena cava thrombi are present (5). There are several treatments for HCC, such as transarterial chemoembolization (TACE), hepatic arterial infusion chemotherapy (HAIC), percutaneous ethanol injection (PEIT), and radiofrequency ablation (RFA) (6). However, a tumor thrombus alters the blood supply route to the liver, reduces nutrient supplement, and further reduces the liver function reserve. Therefore, most treatments are no longer effective. Sorafenib is one of the preferred treatments of choice for this condition (6). However, the overall response rate of HCC with MVI to sorafenib is low, and the associated toxicity is severe (7, 8). It is therefore important to consider other effective treatments.

External beam radiation therapy (EBRT) is one of the promising treatments. Previously, the tolerated liver dose was considered to be lower than the tumor killing dose, and therefore, this treatment could not be used for liver cancer (9, 10). However, in recent years, imaging and dose control techniques have made great progress, with reduced toxicity to normal liver tissue. A meta- analysis showed that the 1-year overall survival (OS) and response rate for stereotactic body radiation therapy (SBRT) were 43.8% and 70.7% %, respectively (11). These data objectively reflect the therapeutic advantage of EBRT for HCC with MVI. Recently, several high-quality studies have reported the advantages of EBRT for unresectable HCC, especially for particle radiotherapy (PRT), which shows the preponderance of high response rate, high control and low toxicity (12). However, due to the lack of PRT centers, it is difficult to conduct a head-to-head comparison study with a large sample size for PRT versus other EBRTs for HCC with MVI. Therefore, we conducted this meta-analysis to compare the safety and effectiveness of PRT and photon therapy for HCC with MVI. Meanwhile, it serves to update findings related to EBRT from a previous meta-analysis (11).

METHODS

Search and Selection Criteria

This study followed the Preferred Reporting Items for Systematic Reviews and Meta-analyses (PRISMA) reporting guidelines (13). The protocol we designed defined inclusion criteria, search strategy, outcomes of interest, and analysis plan.

We searched Medline (Ovid), Embase, Clinicaltrials, Web of Science, the Cochrane Central Register of Controlled Trials, and the Cochrane Database of Systematic Reviews, from the date of inception of each database to November 2021. The following keywords or terms were used: "(hepatocellular carcinoma) OR (HCC) OR (hepatoma)" AND "(external beam radiation therapy) OR (stereotactic body radiation therapy) OR (conformal radiotherapy) OR (particle radiotherapy)" AND "(thrombosis)". Additional references were acquired through manual searches of the reference lists. No filters were used, but only papers written in English were included.

The cohorts in the studies had to meet criteria for inclusion as follows: 1) HCC with macrovascular invasion; 2) treatment with EBRT; 3) reported outcomes of interest (i.e., overall survival, response rate, and adverse events). We excluded case reports with fewer than fifteen patients, reviews, letters, and editorial comments. If more than one available study was conducted from the same treatment center in overlapping timeframes, the study with the biggest group and/or highest quality of article was selected. HCC with microvascular invasion was excluded. The conventional radiotherapy (CRT) included three dimensional conformal radiation therapy (3D-CRT), image-guide radiotherapy (IGRT), intensity-modulated radiotherapy (IMRT). SBRT and CRT are difference type of photon therapies. PRT usually means radiotherapy using beams of protons, carbon ions, or other charged particles. Hematological toxicity includes leukopenia, anemia, thrombocytopenia, etc. Hepatotoxicity includes increased ALT, AST, ALP, bilirubin, GGT level, hypoproteinemia, etc. Dermatological toxicity refers to skin reactions. Gastrointestinal toxicity includes nausea, vomit, anorexia, diarrhea, etc. Objective response rate (ORR) was defined as complete response (CR) plus partial response (PR). Local control rate (LCR) means ORR plus stable disease (SD).

Data Extraction

The details were extracted in a standardized pilot-tested form by two reviewers independently. A third investigator reviewed all data entries. The lists we extracted as follows: study design, country, study period, number of patients, patients' characteristics (percentage of male patients, age, diameter of lesion, Child-Pugh Class, previous treatment), interventions (radiation dose, modality for EBRT), length of follow-up, median overall survival, and outcomes of interest.

Statistical Analysis

We prespecified the analysis plan for this protocol. We transformed the rates using the variance stabilizing double arcsine transformation. Then, we pooled the transformation rates with random-effect models and assessed heterogeneity. Heterogeneity among studies was tested using Cochran's Q and the I^2 statistic. I^2 values greater than 50% indicating high heterogeneity. Q-test was use in comparisons among groups (11). We performed a subgroup analysis and pooled the rates of interest outcomes for the different types of EBRT. Egger's test was used to detect publication bias. When textual information in

the included study was insufficient, two reviewers independently collected the information from the graphs using Engauge Digitizer 11.1. P < 0.5 was considered as statistical significance. All statistical analyses were conducted using STATA, version 15.1 (Stata Corporation, College Station, TX, USA).

Assessment of Study Quality

Because most of the studies included in our systematic review and meta-analysis were non-comparative studies, we used the modified Newcastle-Ottawa quality assessment scale. The evaluation of quality was independently conducted by two investigators. Any disagreements were resolved by a third investigator.

RESULTS

Study Selection and Quality Assessment

The selection process is shown in detail in the PRISMA flowchart (**Figure 1**). According to a previous search strategy, 1050 results were initially identified from the online databases. After removing duplicates, 890 records remained. Then, 770 records were excluded after screening the titles and abstracts. Then, 76 reports were removed for various reasons, of which 34 were excluded because of overlapping timeframes in the same center. Finally, 44 studies were included in this meta-analysis (14–57). The quality assessment is shown in the **Supplementary Material**.

Study Characteristics

The characteristics of the cohorts in the included studies were summarized in **Tables 1** and **2**. Overall, 44 studies involving 3730 patients were included. 1 was Randomized Controlled Trial, 5 were prospective studies, and 38 were retrospective studies. There are 2927 patients in 33 cohorts for CRT group; 614 patients in 13 cohorts in SBRT group; 189 patients in 6 cohorts in PRT group. The median age of the patients was 56 years (range, 47-73 years) in the overall studies, 56 for CRT group, 55.9 for SBRT group, 64.85 for PRT group. The median lesion size was 8 cm (range, 2.5–13.8 cm). The median percentage of previous-treatment patients was 75.6% (range 36.8%-100%) in the overall studies, 78.8% for CRT group, 79.2 for SBRT group, 67.8% for PRT group. The median percentage of patients with a class of no less than B was 20.23% (range 0%-41.18%) in the overall studies, 30.5% for CRT group, 13.89% for SBRT group, 37.25% for PRT group. The median dose was 48 Gy in the overall studies, 50 Gy for CRT group, 41 Gy for SBRT group, 72.6 GyE for PRT group. GyE is equal to the RBE multiplication with Gy; RBE of proton beam is 1.1; RBE of carbon ion is 3.

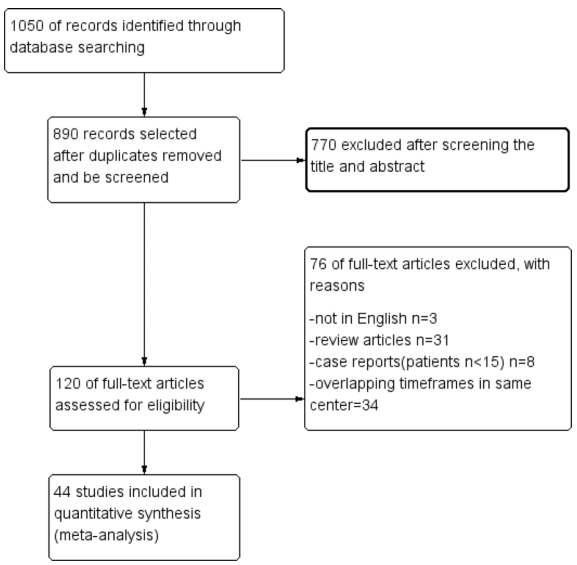

FIGURE 1 | PRISMA flowchart.

Effectiveness Outcomes

A total of 52 cohorts in 44 studies were included in the data synthesis. All valid data were extracted and are displayed in **Table 3**. Pooled data shown in **Table 4** and in Supporting Information. The 1-year pooled OS for CRT, SBRT, PRT were 45.3% (n = 2669, study = 30), 44.9% (n = 592, study = 12), 60.9% (n = 189, study = 6), respectively. The 2-year OS for CRT, SBRT, PRT were 20.4% (n = 2624, study = 29), 19.2% (n = 432, study = 8), 38.5% (n = 155, study = 5), respectively. Except pooled 1-year OS for SBRT group, PRT group; 2-year OS for PRT group with low heterogeneity, other pooled rates with high heterogeneity, respectively. The PRT group showed significantly higher than the CRT group and the SBRT group in OS (PRT vs. CRT: $p = 0.005$ for 1-year OS, $p = 0.001$ for 2-year OS; PRT vs. SBRT: $p = 0.002$ for 1-year OS, $p = 0.004$ for 2-year OS. Compared with previous meta-analysis, the results were stable for the CRT group and SBRT group as the increasing number of patients and studies (11).

The ORR for CRT, SBRT, PRT were 50.4% (n = 1941, study = 26), 72.7% (n = 439, study = 10), 72.1% (n = 137, study = 4), respectively. The LCR for CRT, SBRT, PRT were 86.8% (n = 1915, study = 25), 90.4% (n = 410, study = 9), 95.1% (n = 137, study = 4), respectively. Except pooled LCR for PRT group; other 5 pooled rates with high heterogeneity. The CRT group showed significantly lower than the PRT group ($p = 0.006$) and SBRT group ($p = 0.004$) in ORR. There was no statistical significance between PRT group and SBRT group in ORR ($p = 0.956$). The PRT group showed significantly higher than the CRT group ($p = 0.007$) in LCR.

In recent years, several studies have shown advantage in the combination of RT. We further compared the effects between CRT + TACE, CRT + HAIC, and CRTal groups (CRTal represents CRT alone). CRT + CATE group showed statistically significant advantage in survival prolongation than the CRT alone group ($p = 0.006$ for 1-year OS; $p = 0.014$ for 2-year OS). Pooled ORR and LCR was not statistically significant between three groups. Except pooled 2-year OS for CRT+TACE group; other pooled rates with high heterogeneity.

TABLE 1 | Characteristics of the included studies.

Study	Country	Study design	Period	Type for RT	Patients (n)	Age (median)	Men (%)	Size (median, cm)	Target	CTC ≥B (%)	Dose (median)	Prior treatment (%)
Hou et al.	China	R	2000-2009	CRT	181	51.17	93.9		T 111, TT 70	16.6	50 Gy	90.6
Tan et al.	China	R	2012-2019	CRT	26	<=65 19(73%) >65 7(27%)	85%		TT	22	58 Gy	
Toya et al.	Japan	R	1999-2005	CRT	38	67	84.2	4	T	23.7	40 Gy	78.9
Igaki et al.	Japan	R	1990-2006	CRT	18	70	88.9		T	55.6	50 Gy	83.33
Tanaka et al.	Japan	R	1999-2011	CRT	67	65.5 (mean)	79.1		T	25.4	48.8 Gy (mean)	65.7
Okazaki et al.	Japan	R	2007-2013	CRT	56	69.1	85.7		T	30.5	50Gy	96.4
Iwamoto et al.	Japan	R	2008-2016	CRT	80	68	82.5	7.3	T	42.5	45 Gy	
Yu et al.	Korea	R	1998-2008	CRT	281	54	88.6		TT	16	30-54 Gy	86.1
Rim et al.	Korea	R	2005-2011	CRT	45	50	88.8	5.4	T	37.8	61.2 Gy	93.3
Bae et al.	Korea	R	2007-2015	CRT	47	60	79		T	34	40-45 Gy	74
Huang et al.	Taiwan	R	1997-2005	CRT	326	56.7 (mean)	85.3		T		60 Gy	
Yeh et al.	Taiwan	R	2004-2009	CRT	106	57	80		T	21.7	52 Gy	
Pao et al.	Taiwan	R	2007-2018	CRT	42	63	69		TT	40.5	48.75 Gy	64.3
Onishi et al.	Japan	R	1997-2012	CRT+HAIC	33	63	91	7			50 Gy	
Kodama et al.	Japan	R	–	CRT+HAIC	36	68	89		T	19.4	39 Gy	
Han et al.	Korea	R	2011-2016	CRT+HAIC	152	56	90.1	8.8		15.8	–	36.8
Tang et al.	China	R	2006-2008	CRT+TACE	185	49.7	83.8	9.49		8.6	40 Gy	
Lu et al.	China	R	2008-2011	CRT+TACE	30	58.5	70		T	33.3	40–52.5 Gy	
Yamada et al.	Japan	P	1998-2001	CRT+TACE	19	65.4 (mean)	78.9	5.2 (mean)	T	31.6	60 Gy	
Shirai et al.	Japan	R	2005-2008	CRT+TACE	19	64.8 (mean)	73.7	10.1	TT	31.6	45 Gy	
Yoon et al.	Korea	R	2002-2008	CRT+TACE	412	52	88.1	9.5	T 343, TT 69	35.9	40 Gy	
Yoon et al.	Korea	RCT	2013-2016	CRT+TACE	45	55	84.4	9.8	T		45 Gy	
Yu et al.	Korea	P, P II	2013-2016	CRT+TACE+ hyperthermia	69	56	87	7.2	TT	8.7	47.25 GyE	
Sugahara et al.	Japan	R	1991-2005	PRT	35	63	80	6	TT	20	72.6 GyE	60
Hashimoto et al.	Japan	R	2013-2017	PRT	34	68	79.4			41.2	81.3 GyE	
Komatsu et al.	Japan	R	2001-2016	PRT	31	66.7	83.9	8.3		45.2	52.8-76 GyE	
Sekino et al.	Japan	R	2005-2014	PRT	21	73	80.9	8	TT	42.9	72.6 Gy	57.1
Lee et al.	Korea	R	2008-2011	PRT	27	55	81.5	7	TT	33.3	55 GyE	77.8
Kim et al.	Korea	R	2012-2015	PRT	41	55	85.4	5.8	TT	7.3	HCC 50 Gy, TVT 30 Gy	75.6
Xi et al.	China	R	2010-2012	SBRT	41	54	90.2	2.5	T		36 Gy	–
Shui et al.	China	R	2015-2017	SBRT	70	53.8	84.3		T	35.7	40Gy	
Lou et al.	China	R, multi-center	2008-2016	SBRT	75	53	85		TT	12	38Gy	–

(Continued)

TABLE 1 | Continued

Study	Country	Study design	Period	Type for RT	Patients (n)	Age (median)	Men (%)	Size (median, cm)	Target	CTC ≥B (%)	Dose (median)	Prior treatment (%)
Dutta et al.	India	P, P II	2017-2020	SBRT	72	63	96		TT	14	37.6 Gy	
Kumar et al.	India	R	2018-2020	SBRT	29	56	83	8.6		4	48 Gy	100
Wang et al.	Taiwan	P	2012	SBRT	20	68.55	60		TT	10	50 Gy	
Choi et al.	Korea	R	2010-2016	SBRT	24	56	83.3		T	12.5	45 Gy	79.2
Hou et al.	China	R	2011-2014	CRT	64	54.27	90.6	8.55	TT	21.9	54 Gy	
				CRT	54	54.37	79.6	7.5	TT	14.8	60 Gy	
Zhao et al.	China	R	2015-2018	CRT+TACE +Sorafenib	28	55.5	96.4	7.4	TT		–	
				CRT+TACE	35	54	91.4	6.6	TT		–	
Li et al.	China	R	2000-2017	CRT	154	47	87.7	9	TT	10.1	51 Gy	
				SBRT	133	51	90.2	8.1	TT	13.5	42 Gy	
Nomura et al.	Japan	R	2009-2017	CRT+HAIC	18	68 (mean)	83.3		T	61.1	50 Gy	
				CRT+HAIC +Sorafenib	14	68.5 (mean)	100		T	35.7	50 Gy	
Lin et al.	Taiwan	P	2002-2004	SBRT	22	59.5 (mean)	77.3	6.5	T		45Gy	
				CRT	21	54 (mean)	80.1	13.8	T		45Gy	
Yang et al.	Taiwan	R	2007-2016	SBRT	54	61 (mean)	77.8		T	35.2	45 Gy	55.6
				CRT	86	59.6 (mean)	75.6		T	50	51.5 Gy	38.4
Que et al.	Taiwan	R	2009-2016	SBRT +Sorafenib	18	55.39 (mean)	77.78		T	16.67	40 Gy	
				SBRT	36	59.83 (mean)	80.56			13.89	40 Gy	
Khorprasert et al.	Thailand	R	2007-2019	CRT	140	61.5	–	8.5	TT	31.65	45.8 Gy (mean)	68.1
				SBRT	20	55.9	–	3.9	TT	20	75.9 Gy (mean)	

RT, radiotherapy; CPC, Child–Pugh Class; R, retrospective; P, prospective; P II, phase II trial; RCT, Randomized Controlled Trial; PVT, CRT, conventional radiation therapy; SBRT, stereotactic body radiotherapy; PRT, particle radiotherapy; TT, thrombus and tumor; T, thrombus only; SR, Surgical resection; TACE, transarterial chemoembolization; HAIC, hepatic arterial infusion chemotherapy; GyE = RBE×Gy; RBE of proton beam is 1.1; RBE of carbon ion is 3.

Safety

Toxic effect events for groups showed in **Table 5**. For grade < 3 toxicity, the most common type of toxicity in CRT group was hepatotoxicity (977 events in 1007 patients), in SBRT group was hepatotoxicity as well (152 events in 139 patients), in PRT group was dermatological toxicity (44 events in 56 patients). For grade ≥ 3, the most frequent type of toxicity in CRT, SBRT, PRT group was hematological toxicity, hepatotoxicity, dermatological toxicity, respectively. PRT group showed advantage in avoiding hepatotoxicity than SBRT group (p = 0.003) and CRT group (p = 0.000); in avoiding hematological toxicity than CRT group (p = 0.003). There were no statistical difference among three groups in gastrointestinal toxicity (p = 0.112) and dermatological toxicity (p = 0.183). Five studies definitively reported late toxic events with total of 27 cases, 16 about gastrointestinal toxicity, 11 for dermatological toxicity.

Publication Bias

Egger's test showed publication biases as follows: 1-year OS in the CRT, SBRT PRT groups (p = 0.25, 0.114, 0.390, respectively); 2-year OS in the CRT, SBRT PRT groups (p = 0.725, 0.991, 0.224); ORR in the CRT, SBRT PRT groups (p = 0.863, 0.609, 0.171). LCR in the CRT, SBRT PRT groups (p = 0.872, 0.623, 0.444). 1-year OS in the CRT+TACE, CRT +HAIC, CRTal groups (p = 0.165, 0.128, 0.676); 2-year OS in the CRT+TACE, CRT+HAIC, CRTal groups (p = 0.401, 0.044, 0.977, respectively); ORR in the CRT+TACE, CRTal groups

TABLE 2 | Baseline characteristics of CRT, SBRT and PRT cohorts.

	CRT cohorts	SBRT cohorts	PRT cohorts
Cohorts (n)	33	13	6
Patients (n)	2927	614	189
Median age (median, years)	56	55.9	64.85
Men (median, %)	85.15	83.15	81.2
Median Child-Pugh≥B class (%)	30.5	13.89	37.25
Median radiation dose (GyE = RBE×Gy)	50 Gy	41 Gy	72.6 GyE
Prior treatment (median, %)	78.9	79.2	67.8

GyE = RBE×Gy; RBE of proton beam is 1.1; RBE of carbon ion is 3.

TABLE 3 | Clinical results.

Study	Follow up (month)	MST (months)	Type for RT	Patients (n)	1-year OS (%)	2-year OS (%)	Responser (n)	CR (%)	PR (%)	SD (%)	PD (%)	ORR (%)	LCR (%)
Hou et al.	10		CRT	181			181	29.3	31.5	33.7	5.5	60.8	94.5
Tan et al.	14.3	8	CRT	26	23	4	26	8	31	61		39	
Toya et al.		9.6	CRT	38	39.4	17.5	38	15.8	28.9	44.7	10.5	44.7	89.4
Igaki et al.		5.6	CRT	18	33.3	9	12	16.7	16.7	58.3	8.3	33.4	91.7
Tanaka et al.		9.4	CRT	67	39	9	67	7.5	37.3	23.9	31.3	44.8	68.7
Okazaki et al.	5.3	6.4	CRT	56			50	0	22	44	34	22	66
Iwamoto et al.		13.3	CRT	80	56	26.7							
Yu et al.	8	11.6	CRT	281	48.1	26.9	260	3.85	54.23	27.69	14.23	58.08	85.77
Rim et al.		13.9	CRT	45	51.5		45	6.7	55.6	31	6.7	62.3	93.3
Bae et al.	8		CRT	47	15	15	47	0	40	51	9	40	91
Huang et al.		3.8	CRT	326	16.7	5.5							
Yeh et al.	10	7	CRT	106	34.7	11	106	9.5	52	33	5.5	61.5	94.5
Pao et al.	4.4	6.6	CRT	42	30	19	27	14.8	59.3	25.9	0	74.1	100
Onishi et al.		12.4	CRT+HAIC	33	54.5	22	31	3.2	45.2	45.2	6.5	48.4	93.6
Kodama et al.		9.9	CRT+HAIC	36	47	20.3	36	8.3	41.7	50	0	50	100
Han et al.		13.5	CRT+HAIC	152	60	29.5	152	1.3	46.7	34.2	17.8	48	82.2
Tang et al.	10.7	12.3	CRT+TACE	185	51.6	28.4							
Lu et al.		13.02	CRT+TACE	30	62.4	20.81	30	16.7	53.3	20	10	70	90
Yamada et al.		7	CRT+TACE	19	40.6	10.2	19	0	57.9	42.1	0	57.9	100
Shirai et al.	9.4	10.3	CRT+TACE	19	47.4	23.7	19	0	36.8	52.6	10.5	36.8	89.4
Yoon et al.	10.6	10.6	CRT+TACE	412	42.5	22.8	409	6.6	33	46	14.4	39.6	85.6
Yoon et al.		12.8	CRT+TACE	45	53.3	26.8	45	0	28.9	51.1	20	28.9	80
Yu et al.	11.4		CRT+TACE +hyperthermia	69	85	62.9	69	34	36.2	15.3	14.5	70.2	85.5
Sugahara et al.	21	22	PRT	35	68	48	35	22.8	60	8.6	8.6	82.8	91.4
Hashimoto et al.	8.4		PRT	34	55		34	15	47	35	3	62	97
Komatsu et al.			PRT	31	47	24							
Sekino et al.	21		PRT	21	62	33							
Lee et al.	13.2	13.2	PRT	27	55.6	33.3	27	0	55.6	37	7.4	55.6	92.6
Kim et al.	15.2	34.4	PRT	41	73.2	51.1	41	34.2	48.8	14.3	2.4	83	97.3
Xi et al.	10	13	SBRT	41	50.3		41	36.6	39	17.1	7.3	75.6	92.7
Shui et al.	9.5	10	SBRT	70	40		62	9.7	69.4	6.4	14.5	79.1	85.5
Lou et al.		10	SBRT	75	38.7	13.3	75	22.7	73.3	4	0	96	100
Dutta et al.	6	11.4 (mean)	SBRT	72	38	10	54	0	36	42	22	36	78
Kumar et al.	8	15	SBRT	29	60		29	7	80	13		87	
Wang et al.	7.4	9.6 (mean)	SBRT	20	58		22	36.4	31.8	27.3	4.4	68.2	95.5
Choi et al.	8.4	20.8	SBRT	24	67.5	48.2	24	8.3	45.8	29.2	16.7	54.1	83.3
Hou et al.	11.8	10.46	CRT	64	35.8	16	64	1.6	51.6	12.5	34.3	53.2	65.7
		15.47	CRT	54	59.3	32	54	5.6	64.8	9.3	20.3	70.4	79.7
Zhao et al.	13	19	CRT+TACE+ Sorafenib	28	72.4	48	28	10.7	35.7	28.6	25	46.4	75
	14.1	15.2	CRT+TACE	35	77.5	16	35	0	45.7	31.4	22.9	45.7	77.1
Li et al.	31	10	CRT	154	48.1	25.1							
		10	SBRT	133	46.5	29.3							
Nomura et al.		6.7	CRT+HAIC	18	21	6	32	9.4	50	21.9	18.7	59.4	81.3
		49.2	CRT+HAIC+ Sorafenib	14	75	50							
Lin et al.		6	SBRT	22			14	7	71	21	0	78	100
		6.7	CRT	21									
Yang et al.		10.9	SBRT	54	34.9	15.3	45	11.1	51.1	33.33	4.4	62.2	95.53
		4.7	CRT	86	15.7	8	59	8.5	25.4	45.8	20.3	33.9	79.7
Que et al.	13.22 (mean)	12.5	SBRT+ Sorafenib	18	55.6	17.7	18	33.33	44.44	11.11	11.11	77.77	88.88
	15.33 (mean)	7	SBRT	36	33.3	11.1	36	25	50	2.78	22.22	75	77.78
Khorprasert et al.	8.2	7.9	CRT	140	39.1	16.5	119	18.5	55.5	8.4	17.6	74	82.4
		11.9	SBRT	20	45	22							

Red font means overall survival in 1st year; overall survival in 2nd year.

TABLE 4 | Comparison of pooled outcomes among groups.

Groups	Cohorts (n)	Patients (n)	*p*, Heterogeneity	I^2	Pooled rates (95% CI)	*p* (among three groups)	*p* (between two groups)	*p*, Egger's test,
1-year OS								
Overall	48	3450	0	87.1	47.3 (42.3, 52.4)			0.04
CRT	30	2669	0	89.1	45.3 (38.6, 52.1)	Q=*11.006*, *p*=0.004	PRT vs CRT Q=8.060, *p*=0.005	0.25
SBRT	12	592	0.098	36.6	44.9 (39.5, 50.3)		SBRT vs CRT Q=0.009, *p*=0.926	0.114
PRT	6	189	0.254	22.9	60.9 (52.6, 68.9)		PRT vs SBRT Q=9.922, *p*=0.002	0.39
CRT + TACE	7	745	0.001	73	53.2 (44.2, 62.2)	Q=7.856, *p*= 0.020	CRT+TACE vs CRT+HAIC Q=0.351, *p*=0.554	0.165
CRT + HAIC	4	239	0.0012	72.8	48.0 (33.4, 62.7)		CRT vs CRT+HAIC Q=1.970, *p*=0.160	0.128
CRTal	16	1574	0	90.1	36.1 (28.2, 44.3)		CRT vs CRT+TACE Q=7.612, *p*=0.006	0.676
2-year OS								
Overall	42	3211	0	84.7	21.9 (18.0, 26.1)			0.357
CRT	29	2624	0	81.6	20.4 (15.9, 25.2)	Q=11.412, *p*=0.003	PRT vs CRT Q=10.353, *p*=0.001	0.725
SBRT	8	432	0.001	72.3	19.2 (11.9, 27.5)		SBRT vs CRT Q=0.055, *p*=0.814	0.991
PRT	5	155	0.128	44.1	38.5 (28.2, 49.3)		PRT vs SBRT Q=8.318, *p*=0.004	0.224
CRT + TACE	7	745	0.466	0	23.2 (20.1, 26.4)	Q=6.021, *p*=0.049	CRT+TACE vs CRT+HAIC Q=0.106, *p*=0.744	0.401
CRT + HAIC	4	239	0.106	50.9	21.5 (13.1, 31.2)		CRT vs CRT+HAIC Q=1.483, *p*=0.223	0.044
CRTal	15	1529	0	85.2	15.5 (10.7, 21.0)		CRT vs CRT+TACE Q=6.020, *p*=0.014	0.977
ORR								
Overall	40	2617	0	87	58.1 (52.2, 63.8)			0.151
CRT	26	1941	0	78.1	50.4 (45.1, 55.7)	Q=14.277, *p*=0.001	PRT vs CRT Q=7.455, *p*=0.006	0.863
SBRT	10	439	0	88	72.7 (58.8, 84.7)		SBRT vs CRT Q=8.424,*p*=0.004	0.609
PRT	4	137	0.024	68.3	72.1 (57.6, 84.7)		PRT vs SBRT Q=0.003, *p*=0.956	0.171
CRT + TACE	6	557	0.007	68.4	45.1 (34.4, 56.0)	Q=0.725, *p*=0.696	CRT+TACE vs CRT+HAIC Q=0.247, *p*=0.619	0.403
CRT + HAIC	3	219	–	–	48.4 (41.7, 55.1)		CRT vs CRT+HAIC Q=0.218, *p*=0.641	–
CRTal	14	1036	0	79.1	50.7 (43.4, 58.0)		CRT vs CRT+TACE Q=0.707, *p*=0.400	0.142
LCR								
Overall	38	2562	0	77	88.6 (85.5, 91.4)			0.654
CRT	25	1915	0	77.7	86.8 (83.0, 90.3)	Q=7.257, *p*=0.027	PRT vs CRT Q=7.213, *p*=0.007	0.872
SBRT	9	410	0	78.4	90.4 (82.4, 96.3)		SBRT vs CRT Q=0.645, *p*=0.422	0.623
PRT	4	137	0.638	0	95.1 (90.4, 98.5)		PRT vs SBRT Q=1.410, *p*=0.235	0.444
CRT + TACE	6	557	0.007	68.9	87.0 (80.7, 92.3)	Q=0.962, *p*=0.618	CRT+TACE vs CRT+HAIC Q=0.827, *p*=0.363	0.403
CRT + HAIC	3	219	–	–	93.5 (77.9, 1.0)		CRT vs CRT+HAIC Q=0.949, *p*=0.330	–
CRTal	13	1010	0	84.6	86.1 (79.6, 91.6)		CRT vs CRT+TACE Q=0.019, *p*=0.891	0.599

CRTal, CRT alone group.

Red font means 2-groups comparison in 1-year OS, 2-year OS, ORR, LCR. Subgroups for CRT, SBRT, and PRT; CRT+TACE, CRT+HAIC, and CRTal.

(p = 0.403, 0.142). LCR in the CRT+TACE, CRTal groups (p = 0.403, 0.599).

DISCUSSION

There are 44 studies about external beam radiotherapy for HCC with MVI included in our study. The results showed PRT yields survival prolongation compared with SBRT and CRT. Meanwhile, PRT and SBRT both provide a higher ORR than CRT. In addition, radiotherapy based combination therapies are beneficial to prolong the survival of patients, especially for RT combined with TACE.

In cases of microvascular tumor invasion, especially to the main portal vein, the prognosis is poor. The reasons are as follows: (1) an extensive intrahepatic metastatic spread may

TABLE 5 | Comparison of toxic effect events for groups.

	Cohorts	Events for <grade 3	Total	Cohorts	Events for ≥grade 3	Total	Events rate (95%CI)	I^2	*p* (among three groups)	*p* (among two groups)
Hepatotoxicity										
CRT	11	997	1007	13	178	1303	12.1 (6.8, 18.6)	87.7		PRT vs CRT Q=13.059, *p*=0.000
SBRT	5	152	139	6	40	209	14.7 (4.8, 28.1)	80.2	Q=16.0.39, *p*=0	SBRT vs CRT Q=0.198, *p*=0.656
PRT	2	7	68	4	2	127	6 (0, 3.8)	11		PRT vs SBRT Q=8.605, *p*=0.003
Hematological										
CRT	11	650	774	12	171	658	17.6 (7.8, 30.3)	92.7		PRT vs CRT Q=8.58, *p*=0.003
SBRT	3	87	95	4	18	165	10.8 (11.2, 28.6)	88.3	Q=8.97, *p*=0.011	SBRT vs CRT Q=0.50, *p*=0.482
PRT	3	31	103	4	3	128	2.2 (0.1, 6.9)	45.5		PRT vs SBRT Q=1.996, *p*=0.158
Gastrointestinal										
CRT	20	879	1951	17	62	1529	2.8 (0.6, 6.1)	85.8		PRT vs CRT Q=3.654, *p*=0.056
SBRT	7	141	268	6	1	193	0.1 (0, 1.8)	–	Q=4.374, *p*= 0.112	SBRT vs CRT Q=2.687, *p*=0.101
PRT	1	3	35	4	0	128	0	–		PRT vs SBRT Q=0.201, *p*=0.654
Dermatological										
CRT	5	62	268	4	0	226	0	–		PRT vs SBRT Q=0.080, *p*=0.778
SBRT	8	2	54	2	2	54	0.15 (0, 7.8)	–	Q=3.396, *p*=0.183	PRT vs CRT Q=1.728, *p*=0.189
PRT	2	44	56	4	3	121	0.1 (0, 5.8)	–		SBRT vs CRT Q=2.375, *p*=0.123

Red font means 2-groups comparison in Hepatotoxicity, Hematological, Gastrointestinal, Dermatological. Subgroups for CRT, SBRT, and PRT.

result from shedding of HCC cells along the portal vein thrombosis; (2) when the main portal vein is completely blocked, liver function continues to deteriorate leading to liver failure occurs; and (3) exacerbation of portal hypertension causes refractory ascites and bleeding in the esophagus (58). Such physiological changes not only reduce patient survival, but also limit the choice of treatment. TACE is one of the standard treatments for unresectable liver cancer, especially for BCLC stage B tumors. However, it is contraindicated for portal vein tumor thrombus because post-operative ischemia may cause liver failure. At present, sorafenib is one of the first choices for HCC with MVI (59), but it has a slow-acting effect and is unable effectively alleviate the metastasis of liver cancer cells induced by PVTT. Kim et al. (60) reported that the median duration of efficacy of sorafenib alone in PVTT for liver tumor was less than five months.

Due to the rapid thrombosis of HCC, immediate reduction of macrovascular is important for follow-up treatment of the primary tumor. In our study, radiotherapy achieved a high ORR in a short time, especially SBRT and PRT. EBRT is a promising treatment and can recanalize the portal vein in a short time, improve nutrient supply to the liver, delay liver decompensation, and even reduce the Child–Pugh score, improving the survival rate. In addition, radiotherapy has a synergistic effect with mainstream treatments for HCC. TACE plus RT is an effective combination treatments. Radiotherapy targets vascular invasion and re-opens the portal vein, to facilitate conditions for TACE treatment. TACE can effectively inhibit the intrahepatic primary tumor and prevent recurrence of MVI. In our study, the CRT plus TACE group and the CRT plus HAIC group are superior to CRT group in survival (1-year OS: 53.2%, 48.0% vs 36.1%, p = 0.020; 2-year OS: 23.2%, 21.5% vs 15.5%, p = 0.049). Sorafenib, an inhibitor of RAF kinase and VEGFR, can limit tumor cell proliferation and tumor angiogenesis, decrease radiation-activated NF-κB and increase radiation-induced apoptosis (61–63). RT plus sorafenib displayed clinical benefit and safety for patients with macrovascular invasion (23, 27). A meta-analysis showed concurrent Sorafenib and RT significantly greater benefit in OS than did the non-concurrent treatment, and they recommend vascular tumor involvement as the only target of EBRT to avoid excessive toxicities (64). It illustrated the potential of radiotherapy in combination therapy.

Hepatocellular carcinoma (HCC) is a radiosensitive tumor with a dose-response relationship (65). Some large clinical studies showed that a high cumulative and per fraction dose can significantly improve the response rate, local control rate, and prolong survival in patients with HCC (66, 67). Dose of 40 to 45 Gy in 3 fractions or 40 to 50 Gy in 5 fractions (53 to 84 GyE) have been demonstrated to be safe with good therapeutic effect (65). Recently, conformal radiotherapy technique is converting from 3D to IMRT, which can improve curative effect. IMRT achieved higher biologically effective dose within fewer fractions and a shorter duration of therapeutic method than 3D-CRT. Compared with 3D-CRT, IMRT provides a survival benefit in HCC with MVI (29). Meanwhile, a study showed median OS and

LCR in the IMRT group were similar to those of the SBRT group for HCC with MVI (47). However, study about IMRT for HCC with MVI is scarce, and the clinical efficacy requires more clinical data to support. SBRT and PRT have a dose advantage over conformal radiotherapy by delivering large doses of radiation to the target tumor volume in a small fraction. The treatments can be completed in a short time because of a higher biologically effective dose. A short course of treatment is conducive due to less interference with other therapeutic methods, reducing toxicity. The outcomes in our study are consistent with prevailing views about the dose-response. SBRT and PRT are associated with higher response rates than CRT. PRT show higher survival rates than CRT.

SBRT has made excellent progress in the field of radiation therapy. However, due to the inherent physical characteristics of photons, SBRT has limited advantage with respect to side effects and liver toxicity. Based on the findings, SBRT is inferior to PRT in avoiding hepatotoxicity. Due to its excellent physical properties, PRT can significantly reduce dose exposure to normal tissues when high doses are used to treat target tumors. PRT is expected to be an ideal treatment for HCCs with high Child-Pugh score. The dosimetric superiority of PRT was correlated with the tumor location. A study by Gandhi et al. showed that PRT can reduce radiation toxicity to target tumor located in the dome and of a size >3 cm (68). Some clinical studies have also proven the safety and efficiency of PRT in the treatment of inferior vena cava tumor thrombi (39, 40). In our study, PRT showed an advantage over SBRT and CRT with respect to hepatotoxicity and hematological toxicity in ≥ grade 3 toxic effect events.

This meta-analysis has several limitations. On one side, meta-analysis is controversial for observational studies. It has been known that RCTs are the most effective means of reducing bias, and meta-analyses of RCTs provide the strongest evidence support (69). However, randomized controlled trial of radiation oncology is difficult to carry out. Radiation therapy competes with other treatments. 60% of all patients with cancer have received primarily treatments in other disciplines before receiving radiotherapy (70). Results from RCTs cannot always be feasible to answer clinical questions, especially in oncology. Meta-analysis of observational studies is an effective method to overcome the information gaps resulting from the insufficient RCT-based data (71). Meta-analysis of observational studies with high-quality did not show significantly different effect sizes from those of RCTs (72). On the other side, heterogeneity is inevitable because of the integrated information in studies with the diversities of designs and populations. The radiotherapy standard of HCC with MVI has not reached a consensus. Too strict inclusion criteria can reduce heterogeneity among studies, but cannot help to address clinical challenges in the real world. Heterogeneity should not be seen as an obstacle to the conclusion. Heterogeneity in meta-analysis requires statistical evaluation and interpretation of clinical phenomena to guide clinical decision-making and solve real-world problems (73).

CONCLUSION

When compared with SBRT and CRT groups, PRT can prolong survival and reduces the occurrence of hepatotoxic events in patients with HCC and MVI. PRT and SBRT have advantages over CRT with respect to the ORR. A combination treatment based on radiotherapy can provide survival benefits to these patients. Since some of the included studies were observational studies, high-quality comparative studies are needed to provide reliable conclusions.

DATA AVAILABILITY STATEMENT

The original contributions presented in the study are included in the article/**Supplementary Material**. Further inquiries can be directed to the corresponding authors.

AUTHOR CONTRIBUTIONS

GW designed the study, acquired data, analyzed data, drafted the manuscript and accepted final version. GH designed the study, acquired the data, reviewed the manuscript and accepted final version. JH acquired the data, reviewed the manuscript and accepted final version. LL designed the study, reviewed the manuscript and accepted final version. SP designed the study, reviewed the manuscript and accepted final version. YL designed the study, analyzed data, reviewed the manuscript and accepted final version. WZ designed the study, analyzed data, reviewed the manuscript and accepted final version. All authors contributed to the article and approved the submitted version.

FUNDING

This study is supported by the National Key Research and Development Program of China (2017YFA0205200), the National Natural Science Foundation of China (81901857, 81771957), Guangdong Provincial Key Laboratory of Tumor Interventional Diagnosis and Treatment (2021B1212040004), and the Science and Technology Development Fund, Macau SAR (0011/2019/AKP).

SUPPLEMENTARY MATERIAL

The Supplementary Material for this article can be found online at: https://www.frontiersin.org/articles/10.3389/fonc.2022.829708/full#supplementary-material

REFERENCES

1. Sung H, Ferlay J, Siegel RL, Laversanne M, Soerjomataram I, Jemal A, et al. Global Cancer Statistics 2020: GLOBOCAN Estimates of Incidence and Mortality Worldwide for 36 Cancers in 185 Countries. *CA Cancer J Clin* (2021) 71:209–49. doi: 10.3322/caac.21660
2. Llovet JM, Bustamante J, Castells A, Vilana R, Ayuso Mdel C, Sala M, et al. Natural History of Untreated Nonsurgical Hepatocellular Carcinoma: Rationale for the Design and Evaluation of Therapeutic Trials. *Hepatology* (1999) 29:62–7. doi: 10.1002/hep.510290145
3. Minagawa M, Makuuchi M. Treatment of Hepatocellular Carcinoma Accompanied by Portal Vein Tumor Thrombus. *World J Gastroenterol* (2006) 12:7561–7. doi: 10.3748/wjg.v12.i47.7561
4. Cabibbo G, Enea M, Attanasio M, Bruix J, Craxì A. Cammà C. A Meta-Analysis of Survival Rates of Untreated Patients in Randomized Clinical Trials of Hepatocellular Carcinoma. *Hepatology* (2010) 51:1274–83. doi: 10.1002/hep.23485
5. Kokudo T, Hasegawa K, Yamamoto S, Shindoh J, Takemura N, Aoki T, et al. Surgical Treatment of Hepatocellular Carcinoma Associated With Hepatic Vein Tumor Thrombosis. *J Hepatol* (2014) 61:583–8. doi: 10.1016/j.jhep.2014.04.032
6. Costentin CE, Ferrone CR, Arellano RS, Ganguli S, Hong TS, Zhu AX. Hepatocellular Carcinoma With Macrovascular Invasion: Defining the Optimal Treatment Strategy. *Liver Cancer* (2017) 6:360–74. doi: 10.1159/000481315
7. Llovet JM, Ricci S, Mazzaferro V, Hilgard P, Gane E, Blanc JF, et al. Sorafenib in Advanced Hepatocellular Carcinoma. *N Engl J Med* (2008) 359:378–90. doi: 10.1056/NEJMoa0708857
8. Bruix J, Raoul JL, Sherman M, Mazzaferro V, Bolondi L, Craxi A, et al. Efficacy and Safety of Sorafenib in Patients With Advanced Hepatocellular Carcinoma: Subanalyses of a Phase III Trial. *J Hepatol* (2012) 57:821–9. doi: 10.1016/j.jhep.2012.06.014
9. Lawrence TS, Robertson JM, Anscher MS, Jirtle RL, Ensminger WD, Fajardo LF. Hepatic Toxicity Resulting From Cancer Treatment. *Int J Radiat Oncol Biol Phys* (1995) 31:1237–48. doi: 10.1016/0360-3016(94)00418-k
10. Emami B, Lyman J, Brown A, Coia L, Goitein M, Munzenrider JE, et al. Tolerance of Normal Tissue to Therapeutic Irradiation. *Int J Radiat Oncol Biol Phys* (1991) 21:109–22. doi: 10.1016/0360-3016(91)90171-y
11. Rim CH, Kim CY, Yang DS, Yoon WS. Comparison of Radiation Therapy Modalities for Hepatocellular Carcinoma With Portal Vein Thrombosis: A Meta-Analysis and Systematic Review. *Radiother Oncol* (2018) 129:112–22. doi: 10.1016/j.radonc.2017.11.013
12. Qi WX, Fu S, Zhang Q, Guo XM. Charged Particle Therapy Versus Photon Therapy for Patients With Hepatocellular Carcinoma: A Systematic Review and Meta-Analysis. *Radiother Oncol* (2015) 114:289–95. doi: 10.1016/j.radonc.2014.11.033
13. Moher D, Liberati A, Tetzlaff J, Altman DG. Preferred Reporting Items for Systematic Reviews and Meta-Analyses: The PRISMA Statement. *PloS Med* (2009) 6:e1000097. doi: 10.1371/journal.pmed.1000097
14. Kim DY, Park JW, Kim TH, Kim BH, Moon SH, Kim SS, et al. Risk-Adapted Simultaneous Integrated Boost-Proton Beam Therapy (SIB-PBT) for Advanced Hepatocellular Carcinoma With Tumour Vascular Thrombosis. *Radiother Oncol* (2017) 122:122–9. doi: 10.1016/j.radonc.2016.12.014
15. Hashimoto S, Ogino H, Iwata H, Hattori Y, Nakajima K, Nakanishi M, et al. Efficacy of Proton Beam Therapy for Hepatocellular Carcinoma With Portal Vein or Inferior Vena Cava Tumor Thrombosis. In: *ASTRO 59th Annual Meeting - American Society for Radiation Oncology, Vol. 2099*. San Diego, CA United States: Elsevier Science Inc, International Journal of Radiation Oncology*Biology*Physics (2017). pp. E2152–3.
16. Dutta D, Tatineni T, Yarlagadda S, Gupte A, Reddy SK, Madhavan R, et al. Hepatocellular Carcinoma Patients With Portal Vein Thrombosis Treated With Robotic Radiosurgery: Interim Results of a Prospective Study. *Indian J Gastroenterol* (2021) 40:389–401. doi: 10.1007/s12664-021-01172-w
17. Khorprasert C, Thonglert K, Alisanant P, Amornwichet N. Advanced Radiotherapy Technique in Hepatocellular Carcinoma With Portal Vein Thrombosis: Feasibility and Clinical Outcomes. *PloS One* (2021) 16:e0257556. doi: 10.1371/journal.pone.0257556
18. Tan Z, Lu J, Zhu G, Chen L, Wang Y, Zhang Q, et al. Portal Vein Irradiation Stent Plus Chemoembolization Versus External Radiotherapy Plus Chemoembolization in Hepatocellular Carcinoma With Portal Vein Tumour Thrombus: A Retrospective Study. *Cardiovasc Intervent Radiol* (1414) 44:1414–22. doi: 10.1007/s00270-021-02889-z
19. Onishi H, Nouso K, Nakamura S, Katsui K, Wada N, Morimoto Y, et al. Efficacy of Hepatic Arterial Infusion Chemotherapy in Combination With Irradiation for Advanced Hepatocellular Carcinoma With Portal Vein Invasion. *Hepatol Int* (2015) 9:105–12. doi: 10.1007/s12072-014-9592-y
20. Han S, Lee HW, Park JY, Kim SU, Kim DY, Ahn SH, et al. Appraisal of Long-Term Outcomes of Liver-Directed Concurrent Chemoradiotherapy for Hepatocellular Carcinoma With Major Portal Vein Invasion. *J Hepatocell Carcinoma* (2020) 7:403–12. doi: 10.2147/JHC.S276528
21. Que J, Wu HC, Lin CH, Huang CI, Li LC, Ho CH. Comparison of Stereotactic Body Radiation Therapy With and Without Sorafenib as Treatment for Hepatocellular Carcinoma With Portal Vein Tumor Thrombosis. *Medicine* (2020) 99:1–9. doi: 10.1097/MD.0000000000019660
22. Yang JF, Lo CH, Lee MS, Lin CS, Dai YH, Shen PC, et al. Stereotactic Ablative Radiotherapy Versus Conventionally Fractionated Radiotherapy in the Treatment of Hepatocellular Carcinoma With Portal Vein Invasion: A Retrospective Analysis. *Radiat Oncol* (2019) 14:1–10. doi: 10.1186/s13014-019-1382-1
23. Zhao Y, Wang H, Dong D, Gao S, Zhu X, Wang W. Safety and Efficacy of Transcatheter Arterial Chemoembolization Plus Radiotherapy Combined With Sorafenib in Hepatocellular Carcinoma Showing Macrovascular Invasion. *Front Oncol* (2019) 9:1065. doi: 10.3389/fonc.2019.01065
24. Lou J, Li Y, Liang K, Guo Y, Song C, Chen L, et al. Hypofractionated Radiotherapy as a Salvage Treatment for Recurrent Hepatocellular Carcinoma With Inferior Vena Cava/Right Atrium Tumor Thrombus: A Multi-Center Analysis. *BMC Cancer* (2019) 19:1–7. doi: 10.1186/s12885-019-5870-3
25. Iwamoto H, Nomiyama M, Niizeki T, Shimose S, Shirono T, Nakano M, et al. Dose and Location of Irradiation Determine Survival for Patients With Hepatocellular Carcinoma With Macrovascular Invasion in External Beam Radiation Therapy. *Oncology* (2019) 96:192–9. doi: 10.1159/000495568
26. Shui Y, Yu W, Ren X, Guo Y, Xu J, Ma T, et al. Stereotactic Body Radiotherapy Based Treatment for Hepatocellular Carcinoma With Extensive Portal Vein Tumor Thrombosis. *Radiat Oncol* (2018) 13:1–9. doi: 10.1186/s13014-018-1136-5
27. Kodama K, Kawaoka T, Aikata H, Uchikawa S, Nishida Y, Inagaki Y, et al. Comparison of Outcome of Hepatic Arterial Infusion Chemotherapy Combined With Radiotherapy and Sorafenib for Advanced Hepatocellular Carcinoma Patients With Major Portal Vein Tumor Thrombosis. *Oncology* (2018) 94:215–22. doi: 10.1159/000486483
28. Yu JI, Park HC, Jung SH, Choi C, Shin SW, Cho SK, et al. Combination Treatment With Transarterial Chemoembolization, Radiotherapy, and Hyperthermia (CERT) for Hepatocellular Carcinoma With Portal Vein Tumor Thrombosis: Final Results of a Prospective Phase II Trial. *Oncotarget* (2017) 8:52651–64. doi: 10.18632/oncotarget.17072
29. Hou JZ, Zeng ZC, Wang BL, Yang P, Zhang JY, Mo HF. High Dose Radiotherapy With Image-Guided Hypo-IMRT for Hepatocellular Carcinoma With Portal Vein and/or Inferior Vena Cava Tumor Thrombi Is More Feasible and Efficacious Than Conventional 3D-CRT. *Jpn J Clin Oncol* (2016) 46:357–62. doi: 10.1093/jjco/hyv205
30. Okazaki E, Yamamoto A, Nishida N, Hamuro M, Ogino R, Hosono M, et al. Three-Dimensional Conformal Radiotherapy for Locally Advanced Hepatocellular Carcinoma With Portal Vein Tumour Thrombosis: Evaluating Effectiveness of the Model for End-Stage Liver Disease (MELD) Score Compared With the Child-Pugh Classification. *Br J Radiol* (1063) 89:1–8. doi: 10.1259/bjr.20150945
31. Bae BK, Kim JC. The Response of Thrombosis in the Portal Vein or Hepatic Vein in Hepatocellular Carcinoma to Radiation Therapy. *Radiat Oncol J* (2016) 34:168–76. doi: 10.3857/roj.2016.01669
32. Yeh SA, Chen YS, Perng DS. The Role of Radiotherapy in the Treatment of Hepatocellular Carcinoma With Portal Vein Tumor Thrombus. *J Radiat Res* (2015) 56:325–31. doi: 10.1093/jrr/rru104
33. Wang PM, Hsu WC, Chung NN, Chang FL, Jang CJ, Fogliata A, et al. Feasibility of Stereotactic Body Radiation Therapy With Volumetric Modulated Arc Therapy and High Intensity Photon Beams for Hepatocellular Carcinoma Patients. *Radiat Oncol* (2014) 9:1–9. doi: 10.1186/1748-717X-9-18

34. Tanaka Y, Nakazawa T, Komori S, Hidaka H, Okuwaki Y, Takada J, et al. Radiotherapy for Patients With Unresectable Advanced Hepatocellular Carcinoma With Invasion to Intrahepatic Large Vessels: Efficacy and Outcomes. *J Gastroenterol Hepatol* (2014) 29:352–7. doi: 10.1111/jgh.12333
35. Xi M, Zhang L, Zhao L, Li QQ, Guo SP, Feng ZZ, et al. Effectiveness of Stereotactic Body Radiotherapy for Hepatocellular Carcinoma With Portal Vein and/or Inferior Vena Cava Tumor Thrombosis. *PloS One* (2013) 8:1–7. doi: 10.1371/journal.pone.0063864
36. Tang Q, Li A, Yang G, Lai EC, Zhou W, Jiang Z, et al. Surgical Resection Versus Conformal Radiotherapy Combined With TACE for Resectable Hepatocellular Carcinoma With Portal Vein Tumor Thrombus: A Comparative Study. *World J Surg* (1362) 37:1362–70. doi: 10.1007/s00268-013-1969-x
37. Toya R, Murakami R, Baba Y, Nishimura R, Morishita S, Ikeda O, et al. Conformal Radiation Therapy for Portal Vein Tumor Thrombosis of Hepatocellular Carcinoma. *Radiother Oncol* (2007) 84:266–71. doi: 10.1016/j.radonc.2007.07.005
38. Lin CS, Jen YM, Chiu SY, Hwang JM, Chao HL, Lin HY, et al. Treatment of Portal Vein Tumor Thrombosis of Hepatoma Patients With Either Stereotactic Radiotherapy or Three-Dimensional Conformal Radiotherapy. *Jpn J Clin Oncol* (2006) 36:212–7. doi: 10.1093/jjco/hyl006
39. Sekino Y, Okumura T, Fukumitsu N, Iizumi T, Numajiri H, Mizumoto M, et al. Proton Beam Therapy for Hepatocellular Carcinoma Associated With Inferior Vena Cava Tumor Thrombus. *J Cancer Res Clin Oncol* (2020) 146:711–20. doi: 10.1007/s00432-019-03096-7
40. Komatsu S, Kido M, Asari S, Toyama H, Ajiki T, Demizu Y, et al. Particle Radiotherapy, a Novel External Radiation Therapy, Versus Liver Resection for Hepatocellular Carcinoma Accompanied With Inferior Vena Cava Tumor Thrombus: A Matched-Pair Analysis. *Surgery* (2017) 162:1241–9. doi: 10.1016/j.surg.2017.08.006
41. Lee SU, Park JW, Kim TH, Kim YJ, Woo SM, Koh YH, et al. Effectiveness and Safety of Proton Beam Therapy for Advanced Hepatocellular Carcinoma With Portal Vein Tumor Thrombosis. *Strahlenther u Onkol* (2014) 190:806–14. doi: 10.1007/s00066-014-0604-6
42. Choi HS, Kang KM, Jeong BK, Jeong H, Lee YH, Ha IB, et al. Effectiveness of Stereotactic Body Radiotherapy for Portal Vein Tumor Thrombosis in Patients With Hepatocellular Carcinoma and Underlying Chronic Liver Disease. *Asia-Pac J Clin Oncol* (2021) 17:209–15. doi: 10.1111/ajco.13361
43. Rim CH, Yang DS, Park YJ, Yoon WS, Lee JA, Kim CY. Effectiveness of High-Dose Three-Dimensional Conformal Radiotherapy in Hepatocellular Carcinoma With Portal Vein Thrombosis. *Jpn J Clin Oncol* (2012) 42:721–9. doi: 10.1093/jjco/hys082
44. Shirai S, Sato M, Suwa K, Kishi K, Shimono C, Sonomura T, et al. Feasibility and Efficacy of Single Photon Emission Computed Tomography-Based Three-Dimensional Conformal Radiotherapy for Hepatocellular Carcinoma 8 Cm or More With Portal Vein Tumor Thrombus in Combination With Transcatheter Arterial Chemoembolization. *Int J Radiat Oncol Biol Phys* (2010) 76:1037–44. doi: 10.1016/j.ijrobp.2009.03.023
45. Yamada K, Izaki K, Sugimoto K, Mayahara H, Morita Y, Yoden E, et al. Prospective Trial of Combined Transcatheter Arterial Chemoembolization and Three-Dimensional Conformal Radiotherapy for Portal Vein Tumor Thrombus in Patients With Unresectable Hepatocellular Carcinoma. *Int J Radiat Oncol Biol Phys* (2003) 57:113–9. doi: 10.1016/S0360-3016(03)00434-6
46. Kumar R, Yadav HP, Thaper D, Kamal R, Gupta A, Kirti S. Efficacy and Toxicity of SBRT in Advanced Hepatocellular Carcinoma With Portal Vein Tumor Thrombosis - A Retrospective Study. *Rep Pract Oncol Radiother* (2021) 26:573–81. doi: 10.5603/RPOR.a2021.0048
47. Li L-Q, Zhou Y, Huang Y, Liang P, Liang S-X, Su T-S. Stereotactic Body Radiotherapy Versus Intensity-Modulated Radiotherapy for Hepatocellular Carcinoma With Portal Vein Tumor Thrombosis. *Hepatol Int* (2021) 15:630–41. doi: 10.1007/s12072-021-10173-y
48. Igaki H, Nakagawa K, Shiraishi K, Shiina S, Kokudo N, Terahara A, et al. Three-Dimensional Conformal Radiotherapy for Hepatocellular Carcinoma With Inferior Vena Cava Invasion. *Jpn J Clin Oncol* (2008) 38:438–44. doi: 10.1093/jjco/hyn038
49. Pao T-H, Hsueh W-T, Chang W-L, Chiang N-J, Lin Y-J, Liu Y-S, et al. Radiotherapy for Inferior Vena Cava Tumor Thrombus in Patients With Hepatocellular Carcinoma. *BMC Cancer* (2019) 19:560. doi: 10.1186/s12885-019-5654-9
50. Lu D-H, Fei Z-L, Zhou J-P, Hu Z-T, Hao W-S. A Comparison Between Three-Dimensional Conformal Radiotherapy Combined With Interventional Treatment and Interventional Treatment Alone for Hepatocellular Carcinoma With Portal Vein Tumour Thrombosis. *J Med Imaging Radiat Oncol* (2015) 59:109–14. doi: 10.1111/1754-9485.12207
51. Yoon SM, Ryoo BY, Lee SJ, Kim JH, Shin JH, An JH, et al. Efficacy and Safety of Transarterial Chemoembolization Plus External Beam Radiotherapy vs Sorafenib in Hepatocellular Carcinoma With Macroscopic Vascular Invasion: A Randomized Clinical Trial. *JAMA Oncol* (2018) 4:661–9. doi: 10.1001/jamaoncol.2017.5847
52. Yoon S, Lim Y-S, Won HJ, Kim JH, Kim KM, Lee HC, et al. Radiotherapy Plus Transarterial Chemoembolization for Hepatocellular Carcinoma Invading the Portal Vein: Long-Term Patient Outcomes. *Int J Radiat Oncol Biol Phys* (2012) 82:2004–11. doi: 10.1016/j.ijrobp.2011.03.019
53. Yu JI, Park HC, Lim DH, Park W, Yoo BC, Paik SW, et al. Prognostic Index for Portal Vein Tumor Thrombosis in Patients With Hepatocellular Carcinoma Treated With Radiation Therapy. *J Korean Med Sci* (2011) 26:1014–22. doi: 10.3346/jkms.2011.26.8.1014
54. Huang YJ, Hsu HC, Wang CY, Wang CJ, Chen HC, Huang EY, et al. The Treatment Responses in Cases of Radiation Therapy to Portal Vein Thrombosis in Advanced Hepatocellular Carcinoma. *Int J Radiat Oncol Biol Phys* (2009) 73:1155–63. doi: 10.1016/j.ijrobp.2008.06.1486
55. Nomura T, Tani J, Deguchi A, Nakahara M, Oura K, Tadokoro T, et al. Efficacy of Combined Modality Therapy With Sorafenib Following Hepatic Arterial Injection Chemotherapy and Three-Dimensional Conformal Radiotherapy for Advanced Hepatocellular Carcinoma With Major Vascular Invasion. *Mol Clin Oncol* (2019) 11:447–54. doi: 10.3892/mco.2019.1920
56. Sugahara S, Nakayama H, Fukuda K, Mizumoto M, Tokita M, Abei M, et al. Proton-Beam Therapy for Hepatocellular Carcinoma Associated With Portal Vein Tumor Thrombosis. *Strahlenther Und Onkol* (2009) 185:782–8. doi: 10.1007/s00066-009-2020-x
57. Hou J-Z, Zeng Z-C, Zhang J-Y, Fan J, Zhou J, Zeng M-S. Influence of Tumor Thrombus Location on the Outcome of External-Beam Radiation Therapy in Advanced Hepatocellular Carcinoma With Macrovascular Invasion. *Int J Radiat Oncol Biol Phys* (2012) 84:362–8. doi: 10.1016/j.ijrobp.2011.12.024
58. Lau WY LE, Yu SC. Management of Portal Vein Tumor Thrombus. In: Lau WY, editor. *Hepatocellular Carcinoma*. Singapore: World Scientific Publishing (2008). p. 739–60.
59. Bruix J, Sherman M. Management of Hepatocellular Carcinoma: An Update. *Hepatology* (2011) 53:1020–2. doi: 10.1002/hep.24199
60. Kim GA, Shim JH, Yoon SM, Jung J, Kim JH, Ryu MH, et al. Comparison of Chemoembolization With and Without Radiation Therapy and Sorafenib for Advanced Hepatocellular Carcinoma With Portal Vein Tumor Thrombosis: A Propensity Score Analysis. *J Vasc Interv Radiol* (2015) 26:320–9.e326. doi: 10.1016/j.jvir.2014.10.019
61. Wilhelm SM, Carter C, Tang L, Wilkie D, McNabola A, Rong H, et al. BAY 43-9006 Exhibits Broad Spectrum Oral Antitumor Activity and Targets the RAF/MEK/ERK Pathway and Receptor Tyrosine Kinases Involved in Tumor Progression and Angiogenesis. *Cancer Res* (2004) 64:7099–109. doi: 10.1158/0008-5472.Can-04-1443
62. Huang CY, Lin CS, Tai WT, Hsieh CY, Shiau CW, Cheng AL, et al. Sorafenib Enhances Radiation-Induced Apoptosis in Hepatocellular Carcinoma by Inhibiting STAT3. *Int J Radiat Oncol Biol Phys* (2013) 86:456–62. doi: 10.1016/j.ijrobp.2013.01.025
63. Yu W, Gu K, Yu Z, Yuan D, He M, Ma N, et al. Sorafenib Potentiates Irradiation Effect in Hepatocellular Carcinoma *In Vitro* and *In Vivo*. *Cancer Lett* (2013) 329:109–17. doi: 10.1016/j.canlet.2012.10.024
64. Rim CH, Park S, Shin IS, Yoon WS. Is the Concurrent Use of Sorafenib and External Radiotherapy Feasible for Advanced Hepatocellular Carcinoma? A Meta-Analysis. *Cancers (Basel)* (2021) 13:1–14. doi: 10.3390/cancers13122912
65. Schaub SK, Hartvigson PE, Lock MI, Høyer M, Brunner TB, Cardenes HR, et al. Stereotactic Body Radiation Therapy for Hepatocellular Carcinoma: Current Trends and Controversies. *Technol Cancer Res Treat* (2018) 17:1533033818790217. doi: 10.1177/1533033818790217
66. Jang WI, Kim MS, Bae SH, Cho CK, Yoo HJ, Seo YS, et al. High-Dose Stereotactic Body Radiotherapy Correlates Increased Local Control and Overall Survival in Patients With Inoperable Hepatocellular Carcinoma. *Radiat Oncol* (2013) 8:250. doi: 10.1186/1748-717x-8-250

67. Seong J, Lee IJ, Shim SJ, Lim DH, Kim TH, Kim JH, et al. A Multicenter Retrospective Cohort Study of Practice Patterns and Clinical Outcome on Radiotherapy for Hepatocellular Carcinoma in Korea. *Liver Int* (2009) 29:147–52. doi: 10.1111/j.1478-3231.2008.01873.x
68. Gandhi SJ, Liang X, Ding X, Zhu TC, Ben-Josef E, Plastaras JP, et al. Clinical Decision Tool for Optimal Delivery of Liver Stereotactic Body Radiation Therapy: Photons Versus Protons. *Pract Radiat Oncol* (2015) 5:209–18. doi: 10.1016/j.prro.2015.01.004
69. Berlin JA, Golub RM. Meta-Analysis as Evidence: Building a Better Pyramid. *Jama* (2014) 312:603–5. doi: 10.1001/jama.2014.8167
70. Benzies KM, Premji S, Hayden KA, Serrett K. State-Of-the-Evidence Reviews: Advantages and Challenges of Including Grey Literature. *Worldviews Evid Based Nurs* (2006) 3:55–61. doi: 10.1111/j.1741-6787.2006.00051.x
71. Frieden TR. Evidence for Health Decision Making - Beyond Randomized, Controlled Trials. *N Engl J Med* (2017) 377:465–75. doi: 10.1056/NEJMra1614394
72. Concato J, Shah N, Horwitz RI. Randomized, Controlled Trials, Observational Studies, and the Hierarchy of Research Designs. *N Engl J Med* (2000) 342:1887–92. doi: 10.1056/nejm200006223422507
73. Shin IS, Rim CH. Updating Perspectives on Meta-Analyses in the Field of Radiation Oncology. *Med (Kaunas)* (2021) 57:1–11. doi: 10.3390/medicina57020117

Conflict of Interest: The authors declare that the research was conducted in the absence of any commercial or financial relationships that could be construed as a potential conflict of interest.

Publisher's Note: All claims expressed in this article are solely those of the authors and do not necessarily represent those of their affiliated organizations, or those of the publisher, the editors and the reviewers. Any product that may be evaluated in this article, or claim that may be made by its manufacturer, is not guaranteed or endorsed by the publisher.

frontiers in Oncology

ORIGINAL RESEARCH
published: 25 February 2022
doi: 10.3389/fonc.2022.816678

Evaluation of Multisource Adaptive MRI Fusion for Gross Tumor Volume Delineation of Hepatocellular Carcinoma

Andy Lai-Yin Cheung[1,2†], Lei Zhang[3,4,5†], Chenyang Liu[2], Tian Li[2], Anson Ho-Yin Cheung[6], Chun Leung[6], Angus Kwong-Chuen Leung[7], Sai-Kit Lam[2], Victor Ho-Fun Lee[8] and Jing Cai[2,3]*

[1] Department of Clinical Oncology, Queen Mary Hospital, Hong Kong, Hong Kong SAR, China, [2] Department of Health Technology and Informatics, The Hong Kong Polytechnic University, Hong Kong, Hong Kong SAR, China, [3] Department of Radiation Oncology, Duke University Medical Center, Durham, NC, United States, [4] Medical Physics Graduate Program, Duke University, Durham, NC, United States, [5] Medical Physics Graduate Program, Duke Kunshan University, Kunshan, China, [6] Radiotherapy and Oncology Centre, Hong Kong Baptist Hospital, Hong Kong, Hong Kong SAR, China, [7] AMO Oncology Centre, Hong Kong, Hong Kong SAR, China, [8] Department of Clinical Oncology, The University of Hong Kong, Hong Kong, Hong Kong SAR, China

OPEN ACCESS

Edited by:
Yuming Jiang,
Stanford University, United States

Reviewed by:
Jackie Wu,
Duke University, United States
Guanzhong Gong,
Shandong University, China
Amol Narang,
Johns Hopkins Medicine, United States
Robert Finnegan,
The University of Sydney, Australia

***Correspondence:**
Jing Cai
jing.cai@polyu.edu.hk

†These authors have contributed equally to this work

Specialty section:
This article was submitted to Radiation Oncology, a section of the journal Frontiers in Oncology

Received: *17 November 2021*
Accepted: *27 January 2022*
Published: *25 February 2022*

Citation:
Cheung AL-Y, Zhang L, Liu C, Li T, Cheung AH-Y, Leung C, Leung AK-C, Lam S-K, Lee VH-F and Cai J (2022) Evaluation of Multisource Adaptive MRI Fusion for Gross Tumor Volume Delineation of Hepatocellular Carcinoma. Front. Oncol. 12:816678. doi: 10.3389/fonc.2022.816678

Purpose: Tumor delineation plays a critical role in radiotherapy for hepatocellular carcinoma (HCC) patients. The incorporation of MRI might improve the ability to correctly identify tumor boundaries and delineation consistency. In this study, we evaluated a novel Multisource Adaptive MRI Fusion (MAMF) method in HCC patients for tumor delineation.

Methods: Ten patients with HCC were included in this study retrospectively. Contrast-enhanced T1-weighted MRI at portal-venous phase ($T1W_{PP}$), contrast-enhanced T1-weighted MRI at 19-min delayed phase ($T1W_{DP}$), T2-weighted (T2W), and diffusion-weighted MRI (DWI) were acquired on a 3T MRI scanner and imported to in-house-developed MAMF software to generate synthetic MR fusion images. The original multi-contrast MR image sets were registered to planning CT by deformable image registration (DIR) using MIM. Four observers independently delineated gross tumor volumes (GTVs) on the planning CT, four original MR image sets, and the fused MRI for all patients. Tumor contrast-to-noise ratio (CNR) and Dice similarity coefficient (DSC) of the GTVs between each observer and a reference observer were measured on the six image sets. Inter-observer and inter-patient mean, SD, and coefficient of variation (CV) of the DSC were evaluated.

Results: Fused MRI showed the highest tumor CNR compared to planning CT and original MR sets in the ten patients. The mean ± SD tumor CNR was 0.72 ± 0.73, 3.66 ± 2.96, 4.13 ± 3.98, 4.10 ± 3.17, 5.25 ± 2.44, and 9.82 ± 4.19 for CT, $T1W_{PP}$, T2W, DWI, $T1W_{DP}$, and fused MRI, respectively. Fused MRI has the minimum inter-observer and inter-patient variations as compared to original MR sets and planning CT sets. GTV delineation inter-observer mean DSC across the ten patients was 0.81 ± 0.09, 0.85 ± 0.08, 0.88 ± 0.04, 0.89 ± 0.08, 0.90 ± 0.04, and 0.95 ± 0.02 for planning CT, $T1W_{PP}$,

T2W, DWI, $T1W_{DP}$, and fused MRI, respectively. The patient mean inter-observer CV of DSC was 3.3%, 3.2%, 1.7%, 2.6%, 1.5%, and 0.9% for planning CT, $T1W_{PP}$, T2W, DWI, $T1W_{DP}$, and fused MRI, respectively.

Conclusion: The results demonstrated that the fused MRI generated using the MAMF method can enhance tumor CNR and improve inter-observer consistency of GTV delineation in HCC as compared to planning CT and four commonly used MR image sets ($T1W_{PP}$, $T1W_{DP}$, T2W, and DWI). The MAMF method holds great promise in MRI applications in HCC radiotherapy treatment planning.

Keywords: MRI fusion, tumor contrast, GTV delineation, hepatocellular carcinoma, MR-guided radiotherapy

1 INTRODUCTION

Hepatocellular carcinoma (HCC) is the most common primary liver cancer, which is among the most prominent causes of cancer-related deaths worldwide (1). It is one of the deadliest and most aggressive cancer types, with a general 5-year survival of 18%, depending on the stages being diagnosed (2).

Historically, conventional radiotherapy was not the preferred option for the treatment of liver tumors due to the risk of radiation-induced liver damage (RILD) (3). In recent years, a higher radiation dose can be delivered in hypo-fractionated fractions with reduced risk of RILD owing to the adoption of CT, MRI, and image-guided radiotherapy (IGRT) for improved accuracy in target delineation, as well as the use of a rigid immobilizing device for limiting patient movement and cone-beam CT (CBCT)-based image guidance during patient setup (4–11). Highly conformal dose to the target and sparing of the surrounding normal tissues are believed to contribute to the improved outcomes in HCC patients. Target delineation is therefore a critically important step towards precise treatment with high dose conformation, dose escalation, and eventually the success of modern radiotherapy. Indeed, the benefits of dose escalation in both photon and proton therapy for liver malignancies have been demonstrated in multiple clinical trials (12, 13).

In the current clinical practice of liver cancer radiotherapy treatment planning, MRI has been increasingly used alone or in conjunction with CT for tumor and normal tissue delineations because of its superior soft-tissue contrast (9). The contours of the target are firstly created in MR images and then transferred to planning CT images *via* MRI-CT registration. However, MRI might still be prone to inter-sequence and inter-patient variations in image quality and tumor contrast, and potentially inter-observer variations in tumor identification or delineation (14–23).

To overcome these challenges, we have previously developed a Multisource Adaptive MRI Fusion (MAMF) method that is capable of producing a large number of fused MR images with multifaceted image contrasts for RT applications using a limited number of standard MR images as input (21). This method has shown promise in enhancing the image quality of MRI in radiotherapy treatment planning featuring application-specific adaptation and optimization of image contrast (22). In this study, we evaluated the potential clinical efficacy of MAMF in gross tumor volume (GTV) delineation of HCC patients in terms of both tumor contrast optimization and inter-observer variability improvement.

2 METHODS

2.1 Patient Data and Image Acquisition

Ten HCC patients treated with radiotherapy at the Hong Kong Queen Mary Hospital between 2015 and 2019 were retrospectively recruited for this study with Institutional Review Board approval. The distribution of the Child-Pugh score among the enrolled patients was 7 for grade A, 2 for grade B, and 1 for grade C. The CT scan and MRI scans of each patient were performed within 1 week to ensure minimal anatomical changes between scans. During planning CT image acquisition, patients were scanned under a CT scanner (Aquilion/LB, Toshiba, Tokyo, Japan) with a head-first supine position in a vacuum bag with arms raised above their head. The planning MR image acquisition was conducted under a Philips Achieva 3T MRI scanner (Philips Healthcare, Best, The Netherlands). The patient positioning was equivalent to that during planning CT scanning to minimize variations in patient anatomy between CT and MR scans. A series of four MR image sets were acquired including T1-weighted MRI in portal-venous phase ($T1W_{PP}$), T1-weighted MRI in 19-min delay post-contrast ($T1W_{DP}$), T2-weighted MRI (T2W), and diffusion-weighted MRI (DWI).

The details of the imaging protocols for CT and each MR sequence are as follows. Planning CT: tube voltage = 120 kVp; tube current = 50–400 mA; helical scan; field of view (FOV) = 500 mm × 500 mm; slice thickness = 3 mm. $T1W_{PP}$ and $T1W_{DP}$ MRI: pulse sequence = LAVA; 3D mode; time of repetition (TR) = 3.86 ms; time of echo (TE) = 1.79 ms; FOV = 420 mm × 420 mm; slice thickness = 4 mm; flip angle = 12°; bandwidth = 62.5 Hz/pixel. For T1W contrast enhancement, Primovist was deployed as the contrast agent with a concentration of 0.25 mmol/ml and was injected to the patients *via* a rate of 1.5 ml/s. T2W MRI: pulse sequence = FSE-XL; 2D mode; TR = 2,200 ms; TE = 85 ms; FOV = 400 mm × 400 mm; slice thickness = 7 mm; flip angle = 111°; bandwidth = 62.5 Hz/pixel. DWI: pulse sequence: SE; 2D mode; FOV = 400 mm × 400 mm;

slice thickness = 7 mm; number of diffusion directions, 3 in 1; b-value = 500 s/mm^2; NEX = 8.

Respiratory motion management was performed during image acquisitions. The planning CT images were acquired during the end-of-exhalation (EOE) phase of the patient's respiratory cycle under the breath-holding technique using Varian Real-time Position Management (RPM) (Varian Medical Systems, Palo Alto, CA, USA) in the monitoring of the patient's breathing motion pattern. $T1W_{PP}$, $T1W_{DP}$, and T2W MR images were acquired during the EOE phase with patient breath-holding. DWI MR images were acquired during the EOE phase using respiratory navigation (Philips Bellows system) due to its longer acquisition time. Prior to both CT and MR image acquisitions, coaching was exercised on patients for assessing breathing stability, breathing consistency, and breath-hold duration, in compliance with an international guideline on stereotactic body radiation therapy (SBRT) from the American Association of Physicists in Medicine (AAPM) Task Group 101 (TG-101) report. The acquired MR images were "stationary" images that represent a single phase of the respiratory cycle of the patients, which were then used for the generation of fused MRI using MAMF (see *Section 2.2*).

2.2 Generation of Fused MRI Using Multisource Adaptive MRI Fusion

The MAMF technique consists of five key components: input multiple MRI, image preprocessing, fusion algorithm, adaptation methods, and output fused MRI. For input MRI, the four original MR image sets ($T1W_{PP}$, $T1W_{DP}$, T2W, and DWI) were imported into the in-house-developed MAMF program implemented in Matlab (MathWorks, Natick, MA, USA) to generate a new fused MRI that has enhanced tumor-to-tissue contrast. For image preprocessing, the original four MR image sets were registered to planning CT by deformable image registration (DIR) using MIM Maestro v6.3 (MIM Software Inc., Cleveland, OH, USA). Image intensities were clipped by the 99.5th percentile of each image set and normalized to values between 0 and 1. For image fusion, a linear weighted summation fusion algorithm was used to generate a series of fused MRIs. The fused MRI was synthesized by the following equation:

$$Y_i = \Sigma_{k=1}^{K}\, w_{ik} X_k \qquad [1],$$

where Y is the fused images, X is the input MRI, w ∈ [−1, 1] in an interval of 0.167 is the weight coefficient for each input MRI, and k and i are the indices of input and fused MRI, respectively.

A database of all fused MRI with input image weight coefficients and fused image features was built for each patient. Fused image features in this study included tumor contrast-to-noise ratio (CNR) and liver signal-to-noise ratio (SNR), which are defined as

$$Tumor\ CNR = \left| \frac{\mu_{Tumor} - \mu_{Liver}}{\sigma_{Liver}} \right| \qquad [2],$$

$$Liver\ SNR = \frac{\mu(Liver)}{\sigma(Liver)} \qquad [3],$$

where μ and σ are the mean and SD of the regional intensities, respectively. Tumor and liver represent the GTV and a nearby homogenous liver region, respectively.

Finally, an output- or feature-driven adaptation approach was used for the fused MRI selection. In this study, for the application of tumor contrast enhancement and GTV delineation, tumor CNR was set to maximum, while liver SNR was set as positive. The optimal image set with the highest tumor CNR and a positive liver SNR in the database was selected for each patient automatically and exported in DICOM format for GTV delineation. The input image weight coefficients were therefore not fixed per imaging techniques or patient. Instead, they were independently optimized to achieve optimal tumor CNR with a positive liver SNR for each patient. More details of the MAMF method could be found in previous publications (21, 22).

2.3 Gross Tumor Volume Delineation

Eclipse treatment planning workstation (version 15.6, Varian Medical Systems, Palo Alto, CA, USA) was used for GTV delineation. Four experienced radiation oncologists and medical physicists were recruited from two hospitals to delineate the GTV separately. Identical window and level settings were used for consistency.

2.4 Data Analysis

Two main evaluation metrics were used to assess the clinical efficacy of MAMF for GTV delineation: tumor CNR and GTV Dice similarity coefficient (DSC). The tumor CNR was defined in *Section 2.2*. Absolute values of tumor CNR were measured on all six image sets of all patients. Tumor CNR inter-patient (IP) mean, SD, and coefficient of variation (CV) were calculated. The CV of CNR was defined as

$$CNR_{IPCV} = \frac{\sigma(CNR_i)}{\mu(CNR_i)} \times 100\,\% \qquad [4],$$

where i = 1 to 10 represents the patient number.

The DSC, defined as the overlap of two volumes divided by their average, was applied to quantify consistencies in the GTV delineation. GTV RT structures of all four observers and all six image sets were exported from the treatment planning system to Python for DSC calculation. The DSC was calculated between the most experienced radiation oncologist contour, which was defined as the reference, and each of three observer contours. The DSC was calculated as follows:

$$DSC_i = \frac{2(\left|GTV_{Ref}\right| \cap \left|GTV_i\right|)}{\left|GTV_{Ref}\right| + \left|GTV_i\right|} \qquad [5],$$

where GTV_{Ref} is the reference GTV and GTV_i is one of the three observer GTVs.

Mean, SD, and CV of the three DSCs were calculated for each image set and each patient. The DSC inter-observer (IO) mean and CV were defined as

$$DSC_{IOmean} = \mu(DSC_i) \qquad [6]$$

$$DSC_{IOCV} = \frac{\sigma(DSC_i)}{\mu(DSC_i)} \times 100\,\% \quad [7],$$

where i = 1 to 3 represents the three observer contours for each image set, and μ and σ are the mean and SD among the three DSCs. The DSC_{IOmean} and DSC_{IOCV} were calculated for all image sets and patients. Paired Student's t-tests were performed for the *CNR* and DSC_{IOmean} comparisons between the six image sets.

3 RESULTS

3.1 Patient Demographic Data

Ten patients were included in the study, including seven male and three female patients. The characteristics of the patients are shown in **Table 1**. Patient age ranged from 58 to 86, and the mean ± SD age was 68.4 ± 9.5 years. Ten HCC tumors were roughly evenly distributed in different liver segments. The GTV volume had a range of 5.9 to 83.0 cm^3, and the mean ± SD GTV volume was 33.8 ± 27.9 cm^3.

3.2 Tumor Contrast-to-Noise Ratio

By using the MAMF method, the inter-patient mean ± SD of the optimized weight coefficients for each input imaging technique was as follows: $T1W_{PP}$, 0.63 ± 0.33; $T1W_{DP}$, −0.43 ± 0.21; T2W, 0.50 ± 0.43; and DWI, 0.23 ± 0.38. The details of the weight coefficients for each patient are summarized in **Table 2**.

Figure 1 shows the comparison of tumor CNR between the planning CT, the four original MR image sets, and the fused MR images. Firstly, it can be observed that the fused MR images achieved the highest mean tumor CNR (9.82 ± 4.19) among all image sets, leading to a statistically significant enhancement as compared to that of CT (9.82 ± 4.19 vs. 0.72 ± 0.73, $p < 0.0005$), $T1W_{PP}$ (9.82 ± 4.19 vs. 3.66 ± 2.96, $p < 0.005$), T2W (9.82 ± 4.19 *vs.* 4.13 ± 3.98, $p < 0.001$), DWI (9.82 ± 4.19 vs. 4.10 ± 3.17, $p < 0.005$), and $T1W_{DP}$ (9.82 ± 4.19 vs. 5.25 ± 2.44, $p < 0.01$) images. Secondly, the inter-patient CV of tumor CNR was the lowest in the fused MR images (42.7%), followed by $T1W_{DP}$ (46.5%), DWI (77.5%), $T1W_{DP}$ (81.0%), T2W (96.2%), and planning CT (101.0%), suggesting that the fused MR images achieved minimum tumor CNR variability between patients. Thirdly, the planning CT images had lower mean tumor CNR than $T1W_{PP}$ ($p < 0.01$), T2W ($p < 0.02$), DWI ($p < 0.005$), and $T1W_{DP}$ ($p < 0.0005$).

Figure 2 shows different degrees of tumor visibility on the central tumor plane of the planning CT, the four original MR sets ($T1W_{DP}$, $T1W_{DP}$, T2W, DWI), and the fused MR image of a representative patient. For CT and $T1W_{PP}$ images, the tumor and adjacent normal tissue are not clearly discernible. $T1W_{DP}$, T2W, and DWI images show improved tumor contrast. Of note, the fused MR images demonstrated the highest tumor contrast. These findings are in line with the results of quantitative comparisons in terms of CNR (**Figure 1**).

TABLE 1 | Characteristics of HCC patients enrolled in this study.

Characteristic	Finding
Age (year)*	68.4 ± 9.5 (range: 58–86)
Sex	
Male	7
Female	3
GTV volume (cm^3)*	33.8 ± 27.9 (range: 5.9–83.0)
Tumor location	
Segment 1	0
Segment 2	3
Segment 3	1
Segment 4	2
Segment 5	1
Segment 6	1
Segment 7	2
Segment 8	0

HCC, hepatocellular carcinoma; GTV, gross tumor volume.
**Data: mean ± SD.*

3.3 Inter-Observer and Inter-Patient Consistencies of Gross Tumor Volume Delineation

Figure 3 demonstrates the inter-observer mean of the GTV delineation DSC values (DSC_{IOmean}) of all ten patients in each of the six studied image sets. Firstly, the fused MR images yielded the highest DSC_{IOmean} (0.95 ± 0.02) among all image sets, leading to a statistically significant enhancement as compared to CT (0.95 ± 0.02 vs. 0.81 ± 0.09, $p < 0.0005$), $T1W_{PP}$ (0.95 ± 0.02 vs. 0.85 ± 0.08, $p < 0.002$), T2W (0.95 ± 0.02 vs. 0.88 ± 0.04, $p < 0.001$), DWI (0.95 ± 0.02 vs. 0.89 ± 0.08, $p < 0.05$), and $T1W_{DP}$ (0.95 ± 0.02 vs. 0.90 ± 0.04, $p < 0.005$). Secondly, the inter-patient CV of the DSC_{IOmean} was the lowest in the fused MR images (2.4%), followed by $T1W_{DP}$ (4.6%), T2W (5.1%), DWI (8.5%), $T1W_{PP}$ (9.3%), and planning CT (11.8%). Thirdly, the planning CT images had lower inter-patient mean DSC_{IOmean} of GTV delineations than T2W ($p < 0.05$), DWI ($p < 0.05$), and $T1W_{DP}$ ($p < 0.05$).

Figure 4 illustrates the inter-observer CV of the GTV delineation DSC values (DSC_{IOCV}) of all patients in each of the six image sets. The inter-patient mean DSC_{IOCV} was 3.3%, 3.2%, 1.7%, 2.6%, 1.5%, and 0.9% for planning CT, $T1W_{PP}$, T2W, DWI, $T1W_{DP}$, and fused MR images, respectively. The fused MR exhibited the lowest inter-observer variability in liver HCC tumor delineation in the study.

Figure 5 visualizes GTV contours delineated by all four observers on the (A) planning CT, (B) $T1W_{PP}$, (C) $T1W_{DP}$, (D) T2W, (E) DWI, and (F) fused MR images of a representative patient. The planning CT image (**Figure 5A**) showed the lowest inter-observer consistency in GTV delineations. The four input MR images (**Figures 5B–E**) showed an improved inter-observer consistency in GTV delineation. Notably, the fused MR image (**Figure 5F**) yielded the highest inter-observer consistency in GTV delineation. This agrees with the DSC_{IOmean} and DSC_{IOCV} findings in **Figures 3** and **4**, demonstrating the highest consistency of GTV delineation between observers on the fused MR images.

4 DISCUSSION

With the rapid development in imaging and radiation treatment techniques, modern radiotherapy can deliver high ablative radiation dose more accurately to the tumor, leading to

TABLE 2 | Input MRI weight coefficients for the fused MRI with optimal tumor CNR of each patient.

Patient #	$T1W_{PP}$	$T1W_{DP}$	T2W	DWI
1	0.33	–0.33	1.00	0.17
2	1.00	–0.66	0.66	–0.17
3	0.83	–0.66	0.00	1.00
4	1.00	–0.33	0.00	–0.17
5	0.50	–0.17	0.66	0.66
6	1.00	–0.33	–0.17	0.00
7	0.83	–0.33	0.33	0.17
8	0.17	–0.33	0.66	0.17
9	0.33	–0.83	1.00	0.50
10	0.33	–0.33	0.83	0.00
Mean	0.63	–0.43	0.50	0.23
SD	0.33	0.21	0.43	0.38

CNR, contrast-to-noise ratio; $T1W_{PP}$, T1-weighted MRI at portal-venous phase; $T1W_{DP}$, T1-weighted MRI at 19-min delayed phase; T2W, T2-weighted; DWI, diffusion-weighted MRI.

improvement of the prognosis for unresectable HCC patients (24–27). Regardless of the chosen radiotherapy technique (intensity-modulated radiotherapy, stereotactic body radiotherapy, etc.), precise tumor delineation is a must and prerequisite for successful radiotherapy treatment. Inaccurate tumor delineation is a major source of errors and can lead to missing of the target during the radiotherapy delivery. It has a significant impact on the dose to the tumor and surrounding normal tissues. Visualization of the tumor and the tumor boundaries within normal tissues is critical for tumor delineation. For HCC, MRI provides superior soft-tissue contrast and therefore more clear tumor boundaries than CT and is a preferred modality for target delineation. MRI has been widely used for image registration with radiotherapy planning CT for tumor delineation in radiotherapy (28). It is an essential clinical procedure in the detection and characterization of HCC, with estimated sensitivity and specificity of 97.4% and 100% (29, 30).

However, there are some limitations of the current practice of MRI-based target delineation in radiotherapy: 1) only one set of MR sequences with a single weighting contrast can be reviewed at a time, making it time-consuming to review multiple sets of MR images during target delineation; 2) tumor contrast may vary significantly between patients and increase the variation and therefore uncertainty in target delineation. The MAMF method, as shown in this study, can be used to enhance MRI tumor contrast as well as its consistency between patients. The MAMF method is therefore a promising tool to overcome the abovementioned obstacles of MRI-based target delineation of HCC. To our best knowledge, this is the first study of systematic evaluation of the clinical efficacy of the MAMF method in HCC. It is worth noting that other challenges of MRI-based radiotherapy also exist, such as the potential of geometry distortion and the lack of electron density information for dose calculation. These areas have been actively studied in the research community (31).

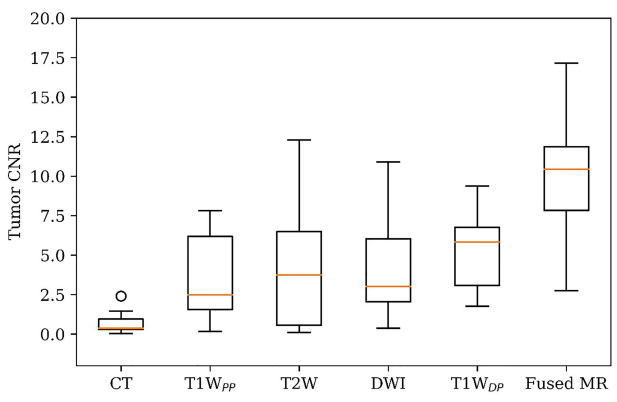

FIGURE 1 | Patient tumor CNR in planning CT, four original MR image sets, and fused MRI. CNR, contrast-to-noise ratio.

With the MAMF method applied in this study, the fused MRI demonstrated the highest tumor CNR and minimum inter-observer variability. It implies that the detectability and accuracy of tumor delineation of HCC could be enhanced in fused MRI. This improvement could reduce the probability of inaccurate GTV delineation and could affect the clinical outcomes of patients such as tumor local control rate and survival rate.

The four original MR image sets ($T1W_{PP}$, $T1W_{DP}$, T2W, and DWI) were used as input for the MAMF method in this study. These images are commonly used in HCC radiotherapy treatment planning and are typically included in routine abdomen MR imaging protocol. Most HCC lesions can be accurately diagnosed by T1W and T2W MR images (32), and DWI and contrast-enhanced MRI have been shown to be useful contributors to improve the accuracy of liver HCC diagnosis (33–36). It is also worth noting that the proposed MAMF method does not require all four types of MR images as input for performing image fusion. When fewer image modalities are applied as input, the model can be re-trained for generating the fused MR images. Apart from this, the MAMF method is not limited to the four studied MR sequences. Other types of MR images, such as T2/T1-weighted MRI using MR steady-state free precession sequences (22, 37), can also be used as input for MAMF and provide unique contributions to the contrast spectrum of the resulting fused MR images. The clinical efficacy of different MRI sequences combinations for MAMF is yet to be investigated. Besides, the fusion algorithm in the

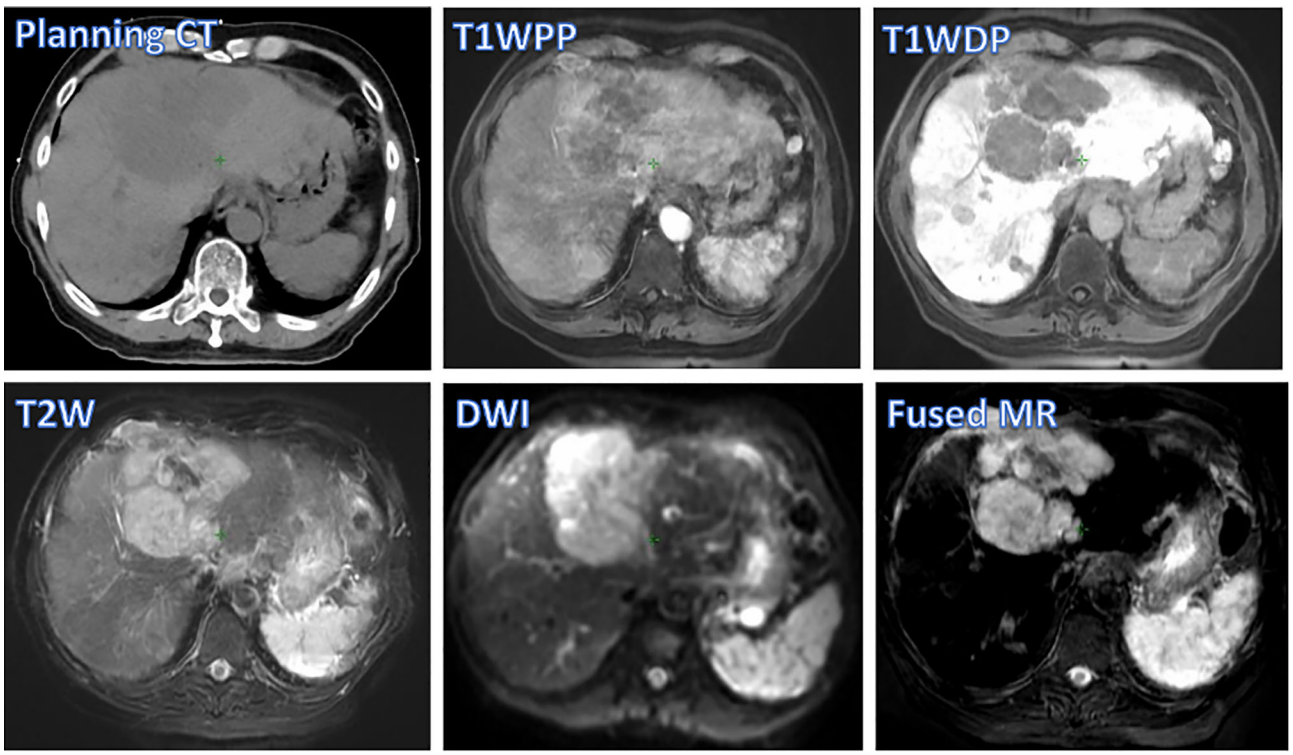

FIGURE 2 | Tumor visibility of a representative patient on various images: planning CT, four original MR sets ($T1W_{PP}$, $T1W_{DP}$, T2W, and DWI), and fused MRI. $T1W_{PP}$, T1-weighted MRI at portal-venous phase; $T1W_{DP}$, T1-weighted MRI at 19-min delayed phase; T2W, T2-weighted; DWI, diffusion-weighted MRI.

MAMF method is not restricted to specific treatment sites. Further exploration of the generalizability of the MAMF method to other treatment sites is warranted.

On the other hand, it is worth noting that respiratory motion has been demonstrated to adversely influence the quality of thoracic and abdominal images and cause uncertainties in tumor delineation (38, 39). Tremendous efforts have been made to assess a patient's respiratory motion during radiotherapy and to mitigate its impact on accurate treatment delivery (40–43). Therefore, to minimize the impact of the

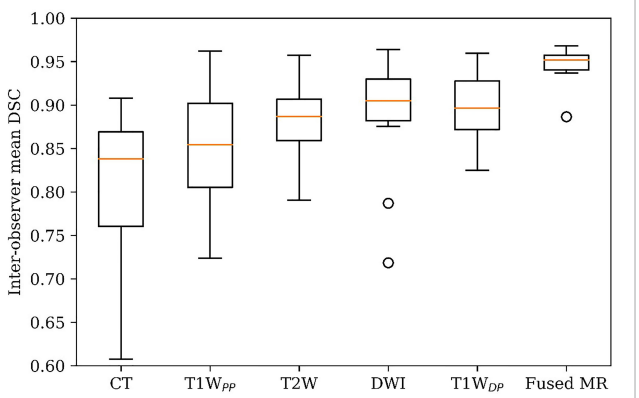

FIGURE 3 | GTV delineation inter-observer mean DSC on planning CT, four original MR image sets, and fused MRI. GTV, gross tumor volume; DSC, Dice similarity coefficient.

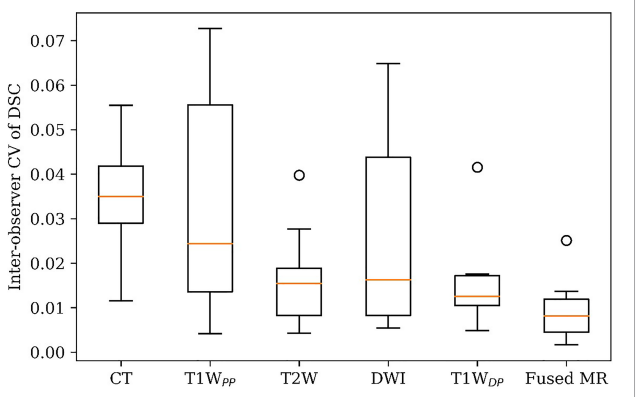

FIGURE 4 | GTV delineation inter-observer coefficient of variation (CV) of DSC on planning CT, four original MR sets, and fused MRI. GTV, gross tumor volume; DSC, Dice similarity coefficient.

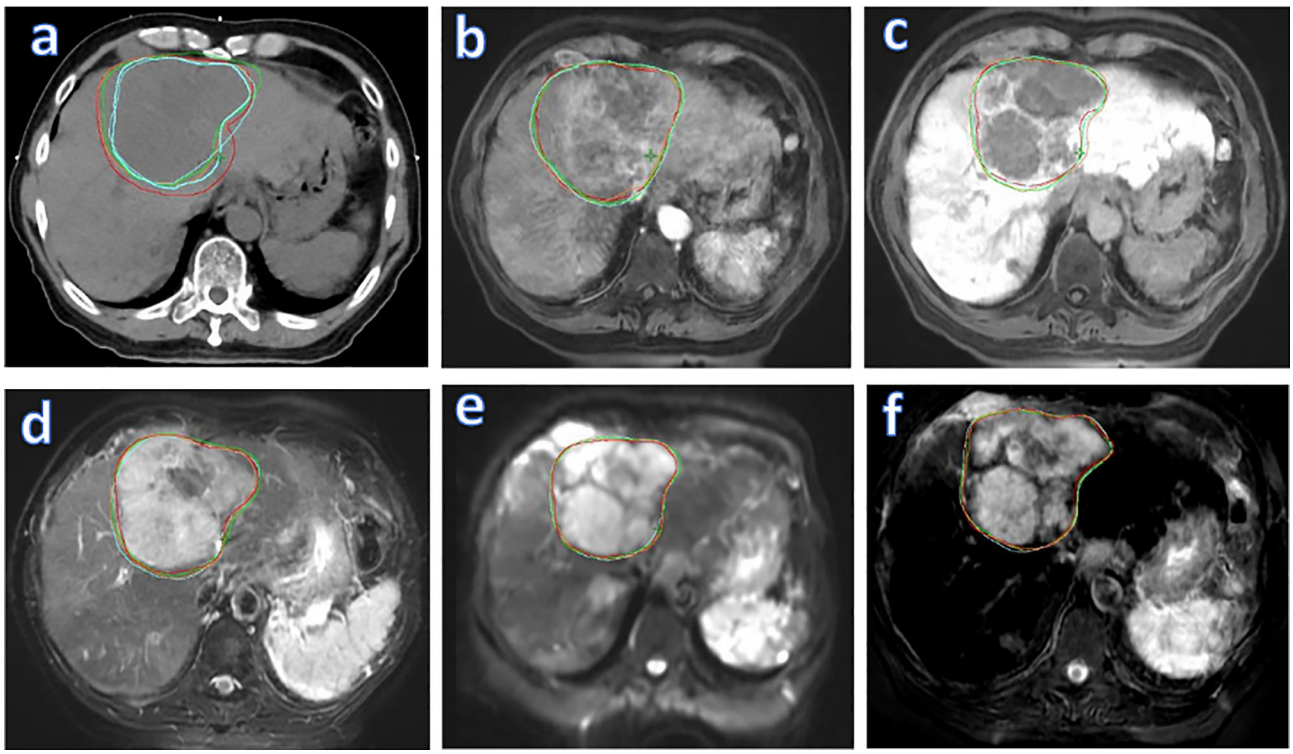

FIGURE 5 | Liver tumor delineation in a representative patient, illustrating different degrees of GTV contouring inter-observer consistency on various images: planning CT **(A)**, four original MR sets ($T1W_{PP}$ **(B)**, $T1W_{DP}$ **(C)**, T2W **(D)**, and DWI **(E)**], and fused MRI **(F)**. GTV, gross tumor volume; $T1W_{PP}$, T1-weighted MRI at portal-venous phase; $T1W_{DP}$, T1-weighted MRI at 19-min delayed phase; T2W, T2-weighted; DWI, diffusion-weighted MRI.

respiratory motion on the image quality, the acquisitions of the planning CT, $T1W_{PP}$, $T1W_{DP}$, and T2W MR images were performed during breath-holding. DWI images were acquired during the EOE phase using respiratory navigation due to its longer acquisition time. Intrinsically, the acquired "stationary" MR images might still have slight variations in the anatomic position due to potential different breathing depths (44, 45). To tackle this, the four input MR image sets were registered to planning CT by DIR prior to image fusion. It is worth noting that being a group of state-of-the-art registration methods, the DIR methods and their accuracy have been actively studied (46, 47). Advances in the DIR methods would further improve the accuracy of the multisource MRI fusion.

Recently, four-dimensional MRI (4D-MRI) has been an emerging technique for studying the impact of respiratory motion (23, 48, 49). Initial incorporation of 4D-MRI with the MAMF fusion method has been reported (22), suggesting that the MAMF method could be combined with 4D-MRI for enhanced tumor contrast and inter-observer target delineation consistency. One limitation of the study is a relatively small cohort size. As a feasibility study and initial evaluation, the results have demonstrated the capability of tumor CNR enhancements and GTV delineation consistency improvement by the MAMF method. The proposed method can benefit from more validation and testing in a larger cohort study before its consideration for clinical implementation. In future studies, we plan to use more patient cases and digital human phantoms, such as the 4D Digital Extended Cardiac-Torso (XCAT) phantom (50, 51), to more comprehensively evaluate the robustness and accuracy of the proposed method for mobile tumors.

5 CONCLUSION

The preliminary results in ten HCC patients demonstrated that the fused MRI generated using the MAMF method can enhance tumor CNR in HCC as compared with planning CT and four commonly used MR image sets ($T1W_{PP}$, $T1W_{DP}$, T2W, and DWI). The fused MRI can also improve the inter-observer consistency of GTV delineation. The MAMF method holds great promises for HCC tumor delineation and radiotherapy treatment planning.

DATA AVAILABILITY STATEMENT

The original contributions presented in the study are included in the article/supplementary material. Further inquiries can be directed to the corresponding author.

ETHICS STATEMENT

The studies involving human participants were reviewed and approved by The University of Hong Kong/Hospital Authority Institutional Review Board (HKU/HA HKW IRB). IRB/REC No. UW 21-397. Written informed consent for participation was not required for this study in accordance with the national legislation and the institutional requirements.

AUTHOR CONTRIBUTIONS

JC designed and directed the study. JC and ALC applied for study ethical approval. ALC and LZ designed and developed the methods and performed the experiments. ALC, AHC, CYL, AL, and VL managed the patient selection, data collection, and target delineation. ALC, LZ, and CYL performed the data analysis. ALC wrote the first draft. LZ, CL, TL, SKL, and JC revised the manuscript. JC approved the final version. All authors listed have made a substantial, direct, and intellectual contribution to the work and approved it for publication.

FUNDING

This work was partly supported by research grants of General Research Fund (GRF 15102118, GRF 15102219), the University Grants Committee; and Health and Medical Research Fund (HMRF 06173276), the Food and Health Bureau, The Government of the Hong Kong Special Administrative Regions.

REFERENCES

1. Sung H, Ferlay J, Siegel RL, Laversanne M, Soerjomataram I, Jemal A, et al. Global Cancer Statistics 2020: GLOBOCAN Estimates of Incidence and Mortality Worldwide for 36 Cancers in 185 Countries. *CA Cancer J Clin* (2021) 71:209–49. doi: 10.3322/caac.21660
2. Viale PH. The American Cancer Society's Facts & Figures: 2020 Edition. *J Adv Pract Oncol* (2020) 11:135–6. doi: 10.6004/jadpro.2020.11.2.1
3. Cheng JC, Wu JK, Huang CM, Huang DY, Cheng SH, Lin YM, et al. Radiation-Induced Liver Disease After Radiotherapy for Hepatocellular Carcinoma: Clinical Manifestation and Dosimetric Description. *Radiother Oncol* (2002) 63:41–5. doi: 10.1016/S0167-8140(02)00061-0
4. Boldrini L, Corradini S, Gani C, Henke L, Hosni A, Romano A, et al. MR-Guided Radiotherapy for Liver Malignancies. *Front Oncol* (2021) 11:616027. doi: 10.3389/fonc.2021.616027
5. Lanciano R, Lamond J, Yang J, Feng J, Arrigo S, Good M, et al. Stereotactic Body Radiation Therapy for Patients With Heavily Pretreated Liver Metastases and Liver Tumors. *Front Oncol* (2012) 2:23. doi: 10.3389/fonc.2012.00023
6. Hawkins MA, Brock KK, Eccles C, Moseley D, Jaffray D, Dawson LA. Assessment of Residual Error in Liver Position Using kV Cone-Beam Computed Tomography for Liver Cancer High-Precision Radiation Therapy. *Int J Radiat Oncol Biol Phys* (2006) 66:610–9. doi: 10.1016/j.ijrobp.2006.03.026
7. Yin FF, Wang Z, Yoo S, Wu QJ, Kirkpatrick J, Larrier N, et al. Integration of Cone-Beam CT in Stereotactic Body Radiation Therapy. *Technol Cancer Res Treat* (2008) 7:133–9. doi: 10.1177/153303460800700206
8. Rosenberg SA, Henke LE, Shaverdian N, Mittauer K, Wojcieszynski AP, Hullett CR, et al. A Multi-Institutional Experience of MR-Guided Liver Stereotactic Body Radiation Therapy. *Adv Radiat Oncol* (2019) 4:142–9. doi: 10.1016/j.adro.2018.08.005
9. Witt JS, Rosenberg SA, Bassetti MF. MRI-Guided Adaptive Radiotherapy for Liver Tumours: Visualising the Future. *Lancet Oncol* (2020) 21:e74–82. doi: 10.1016/S1470-2045(20)30034-6
10. Yang J, Cai J, Wang H, Chang Z, Czito BG, Bashir MR, et al. Four-Dimensional Magnetic Resonance Imaging Using Axial Body Area as Respiratory Surrogate: Initial Patient Results. *Int J Radiat Oncol Biol Phys* (2014) 88:907–12. doi: 10.1016/j.ijrobp.2013.11.245
11. Harris W, Wang C, Yin FF, Cai J, Ren L. A Novel Method to Generate on-Board 4D MRI Using Prior 4D MRI and on-Board kV Projections From a Conventional LINAC for Target Localization in Liver SBRT. *Med Phys* (2018) 45:3238–45. doi: 10.1002/mp.12998
12. Goodman KA, Wiegner EA, Maturen KE, Zhang Z, Mo Q, Yang G, et al. Dose-Escalation Study of Single-Fraction Stereotactic Body Radiotherapy for Liver Malignancies. *Int J Radiat Oncol Biol Phys* (2010) 78:486–93. doi: 10.1016/j.ijrobp.2009.08.020
13. Hong TS, Wo JY, Yeap BY, Ben-Josef E, McDonnell EI, Blaszkowsky LS, et al. Multi-Institutional Phase II Study of High-Dose Hypofractionated Proton Beam Therapy in Patients With Localized, Unresectable Hepatocellular Carcinoma and Intrahepatic Cholangiocarcinoma. *J Clin Oncol* (2016) 34:460–8. doi: 10.1200/JCO.2015.64.2710
14. Zhou N, Hu A, Shi Z, Wang X, Zhu Q, Zhou Q, et al. Inter-Observer Agreement of Computed Tomography and Magnetic Resonance Imaging on Gross Tumor Volume Delineation of Intrahepatic Cholangiocarcinoma: An Initial Study. *Quant Imaging Med Surg* (2021) 11:579–85. doi: 10.21037/qims-19-1093
15. Hong TS, Bosch WR, Krishnan S, Kim TK, Mamon HJ, Shyn P, et al. Interobserver Variability in Target Definition for Hepatocellular Carcinoma With and Without Portal Vein Thrombus: Radiation Therapy Oncology Group Consensus Guidelines. *Int J Radiat Oncol Biol Phys* (2014) 89:804–13. doi: 10.1016/j.ijrobp.2014.03.041
16. Bundschuh RA, Andratschke N, Dinges J, Duma MN, Astner ST, Brügel M, et al. Respiratory Gated [18F]FDG PET/CT for Target Volume Delineation in Stereotactic Radiation Treatment of Liver Metastases. *Strahlenther Onkol* (2012) 188:592–8. doi: 10.1007/s00066-012-0094-3
17. Barboriak DP, Zhang Z, Desai P, Snyder BS, Safriel Y, McKinstry RC, et al. Interreader Variability of Dynamic Contrast-Enhanced MRI of Recurrent Glioblastoma: The Multicenter ACRIN 6677/RTOG 0625 Study. *Radiology* (2019) 290:467–76. doi: 10.1148/radiol.2019181296
18. Lestra T, Kanagaratnam L, Mule S, Janvier A, Brixi H, Cadiot G, et al. Measurement Variability of Liver Metastases From Neuroendocrine Tumors on Different Magnetic Resonance Imaging Sequences. *Diagn Interv Imaging* (2018) 99:73–81. doi: 10.1016/j.diii.2017.12.009
19. Vinod SK, Jameson MG, Min M, Holloway LC. Uncertainties in Volume Delineation in Radiation Oncology: A Systematic Review and Recommendations for Future Studies. *Radiother Oncol* (2016) 121:169–79. doi: 10.1016/j.radonc.2016.09.009
20. Zhang J, Srivastava S, Wang C, Beckham T, Johnson C, Dutta P, et al. Clinical Evaluation of 4D MRI in the Delineation of Gross and Internal Tumor Volumes in Comparison With 4DCT. *J Appl Clin Med Phys* (2019) 20:51–60. doi: 10.1002/acm2.12699
21. Zhang L, Yin FF, Moore B, Han S, Cai J. A Multisource Adaptive Magnetic Resonance Image Fusion Technique for Versatile Contrast Magnetic Resonance Imaging. *Cancer Transl Med* (2018) 4:65–9. doi: 10.4103/ctm.ctm_21_18
22. Zhang L, Yin FF, Li T, Teng X, Xiao H, Harris W, et al. Multi-Contrast Four-Dimensional Magnetic Resonance Imaging (MC-4D-MRI): Development and Initial Evaluation in Liver Tumor Patients. *Med Phys* (2021) 48:7984–97. doi: 10.1002/mp.15314
23. Liu Y, Yin FF, Czito BG, Bashir MR, Cai J. T2-Weighted Four Dimensional Magnetic Resonance Imaging With Result-Driven Phase Sorting. *Med Phys* (2015) 42:4460–71. doi: 10.1118/1.4923168

24. Feng M, Ben-Josef E. Radiation Therapy for Hepatocellular Carcinoma. *Semin Radiat Oncol* (2011) 21:271–7. doi: 10.1016/j.semradonc.2011.05.002
25. Dawson LA. Overview: Where Does Radiation Therapy Fit in the Spectrum of Liver Cancer Local-Regional Therapies? *Semin Radiat Oncol* (2011) 21:241–6. doi: 10.1016/j.semradonc.2011.05.009
26. Kele PG, van der Jagt EJ. Diffusion Weighted Imaging in the Liver. *World J Gastroenterol* (2010) 16:1567–76. doi: 10.3748/wjg.v16.i13.1567
27. Marin D, Di Martino M, Guerrisi A, De Filippis G, Rossi M, Ginanni Corradini S, et al. Hepatocellular Carcinoma in Patients With Cirrhosis: Qualitative Comparison of Gadobenate Dimeglumine-Enhanced MR Imaging and Multiphasic 64-Section CT. *Radiology* (2009) 251:85–95. doi: 10.1148/radiol.2511080400
28. Dirix P, Haustermans K, Vandecaveye V. The Value of Magnetic Resonance Imaging for Radiotherapy Planning. *Semin Radiat Oncol* (2014) 24:151–9. doi: 10.1016/j.semradonc.2014.02.003
29. Becker-Weidman DJ, Kalb B, Sharma P, Kitajima HD, Lurie CR, Chen Z, et al. Hepatocellular Carcinoma Lesion Characterization: Single-Institution Clinical Performance Review of Multiphase Gadolinium-Enhanced MR Imaging–Comparison to Prior Same-Center Results After MR Systems Improvements. *Radiology* (2011) 261:824–33. doi: 10.1148/radiol.11110157
30. Ayuso C, Rimola J, García-Criado Á. Imaging of HCC. *Abdom Imaging* (2012) 37:215–30. doi: 10.1007/s00261-011-9794-x
31. Owrangi AM, Greer PB, Glide-Hurst CK. MRI-Only Treatment Planning: Benefits and Challenges. *Phys Med Biol* (2018) 63:05TR1. doi: 10.1088/1361-6560/aaaca4
32. Yu NC, Chaudhari V, Raman SS, Lassman C, Tong MJ, Busuttil RW, et al. CT and MRI Improve Detection of Hepatocellular Carcinoma, Compared With Ultrasound Alone, in Patients With Cirrhosis. *Clin Gastroenterol Hepatol* (2011) 9:161–7. doi: 10.1016/j.cgh.2010.09.017
33. Sandrasegaran K, Akisik FM, Lin C, Tahir B, Rajan J, Aisen AM. The Value of Diffusion-Weighted Imaging in Characterizing Focal Liver Masses. *Acad Radiol* (2009) 16:1208–14. doi: 10.1016/j.acra.2009.05.013
34. Taouli B, Koh D-M. Diffusion-Weighted MR Imaging of the Liver. *Radiology* (2010) 254:47–66. doi: 10.1148/radiol.09090021
35. Culverwell AD, Sheridan MB, Guthrie JA, Scarsbrook AF. Diffusion-Weighted MRI of the Liver-Interpretative Pearls and Pitfalls. *Clin Radiol* (2013) 68:406–14. doi: 10.1016/j.crad.2012.08.008
36. Gandhi SN, Brown MA, Wong JG, Aguirre DA, Sirlin CB. MR Contrast Agents for Liver Imaging: What, When, How. *Radiographics* (2006) 26:1621–36. doi: 10.1148/rg.266065014
37. Fernandes AT, Apisarnthanarax S, Yin L, Zou W, Rosen M, Plastaras JP, et al. Comparative Assessment of Liver Tumor Motion Using Cine-Magnetic Resonance Imaging Versus 4-Dimensional Computed Tomography. *Int J Radiat Oncol Biol Phys* (2015) 91:1034–40. doi: 10.1016/j.ijrobp.2014.12.048
38. Ge H, Cai J, Kelsey CR, Yin FF. Quantification and Minimization of Uncertainties of Internal Target Volume for Stereotactic Body Radiation Therapy of Lung Cancer. *Int J Radiat Oncol Biol Phys* (2013) 85:438–43. doi: 10.1016/j.ijrobp.2012.04.032
39. Liu C, Pierce LA2nd, Alessio AM, Kinahan PE. The Impact of Respiratory Motion on Tumor Quantification and Delineation in Static PET/CT Imaging. *Phys Med Biol* (2009) 54:7345–62. doi: 10.1088/0031-9155/54/24/007
40. Cai J, Read PW, Larner JM, Jones DR, Benedict SH, Sheng K. Reproducibility of Interfraction Lung Motion Probability Distribution Function Using Dynamic MRI: Statistical Analysis. *Int J Radiat Oncol Biol Phys* (2008) 72:1228–35. doi: 10.1016/j.ijrobp.2008.07.028
41. Chang Z, Liu T, Cai J, Chen Q, Wang Z, Yin FF. Evaluation of Integrated Respiratory Gating Systems on a Novalis Tx System. *J Appl Clin Med Phys* (2011) 12:3495. doi: 10.1120/jacmp.v12i3.3495
42. Harris W, Yin FF, Wang C, Zhang Y, Cai J, Ren L. Accelerating Volumetric Cine MRI (VC-MRI) Using Undersampling for Real-Time 3D Target Localization/Tracking in Radiation Therapy: A Feasibility Study. *Phys Med Biol* (2017) 63:01NT. doi: 10.1088/1361-6560/aa9746
43. Liu Y, Yin FF, Rhee D, Cai J. Accuracy of Respiratory Motion Measurement of 4D-MRI: A Comparison Between Cine and Sequential Acquisition. *Med Phys* (2016) 43:179. doi: 10.1118/1.4938066
44. Dawson LA, Eccles C, Bissonnette JP, Brock KK. Accuracy of Daily Image Guidance for Hypofractionated Liver Radiotherapy With Active Breathing Control. *Int J Radiat Oncol Biol Phys* (2005) 62:1247–52. doi: 10.1016/j.ijrobp.2005.03.072
45. Mast M, Kouwenhoven E, Roos J, van Geen S, van Egmond J, van Santvoort J, et al. Two Years' Experience With Inspiration Breath-Hold in Liver SBRT. *Tech Innov Patient Support Radiat Oncol* (2018) 7:1–5. doi: 10.1016/j.tipsro.2018.04.001
46. Rigaud B, Simon A, Castelli J, Lafond C, Acosta O, Haigron P, et al. Deformable Image Registration for Radiation Therapy: Principle, Methods, Applications and Evaluation. *Acta Oncol* (2019) 58:1225–37. doi: 10.1080/0284186X.2019.1620331
47. Wu RY, Liu AY, Yang J, Williamson TD, Wisdom PG, Bronk L, et al. Evaluation of the Accuracy of Deformable Image Registration on MRI With a Physical Phantom. *J Appl Clin Med Phys* (2020) 21:166–73. doi: 10.1002/acm2.12789
48. Du D, Caruthers SD, Glide-Hurst C, Low DA, Li HH, Mutic S, et al. High-Quality T2-Weighted 4-Dimensional Magnetic Resonance Imaging for Radiation Therapy Applications. *Int J Radiat Oncol Biol Phys* (2015) 92:430–7. doi: 10.1016/j.ijrobp.2015.01.035
49. Hu Y, Caruthers SD, Low DA, Parikh PJ, Mutic S. Respiratory Amplitude Guided 4-Dimensional Magnetic Resonance Imaging. *Int J Radiat Oncol Biol Phys* (2013) 86:198–204. doi: 10.1016/j.ijrobp.2012.12.014
50. Panta RK, Segars P, Yin FF, Cai J. Establishing a Framework to Implement 4D XCAT Phantom for 4D Radiotherapy Research. *J Cancer Res Ther* (2012) 8:565–70. doi: 10.4103/0973-1482.106539
51. Segars WP, Tsui BMW, Cai J, Yin FF, Fung GSK, Samei E. Application of the 4-D XCAT Phantoms in Biomedical Imaging and Beyond. *IEEE Trans Med Imaging* (2018) 37:680–92. doi: 10.1109/TMI.2017.2738448

Conflict of Interest: The authors declare that the research was conducted in the absence of any commercial or financial relationships that could be construed as a potential conflict of interest.

The reviewer JW declared a shared affiliation, with no collaboration, with two of the authors, LZ, JC, to the handling editor at the time of the review.

frontiers | Frontiers in Oncology

ORIGINAL RESEARCH
published: 27 April 2022
doi: 10.3389/fonc.2022.882272

Hypofractionated Radiotherapy for Palliation of Main Portal Vein Tumor Thrombosis

Fang Fang[1†], *Bin Qiu*[2†], *Peng Zhen*[1*] *and Junjie Wang*[2*]

[1] Department of Radiation Oncology, Chifeng Tumor Hospital, Chifeng, China, [2] Department of Radiation Oncology, Peking University Third Hospital, Beijing, China

OPEN ACCESS

Edited by:
An Liu,
City of Hope National Medical Center, United States

Reviewed by:
Alessandro Granito, University of Bologna, Italy
Yasuo Yoshioka, Japanese Foundation for Cancer Research, Japan

***Correspondence:**
Peng Zhen
d_roc@sina.com
Junjie Wang
junjiewang@pku.edu.cn

[†]These authors have contributed equally to this work

Specialty section:
This article was submitted to Radiation Oncology, a section of the journal Frontiers in Oncology

Received: 23 February 2022
Accepted: 30 March 2022
Published: 27 April 2022

Citation:
Fang F, Qiu B, Zhen P and Wang J (2022) Hypofractionated Radiotherapy for Palliation of Main Portal Vein Tumor Thrombosis. Front. Oncol. 12:882272. doi: 10.3389/fonc.2022.882272

Background: Hypofractionated radiotherapy delivered for portal vein tumor thrombosis (PVTT) located in the main portal vein is rarely exploited. The study aimed to evaluate the efficacy and safety of hypofractionated radiotherapy as palliative treatment for PVTT in cirrhotic patients with hepatocellular carcinoma.

Methods: From March 2016 to July 2020, 16 patients (mean age, 59.1 ± 6.3 years; 15 men) with hepatocellular carcinoma and hepatitis virus-related cirrhosis who underwent hypofractionated radiotherapy for PVTT (located in the main portal vein) in our institute were retrospectively reviewed.

Results: Complete response of the PVTT was observed in 4 cases (25%) with partial response in 7 cases (43.75%) and stable disease in 5 cases (31.25%). Symptom relief was observed in all 7 patients suffering from ventosity. The median time to progression was 6 months (interquartile range, IQR: 6–12 months). Eight patients (50%) failed due to primary cancer progression, 7 patients failed due to extrahepatic metastasis, and only 1 patient failed due to PVTT progression. The median overall survival was 17.4 months (IQR: 8–25 months). Grade I/II anorexia/nausea was observed in 14 patients (87.5%) and Grade I/II leukopenia was observed in 14 patients (87.5%). No complications ≥ Grade III were observed.

Conclusions: Hypofractionated radiotherapy as palliative treatment appears effective and safe for PVTT located in the main portal vein in cirrhotic patients with advanced hepatocellular carcinoma, yielding a high rate of tumor response. Further study is warranted.

Keywords: hypofractionated radiotherapy, portal vein tumor thrombosis, hepatocellular carcinoma, cirrhosis, palliation

BACKGROUND

Hepatocellular carcinoma (HCC) is the third leading cause of cancer-related death worldwide. Advanced HCC is usually the case when the cancer is initially diagnosed due to the asymptomatic nature of HCC. Portal vein tumor thrombosis (PVTT) is frequent in patients with advanced HCC and has been reported in as many as 44%–84% of patients from autopsy data and in 31%–50% from clinical data (1). The prognosis for these patients remains discouraging with a median survival of only 2.7 months without treatment (2).

The recommended therapeutic methods for PVTT are systemic therapy usually with targeted drugs or recently reported atezolizumab plus bevacizumab regimen (3–8), which is promising while unlikely to be a cost-effective option (9). Notably, PVTT can obstruct portal venous flow and worsen portal hypertension (10). An approach using local therapy and systemic agents before progression should be investigated (11). In selected patients with good hepatic reserves, surgical resection and radioembolization may be attempted (11–13). However, these local therapies were either invasive or inexhaustive and only applicable to a small range of patients.

Recently, external beam radiation therapy (EBRT) was recommended as a non-invasive local therapeutic option for PVTT, and promising results have been noted (12–17). However, hypofractionated radiotherapy for PVTT located in the main portal vein is rarely exploited (18). Hypofractionated radiotherapy was conducted as a palliative treatment for PVTT of the main portal vein in our institute. Here, the study aimed to evaluate the efficacy and safety of hypofractionated radiotherapy as palliative treatment for PVTT located in the main portal vein only in cirrhotic patients with hepatocellular carcinoma.

METHODS

Study Design

The retrospective study complies with the Declaration of Helsinki and was approved by our institutional review board. The written informed consent was obtained. The documented clinical data from March 2016 to July 2020 in our institute were retrospectively reviewed. Cirrhotic patients with advanced hepatocellular carcinoma who underwent hypofractionated radiotherapy for the main PVTT only were included. The indication of hypofractionated radiotherapy was the intent to control PVTT in the main portal vein in cirrhotic patients with or without portal hypertension symptoms. The contraindications of hypofractionated radiotherapy were as follows: (i) uncontrolled intrahepatic/extrahepatic lesion; (ii) liver function of Child–Pugh Class C; (iii) renal failure; (iv) active portal hypertension, confirmed by upper endoscopy and the presence of symptoms (i.e., gastrointestinal bleeding or refractory ascites); (v) poor condition with Eastern Cooperative Oncology Group (ECOG) score > 2 or expected life span < 1 month; and (vi) pregnancy. All patients had signed an informed consent form for hypofractionated radiotherapy using Gamma-knife.

Definitions

The PVTT response, symptom relief, time to progression (TTP), overall survival, and complication after hypofractionated radiotherapy were recorded. The PVTT response was evaluated based on the consensus of 2 investigators according to the Response Evaluation Criteria in Solid Tumors on the first computed tomography (CT) or magnetic resonance imaging (MRI) image within 3 months after hypofractionated radiotherapy (19). Symptom relief was recorded according to the patient's complaint at the first-time follow-up after hypofractionated radiotherapy. TTP was defined as the time from the hypofractionated radiotherapy initialization until tumor progression including not only PVTT but also any intrahepatic or extrahepatic tumor progression. Overall survival was defined as the interval between hypofractionated radiotherapy initialization and death from any cause. Complications were determined by the Common Terminology Criteria for Adverse Events (CTCAE) v4.0 (CTCA) (20).

Study Population

A total of 16 patients (mean age, 59.1 ± 6.3 years; 15 men) were included in the analysis. All the patients were clinically diagnosed with Barcelona Clinical Liver Cancer (BCLC) stage C HCC according to the European Society for Medical Oncology (ESMO) Clinical Practice Guidelines (21), along with hepatitis B (n = 15)/C (n = 1) virus-related cirrhosis. The PVTTs were all in the main portal vein (Vp4) and diagnosed by both enhanced CT and MRI according to the Japan criterion (22). Fourteen (87.5%) patients had portal hypertension, while only 1 (6.25%) patient had ascites and 7 (43.8%) patients had ventosity. The liver function of the patients was Child–Pugh stage A in 12 patients and stage B in 4 patients, all with ECOG performance score 1. The summary of the patients is listed in **Table 1**. Ten (62.5%) patients combined with previous or post-treatment for primary tumor control. Only one patient (No. 16) received Lenvatinib and another patient (No. 13) received anti-PD-1; the remaining patients refused systemic therapy due to medical charges. Two patients (Nos. 2 and 14) could not receive transarterial chemoembolization (TACE) before radiotherapy because of PVTT and portal vein recanalization after radiotherapy provides TACE treatment opportunity.

Hypofractionated Radiotherapy

Hypofractionated radiotherapy was performed using a Gamma-knife (OUR-QGD/B Version, Shenzhen Aowo Medical New Technology Co., Ltd) loaded with $Cobalt^{60}$. All patients underwent enhanced CT with a slice thickness of 2 mm for detection of the lesion after placing the stereotactic frame. Contouring of the PVTT and organ at risk (OAR) was then conducted. The treatment plans were developed using treatment

Abbreviations: PVTT, portal vein tumor thrombosis; SD, stable disease; IQR, interquartile range; HCC, hepatocellular carcinoma; EBRT, external beam radiation therapy; TACE, transarterial chemoembolization; ECOG, Eastern Cooperative Oncology Group; TTP, time to progression; CT, computed tomography; MRI, magnetic resonance imaging; CTCAE, Common Terminology Criteria for Adverse Events; BCLC, Barcelona Clinical Liver Cancer; ESMO, European Society for Medical Oncology; OAR, organ at risk; CR, complete response; PR, partial response; SD, stable disease; PD, progressive disease; 3D-CRT, three-dimensional conformal radiotherapy.

TABLE 1 | Summary of the 16 patients.

Patients	Sex	Age	CP	PH	Combined treatment	Dose/fraction	Symptom relief	PVTT-R	Failure	TTP	OS	Complications	Prognosis
1	M	55	B	Yes	Pre-TACE (PD)	45 Gy/15F	Ventosity relief; Ascites reduced	SD	Primary cancer progression	3	6.9	None	Died due to primary tumor progression
2	F	66	A	Yes	Post-TACE	8.8 Gy/4F +26.4 Gy/11F	Ventosity relief	PR	Extrahepatic metastasis	24	31.3	Grade 2 anorexia/nausea	Died due to extrahepatic metastasis
3	M	55	B	Yes	None	45 Gy/15F	Ventosity relief	CR	Extrahepatic metastasis	6	20.5	Grade 2 anorexia/nausea; Grade 1 leukopenia	Died due to extrahepatic metastasis
4	M	47	A	Yes	None	36.4 Gy/13F	Ventosity relief	PR	Primary cancer progression	12	25.0	Grade 1 anorexia/nausea; Grade 1 leukopenia	Died due to cachexia
5	M	58	A	Yes	Pre-TACE (PD)	33.8 Gy/13F	Without Symptom	PR	Extrahepatic metastasis	12	17.6	Grade 2 anorexia/nausea; Grade 2 leukopenia	Died due to cachexia
6	M	63	A	Yes	Post-HIFU for primary	25 Gy/10F	Ventosity relief	SD	Primary cancer progression	3	7.7	Grade 2 anorexia/nausea; Grade 1 leukopenia	Died due to hepatorenal syndrome and extrahepatic metastasis
7	M	56	A	Yes	Pre-TACE+ RT (PR); Post-TACE	45 Gy/15F	Without symptom	CR	Primary cancer progression	12	44.2	Grade 1 anorexia/nausea; Grade 1 leukopenia	Died due to tumor progression
8	M	64	A	Yes	None	39 Gy/13F	Without symptom	CR	Extrahepatic metastasis	12	17.4	Grade 2 anorexia/nausea; Grade 2 leukopenia	Died due to liver failure and extrahepatic metastasis
9	M	58	A	Yes	None	45 Gy/15F	Ventosity relief	PR	Extrahepatic metastasis	12	16.4	Grade 2 anorexia/nausea; Grade 2 leukopenia	Died due to liver failure and extrahepatic metastasis
10	M	58	A	Yes	Pre-HAIC	39 Gy/13F	Without symptom	PR	Extrahepatic metastasis	12	14.6	Grade 1 anorexia/nausea; Grade 2 leukopenia	Died due to cachexia and extrahepatic metastasis
11	M	55	A	Yes	Pre-+post-TACE	45 Gy/15F	Without symptom	CR	Primary cancer progression	36	40.5	Grade 2 anorexia/nausea; Grade 2 leukopenia	Alive
12	M	51	A	Yes	None	39 Gy/13F	Without symptom	PR	PVTT progression	3	12	Grade 2 anorexia/nausea; Grade 2 leukopenia	Alive
13	M	68	A	Yes	Post-anti-PD-1	45 Gy/15F	Ventosity relief	SD	Primary cancer progression	6	8.6	Grade 1 anorexia/nausea; Grade 1 leukopenia	Died due to variceal bleeding
14	M	71	B	Yes	Pre-RFA (CR); Post-TACE	45 Gy/15f	Without symptom	PR	Primary cancer progression	6	10.2	Grade 1 anorexia/nausea; Grade 1 leukopenia	Alive
15	M	62	A	No	None	30 Gy/10F	Without symptom	SD	Primary cancer progression	6	6	Grade 2 anorexia/nausea; Grade 1 leukopenia	Died due to tumor progression
16	M	58	B	No	Pre-TACE+ Lenvatinib	45 Gy/15f	Without symptom	SD	Extrahepatic metastasis	6	6.4	Grade 1 leukopenia	Alive

CP, Child–Pugh; PH, portal hypertension; M, male; F, female; Pre-, previous; Post-, post-Gamma-knife radiotherapy; PVTT-R, portal vein tumor thrombosis response; TACE, transarterial chemoembolization; HIFU, high-intensity focused ultrasound; RT, radiotherapy; PD, progression disease; PR, partial response; CR, complete response; TTP, time to progression; OS, overall survival.

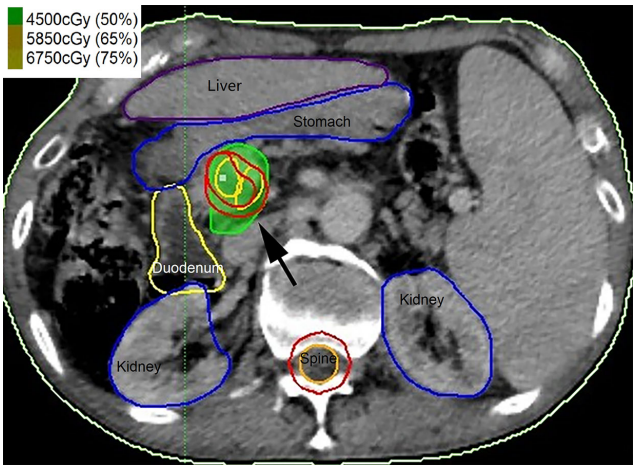

FIGURE 1 | Contouring of the portal vein tumor thrombosis (PVTT) (black arrow) and organ at risk (OAR) and the treatment plans were developed.

plan systems (Shenzhen Aowo Medical New Technology Co., Ltd) (**Figure 1**). The prescription dose was individualized and usually 30–45 Gy delivered in 10–15 fractions. The actual dosimetry parameter of the OARs for the patient is listed in **Table 2**.

Follow-Up

The patients were routinely followed within the first month, 2- to 3-month intervals within the first 2 years, and 3- to 6-month intervals thereafter. Enhanced CT/MRI was conducted to assess the response of the tumor 1–3 months after hypofractionated radiotherapy.

Statistical Analysis

The data were expressed as mean ± standard deviation or median (interquartile range, IQR). The TTP and overall survival analysis were evaluated by the Kaplan–Meier method. SPSS statistical software (version 26.0) was used.

TABLE 2 | The actual dosimetry parameter of the OARs for the 16 patients.

Patients	Stomach Dmax (cGy)	Duodenum Dmax (cGy)	Liver mean dose (cGy)	Cord Dmax (cGy)
1	3,604.4	2,809.4	1,445.2	507.6
2	2,709.1	3,200.6	1,167.2	669.1
3	3,098.2	2,760.6	1,203.4	612.9
4	2,908.5	3,400.7	1,156.7	709.8
5	2,557.8	2,908.7	1,321.5	700
6	3,120.6	3,320.5	899.2	601.6
7	1,600.8	3,609.5	1,006.7	907.6
8	2,099.5	2,500.8	954.5	812.9
9	1,870.5	3,509	1,207.7	615
10	2,234.9	3,621.3	1,165.5	652
11	1,866.3	3,456.7	1,098.4	602.6
12	1,504.7	2,318.9	1,149.6	737.9
13	3,550.8	2,710.6	1,151.4	281.5
14	1,455.6	2,730.5	1,045.7	723.6
15	3,145.4	3,579.9	987.7	908.8
16	3,500.6	3,764.8	1,380.4	642.8

Dmax, maximum dose; OARs, organs at risk.

RESULTS

PVTT Response

Complete response (CR) was observed in 4 cases (25%), partial response (PR) was observed in 7 cases (43.75%), stable disease (SD) was observed in 5 cases (31.25%), and progressive disease (PD) was not found (**Figure 2**). Symptom relief was observed in all 7 patients with ventosity.

Treatment Failure and Overall Survival

The median TTP was 6 months (IQR: 6–12 months). Eight patients (50%) failed due to primary cancer progression, 7 patients failed due to extrahepatic metastasis, and only 1 patient failed due to PVTT progression (patient no. 12).

The median overall survival was 17.4 months (IQR: 8–25 months) (**Figure 3**). Patients with CR/PR were associated with longer OS (6–36 months) compared with that of SD (3–6 months).

Until January 17, 2021, 4 patients (25%) were still alive and 8 patients died due to cachexia, liver failure, primary tumor progression, extrahepatic metastasis, hepatorenal syndrome, or variceal bleeding.

Complications

Grade I/II anorexia/nausea was observed in 14 patients (87.5%) and Grade I/II leukopenia was observed in 14 patients (87.5%). All recovered without a prolonged hospital stay. No complications ≥ Grade III were observed (**Table 1**).

DISCUSSION

In the retrospective study of 16 patients, hypofractionated radiotherapy as palliative treatment appears effective and safe for PVTT located in the main portal vein only in cirrhotic patients with advanced hepatocellular carcinoma yielding a high rate of tumor response.

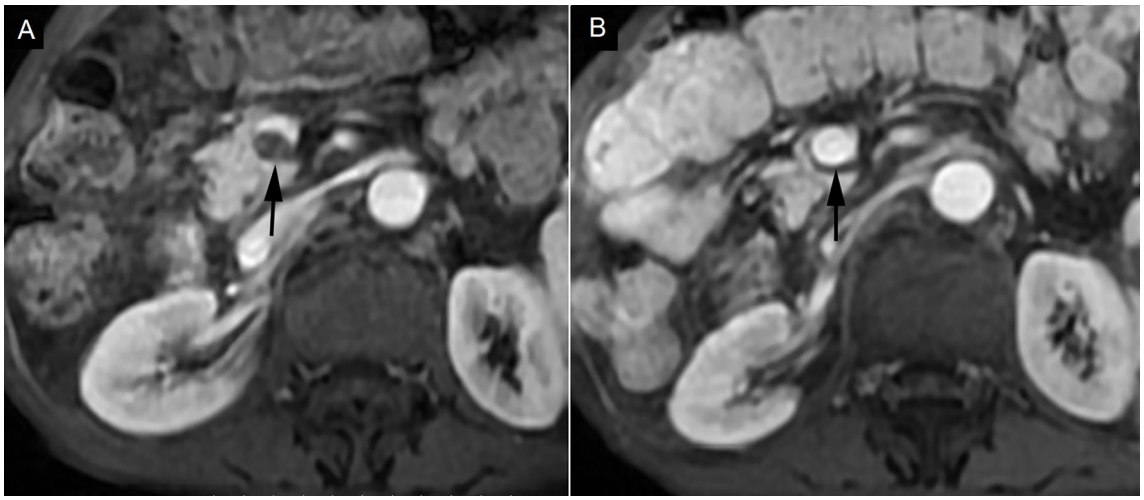

FIGURE 2 | Complete response in a patient with portal vein tumor thrombosis (PVTT). **(A)** PVTT was shown in the main portal vein (black arrow). **(B)** PVTT was eliminated 3 months after hypofractionated radiotherapy (black arrow).

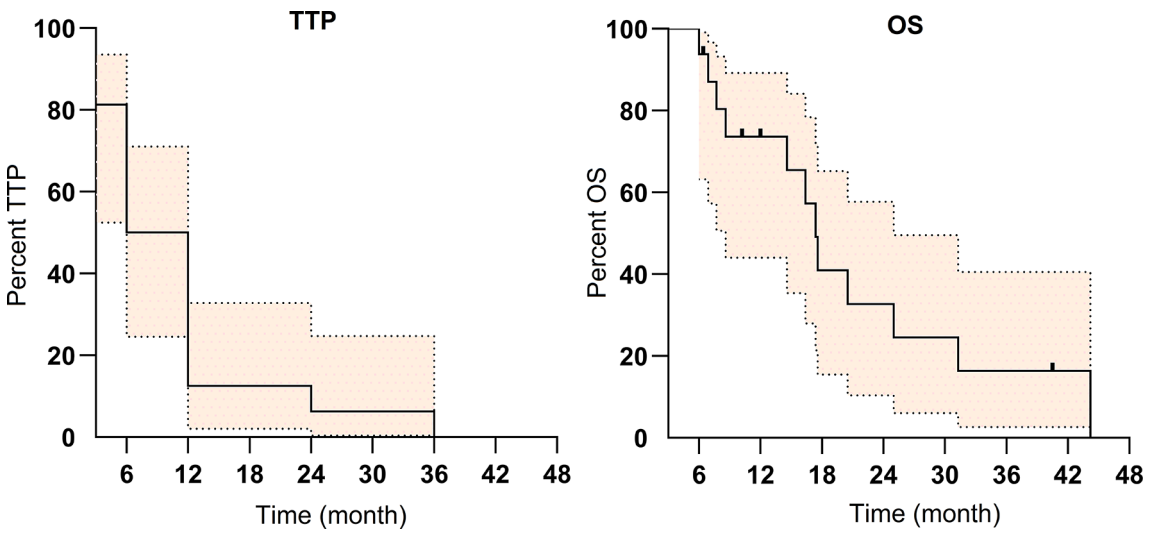

FIGURE 3 | The Kaplan–Meier survival curve of time to progression (TTP) and overall survival (OS) for the 16 patients with portal vein tumor thrombosis (PVTT) (colored area refers to 95% confidence interval).

Both the response rate of PVTT and patient survival in the present study were superior to the previously published studies involving EBRT for PVTT (14). In an overview reported by Lee et al. (14), the response rate of three-dimensional conformal radiotherapy (3D-CRT) delivered to PVTT alone was about 50%–75% and that was 40%–50% when delivered to both the PVTT and primary cancer (14). The median survival was reported at 7–8 months for EBRT delivered to PVTT alone and 5 months for non-responders/20 months for responders when delivered to both the PVTT and primary cancer (14). Kim et al. reported hypofractionated radiotherapy using helical tomotherapy for PVTT in 35 patients, and there was a CR in 5 patients (14.3%), PR only in 10 patients (28.6%), SD in 18 patients (51.4%), and PD in 2 patients (5.7%) (16). These historical data were all inferior to that of the present study. The reason for the difference may be that the PVTT located in the main portal may benefit more from focused radiotherapy (23, 24). In the present study, the combination with other treatments, e.g., transarterial chemoembolization in some patients (25–27), and relative high response rate of PVTT may contribute to the relatively long survival time of the patients (median 17.4 months), as responders seem to have significantly lived longer

than non-responders (22.0 months vs. 5.0 months) (28, 29). Treatment-related toxicities were reported in most studies, but the specific toxic effect of PVTT treatment was seldom found, and most cases were of non-specific liver toxicities or were associated with RT-related toxicity (14). The complications in the present study were also non-specific and all recovered without a prolonged hospital stay.

Although hypofractionated EBRT or stereotactic body radiotherapy (SBRT) for primary HCC targeting has been broadly studied, the use of these regimens for PVTT treatment has rarely been reported (14). In a multi-center analysis by Lou et al. (17), 75 patients with HCC and inferior vena cava/right atrium tumor thrombus who underwent hypofractionated radiotherapy were retrospectively reviewed. The tumor thrombus completely disappeared (CR) in 17 patients (22.7%), 55 patients (73.3%) had a PR, and 3 patients (4.0%) had an SD, which seems superior to the current study. Patients with inferior vena cava thrombus treated with EBRT tend to have a better response rate and longer survival than those with PVTT (1). A study by Wu et al. evaluated the efficacy of 3-dimensional conformal hypofractionated radiotherapy combined with transcatheter arterial chemoembolization for PVTT; radiotherapy was performed at an exposure of 4–8 Gy/time, 3 times/week, 48–60 Gy, 8–12 times, 3.0–3.5 weeks. The objective response was 71.4%. The overall survival rates were 59.3%, 31.6%, and 26.6% at 1, 2, and 3 years, respectively, with a median survival time of 11 months, which were similar to that reported here and were superior to the previously published studies involving conventionally fractionated radiotherapy for PVTT. Further study is warranted for hypofractionated radiotherapy to evaluate the potential benefit over conventionally fractionated radiotherapy.

PVTT is one of the treatment dilemmas that need to be addressed for patients with HCC. With the advance in modern radiotherapies, such as MRI-guided radiotherapy, helical tomotherapy, or charged particle hypofractionated radiotherapy, focused radiotherapy with precise dose carving and the high prescription dose may be delivered and may shed light on the fields (16, 30, 31). As indicated by the current studies, focused radiotherapy may benefit the patients with high local control. However, primary cancer progression, extrahepatic metastasis, poor liver function, and related events could still be stumbling blocks on patients' survival improvement. In particular, for patients with HCC and Child–Pugh class B, owing to borderline liver function, any intervention might be offset by liver function deterioration (32), and these patients also yield relatively poor TTP in the present study. Though hypofractionated radiotherapy shows acceptable toxicity in the present study, careful attention should be paid to low-dose volumes that could potentially result in increased liver toxicity (33). Therefore, stricter patient selection may maximize the potential benefits of this treatment (16). In the phase III RESORCE trial, median OS from the start of sorafenib to death was 19.2 months and 26.0 months for patients with sequential regorafenib treatment (34). The median OS (17.4 months) in the present study seems to approach that of sorafenib and significantly inferior to patients with sequential regorafenib treatment. However, only two patients in the present study received systemic therapies (Lenvatinib and anti-PD-1) (35). Therefore, the combination of hypofractionated radiotherapy with a moderate systemic therapy, e.g., immune checkpoint blockade, is warranted (7).

There are several limitations of this study. Firstly, the study is a retrospective study with a small group of patients, which may lead to a certain bias. Secondly, the hypofractionated radiotherapy regimen varied for the patients and lacked a control group with conventionally fractionated radiotherapy. Therefore, the potential benefit of hypofractionated radiotherapy using Gamma-knife over conventionally fractionated radiotherapy was impossible to verify while a relatively high response rate was observed. Finally, the PVTT diagnosis was based on an enhanced CT and MRI image without pathological confirmation and may be biased by the potential onset of portal vein thrombosis. However, this is currently the accepted diagnostic regimen.

CONCLUSION

Hypofractionated radiotherapy as palliative treatment appears effective and safe for PVTT located in the main portal vein in cirrhotic patients with advanced hepatocellular carcinoma, yielding a high rate of tumor response. Further study is warranted.

DATA AVAILABILITY STATEMENT

The raw data supporting the conclusions of this article will be made available by the authors, without undue reservation.

ETHICS STATEMENT

The studies involving human participants were reviewed and approved by Chifeng Tumor Hospital institutional review board. The ethics committee waived the requirement of written informed consent for participation.

AUTHOR CONTRIBUTIONS

FF and PZ are responsible for the data collection. FF and BQ are responsible for data analysis and drafting the manuscript. JW and PZ are responsible for reviewing and revising the manuscript and supervising the project. All authors contributed to the article and approved the submitted version.

FUNDING

The National Key Research and Development Program of China (Grant No. 2019YFB1311300 to JW) supports the implementation (e.g., labor cost and data collection) and publication of the project.

REFERENCES

1. Hou JZ, Zeng ZC, Zhang JY, Fan J, Zhou J, Zeng MS. Influence of Tumor Thrombus Location on the Outcome of External-Beam Radiation Therapy in Advanced Hepatocellular Carcinoma With Macrovascular Invasion. *Int J Radiat Oncol Biol Phys* (2012) 84(2):362–8. doi: 10.1016/j.ijrobp.2011.12.024
2. Llovet JM, Bustamante J, Castells A, Vilana R, Ayuso Mdel C, Sala M, et al. Natural History of Untreated Nonsurgical Hepatocellular Carcinoma: Rationale for the Design and Evaluation of Therapeutic Trials. *Hepatology* (1999) 29(1):62–7. doi: 10.1002/hep.510290145
3. Finn RS, Qin S, Ikeda M, Galle PR, Ducreux M, Kim TY, et al. Atezolizumab Plus Bevacizumab in Unresectable Hepatocellular Carcinoma. *N Engl J Med* (2020) 382(20):1894–905. doi: 10.1056/NEJMoa1915745
4. Lee MS, Ryoo BY, Hsu CH, Numata K, Stein S, Verret W, et al. Atezolizumab With or Without Bevacizumab in Unresectable Hepatocellular Carcinoma (GO30140): An Open-Label, Multicentre, Phase 1b Study. *Lancet Oncol* (2020) 21(6):808–20. doi: 10.1016/S1470-2045(20)30156-X
5. Jelic S, Sotiropoulos GC, Group EGW. Hepatocellular Carcinoma: ESMO Clinical Practice Guidelines for Diagnosis, Treatment and Follow-Up. *Ann Oncol* (2010) 21Suppl 5:v59–64. doi: 10.1093/annonc/mdq166
6. Rizzo A, Ricci AD, Brandi G. Atezolizumab in Advanced Hepatocellular Carcinoma: Good Things Come to Those Who Wait. *Immunotherapy* (2021) 13(8):637–44. doi: 10.2217/imt-2021-0026
7. Choi C, Yoo GS, Cho WK, Park HC. Optimizing Radiotherapy With Immune Checkpoint Blockade in Hepatocellular Carcinoma. *World J Gastroenterol* (2019) 25(20):2416–29. doi: 10.3748/wjg.v25.i20.2416
8. Rizzo A, Ricci AD, Brandi G. Immune-Based Combinations for Advanced Hepatocellular Carcinoma: Shaping the Direction of First-Line Therapy. *Future Oncol* (2021) 17(7):755–7. doi: 10.2217/fon-2020-0986
9. Su D, Wu B, Shi L. Cost-Effectiveness of Atezolizumab Plus Bevacizumab vs Sorafenib as First-Line Treatment of Unresectable Hepatocellular Carcinoma. *JAMA Netw Open* (2021) 4(2):e210037. doi: 10.1001/jamanetworkopen.2021.0037
10. Qiu B, Li K, Dong X, Liu FQ. Transjugular Intrahepatic Portosystemic Shunt for Portal Hypertension in Hepatocellular Carcinoma With Portal Vein Tumor Thrombus. *Cardiovasc Intervent Radiol* (2017) 40(9):1372–82. doi: 10.1007/s00270-017-1655-8
11. Memon K, Kulik L, Lewandowski RJ, Mulcahy MF, Benson AB, Ganger D, et al. Radioembolization for Hepatocellular Carcinoma With Portal Vein Thrombosis: Impact of Liver Function on Systemic Treatment Options at Disease Progression. *J Hepatol* (2013) 58(1):73–80. doi: 10.1016/j.jhep.2012.09.003
12. Chen LT, Martinelli E, Cheng AL, Pentheroudakis G, Qin S, Bhattacharyya GS, et al. Pan-Asian Adapted ESMO Clinical Practice Guidelines for the Management of Patients With Intermediate and Advanced/Relapsed Hepatocellular Carcinoma: A TOS-ESMO Initiative Endorsed by CSCO, ISMPO, JSMO, KSMO, MOS and SSO. *Ann Oncol* (2020) 31(3):334–51. doi: 10.1016/j.annonc.2019.12.001
13. Wei X, Jiang Y, Zhang X, Feng S, Zhou B, Ye X, et al. Neoadjuvant Three-Dimensional Conformal Radiotherapy for Resectable Hepatocellular Carcinoma With Portal Vein Tumor Thrombus: A Randomized, Open-Label, Multicenter Controlled Study. *J Clin Oncol* (2019) 37(24):2141–51. doi: 10.1200/JCO.18.02184
14. Lee DS, Seong J. Radiotherapeutic Options for Hepatocellular Carcinoma With Portal Vein Tumor Thrombosis. *Liver Cancer* (2014) 3(1):18–30. doi: 10.1159/000343855
15. Toya R, Murakami R, Baba Y, Nishimura R, Morishita S, Ikeda O, et al. Conformal Radiation Therapy for Portal Vein Tumor Thrombosis of Hepatocellular Carcinoma. *Radiother Oncol* (2007) 84(3):266–71. doi: 10.1016/j.radonc.2007.07.005
16. Kim JY, Yoo EJ, Jang JW, Kwon JH, Kim KJ, Kay CS. Hypofractionated Radiotheapy Using Helical Tomotherapy for Advanced Hepatocellular Carcinoma With Portal Vein Tumor Thrombosis. *Radiat Oncol* (2013) 8:15. doi: 10.1186/1748-717X-8-15
17. Lou J, Li Y, Liang K, Guo Y, Song C, Chen L, et al. Hypofractionated Radiotherapy as a Salvage Treatment for Recurrent Hepatocellular Carcinoma With Inferior Vena Cava/Right Atrium Tumor Thrombus: A Multi-Center Analysis. *BMC Cancer* (2019) 19(1):668. doi: 10.1186/s12885-019-5870-3
18. Lu XJ, Dong J, Ji LJ, Xiao LX, Ling CQ, Zhou J. Tolerability and Efficacy of Gamma Knife Radiosurgery on Hepatocellular Carcinoma With Portal Vein Tumor Thrombosis. *Oncotarget* (2016) 7(3):3614–22. doi: 10.18632/oncotarget.6118
19. Lencioni R, Llovet JM. Modified RECIST (mRECIST) Assessment for Hepatocellular Carcinoma. *Semin Liver Dis* (2010) 30(1):52–60. doi: 10.1055/s-0030-1247132
20. Chen AP, Setser A, Anadkat MJ, Cotliar J, Olsen EA, Garden BC, et al. Grading Dermatologic Adverse Events of Cancer Treatments: The Common Terminology Criteria for Adverse Events Version 4.0. *J Am Acad Dermatol* (2012) 67(5):1025–39. doi: 10.1016/j.jaad.2012.02.010
21. Verslype C, Rosmorduc O, Rougier P, Group EGW. Hepatocellular Carcinoma: ESMO-ESDO Clinical Practice Guidelines for Diagnosis, Treatment and Follow-Up. *Ann Oncol* (2012) 23 Suppl 7:vii41–8. doi: 10.1093/annonc/mds225
22. Kudo M, Kitano M, Sakurai T, Nishida N. General Rules for the Clinical and Pathological Study of Primary Liver Cancer, Nationwide Follow-Up Survey and Clinical Practice Guidelines: The Outstanding Achievements of the Liver Cancer Study Group of Japan. *Dig Dis* (2015) 33(6):765–70. doi: 10.1159/000439101
23. Li XL, Guo WX, Hong XD, Yang L, Wang K, Shi J, et al. Efficacy of the Treatment of Transarterial Chemoembolization Combined With Radiotherapy for Hepatocellular Carcinoma With Portal Vein Tumor Thrombus: A Propensity Score Analysis. *Hepatol Res* (2016) 46(11):1088–98. doi: 10.1111/hepr.12657
24. Shirai S, Sato M, Suwa K, Kishi K, Shimono C, Kawai N, et al. Single Photon Emission Computed Tomography-Based Three-Dimensional Conformal Radiotherapy for Hepatocellular Carcinoma With Portal Vein Tumor Thrombus. *Int J Radiat Oncol Biol Phys* (2009) 73(3):824–31. doi: 10.1016/j.ijrobp.2008.04.055
25. Kim YJ, Jung J, Joo JH, Kim SY, Kim JH, Lim YS, et al. Combined Transarterial Chemoembolization and Radiotherapy as a First-Line Treatment for Hepatocellular Carcinoma With Macroscopic Vascular Invasion: Necessity to Subclassify Barcelona Clinic Liver Cancer Stage C. *Radiother Oncol* (2019) 141:95–100. doi: 10.1016/j.radonc.2019.08.009
26. Yoon SM, Lim YS, Won HJ, Kim JH, Kim KM, Lee HC, et al. Radiotherapy Plus Transarterial Chemoembolization for Hepatocellular Carcinoma Invading the Portal Vein: Long-Term Patient Outcomes. *Int J Radiat Oncol Biol Phys* (2012) 82(5):2004–11. doi: 10.1016/j.ijrobp.2011.03.019
27. Zhang XB, Wang JH, Yan ZP, Qian S, Du SS, Zeng ZC. Hepatocellular Carcinoma With Main Portal Vein Tumor Thrombus: Treatment With 3-Dimensional Conformal Radiotherapy After Portal Vein Stenting and Transarterial Chemoembolization. *Cancer* (2009) 115(6):1245–52. doi: 10.1002/cncr.24139
28. Kim TH, Kim DY, Park JW, Kim YI, Kim SH, Park HS, et al. Three-Dimensional Conformal Radiotherapy of Unresectable Hepatocellular Carcinoma Patients for Whom Transcatheter Arterial Chemoembolization was Ineffective or Unsuitable. *Am J Clin Oncol* (2006) 29(6):568–75. doi: 10.1097/01.coc.0000239147.60196.11
29. Yu JI, Park HC, Lim DH, Park W, Yoo BC, Paik SW, et al. Prognostic Index for Portal Vein Tumor Thrombosis in Patients With Hepatocellular Carcinoma Treated With Radiation Therapy. *J Korean Med Sci* (2011) 26(8):1014–22. doi: 10.3346/jkms.2011.26.8.1014
30. Lee SJ, Kim M, Kwak YK, Kang HJ. MRI-Guided Radiotherapy for PVTT in HCC Patients: Evaluation of the Efficacy and Safety. *J Cancer Res Clin Oncol* (2021). doi: 10.1007/s00432-021-03788-z
31. Shiba S, Shibuya K, Okamoto M, Okazaki S, Komatsu S, Kubota Y, et al. Clinical Impact of Hypofractionated Carbon Ion Radiotherapy on Locally Advanced Hepatocellular Carcinoma. *Radiat Oncol* (2020) 15(1):195. doi: 10.1186/s13014-020-01634-z
32. Granito A, Bolondi L. Non-Transplant Therapies for Patients With Hepatocellular Carcinoma and Child-Pugh-Turcotte Class B Cirrhosis. *Lancet Oncol* (2017) 18(2):e101–e12. doi: 10.1016/S1470-2045(16)30569-1
33. Lasley FD, Mannina EM, Johnson CS, Perkins SM, Althouse S, Maluccio M, et al. Treatment Variables Related to Liver Toxicity in Patients With Hepatocellular Carcinoma, Child-Pugh Class A and B Enrolled in a Phase

1-2 Trial of Stereotactic Body Radiation Therapy. *Pract Radiat Oncol* (2015) 5 (5):e443–e9. doi: 10.1016/j.prro.2015.02.007
34. Finn RS, Merle P, Granito A, Huang YH, Bodoky G, Pracht M, et al. Outcomes of Sequential Treatment With Sorafenib Followed by Regorafenib for HCC: Additional Analyses From the Phase III RESORCE Trial. *J Hepatol* (2018) 69 (2):353–8. doi: 10.1016/j.jhep.2018.04.010
35. Granito A, Forgione A, Marinelli S, Renzulli M, Ielasi L, Sansone V, et al. Experience With Regorafenib in the Treatment of Hepatocellular Carcinoma. *Therap Adv Gastroenterol* (2021) 14:17562848211016959. doi: 10.1177/17562848211016959

Conflict of Interest: The authors declare that the research was conducted in the absence of any commercial or financial relationships that could be construed as a potential conflict of interest.

Publisher's Note: All claims expressed in this article are solely those of the authors and do not necessarily represent those of their affiliated organizations, or those of the publisher, the editors and the reviewers. Any product that may be evaluated in this article, or claim that may be made by its manufacturer, is not guaranteed or endorsed by the publisher.

frontiers | Frontiers in Oncology

CASE REPORT
published: 12 May 2022
doi: 10.3389/fonc.2022.879454

Case Report: Radiotherapy Plus Immunotherapy and Lenvatinib for the Treatment of Recurrent Hepatocellular Carcinoma With a Right Atrium and Inferior Vena Cava Tumor Thrombus

*Yuting Qian†, Long Gong†, Su Li†, Kun Mao, Xianming Li and Guixiang Liao**

Department of Radiation Oncology, Shenzhen People's Hospital, The Second Clinical Medical College, Jinan University, Shenzhen, China

OPEN ACCESS

Edited by:
John Varlotto, Marshall University, United States

Reviewed by:
Antonio Giovanni Solimando, University of Bari Aldo Moro, Italy
Wei Li, Capital Medical University, China

***Correspondence:**
Guixiang Liao
liaoguixiang@163.com

†These authors have contributed equally to this work

Specialty section:
This article was submitted to Radiation Oncology, a section of the journal Frontiers in Oncology

Received: *19 February 2022*
Accepted: *11 April 2022*
Published: *12 May 2022*

Citation:
Qian Y, Gong L, Li S, Mao K, Li X and Liao G (2022) Case Report: Radiotherapy Plus Immunotherapy and Lenvatinib for the Treatment of Recurrent Hepatocellular Carcinoma With a Right Atrium and Inferior Vena Cava Tumor Thrombus. Front. Oncol. 12:879454. doi: 10.3389/fonc.2022.879454

Background: The treatment of hepatocellular carcinoma (HCC) with right atrium (RA) and inferior vena cava (IVC) tumor thrombi is challenging, with the standard treatment being not well established. Immunotherapy plus antiangiogenic therapy is a potentially effective treatment for patients with advanced HCC. Here, we described the case of a patient with HCC with RA and IVC tumor thrombi who achieved a successful response from radiotherapy and targeted therapy plus immunotherapy.

Case Summary: A 62-year-old women presented with severe bilateral lower extremity edema identified as recurrent HCC with RA and IVC tumor thrombi based on past medical history and computed tomography. The patient received palliative radiotherapy plus pembrolizumab and lenvatinib treatment and was relieved of disease symptoms of bilateral lower extremity edema. The HCC with RA and IVC tumor thrombi shrunk, and the progression-free survival of this patient was > seven months.

Conclusion: Tumor thrombus-directed radiotherapy plus concurrent immunotherapy and targeted therapy might be a feasible and safe approach for patients with HCC with RA and IVC tumor thrombi.

Keywords: hepatocellular carcinoma, immune checkpoint inhibitor, radiotherapy, lenvatinib, case report

INTRODUCTION

Primary liver cancer is the sixth most commonly diagnosed cancer and the third leading cause of cancer-related deaths worldwide in 2020, with approximately 906,000 new cases and 830,000 deaths (1). Nevertheless, in China, hepatocellular carcinoma (HCC) is the fourth leading cause of cancer-related deaths (accounting 326,000 deaths), with 370,000 new cases in 2015 (2). HCC with a tumor thrombus extending into the inferior vena cava (IVC) or the right atrium (RA) is rare, accounting for 3.8% of the HCC cases (3, 4). In addition, vasculature invasion is a poor prognostic factor in

patients with HCC (5). The median survival of patients with untreated macrovascular thrombi is approximately five months (6). The causes of mortality include heart failure, pulmonary embolism, Budd–Chiari syndrome, and other events (7).

Lenvatinib and sorafenib are both multi-kinase inhibitors. Sorafenib can simultaneously inhibit various intracellular and cell surface kinases, including rapidly accelerated fibrosarcoma (RAF) kinase, vascular endothelial growth factor receptor-2 (VEGFR-2), VEGFR-3, and platelet-derived growth factor receptor-beta (PDGFR-β). Lenvatinib and sorafenib have dual antitumor effects. On the one hand, they can directly inhibit tumor growth by inhibiting the RAF/MEK/ERK signaling pathway; on the other hand, they can block VEGFR and PDGFR. Both sorafenib and lenvatinib have survival benefits and are recommended for managing patients with advanced HCC (8, 9). However, the efficacy of sorafenib is limited due to developed drug resistance.

The major neuronal allotypes of RAF, BRAF, and MEK pathways play a key role in HCC evasion of tyrosine kinase inhibitor (TKI) activity (10). Immune checkpoint inhibitors (ICIs) have been approved as second-line therapy for HCC in patients who previously received sorafenib (11). Pembrolizumab has shown substantial antitumor activity and a favorable toxicity profile as a second-line treatment for HCC (12). Moreover, according to the IMbrave150 trial, atezolizumab plus bevacizumab is recommended for treating unresectable HCC (13). In a clinical trial (NCT03006926), 104 patients with unresectable HCC received lenvatinib orally daily and 200 mg pembrolizumab every three weeks (q3w), the objective response rate was 46%, with median overall survival (OS) of 22 months (14).

Radiation therapy, especially image-guided radiation therapy, can be used to treat liver cancer. For HCC, stereotactic body radiation therapy (SBRT) can achieve adequate local tumor control and survival benefits (15). SBRT plus immunotherapy showed a 100% response in five advanced HCC patients (16).

Here, we report a case of recurrent HCC with RA and IVC tumor thrombus that received radiation plus pembrolizumab and lenvatinib treatment.

CASE DESCRIPTION

This case report was conducted per the CARE Guidelines (17). In July 2021, a 66-year-old Chinese woman was hospitalized due to severe bilateral lower extremity edema and palpitation, without any accompanying symptoms, such as abdominal pain or bloating. She had no history of high blood pressure, diabetes, or hepatitis. She had been diagnosed with HCC nine years ago and had undergone surgical resection. Postoperative pathology revealed a highly differentiated HCC. She had received radiofrequency ablation because of local HCC recurrence in November 2013 and May 2014. Subsequently, the patient did not undergo medical examination until July 2021. In July 2021, an enhanced computed tomography (CT) showed HCC recurrence at the junction of the anterior segment (S5/S8) of the liver, with approximately 1.8 × 1.4 cm size. The mass wrapped and invaded the adjacent IVC and grew into the IVC, RA, and left renal vein. The diagnosis was HCC with RA and IVC tumor thrombi with Barcelona clinic liver cancer (BCLC) stage-C (**Figure 1**). Then, the patient received sorafenib treatment and developed grade 4 (the US National Cancer Institute Common Terminology Criteria for Adverse Events [CTCAE v4.03]) skin rash and discontinued the sorafenib treatment. Hormones and proglobulin were used to treat dermatitis, and adverse skin reactions were reversed.

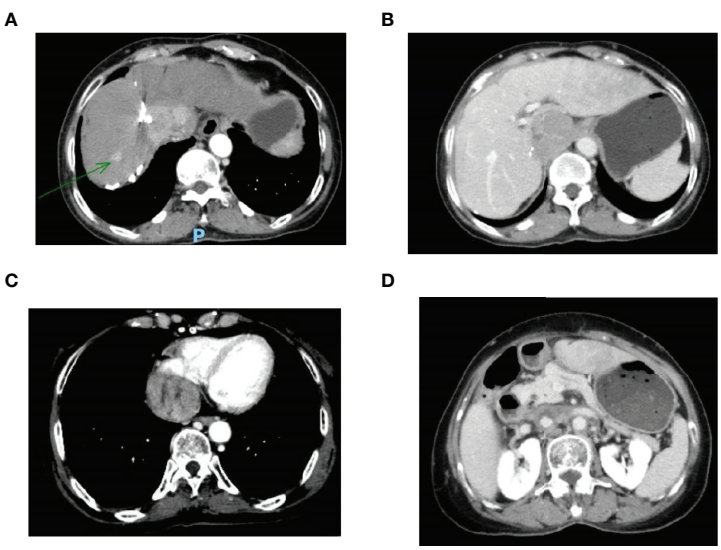

FIGURE 1 | **(A)** Enhanced CT revealed a mass tumor in the S5/S8 segment of the liver; **(B)** The tumor thrombus in the inferior vena cava; **(C)** The tumor thrombus in the right atrium; **(D)** The tumor thrombus in the left renal vein. CT, computed tomography.

According to a published study, radiotherapy can be used to treat liver cancer with RA and IVC tumor thrombi (18). Moreover, immunotherapy plus radiotherapy and antiangiogenic therapy is a safe and effective approach for advanced HCC (19). Therefore, we administrated radiotherapy, immunotherapy, and lenvatinib. The patient received radiotherapy in August 2021 through volumetric modulated arc therapy and respiratory gating technology. The dose for HCC recurrence was 50 Gy/25 fractions and for HCC with RA and IVC tumor thrombi was 45 Gy/25 fractions (**Figure 2**). She simultaneously received pembrolizumab (100 mg; 2 mg/kg, q3w) and lenvatinib (8 mg/day). Lower extremity edema and palpitations resolved after radiotherapy. Toxicity was well tolerated with no liver toxicity, and grade ≥ 3 adverse events were observed. After four cycles of pembrolizumab plus lenvatinib treatment, the CT scan indicated that the patient had a partial response and a decreased thrombus according to the Response Evaluation Criteria in Solid Tumors (RECIST) v.1.1. The HCC lesion at the junction of S5/S8 segment disappeared, and the IVC/RA thrombus decreased in size (**Figure 3**). No disease progression was observed. The patient continued to receive the pembrolizumab plus lenvatinib treatment (the last pembrolizumab treatment day was March 26, 2022). The patient remained stable at the time of writing (> 7 months). During the treatment period, there was no grade ≥ 3 adverse events or liver toxicity. Leukopenia (grade 2), thrombocytopenia (grade 1), hypoalbuminemia (grade 1), and hypertension (grade 2) were resolved using symptomatic drug treatment. Granulocyte colony-stimulating factor was administered to deal with white blood loss. A CT scan was regularly performed for every 3 months. Blood routine, liver function, kidney function, electrolyte, thyroid function, and pituitary function were regularly measured. The timeline scheme of the major clinical events of the patient since HCC diagnosis is shown in **Figure 4**.

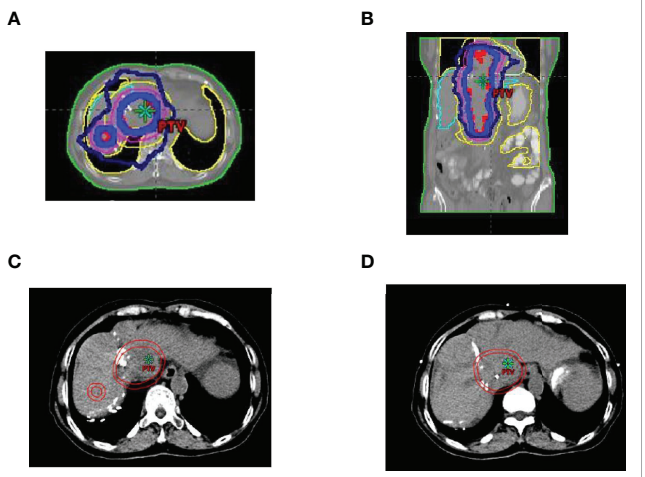

FIGURE 2 | Region of image-guided radiotherapy. **(A)** cross-sectional dose distribution map; **(B)** coronal dose distribution map; **(C, D)** target delineation of gross tumor volume (GTV) and planted target volume (PTV), the inner circle line is GTV, and the outer circle line is PTV.

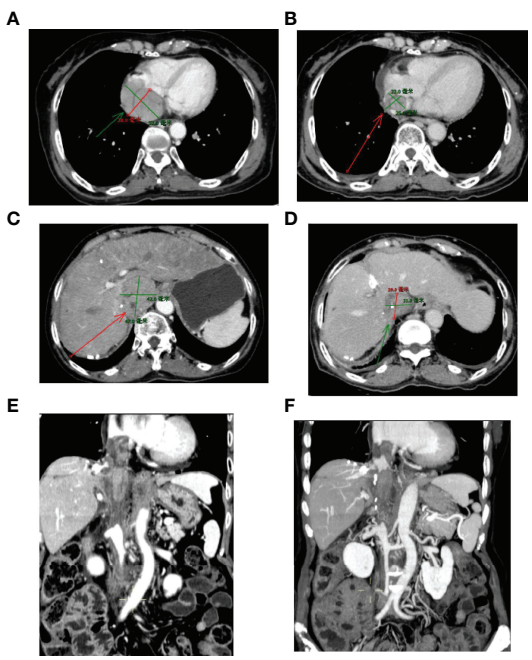

FIGURE 3 | Sizes of RA and IVC tumor thrombi before and after 3-month treatment. **(A, C, E)** Before treatment; **(B, D, F)** Three months after treatment. IVC, inferior vena cava; RA, right atrium.

DISCUSSION

In this case, the patient with HCC recurrence with RA and IVC tumor thrombi received radiotherapy, and pembrolizumab plus lenvatinib was administered to the patient. Partial responses after three months of treatment were observed. The patient was treated with (100 mg; 2 mg/kg, q3w) and lenvatinib (8 mg/day) regularly. Blood routine, liver function, kidney function, electrolyte, thyroid function, and pituitary function were regularly measured. A CT scan was regularly performed for every 3 months.

The progression-free survival (PFS) was > 7 months at the last calculation with no grade ≥ 3 adverse events.

The treatment of HCC with RA tumor thrombus *via* progression through the hepatic veins into the IVC is challenging (18). Treatment with sorafenib and best supportive care (20) as well as pembrolizumab plus lenvatinib treatment has been recommended (21). However, the prognosis of RA tumor thrombi is poor, and the identification of safe and effective local therapies is required. Local therapies include surgical resection (4), microwave ablation, transarterial chemoembolization, and radiotherapy.

A radiotherapy is an effective approach for managing unresectable HCC, with radiographic response rates of 49–98% and local control rates of 68–100% (22, 23). Bitterman et al.

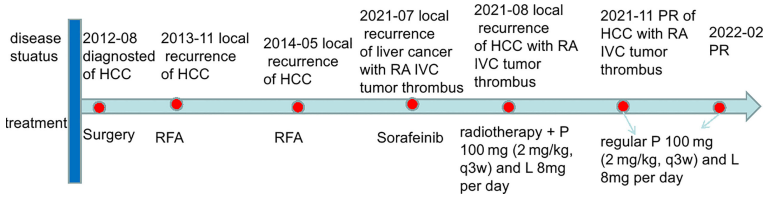

FIGURE 4 | The timeline scheme of the major clinical events of the patient since diagnosis. HCC, hepatocellular carcinoma; IVC, inferior vena cava; RA, right atrium; RFA, radiofrequency ablation; P, pembrolizumab; L, lenvatinib; PR, partial response.

reported 10 patients with HCC and IVC and RA thrombi receiving a median of 50.6 Gy radiation. The median follow-up was 5 months, and no grade ≥ 3 acute toxicities occurred (18). Duan et al. reported 11 patients with IVC and RA who received transarterial chemoembolization and 60 Gy/30 fraction radiotherapy. Radiographic responses with no severe toxicity were observed in all patients. The median OS was 21 months (24). A recent review included 105 patients with HCC with IVC and RA thrombi, with a median age of 58.7 ± 12.4 years. Different groups were classified according to their treatment choices. The OS was 40.8% in these patients, indicating effective radiotherapy. The major morbidity was due to intra or extrahepatic recurrence of HCC (25). Fleckenstein et al. reported that a patient with HCC thrombus extending into the RA received CT-guided high-dose-rate brachytherapy; the patient showed relieving disease symptoms and good radiologic response (26).

Immunotherapy is a therapeutic modality in many solid tumors. Patients with advanced HCC may benefit from ICIs (21). Anti-programmed cell death-1(anti-PD-1) therapy in 413 patients with HCC was investigated in the Keynote-240 trial. The median OS was 13.9 months in the anti-PD-1 group and 10.6 months in the best supportive care group. The response rates were 18.3% and 4.4% in the anti-PD-1 and best supportive care groups, respectively. Moreover, the toxicity of ICIs was well tolerated (27). Furthermore, Keynote-224 investigated the effect of pembrolizumab in patients with advanced HCC, who had previously been treated using sorafenib, and showed that pembrolizumab might be an effective way for this group of patients (28). Sorafenib is a molecularly-targeted drug approved by the U.S. Food and Drug Administration (FDA) for treating advanced HCC. The antiangiogenic agent lenvatinib is a targeted small molecule approved for the first-line treatment of advanced HCC. However, only approximately 30% of patients with advanced HCC showed good treatment response after receiving sorafenib, and many patients gradually progressed to insensitivity or resistance to sorafenib within six months. Drug resistance involves many signaling pathways, such as the RAF, BRAF, and MEK pathways. Advanced HCC patients with BRAF mutations display multifocal or more aggressive behavior with resistance to TKI. Long non-coding RNA may play a vital role in BRAF aggressiveness in HCC (10). Tumors grow and evolve through constant crosstalk with the surrounding microenvironment. Emerging evidence indicates that angiogenesis and immunosuppression frequently occur simultaneously in response to this crosstalk (10). Accordingly, strategies combining antiangiogenic therapy and immunotherapy have the potential to balance the tumor microenvironment and improve treatment response (10). The combination of antiangiogenic therapy with immunotherapy (atezolizumab plus bevacizumab) was also demonstrated in the IMBRAVE 150 study to provide a survival benefit for advanced HCC (13). Moreover, low-dose antiangiogenic therapy and immunotherapy improved the treatment effect in patients with breast cancer (29). Two HCC patients with lung metastases treated with lenvatinib plus pembrolizumab showed a good radiologic response and median PFS of > 12 months (30). The objective response rate of 29 patients receiving ICIs plus lenvatinib was approximately 25.9%, with one patient having a complete response, 6-month OS was 62.6%, 12-month OS was 53.7%, and 6-month PFS rate was 43.5% (31).

One study included 65 patients who received lenvatinib plus immunotherapy and 45 patients who received lenvatinib monotherapy. Lenvatinib plus ICI provided significantly higher OS and PFS than lenvatinib monotherapy. The objective response rate and disease control rate were significantly higher in the lenvatinib plus ICI group than in the lenvatinib monotherapy group. No treatment-related deaths occurred. Grade 3 or higher hypertension and palmar-plantar erythrodysesthesia were observed in 20% and 10.8% of the patients in the combination group and 17.8% and 4.4% of the patients in the single-agent group, respectively (32). In another study, patients with HCC showed complete response after lenvatinib plus pembrolizumab treatment (33). An HCC patient with IVC and RA tumor thrombi and left adrenal gland metastasis received transarterial chemoembolization, immunotherapy, and subsequent radiotherapy. The patient survived for > 34 months since the disease diagnosis (34).

The tumor microenvironment has a strong immunosuppressive effect. Although there is considerable intratumoral heterogeneity in tumors, various mechanisms may play an immunosuppressive role, including altered cytokine signaling and the presence of immunosuppressive cells. Radiotherapy for tumors can transform an immunosuppressive environment into an immunostimulatory environment. Ionizing radiation can also promote both immunosuppressive and carcinogenic effects. Regulating the immune microenvironment by radiotherapy may involve the following mechanisms: (1) local production of chemokines, cytokines, and other soluble factors; (2) changes in

the tumor-associated stroma and endothelium; (3) transport or regulation of immune cell subsets into the tumor microenvironment (35). Radiation activates the immune system, exerts a synergistic antitumor effect through a combination of immunotherapy, and can increase the expression of the immune cells (36, 37). Yttrium-90 radioembolization (Y-90 RE) plus immunotherapy was safe and effective in patients with advanced HCC, with an objective response rate of 31% (38). The combination of radiotherapy and immunotherapy in patients with HCC showed 1- and 2-year PFS of 93.3% and 77.8%, respectively (39). A phase I trial reported that radiotherapy plus ipilimumab had clinical benefits in 23% of patients with liver/lung cancer (40). One study included 76 patients with HCC treated with nivolumab. Of those patients, 54 (71.1%) received radiotherapy before or during immunotherapy. The patients who had received radiotherapy had significantly longer PFS and OS than patients who had not received radiotherapy (41). Some clinical trials are ongoing to evaluate the treatment of programmed cell death-1 antibody plus radiotherapy for advanced HCC. One clinical trial investigated radiation plus intravenous administration of 200 mg camrelizumab (q3w, five times since the first day of radiotherapy until disease progression or intolerable toxicity) in advanced HCC (https://clinicaltrials.gov/ct2/show/NCT04193696). The primary outcome was the objective response rate, and the secondary outcomes were OS and toxicity. Another clinical trial investigated the efficacy and safety of SBRT followed by immunotherapy compared to SBRT alone for HCC with portal vein invasion after arterially directed therapy. Patients underwent SBRT using volumetric arc therapy, and the prescribed dose was 30–54 Gy in 3–6 fractions over 1–2 weeks (https://clinicaltrials.gov/ct2/show/NCT04167293). Further research on radiotherapy plus immunotherapy for HCC is required.

In a recent randomized phase III trial, 91 patients with locally advanced cervical squamous cell carcinoma were included. Of which 43 patients received radiochemotherapy, and 48 received chemotherapy plus Endostar (an antiangiogenic agent). The study indicated that the completed response rate was significantly higher in the chemotherapy plus Endostar group than in the radiochemotherapy group (83.33% *vs.* 65.12%) (42). Whether the three treatments have synergistic effects is worth exploring. A few studies have focused on the combination of the three treatments. A study indicated that all three treatments in murine lung tumors could inhibit tumor growth and increase immune memory protecting against tumor recurrence (43).

Although radiotherapy combined with antiangiogenic therapy or immunotherapy has been extensively studied, only a few phase III controlled studies have been successfully conducted. Owing to the complex relationship between cancer cells and tumors in the tumor microenvironment, combination therapy still requires overcoming many difficulties in achieving therapeutic benefits. Further studies are necessary to determine the optimal timing and dose of treatment (44).

Regarding treatment toxicity, no evidence of liver toxicity was observed. According to the study reported by Zhong et al. (19), the combination of immunotherapy and targeted therapy often results in toxicity. Additional radiotherapy did not increase the side effects in our case. A previous study suggested that radiotherapy plus immunotherapy did not cause radiation-induced liver disease and treatment-related deaths (39).

However, this case report also has some limitations. Most importantly, the recurrent HCC, in this case, did not undergo pathological biopsy, and the PD-L1 level in the tumor tissue could not be measured.

In conclusion, radiotherapy plus immunotherapy and targeted therapy for HCC with RA and IVC tumor thrombi might be a feasible and safe approach.

DATA AVAILABILITY STATEMENT

The original contributions presented in the study are included in the article/supplementary material. Further inquiries can be directed to the corresponding author.

ETHICS STATEMENT

The studies involving human participants were reviewed and approved by Ethic Committee of Shenzhen People's Hospital. The patients/participants provided their written informed consent to participate in this study. Written informed consent was obtained from the individual(s) for the publication of any potentially identifiable images or data included in this article.

AUTHOR CONTRIBUTIONS

GL, SL, LG, and XL treated the patient. YQ, KM, and GL wrote the paper. All authors contributed to the article and approved the submitted version.

ACKNOWLEDGMENTS

We acknowledged the patient and her son that agreed us to publish the case.

REFERENCES

1. Sung H, Ferlay J, Siegel RL, Laversanne M, Soerjomataram I, Jemal A, et al. Global Cancer Statistics 2020: GLOBOCAN Estimates of Incidence and Mortality Worldwide for 36 Cancers in 185 Countries. *CA Cancer J Clin* (2021) 71:209–49. doi: 10.3322/caac.21660
2. Zhang S, Sun K, Zheng R, Zeng H, Wang S, Chen R, et al. Cancer Incidence and Mortality in China, 2015. *J Natl Cancer Center* (2021) 1:2–11. doi: 10.1016/j.jncc.2020.12.001
3. Lee IJ, Chung JW, Kim HC, Yin YH, So YH, Jeon UB, et al. Extrahepatic Collateral Artery Supply to the Tumor Thrombi of Hepatocellular Carcinoma Invading Inferior Vena Cava: The Prevalence and Determinant

Factors. *J Vasc Iinerv Radiol* (2009) 20:22–9. doi: 10.1016/j.jvir.2008.09.030
4. Chang YL, Lin KH, Lee KC, Chen YL. The Inferior Vena Cava Hanging Maneuver for Hepatocellular Carcinoma With Right Atrial Tumor Thrombus. *Asian J Surg* (2020) 43:705–6. doi: 10.1016/j.asjsur.2020.01.006
5. Llovet JM, Bustamante J, Castells A, Vilana R, Ayuso MC, Sala M, et al. Natural History of Untreated Nonsurgical Hepatocellular Carcinoma: Rationale for The Design and Evaluation of Therapeutic Trials. *Hepatology* (1999) 29:62–7. doi: 10.1002/hep.510290145
6. Wang Y, Yuan L, Ge RL, Sun Y, Wei G. Survival Benefit of Surgical Treatment for Hepatocellular Carcinoma With Inferior Vena Cava/Right Atrium Tumor Thrombus: Results of a Retrospective Cohort Study. *Ann Surg Oncol* (2013) 20:914–22. doi: 10.1245/s10434-012-2646-2
7. Ohta M, Nakanishi C, Kawagishi N, Hara Y, Maida K, Kashiwadate T, et al. Surgical Resection of Recurrent Extrahepatic Hepatocellular Carcinoma With Tumor Thrombus Extending Into the Right Atrium Under Cardiopulmonary Bypass: A Case Report and Review of the Literature. *Surg Case Rep* (2016) 2:110. doi: 10.1186/s40792-016-0241-7
8. Llovet JM, Ricci S, Mazzaferro V, Hilgard P, Gane E, Blanc JF, et al. Sorafenib in Advanced Hepatocellular Carcinoma. *N Engl J Med* (2008) 359:378–90. doi: 10.1056/NEJMoa0708857
9. Nair A, Reece K, Donoghue MB, Yuan WV, Rodriguez L, Keegan P, et al. FDA Supplemental Approval Summary: Lenvatinib for the Treatment of Unresectable Hepatocellular Carcinoma. *Oncologist* (2021) 26:e484–91. doi: 10.1002/onco.13566
10. Gnoni A, Licchetta A, Memeo R, Argentiero A, Solimando AG, Longo V, et al. Role of BRAF in Hepatocellular Carcinoma: A Rationale for Future Targeted Cancer Therapies. *Med (Kaunas)* (2019) 55:754. doi: 10.3390/medicina55120754
11. Cheng H, Sun G, Chen H, Li Y, Han Z, Li Y, et al. Trends in the Treatment of Advanced Hepatocellular Carcinoma: Immune Checkpoint Blockade Immunotherapy and Related Combination Therapies. *Am J Cancer Res* (2019) 9:1536–45.
12. Chiang CL, Chan SK, Lee SF, Wong IO, Choi HC. Cost-Effectiveness of Pembrolizumab as a Second-Line Therapy for Hepatocellular Carcinoma. *JAMA Netw Open* (2021) 4:e2033761. doi: 10.1001/jamanetworkopen.2020.33761
13. Finn RS, Qin S, Ikeda M, Galle PR, Ducreux M, Kim TY, et al. Atezolizumab Plus Bevacizumab in Unresectable Hepatocellular Carcinoma. *N Engl J Med* (2020) 382:1894–905. doi: 10.1056/NEJMoa1915745
14. Finn RS, Ikeda M, Zhu AX, Sung MW, Baron AD, Kudo M, et al. Phase Ib Study of Lenvatinib Plus Pembrolizumab in Patients With Unresectable Hepatocellular Carcinoma. *J Clin Oncol* (2020) 38:2960–70. doi: 10.1200/JCO.20.00808
15. Ohri N, Dawson LA, Krishnan S, Seong J, Cheng JC, Sarin SK, et al. Radiotherapy for Hepatocellular Carcinoma: New Indications and Directions for Future Study. *J Natl Cancer Inst* (2016) 108:djw133. doi: 10.1093/jnci/djw133
16. Chiang CL, Chan A, Chiu K, Kong FS. Combined Stereotactic Body Radiotherapy and Checkpoint Inhibition in Unresectable Hepatocellular Carcinoma: A Potential Synergistic Treatment Strategy. *Front Oncol* (2019) 9:1157. doi: 10.3389/fonc.2019.01157
17. Riley DS, Barber MS, Kienle GS, Aronson JK, von Schoen-Angerer T, Tugwell P, et al. CARE Guidelines for Case Reports: Explanation and Elaboration Document. *J Clin Epidemiol* (2017) 89:218–35. doi: 10.1016/j.jclinepi.2017.04.026
18. Bitterman DS, Edgington SK, Kilcoyne A, Kim DW, Eyler CE, Qadan M, et al. Palliative External Beam Radiation Therapy for Hepatocellular Carcinoma With Right Atrial Tumor Thrombus. *Pract Radiat Oncol* (2020) 10:e183–7. doi: 10.1016/j.prro.2019.12.010
19. Zhong L, Wu D, Peng W, Sheng H, Xiao Y, Zhang X, et al. Safety of PD-1/PD-L1 Inhibitors Combined With Palliative Radiotherapy and Anti-Angiogenic Therapy in Advanced Hepatocellular Carcinoma. *Front Oncol* (2021) 11:686621. doi: 10.3389/fonc.2021.686621
20. Tao ZW, Cheng BQ, Zhou T, Gao YJ. Management of Hepatocellular Carcinoma Patients With Portal Vein Tumor Thrombosis: A Narrative Review. *Hepatobil Pancreat Dis Int* (2021) 21:134–44. doi: 10.1016/j.hbpd.2021.12.004
21. Llovet JM, Castet F, Heikenwalder M, Maini MK, Mazzaferro V, Pinato DJ, et al. Immunotherapies for Hepatocellular Carcinoma. *Nat Rev Clin Oncol* (2021) 19:172. doi: 10.1038/s41571-021-00573-2
22. Park HC, Yu JI, Cheng JC, Zeng ZC, Hong JH, Wang ML, et al. Consensus for Radiotherapy in Hepatocellular Carcinoma From The 5th Asia-Pacific Primary Liver Cancer Expert Meeting (APPLE 2014): Current Practice and Future Clinical Trials. *Liver Cancer* (2016) 5:162–74. doi: 10.1159/000367766
23. Chen CP. Role of External Beam Radiotherapy in Hepatocellular Carcinoma. *Clin Liver Dis* (2020) 24:701–17. doi: 10.1016/j.cld.2020.07.006
24. Duan F, Yu W, Wang Y, Liu FY, Song P, Wang ZJ, et al. Trans-Arterial Chemoembolization and External Beam Radiation Therapy for Treatment of Hepatocellular Carcinoma With a Tumor Thrombus in the Inferior Vena Cava and Right Atrium. *Cancer Imaging* (2015) 15:7. doi: 10.1186/s40644-015-0043-3
25. Guo YX. Hepatocellular Carcinoma With Right Atrial Tumor Thrombus. *Z Gastroenterol* (2021) 59:153–61. doi: 10.1055/a-1275-3780
26. Fleckenstein FN, Jonczyk M, Can E, Ludemann WM, Savic L, Maleitzke T, et al. Hepatocellular Carcinoma Tumor Thrombus Entering the Right Atrium Treated With Combining Percutaneous and Intravenous High-Dose-Rate Brachytherapy: A Case Report. *CVIR Endovasc* (2021) 4:71. doi: 10.1186/s42155-021-00259-x
27. Finn RS, Ryoo BY, Merle P, Kudo M, Bouattour M, Lim HY, et al. Pembrolizumab As Second-Line Therapy in Patients With Advanced Hepatocellular Carcinoma in KEYNOTE-240: A Randomized, Double-Blind, Phase III Trial. *J Clin Oncol* (2020) 38:193–202. doi: 10.1200/JCO.19.01307
28. Zhu AX, Finn RS, Edeline J, Cattan S, Ogasawara S, Palmer D, et al. Pembrolizumab in Patients With Advanced Hepatocellular Carcinoma Previously Treated With Sorafenib (KEYNOTE-224): A non-Randomised, Open-Label Phase 2 Trial. *Lancet Oncol* (2018) 19:940–52. doi: 10.1016/S1470-2045(18)30351-6
29. Li Q, Wang Y, Jia W, Deng H, Li G, Deng W, et al. Low-Dose Anti-Angiogenic Therapy Sensitizes Breast Cancer to PD-1 Blockade. *Clin Cancer Res* (2020) 26:1712–24. doi: 10.1158/1078-0432.CCR-19-217
30. Li J, Chen T, Bi F, Yang Y. Efficacy of Lenvatinib Plus Pembrolizumab in Hepatocellular Carcinoma With Metachronous Lung Metastasis: A Report of Two Cases. *Tumori* (2021) 107:P114–9. doi: 10.1177/03008916211033353
31. Huang X, Xu L, Ma T, Yin X, Huang Z, Ran Y, et al. Lenvatinib Plus Immune Checkpoint Inhibitors Improve Survival in Advanced Hepatocellular Carcinoma: A Retrospective Study. *Front Oncol* (2021) 11:751159. doi: 10.3389/fonc.2021.751159
32. Chen K, Wei W, Liu L, Deng ZJ, Li L, Liang XM, et al. Lenvatinib With or Without Immune Checkpoint Inhibitors for Patients With Unresectable Hepatocellular Carcinoma in Real-World Clinical Practice. *Cancer Immunol Immunother* (2021) 71:1063–74. doi: 10.1007/s00262-021-03060-w
33. Liu Z, Li X, He X, Xu Y, Wang X. Complete Response to the Combination of Lenvatinib and Pembrolizumab in an Advanced Hepatocellular Carcinoma Patient: A Case Report. *BMC Cancer* (2019) 19:1062. doi: 10.1186/s12885-019-6287-8
34. Sun N, Zhang J, Li B, Li A, Lv M, Zhang C. Favorable Response to Multimodal Treatment in Hepatocellular Carcinoma With Inferior Vena Cava and Right Atrial Tumor Thrombus and Left Adrenal Gland Metastasis: A Case Report and Literature Review. *Med (Baltimore)* (2021) 100:e27987. doi: 10.1097/MD.0000000000027987
35. Marciscano AE, Haimovitz-Friedman A, Lee P, Tran PT, Tome WA, Guha C, et al. Immunomodulatory Effects of Stereotactic Body Radiation Therapy: Preclinical Insights and Clinical Opportunities. *Int J Radiat Oncol Biol Phys* (2021) 110:35–52. doi: 10.1016/j.ijrobp.2019.02.046
36. Lee YH, Tai D, Yip C, Choo SP, Chew V. Combinational Immunotherapy for Hepatocellular Carcinoma: Radiotherapy, Immune Checkpoint Blockade and Beyond. *Front Immunol* (2020) 11:568759. doi: 10.3389/fimmu.2020.568759
37. Choi C, Yoo GS, Cho WK, Park HC. Optimizing Radiotherapy With Immune Checkpoint Blockade in Hepatocellular Carcinoma. *World J Gastroenterol* (2019) 25:2416–29. doi: 10.3748/wjg.v25.i20.2416
38. Tai D, Loke K, Gogna A, Kaya NA, Tan SH, Hennedige T, et al. Radioembolisation With Y90-Resin Microspheres Followed by Nivolumab for Advanced Hepatocellular Carcinoma (CA 209-678): A Single Arm, Single Centre, Phase 2 Trial. *Lancet Gastroenterol Hepatol* (2021) 6:1025–35. doi: 10.1016/S2468-1253(21)00305-8
39. Chiang CL, Chiu KW, Lee FA, Kong FS, Chan AC. Combined Stereotactic Body Radiotherapy and Immunotherapy Versus Transarterial Chemoembolization in Locally Advanced Hepatocellular Carcinoma: A

Propensity Score Matching Analysis. *Front Oncol* (2021) 11:798832. doi: 10.3389/fonc.2021.798832
40. Tang C, Welsh JW, de Groot P, Massarelli E, Chang JY, Hess KR, et al. Ipilimumab With Stereotactic Ablative Radiation Therapy: Phase I Results and Immunologic Correlates From Peripheral T Cells. *Clin Cancer Res* (2017) 23:1388–96. doi: 10.1158/1078-0432.CCR-16-1432
41. Yu JI, Lee SJ, Lee J, Lim HY, Paik SW, Yoo GS, et al. Clinical Significance of Radiotherapy Before and/or During Nivolumab Treatment in Hepatocellular Carcinoma. *Cancer Med* (2019) 8:6986–94. doi: 10.1002/cam4.2570
42. Shu H, Dong Y, Xu Z, Luo W, Xu L, Zhu H, et al. The Efficacy and Safety of Continuous Intravenous Endostar Treatment Combined With Concurrent Chemoradiotherapy in Patients With Locally Advanced Cervical Squamous Cell Carcinoma: A Randomized Controlled Trial. *Front Oncol* (2021) 11:723193. doi: 10.3389/fonc.2021.723193
43. Chen JL, Pan CK, Huang YS, Tsai CY, Wang CW, Lin YL, et al. Evaluation of Antitumor Immunity by a Combination Treatment of High-Dose Irradiation, Anti-PDL1, and Anti-Angiogenic Therapy in Murine Lung Tumors. *Cancer Immunol Immunother* (2021) 70:391–404. doi: 10.1007/s00262-020-02690-w
44. Goedegebuure R, de Klerk LK, Bass AJ, Derks S, Thijssen V. Combining Radiotherapy With Anti-Angiogenic Therapy and Immunotherapy; A Therapeutic Triad for Cancer? *Front Immunol* (2018) 9:3107. doi: 10.3389/fimmu.2018.03107

Conflict of Interest: The authors declare that the research was conducted in the absence of any commercial or financial relationships that could be construed as a potential conflict of interest.

Publisher's Note: All claims expressed in this article are solely those of the authors and do not necessarily represent those of their affiliated organizations, or those of the publisher, the editors and the reviewers. Any product that may be evaluated in this article, or claim that may be made by its manufacturer, is not guaranteed or endorsed by the publisher.

frontiers | Frontiers in Oncology

ORIGINAL RESEARCH
published: 30 June 2022
doi: 10.3389/fonc.2022.868076

Association Between Internal Organ/Liver Tumor and External Surface Motion From Cine MR Images on an MRI-Linac

*Weihua Mao**, *Joshua Kim* and *Indrin J. Chetty*

Department of Radiation Oncology, Henry Ford Health System, Detroit, MI, United States

Purposes/Objectives: Historically, motion correlation between internal tumor and external surrogates have been based on limited sets of X-ray or magnetic resonance (MR) images. With the recent clinical implementation of MR-guided linear accelerators, a vast quantity of continuous planar real-time MR imaging data is acquired. In this study, information was extracted from MR cine imaging during liver cancer treatments to establish associations between internal tumor/diaphragm and external surface/skin movement.

Methods and Materials: This retrospective study used 305,644 MR image frames acquired over 118 treatment/imaging sessions of the first 23 liver cancer patients treated on an MRI-linac. 9 features were automatically determined on each MR image frame: Lung_Area, the posterior (Dia_Post), dome (Dia_Dome), and anterior (Dia_Ant) points of a diaphragmatic curve and the diaphragm curve point (Dia_Max), the chest (Chest) and the belly (Belly) skin points experiencing the maximum motion ranges; the superior-interior (SI) and posterior-anterior (PA) positions of a target. For every session, correlation analyses were performed twice among the 9 features: 1) over a breath-hold (BH) set and 2) on a pseudo free-breathing (PFB) generated by removing breath-holding frames.

Results: 303,123 frames of images were successfully analyzed. For BH set analysis, correlation coefficients were as follows: 0.94 ± 0.07 between any two features among Dia_Post, Dia_Dome, Dia_Max, and Lung_Area; 0.95 ± 0.06 between SI and any feature among Dia_Post, Dia_Dome, Dia_Max, or Lung_Area; 0.76 ± 0.29 between SI and Belly (with 50% of correlations ≥ 0.87). The PFB set had 142,862 frames of images. For this set, correlation coefficients were 0.96 ± 0.06 between any two features among Dia_Post, Dia_Dome, Dia_Max, and Lung_Area; 0.95 ± 0.06 between SI and any feature among Dia_Post, Dia_Dome, Dia_Max, or Lung_Area; 0.80 ± 0.26 between SI and Belly (with 50% of correlations ≥ 0.91).

OPEN ACCESS

Edited by:
John Varlotto,
Marshall University, United States

Reviewed by:
Gage Redler,
Moffitt Cancer Center, United States
Niek Huttinga,
University Medical Center Utrecht, Netherlands

****Correspondence:***
Weihua Mao
wmao1@hfhs.org

Specialty section:
This article was submitted to Radiation Oncology, a section of the journal Frontiers in Oncology

Received: *02 February 2022*
Accepted: *08 June 2022*
Published: *30 June 2022*

Citation:
Mao W, Kim J and Chetty IJ (2022) Association Between Internal Organ/Liver Tumor and External Surface Motion From Cine MR Images on an MRI-Linac. Front. Oncol. 12:868076. doi: 10.3389/fonc.2022.868076

Conclusion: Diaphragmatic motion as assessed by cine MR imaging is highly correlated with liver tumor motion. Belly vertical motion is highly correlated with liver tumor longitudinal motion in approximately half of the cases. More detailed analyses of those cases displaying weak correlations are in progress.

Keywords: motion correlation, MR cine imaging, liver cancer, tumor motion, diaphragm motion, skin motion

INTRODUCTION

Internal tumor motion due to respiration compromises the precision of radiation therapy and efficacy at delivering high radiation doses to control the tumor while minimizing side effects to adjacent normal tissues. Large margins have been added to expand the clinical target volume to a much larger planning treatment volume (PTV) (1–3). It is vital to locate tumors and critical structures in real-time to minimize irradiation of normal tissue (4–7). However, it is difficult to directly track internal organ motions in real-time by common radiation therapy equipment. X-ray based fluoroscopy imaging delivers too much extra imaging dose with limited soft tissue contrast (8). Implanted fiducial markers only provide locations of limited points with the risk of side effects from fiducial implantation and marker migration (9). Intensive studies have been reported to identify the correlation between internal tumor motion and external surrogates (10–23). Correlations between internal tumor motions and external surrogates have been based on computed tomography (CT) or magnetic resonance (MR) volumetric image sets or dynamically updated with intermittent X-ray or MR images during treatment. All these studies were performed based on limited patient data. Previous reports that focused on cine MR images to define correlations between different surrogates have used MR images acquired over a limited time period and outside the context of actual radiation therapy treatment delivery. For example, Paganelli et al. reported correlation studies between internal features and external surrogates based on 120 frames of MR cine images over 74.4 seconds per patient (24); Yang et al. reported correlation between diaphragm and liver tumor based on MR images within 15~30 seconds (25). It is clinically important to study the correlation over a time period covering an entire radiation therapy treatment from positioning patient to completing dose delivery, which lasts for at least 10 minutes. Moreover, breathing patterns acquired at simulation can often be different than those at time of actual treatment. With the recent clinical implementation of MR-guided linear accelerators, a vast quantity of continuous planar real-time MR imaging data is acquired at 4 frames/second as part of the radiation therapy treatment delivery process (5–7). In the first 9-months after installation of an MR-guided linear accelerator at our institution, 23 liver cancer patients had been treated by stereotactic body radiation therapy (SBRT). MR cine images were acquired for about one hour per patient. In this study, liver tumor motion data was extracted from the treatment MR cine imaging data to establish associations between internal tumor/diaphragm and external surface/skin movement from the same image sets for the entire treatment session. This would be the first report that includes a large quantity of cine images acquired during actual treatment for the full treatment session. This is very different from reports in the literature, which were based on patient data over a short period of time. With such an enormous amount of data, patient respiratory diversity and variation were represented by the changing respiratory pattern over the course of a full treatment. This is different from irregular breathing usually observed during 4D CT scans, which might be due to irregular respiration amplitude.

METHODS AND MATERIALS

This retrospective study used patient cine images acquired during routine stereotactic body radiation therapy (SBRT) treatments on a low field (0.35 T) MRI-linac (MRIdian, ViewRay, Mountain View, CA). 23 liver cancer patients (listed in **Table 1**) were enrolled in this Internal Review Board (IRB)-approved (IRB #12934) study. All patients were prescribed to 50 Gy in 5 fractions. In certain cases, one planned fraction of treatment might be interrupted and the remainder of this fraction of treatment would be resumed later. In that case, one planned fraction of treatment could span multiple sessions. 305,644 frames of MR sagittal images were acquired as a part of the radiation therapy process.

After 3-dimensional (3D) MRI images were acquired to setup patients for treatment, this MRI-linac continuously acquired four sagittal MR image frames per second during treatment. Dimensions of each frame were 100 x 100 and pixel sizes were 3.5 mm x 3.5 mm. After a patient was positioned for treatment, an initial target tracking structure was manually contoured on the initial volumetric image set and a tracking boundary structure was automatically generated as an isotropic 3 mm expansion of the tracking structure. The treatment software routinely monitored target motion. It deformably propagated the target tracking structure automatically onto each newly acquired image frame. Additionally, the tracking boundary structure was statically copied onto each image frame. The treatment software continuously monitored whether the detected target was within this boundary. Treatment beam delivery would be held whenever the target was out of the boundary by a preset percentage (5% for liver SBRT treatment) and the beam delivery would resume when the target moved back in the boundary. The tracking structure may be different from the target but must represent target motion. In this article, we regard tracking structures as targets. Targets were mapped as red contours and target boundaries were mapped as yellow contours (as shown in **Figure 1A**). They were overlaid on grayscale MR images. Cine images were saved and exported as videos for each treatment session. The videos have dimensions of

TABLE 1 | List of patients with planning target volume (PTV) size and average longitudinal and lateral locations.

Patients	Gender	Age	Diagnosis	PTV (cm^3)	Longitudinal location (mm)	Lateral location
LV01	F	89	Secondary malignant neoplasm of bone	40	40	0.60
LV02	M	71	Liver cell carcinoma	148	69	0.70
LV03	M	85	Secondary malignant neoplasm of liver and intrahepatic bile duct	50	106	0.45
LV04	F	54	Liver cell carcinoma	46	61	0.58
LV05	M	65	Liver cell carcinoma	181	49	0.66
LV06	M	68	Liver cell carcinoma	71	69	0.47
LV07	M	72	Liver cell carcinoma	937	71	0.68
LV08	M	89	Liver cell carcinoma	24	39	0.53
LV09	F	90	Intrahepatic bile duct carcinoma	111	83	0.72
LV10	M	56	Liver cell carcinoma	63	57	0.69
LV11	M	71	Secondary malignant neoplasm of liver and intrahepatic bile duct	118	61	0.55
LV12	M	78	Liver cell carcinoma	12	108	0.52
LV13	M	88	Intrahepatic bile duct carcinoma	121	49	0.55
LV14	M	68	Liver cell carcinoma	253	84	0.57
LV15	M	68	Liver cell carcinoma	48	89	0.31
LV16	F	86	Secondary malignant neoplasm of liver and intrahepatic bile duct	29	14	0.55
LV17	M	83	Secondary malignant neoplasm of liver and intrahepatic bile duct	231	95	0.78
LV18	M	68	Secondary malignant neoplasm of liver and intrahepatic bile duct	48	51	0.53
LV19	F	65	Liver cell carcinoma	65	20	0.53
LV20	M	78	Intrahepatic bile duct carcinoma	59	61	0.57
LV21	F	70	Intrahepatic bile duct carcinoma	281	27	0.75
LV22	F	76	Liver cell carcinoma	115	57	0.49
LV23	M	71	Liver cell carcinoma	60	82	0.48

Longitudinal location is the longitudinal distance between the target center and diaphragmatic dome. Lateral location is the lateral off-center ratio, which is the lateral distance between target center and spine as a ratio of the lateral distance between inner edge of the thoracic cage and spine.

512 x 512 and pixel sizes are 0.79 mm x 0.79 mm. In-house software was developed to analyze images in Matlab (MathWorks, Natic, MA) following the below steps:

1. Read video files and load each frame of MR images.
2. Crop images to remove embedded borders and keep MR images only.
3. Detect the contours of targets and target boundaries. Fill target structures and calculate the center of mass in Posterior-Anterior direction (PA) and Superior-Inferior direction (SI). PA and SI will be used throughout as referring to the target positions in two directions. Remove contours and fill blank pixels with the average of surrounding pixels, as shown in **Figure 1B**.

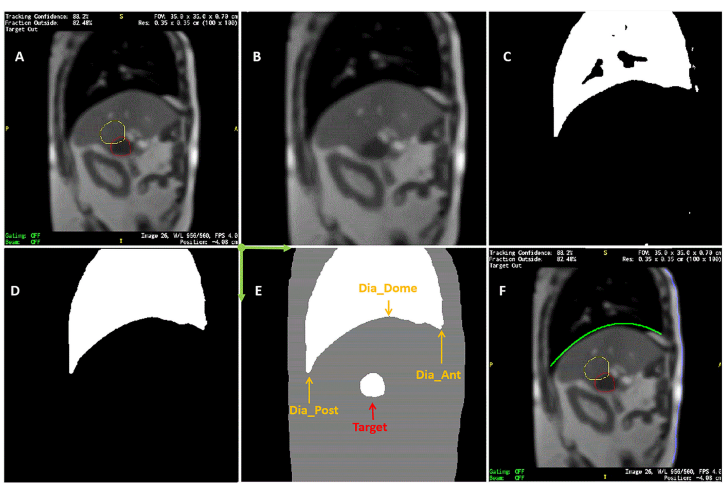

FIGURE 1 | Sample of MR image detection. **(A)** Acquired image. Yellow line contoured the expected target boundary and red line contoured the detected target. Every MR image frame had blank frame borders with information texts attached to four sides of MR images. **(B)** Cropped image after contours were removed. **(C)** Initially detected lung based on intensity threshold. **(D)** refined lung structure. **(E)** Detected body, lung, and target contours superimposed. Dia_Dome, Dia_Post, Dia_Ant, are Target are labeled. Coordinate system origin locates at the upper-left corner and axis directions were illustrated in green arrows. **(F)** Detected body and diaphragmatic curve superimposed back to the original image.

4. Use an intensity threshold to detect the body contour on the image.
5. Use an intensity threshold in the body to detect lungs as shown in **Figure 1C**. Matlab functions including hole filling, eroding, expanding, and selection of the largest areas were used to refine lung detection as shown in **Figure 1D**. Parabolic curves were used to fit diaphragmatic curve (upper portions). **Figure 1E** superimposed the lung structures and filled target onto the body contour.
6. Parabolic curve fitting results and anterior body contours were mapped back to the original images as a record (**Figure 1F**).

On each frame of the cine MR treatment acquisition, in addition to target positions PA and SI, our Matlab program automatically determined the following four lung area features as illustrated in **Figure 1E** (26): (1) Lung_Area - the total area of the detected lung; (2) Dia_Post - the most posterior point on the patient diaphragmatic curve; (3) Dia_Dome - the dome or apex of the diaphragmatic curve after curve-fitting; (4) Dia_Ant - the most anterior point of the patient diaphragmatic curve. Three more features were determined after analyzing motion of each session. The point on the diaphragm that experienced the maximum range of longitudinal motion over a treatment session was selected, and its longitudinal positions were extracted as Dia_Max. The average Dia_Ant point per session was used to separate chest and belly regions on the anterior body surface. The chest skin point and the belly skin point that experienced the maximum range of vertical motion at the chest and belly region, respectively, were selected. Their vertical positions are Chest and Belly. Typically, respiratory motion is usually estimated using external surrogates such as the vertical motion of surface points on the upper abdomen. For example, the Varian Real-time Position Management (RPM) system uses an infrared camera to track the vertical motion of a block placed on the patient's anterior upper abdominal skin surface while the Philips bellows belt system is placed around the patient's belly to measure pressure changes due to respiration. We searched for the skin point with maximum motion range to simulate the optimal external surrogate.

A pre-analysis screening process was automatically carried out for every session. There were certain situations when the target tracking structure was not tracked correctly due to sudden large target excursions. Therefore, a pre-analysis screening process was automatically carried out for every session. Histograms with a bin width of 3.5 mm (the pixel size of original images) were generated for both target positions (SI and PA) and the Belly position. A cutoff frequency was defined as 1% of the maximum frequency, which was used to determine cutoff position thresholds on the upper and lower sides of the target position that occurred most frequently on the histogram. Frames falling outside of the cutoff positions were regarded as outliers (extreme and isolated positions), and they were excluded from correlation analysis.

Pearson correlation coefficients were calculated twice for each pair of features among the 9 features described above for every session. The first correlation analysis was computed over the full set of image frames, which was designated as the breath-hold (BH) set. The MR images were acquired during breath-hold treatment and about half of the image frames were acquired while patients were holding their breath. To eliminate the adverse effects of such unbalanced distribution of motion positions, the second analysis was performed on pseudo free-breathing (PFB) data sets, which were generated by removing image frames identified as being at breath-holding from the BH set. The analysis program automatically compared the Dia_Dome position of each frame with the Dia_Dome positions of the 3 immediately preceding and following frames. If the Dia_Dome range was less than one pixel (3.5 mm), this frame would be regarded as a breath-holding frame. **Figure 2** illustrated a BH set of images and its PFB set. Statistical analyses of comparisons between BH and PFB set analysis results were performed using Student's *t*-test (1 tail, at the alpha = 0.05 significance level).

For every session, the sagittal plane to be tracked during cine imaging was selected using the initial volumetric MRI image. The lateral position of the selected sagittal plane was recorded for each session. The lateral positions of the target center, spine, and inner edge of the thoracic cage were manually detected using an

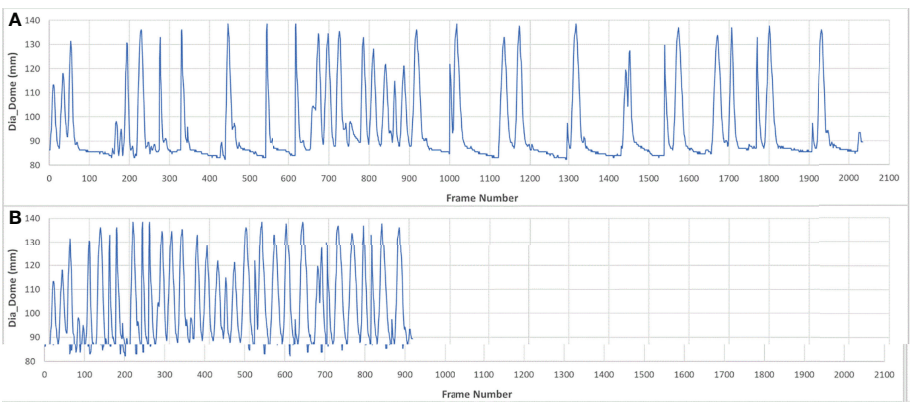

FIGURE 2 | Sample of breath-hold (BH) data set **(A)** and its pseudo free-breathing (PFB) set **(B)**.

axial slice of the initial volumetric MRI that was located at the center of the tracking target. Lateral off-center ratio was calculated as the lateral distance between target center and spine divided by the distance between lateral thoracic cage edge and spine. The smaller the ratio, the closer to the body midline. Average lateral off-center ratios were listed in **Table 1**.

RESULTS

303,123 frames of 2D MR images were analyzed in the BH set over 118 imaging sessions for 23 patients. Less than 1% of images were excluded where the target was not correctly detected by the system. The PFB set analysis used 142,862 of the image frames. **Figure 3** illustrates selected correlation coefficients of 36 feature pairs among the 9 features defined above for BH and PFB analyses. **Figure 3** shows that correlation results of the PFB set are slightly better than BH set analysis results. Analysis was done to compare correlation coefficients per session. The PFB set showed slightly better correlation coefficients among diaphragmatic features (differences of 0.01 ± 0.04 with p-value < 0.01) and similar correlation coefficients between SI and any one of the four diaphragmatic features (differences of 0.00 ± 0.03) while the analysis using PFB set showed better correlation coefficients between Belly and SI (differences of 0.04 ± 0.08 with p-value < 0.01). This shows that excessive breath-holding image frames at end exhalation would affect correlation analysis and the PFB results should be used for the free breathing scenario.

Five lung/diaphragmatic features behave differently, and it is essential to focus on the feature with the best correlation to external motion. High aggregate cross correlations occur between any two features among Dia_Post, Dia_Dome, Dia_Max, and Lung Area, as the left 6 groups of boxplots in **Figure 3** demonstrate. They are 0.94 ± 0.07 and 0.96 ± 0.06 for BH and PFB set analyses, respectively. However, the fifth feature, Dia_Ant, did not have high aggregate correlations with other features. They are 0.77 ± 0.23 and 0.81 ± 0.17 for BH and PFB set analyses, respectively. After reviewing the Dia_Ant results, we found a complex intensity scheme. This may be due to the proximity of the diaphragm to bones as well as possible effects of ascites on the precision of identifying the proper Dia_Ant position. Among the four features, Dia_Dome results achieved the highest correlation with SI. This suggests that Dia_Dome is the best landmark to represent diaphragmatic motions, which is consistent with findings reported by Yang et al. (25). It should be noted that the superior regions of the lungs may sometimes be outside of the field of view. Therefore, the Lung_Area parameter may not represent the full lung area which may degrade the accuracy of the correlation between Lung_Area and other features.

High correlation coefficients (0.95 ± 0.06) occurred as combined result of all feature pairs between SI and any of Dia_Post, Dia_Dome, Dia_Max, and Lung_Area for either BH or PFB set analyses. SI-Belly Correlation coefficients are 0.76 ± 0.29 (with 50% of correlations ≥ 0.86) and 0.80 ± 0.26 (with 50% of correlations ≥ 0.91) for BH and PFB set analyses, respectively. SI-Belly correlation is patient dependent and may vary in different sessions as summarized in **Table 2**. To verify and further study SI-Belly correlation variations, motion details were compared. Particularly, patient LV13 SI-Belly correlation coefficients varied between 0.65 and 0.98 among four sessions. **Figure 4** illustrates portions of SI and Belly results as functions of time of the same patient, LV13, over Sessions #3 and #4. **Figure 5** shows four frames selected from the two sessions of patient LV13 displayed in **Figure 4**. **Figure 6** compares correlations with Belly

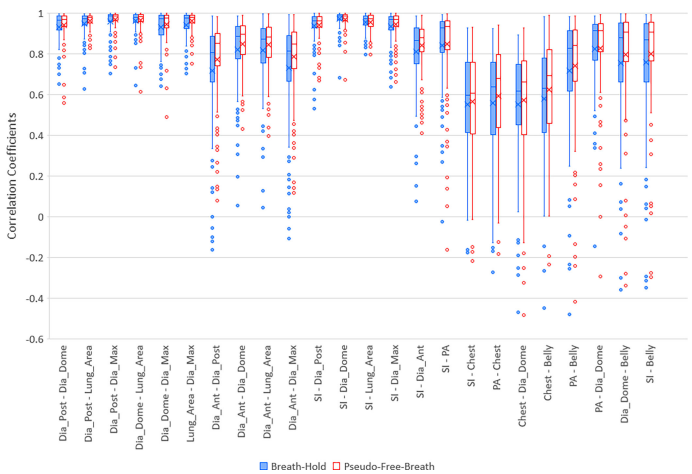

FIGURE 3 | Boxplots of selected correlation coefficients between two of 9 parameters, PA, SI, Dia_Post, Dia_Dome, Dia_Ant, Lung_Area, Dia_Max, Chest, and Belly for Breath-Hold and Pseudo-Free-Breath. Median and Average correlation coefficients are marked by horizontal line and "x" in each box, respectively. Interquartile range (IQR) is the difference between the 3rd quartile (Q3, the upper side of each box) and the 1st quartile (Q1, the lower side of each box). The upper whisker ends at maximum correlation coefficients while bottom whisker ends at Q1 – 1.5 * IQR. Any correlation coefficients smaller than Q1 – 1.5 * IQR are considered to be outliers and are displayed represented by dots.

TABLE 2 | List of average, standard deviation (Stdev), minimum, and maximum correlation coefficients between SI and Belly for each patient.

Patient	Number of Sessions	Average	Stdev	Minimum	Maximum	Stdev/Average	Range/Average/2
LV01	5	0.75	0.17	0.52	0.95	0.22	0.29
LV02	6	0.89	0.05	0.81	0.95	0.06	0.08
LV03	5	0.94	0.03	0.90	0.97	0.03	0.04
LV04	6	0.93	0.09	0.76	0.98	0.09	0.12
LV05	6	0.84	0.07	0.74	0.89	0.09	0.09
LV06	5	0.85	0.05	0.77	0.91	0.06	0.08
LV07	5	0.24	0.27	0.02	0.61	1.14	1.23
LV08	5	0.63	0.23	0.37	0.88	0.36	0.40
LV09	5	0.56	0.23	0.30	0.78	0.42	0.43
LV10	5	0.73	0.12	0.63	0.92	0.17	0.20
LV11	5	0.98	0.01	0.98	0.99	0.01	0.01
LV12	5	0.88	0.06	0.78	0.93	0.07	0.08
LV13	4	0.89	0.16	0.65	0.98	0.18	0.19
LV14	6	0.95	0.04	0.90	0.98	0.04	0.05
LV15	7	0.85	0.16	0.52	0.97	0.19	0.27
LV16	5	0.96	0.03	0.91	0.98	0.03	0.04
LV17	5	0.65	0.10	0.51	0.77	0.15	0.20
LV18	5	0.90	0.06	0.81	0.96	0.07	0.09
LV19	5	0.93	0.01	0.92	0.94	0.01	0.01
LV20	5	0.94	0.02	0.93	0.97	0.02	0.02
LV21	5	0.18	0.63	-0.30	0.87	3.56	3.31
LV22	5	0.93	0.05	0.83	0.96	0.06	0.06
LV23	3	0.91	0.07	0.83	0.97	0.08	0.07

Patients with the most linear correlations were highlighted in green. Patients with the least linear correlations were highlighted in yellow.

between the two sessions. These two sessions showed very different internal-external motion correlations. Furthermore, **Figure 7** illustrates SI-Belly correlations for the sessions with the lowest 20 correlation coefficients.

DISCUSSION

It should be noted that although PFB results show better internal-external correlations, both PFB and BH are different from natural free breathing. When patients were asked to hold their breath at the end of exhale, their lung volumes were generally smaller than those at the end of exhale during a free breathing cycle. Immediately after stressful breath-holds, patients might breathe faster than during free breathing. One limitation of this study is that all cine images available to authors were from breath-hold treatments. The conclusions are valid for breath-hold treatment. In addition, if a patient always breathes with the same respiratory pattern, the internal-external motion correlation should be identical for PFB and free-breathing. During PFB the patient may experience a slightly larger motion range due to deep breath-hold relative to free

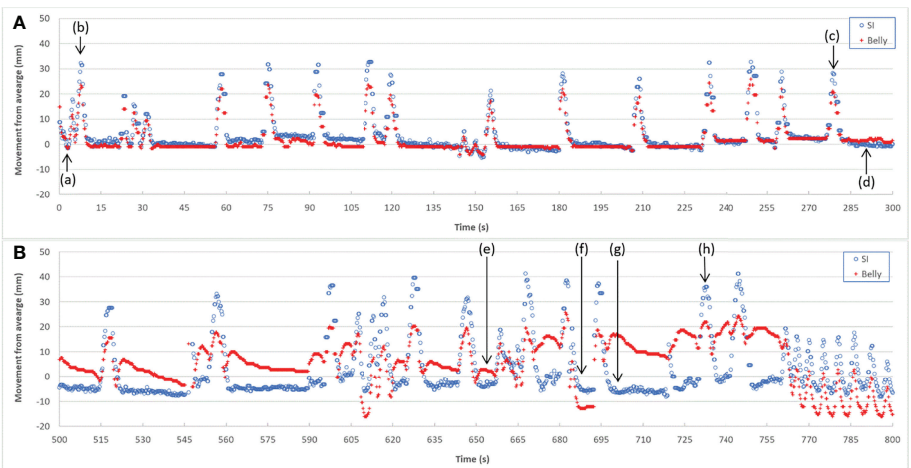

FIGURE 4 | Target SI and Belly motion as functions of time for Session #3 **(A)** and Session #4 **(B)** of patient LV13.

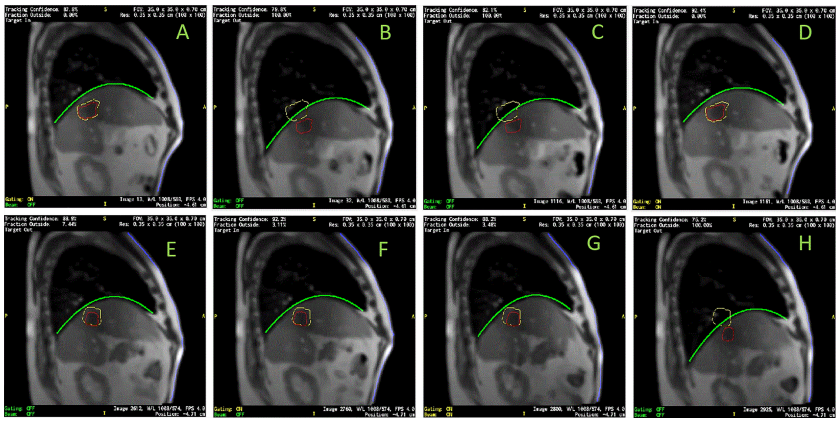

FIGURE 5 | Images selected from two sessions of patient LV13. **(A–D)** were from Session #3 and **(E–H)** were from Session #4 as labeled in **Figure 4**. Target/tracking structures are in red; boundaries of tracking structure are in yellow; curve-fitting results of diaphragmatic curves are in green; anterior skin extracted from body contours are in blue. Frames **(A–H)** indicate the frames (a-h) labeled in **Figure 4**.

breathing. In this case, PFB results should be identical to free-breathing results. However, stressful breath-holds might trigger different respiratory patterns, which could alter the internal-external correlations.

Both Chest and Belly features represent external surrogates but behave very differently. Chest has weaker correlation in aggregate than any other feature. If a patient only performs chest breathing, Dia_Dome and SI would move linearly with Chest while minimal motion of the Belly would be expected. However, observed correlation coefficients between Chest and Dia_Dome were 0.55 ± 0.27 and 0.57 ± 0.28 for BH and PFB set analyses, respectively. Correlation coefficients between Chest and SI were only 0.55 ± 0.26 and 0.57 ± 0.25 for BH and PFB set analyses, respectively. This indicates that no patient experienced

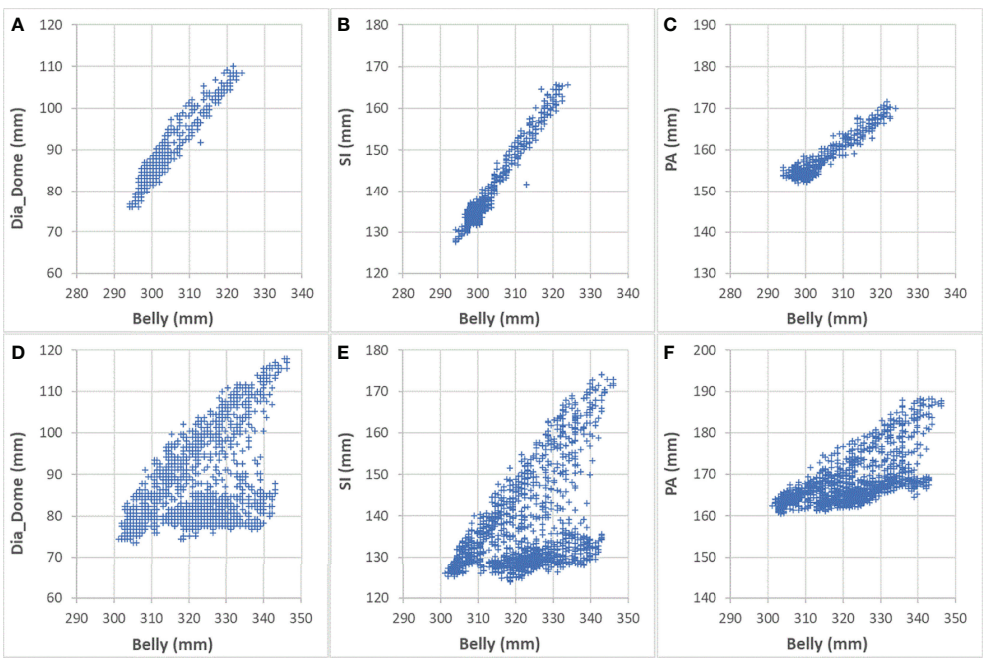

FIGURE 6 | Comparing correlations with Belly for Sessions #3 and #4 of patient LV13. **(A)** Dia_Dome as a function of Belly in Session #3; **(B)** SI as a function of Belly in Session #3; **(C)** PA as a function of Belly in Session #3; **(D)** Dia_Dome as a function of Belly in Session #4; **(E)** SI as a function of Belly in Session #4; **(F)** PA as a function of Belly in Session #4.

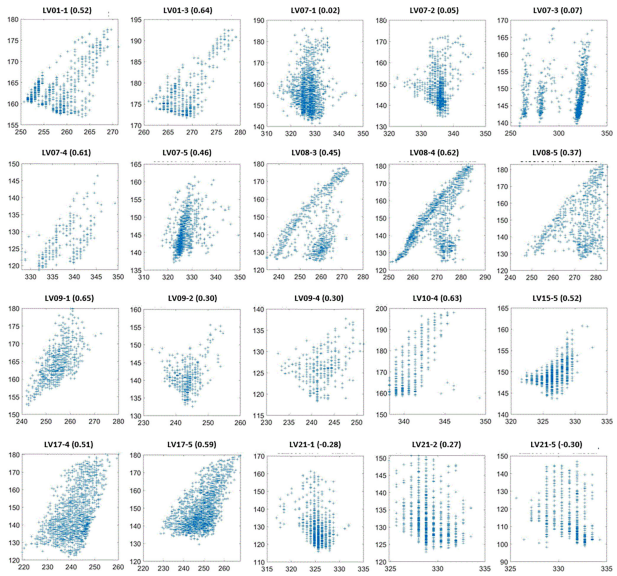

FIGURE 7 | SI (vertical axes in mm) as a function of Belly (horizontal axes in mm) for the sessions with the lowest 20 SI-Belly correlation coefficients. Figure titles include patient ID and Session #. Correlation coefficients are in parentheses.

pure chest breathing, and the position of the chest during chest breathing is not always a good surrogate for the breathing pattern. Another reason could be that Chest experienced the smallest range of motion among the 9 features investigated. Motion ranges were 16 ± 6 mm, 19 ± 8 mm, and 25 ± 11 mm for Chest, PA, and Belly, respectively. Small motion ranges might result in larger uncertainties, especially when the pixel size of the original MR images was relatively large (3.5 mm). Belly motion showed improved correlation with both diaphragmatic and target motions compared to Chest motion. Correlation coefficients between Belly and Dia_Dome are 0.76 ± 0.30 and 0.80 ± 0.28 for BH and PFB set analyses, respectively.

One of our goals was to determine the correlation between Belly and target motion. The correlation coefficient between Belly and SI was 0.76 ± 0.29 using the BH set. Half of the imaging sessions had correlation coefficients between Belly and SI greater than or equal to 0.87. As listed in **Table 2**, 9 patients, highlighted in green, have linear correlation between SI and Belly (with minimum correlation coefficients ≥ 0.81) in every imaging session. Their inter-session correlation coefficient variations are presented by ratio of standard deviation over average (0.06 or less) and ratio of half range over average (0.09 or less) as listed in **Table 2**. **Table 2** shows that more than half (12/23) of the patients have average correlation coefficients greater than 0.88 in their imaging sessions. The remaining patients have average correlation coefficients less than 0.86. As highlighted in yellow in **Table 2**, five patients had weak SI-Belly correlations (with maximum correlation coefficients ≤ 0.88) in every imaging session. If these data were excluded as outliers, PFB correlation coefficients between SI and Belly would be 0.89 ± 0.10 for the 93 sessions of 18 patients. Except for the nine patients with high linear SI-Belly correlations (highlighted in green in **Table 2**), 15 patients changed their respiratory patterns in at least one imaging session. As an example, **Figures 4–6** compare Belly and SI motions of patient LV13 over two different sessions. The PFB correlation coefficients were 0.98 and 0.65 for Sessions #3 and #4, respectively. Compared with **Figures 5A** and **D or B** and **C, E–G** shows that the Belly moved while the diaphragm (Dia_Dome) and target (SI) position remained stationary, causing a wide spread of data points along the Belly position axis at breath-holding positions. The position of each figure along the breathing trace were illustrated in **Figure 4B**. This means that the baseline Belly position varies over a period of just 60 seconds. In the same session, the right portion of the breathing trace displayed in **Figure 4B** plots a period of greater than 30 seconds when the target moves over a range of 25 mm while the Belly moved correspondingly but at a very different Belly baseline. More specifically, **Figure 4B** illustrated a repeating trend that at breath hold, Belly (red "+") tended to gradually drift along the posterior direction while SI (blue "o") and diaphragm remained stationary. This is a potential limitation of breath-hold studies. Patients might change their breathing patterns relative to their normal free breathing pattern. This deviation from normal breathing pattern more likely happened at breath-holding phases. The PFB set was created from the full image set by removing breath-holding frames based on diaphragm positions and some frames with belly drifting were removed. This resulted in a better SI-Belly correlation relative to the full BH set analysis. It should be noted that Pt LV21 had the least linear correlation between SI and Belly as shown in **Figure 7**. Video review found that this patient's belly was located on the border of the MR imaging field of view (FOV) due to patient size, and a portion of the belly kept moving in and out of imaging FOV during treatment. As a result, the extracted Belly results won't represent the optimal external motion.

This study utilized over 300,000 frames of images, which recorded respiratory information, including both internal tumor/organs and external skin motions, lasting for an average of 54 minutes per patient over different days. For lung inhalation, chest breathing may expand the thoracic cage only while abdominal breathing engages the belly and abdomen. A combination of chest and abdominal breathing or even more complicated breathing patterns may occur during radiation therapy treatment. For example, chest breathing may be performed while the belly/abdomen holds at different levels. Once the respiratory pattern changed, the relationship between SI and Belly would cease to be linear. **Figure 7** indicates that several sessions have multiple breathing patterns. This implies that an internal-external correlation model cannot be fully determined during a single session. It is unclear how or when a patient may change his/her respiratory pattern. The respiratory pattern may be interrupted by breath holding, particularly when patients were frequently asked to adjust the breath hold level to ensure that the target remains inside the target boundary. On the other hand, patient body movement, such as body rolling, might result in additional belly shift on the sagittal MR cine images, which contributes to respiratory pattern changes. This should be more likely to happen when the sagittal imaging plane is located farther away from the body midline, where the lateral skin slope becomes larger. The SI-Belly correlation coefficient is

illustrated as a function of the lateral off-center ratio in **Figure 8**. This indicates that the dispersion of SI-Belly correlation coefficients increases with the lateral off-center ratio. Further studies should involve 3-dimensional patient movement. Later treatment software versions allow for acquiring cine images on multiple planes, which would help to eliminate this kind of uncertainty.

A hysteresis relationship or phase shift between internal (SI) and external (Belly) features has been suggested by many reports (2, 16, 17, 20, 23, 27). However, this was not observed from the data acquired in this study. **Figure 7** illustrates the 20 sessions with the lowest SI-Belly correlation coefficients. The non-linear relationship between SI and Belly could not be explained by a hysteresis loop. As illustrated in **Figures 4–6**, Pt LV13 changed respiratory patterns within a single session. **Figures 4E–G** show that the abdomen was changing position even while the target (red contour) remained stationary (within the boundary in yellow). Generally, when a patient exhales during abdominal respiration, the diaphragm moves superiorly and the belly moves posteriorly, which leads to a linear relationship between SI and Belly. However, the patient may hold either with the belly fully (**Figure 4G**) or partially (**Figure 4E**) expanded, which leads to uncertainty in the Belly position at a given breathing phase. As illustrated in **Figure 7**, the sessions with the lowest SI-Belly correlation coefficients demonstrated that even when looking at a single phase (end inhalation), the Belly position would migrate over the course of treatment, which is shown as a wide spread of Belly positions at superior SI locations during holding-breath. This could not be explained by hysteresis.

The linear relationship between diaphragm and target longitudinal motion was confirmed. Correlation coefficients between SI and Dia_Dome were 0.97 ± 0.04 for either BH or PFB set analyses. This is reasonable since the target is underneath the diaphragmatic curve. Although this study is based on liver cancer radiation therapy, the correlation between target and internal diaphragmatic motion could be extended to lung tumor motions. In addition to MR imaging, ultrasound may be used to monitor diaphragmatic motion non-invasively. This also suggests that tracking diaphragmatic motions using an ultrasound technique could be used to monitor liver or lung tumor motions efficiently (28). Chest and Belly motion can be monitored by external surrogates, such as Varian RPM, Philips Bellows, or optical surface imaging systems.

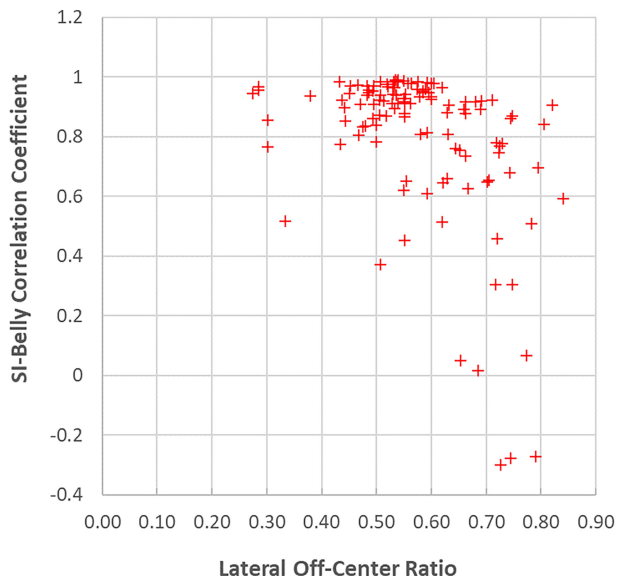

FIGURE 8 | SI-Belly correlation coefficients as a function of the lateral off-center ratio.

CONCLUSIONS

Diaphragmatic motion as assessed by cine imaging on an MRI-linac is highly correlated with liver tumor motion, and the diaphragmatic dome could be a good indicator of liver tumor motion. Care should be taken when using an external skin motion surrogate positioned at the belly, since this surrogate only has linear correlation with liver tumor longitudinal motion in approximately half of the cases. More detailed analyses of those cases displaying weak correlations are under further investigation.

DATA AVAILABILITY STATEMENT

The raw data supporting the conclusions of this article will be made available by the authors, without undue reservation.

ETHICS STATEMENT

The studies involving human participants were reviewed and approved by Henry Ford Health System Internal Review Board. Written informed consent for participation was not required for this study in accordance with the national legislation and the institutional requirements.

AUTHOR CONTRIBUTIONS

WM was responsible for the research design, data collection and analysis, and manuscript preparation. JK and IC participated into the research design and manuscript preparation. All authors contributed to the article and approved the submitted version.

SUPPLEMENTARY MATERIAL

The Supplementary Material for this article can be found online at: https://www.frontiersin.org/articles/10.3389/fonc.2022.868076/full#supplementary-material

REFERENCES

1. Verellen D, De Ridder M, Linthout N, Tournel K, Soete G, Storme G. Innovations in Image-Guided Radiotherapy. *Nat Rev Cancer* (2007) 7 (12):949–60. doi: 10.1038/nrc2288
2. Keall PJ, Mageras GS, Balter JM, Emery RS, Forster KM, Jiang SB, et al. The Management of Respiratory Motion in Radiation Oncology Report of AAPM Task Group 76. *Med Phys* (2006) 33(10):3874–900. doi: 10.1118/1.2349696
3. Jiang SB. Radiotherapy of Mobile Tumors. *Semin Radiat Oncol* (2006) 16 (4):239–48. doi: 10.1016/j.semradonc.2006.04.007
4. Lujan AE, Larsen EW, Balter JM, Ten Haken RK. A Method for Incorporating Organ Motion Due to Breathing Into 3D Dose Calculations. *Med Phys* (1999) 26(5):715–20. doi: 10.1118/1.598577
5. Hu Y, Rankine L, Green OL, Kashani R, Li HH, Li H, et al. Characterization of the Onboard Imaging Unit for the First Clinical Magnetic Resonance Image Guided Radiation Therapy System. *Med Phys* (2015) 42(10):5828–37. doi: 10.1118/1.4930249
6. Mutic S, Dempsey JF. The ViewRay System: Magnetic Resonance-Guided and Controlled Radiotherapy. *Semin Radiat Oncol* (2014) 24(3):196–9. doi: 10.1016/j.semradonc.2014.02.008
7. Wen N, Kim J, Doemer A, Glide-Hurst C, Chetty IJ, Liu C, et al. Evaluation of a Magnetic Resonance Guided Linear Accelerator for Stereotactic Radiosurgery Treatment. *Radiother Oncol* (2018) 127(3):460–6. doi: 10.1016/j.radonc.2018.04.034
8. Xu Q, Hamilton RJ, Schowengerdt RA, Alexander B, Jiang SB. Lung Tumor Tracking in Fluoroscopic Video Based on Optical Flow. *Med Phys* (2008) 35 (12):5351–9. doi: 10.1118/1.3002323
9. Imura M, Yamazaki K, Shirato H, Onimaru R, Fujino M, Shimizu S, et al. Insertion and Fixation of Fiducial Markers for Setup and Tracking of Lung Tumors in Radiotherapy. *Int J Radiat Oncol Biol Phys* (2005) 63(5):1442–7. doi: 10.1016/j.ijrobp.2005.04.024
10. Hoisak JD, Sixel KE, Tirona R, Cheung PC, Pignol JP. Correlation of Lung Tumor Motion With External Surrogate Indicators of Respiration. *Int J Radiat Oncol Biol Phys* (2004) 60(4):1298–306. doi: 10.1016/j.ijrobp.2004.07.681
11. Ahn S, Yi B, Suh Y, Kim J, Lee S, Shin S, et al. A Feasibility Study on the Prediction of Tumour Location in the Lung From Skin Motion. *Br J Radiol* (2004) 77(919):588–96. doi: 10.1259/bjr/64800801
12. Tsunashima Y, Sakae T, Shioyama Y, Kagei K, Terunuma T, Nohtomi A, et al. Correlation Between the Respiratory Waveform Measured Using a Respiratory Sensor and 3D Tumor Motion in Gated Radiotherapy. *Int J Radiat Oncol Biol Phys* (2004) 60(3):951–8. doi: 10.1016/j.ijrobp.2004.06.026
13. Chen H, Zhong Z, Yang Y, Chen J, Zhou L, Zhen X, et al. Internal Motion Estimation by Internal-External Motion Modeling for Lung Cancer Radiotherapy. *Sci Rep* (2018) 8(1):3677. doi: 10.1038/s41598-018-22023-3
14. Koch N, Liu HH, Starkschall G, Jacobson M, Forster K, Liao Z, et al. Evaluation of Internal Lung Motion for Respiratory-Gated Radiotherapy Using MRI: Part I–correlating Internal Lung Motion With Skin Fiducial Motion. *Int J Radiat Oncol Biol Phys* (2004) 60(5):1459–72. doi: 10.1016/j.ijrobp.2004.05.055
15. Kanoulas E, Aslam JA, Sharp GC, Berbeco RI, Nishioka S, Shirato H, et al. Derivation of the Tumor Position From External Respiratory Surrogates With Periodical Updating of the Internal/External Correlation. *Phys Med Biol* (2007) 52(17):5443–56. doi: 10.1088/0031-9155/52/17/023
16. Li G, Wei J, Olek D, Kadbi M, Tyagi N, Zakian K, et al. Direct Comparison of Respiration-Correlated Four-Dimensional Magnetic Resonance Imaging Reconstructed Using Concurrent Internal Navigator and External Bellows. *Int J Radiat Oncol Biol Phys* (2017) 97(3):596–605. doi: 10.1016/j.ijrobp.2016.11.004
17. Milewski AR, Olek D, Deasy JO, Rimner A, Li G. Enhancement of Long-Term External-Internal Correlation by Phase-Shift Detection and Correction Based on Concurrent External Bellows and Internal Navigator Signals. *Adv Radiat Oncol* (2019) 4(2):377–89. doi: 10.1016/j.adro.2019.02.001
18. Antoni ST, Rinast J, Ma XT, Schupp S, Schlaefer A. Online Model Checking for Monitoring Surrogate-Based Respiratory Motion Tracking in Radiation Therapy. *Int J Comput Assisted Radiol Surg* (2016) 11(11):2085–96. doi: 10.1007/s11548-016-1423-2
19. Cho B, Poulsen PR, Keall PJ. Real-Time Tumor Tracking Using Sequential kV Imaging Combined With Respiratory Monitoring: A General Framework Applicable to Commonly Used IGRT Systems. *Phys Med Biol* (2010) 55 (12):3299–316. doi: 10.1088/0031-9155/55/12/003
20. Ionascu D, Jiang SB, Nishioka S, Shirato H, Berbeco RI. Internal-External Correlation Investigations of Respiratory Induced Motion of Lung Tumors. *Med Phys* (2007) 34(10):3893–903. doi: 10.1118/1.2779941
21. Mukumoto N, Nakamura M, Sawada A, Suzuki Y, Takahashi K, Miyabe Y, et al. Accuracy Verification of Infrared Marker-Based Dynamic Tumor-Tracking Irradiation Using the Gimbaled X-Ray Head of the Vero4DRT (MHI-Tm2000). *Med Phys* (2013) 40(4):041706. doi: 10.1118/1.4794506
22. Ren Q, Nishioka S, Shirato H, Berbeco R. Adaptive External Gating Based on the Updating Method of Internal/External Correlation and Gating Window Before Each Beam Delivery. *Phys Med Biol* (2012) 57(9):N145–57. doi: 10.1088/0031-9155/57/9/N145
23. Wu H, Zhao Q, Berbeco RI, Nishioka S, Shirato H, Jiang SB. Gating Based on Internal/External Signals With Dynamic Correlation Updates. *Phys Med Biol* (2008) 53(24):7137–50. doi: 10.1088/0031-9155/53/24/009
24. Paganelli C, Seregni M, Fattori G, Summers P, Bellomi M, Baroni G, et al. Magnetic Resonance Imaging-Guided Versus Surrogate-Based Motion Tracking in Liver Radiation Therapy: A Prospective Comparative Study. *Int J Radiat Oncol Biol Phys* (2015) 91(4):840–8. doi: 10.1016/j.ijrobp.2014.12.013
25. Yang J, Cai J, Wang HJ, Chang Z, Czito BG, Bashir MR, et al. Is Diaphragm Motion a Good Surrogate for Liver Tumor Motion? *Int J Radiat Oncol Biol Phys* (2014) 90(4):952–8. doi: 10.1016/j.ijrobp.2014.07.028
26. Bishop CA, Ricotti V, Sinclair CDJ, Evans MRB, Butler JW, Morrow JM, et al. Semi-Automated Analysis of Diaphragmatic Motion With Dynamic Magnetic Resonance Imaging in Healthy Controls and Non-Ambulant Subjects With Duchenne Muscular Dystrophy. *Front Neurol* (2018) 9. doi: 10.3389/fneur.2018.00009
27. Seppenwoolde Y, Shirato H, Kitamura K, Shimizu S, van Herk M, Lebesque JV, et al. Precise and Real-Time Measurement of 3D Tumor Motion in Lung Due to Breathing and Heartbeat, Measured During Radiotherapy. *Int J Radiat Oncol Biol Phys* (2002) 53(4):822–34. doi: 10.1016/S0360-3016(02)02803-1
28. Vogel L, Sihono DSK, Weiss C, Lohr F, Stieler F, Wertz H, et al. Intra-Breath-Hold Residual Motion of Image-Guided DIBH Liver-SBRT: An Estimation by Ultrasound-Based Monitoring Correlated With Diaphragm Position in CBCT. *Radiother Oncol* (2018) 129(3):441–8. doi: 10.1016/j.radonc.2018.07.007

Conflict of Interest: The authors declare that the research was conducted in the absence of any commercial or financial relationships that could be construed as a potential conflict of interest.

Advantages of publishing in Frontiers

OPEN ACCESS
Articles are free to read for greatest visibility and readership

FAST PUBLICATION
Around 90 days from submission to decision

HIGH QUALITY PEER-REVIEW
Rigorous, collaborative, and constructive peer-review

TRANSPARENT PEER-REVIEW
Editors and reviewers acknowledged by name on published articles

Frontiers
Avenue du Tribunal-Fédéral 34
1005 Lausanne | Switzerland

Visit us: www.frontiersin.org
Contact us: frontiersin.org/about/contact

REPRODUCIBILITY OF RESEARCH
Support open data and methods to enhance research reproducibility

DIGITAL PUBLISHING
Articles designed for optimal readership across devices

FOLLOW US
@frontiersin

IMPACT METRICS
Advanced article metrics track visibility across digital media

EXTENSIVE PROMOTION
Marketing and promotion of impactful research

LOOP RESEARCH NETWORK
Our network increases your article's readership